Zeolite A, X and Cancrinite from South African coal fly ash: mechanism of crystallization, routes to rapid synthesis and new morphology

By

Nicholas Mulei Musyoka
MSc Chemistry - University of the Western Cape
BSc Chemistry (honours) - University of Nairobi

A thesis submitted in fulfilment of the requirements for the degree of Doctor of Philosophy in Chemistry
In the Department of Chemistry, University of the Western Cape.

Supervisors: Prof. Leslie F. Petrik
Dr. Eric Hums

May 2012

ABSTRACT

In South Africa, almost 90 % of the country's electricity is generated from coal combustion. This reliance on coal for energy production is projected to continue in the near and medium term due to the increasing demand for industrial and domestic energy. During coal combustion, a large quantity of fly ash is produced as the main waste product and in South Africa approximately 36 - 37 million tons of fly ash is produced on a yearly basis. The management of huge quantities of fly ash has been and still is a continuing challenge that requires urgent intervention. In this regard, there exists an urgent need to maximize fly ash beneficiation, thus forming the motivation for this research.

The overall objectives of this thesis was to synthesize high pure phase zeolites A and X from South African fly ash, study their formation mechanism, and explore the potential of mine waters during the synthesis process as well as developing new and efficient zeolite synthetic protocols by the use of ultrasound. In order to address these objectives, the research was designed in a sequential manner so that the preceding results could act as a platform for the attainment of the next objective. In this case, the identification and optimization of synthesis conditions for producing zeolite A and X acted as a basis for understanding the influence of use of mine waters as a substitute for pure water. This further laid the foundation for the in-situ ultrasonic monitoring of the formation process of zeolite A and X from fly ash. The final stages of the study involved use of ultrasonic energy as an ageing tool to improve the conditions obtained during the hydrothermal synthesis of zeolite A as well as investigate the potential to synthesize zeolites directly by use of ultrasound without the need for the fusion, aging or conventional hydrothermal treatment step.

The result of the optimized synthesis conditions for producing zeolite A starting either from clear extract of fused fly ash or unseparated, fused South African class F fly ash slurry were molar regimes of 1 Al_2O_3 : 30.84 Na_2O : 4 SiO_2 : 414.42 H_2O or 1 Al_2O_3 : 5.39 Na_2O : 2.75 SiO_2 : 111.82 H_2O respectively and at a hydrothermal synthesis temperature of 100 °C for 2 hours. The optimized procedure was simple, efficient and resulted in a considerable improvement of the quality and phase purity of the zeolite A product when the clear extract of fused fly ash was used

instead of starting from unseparated, fused fly ash slurry. On the other hand, the optimized synthesis conditions for preparing the typical octahedral shaped zeolite X from South African fly ash was found to be a molar regime of 1 Al_2O_3 : 4.90 Na_2O : 3.63 SiO_2 : 115.92 H_2O at a hydrothermal synthesis temperature of 80 ºC for 9 hours.

When the optimized procedure for synthesis of zeolite A was applied using circumneutral mine waters as a substitute for pure water during the synthesis process, an almost similar quality zeolite A was obtained whereas a mixture of mainly zeolite A with co-crystallization of hydroxy-sodalite was obtained when acidic mine water was used. Similarly, it was also proved that zeolite X could crystallize when mine water was used as a synthesis solvent though not in its pure form. This finding highlight the fact that the quality of the zeolite formed was dependent on the type of mine water used but that mine water could be used as a substitute for ultrapure water. The novelty of this process of using mine water during the synthesis process is that it has the potential of enabling the coal mining and combustion industries to move closer to the attainment of the goal of zero waste production.

A novel zeolite X with hierarchical morphology was successfully synthesized from clear extract slurry obtained from fused South African class F fly ash. The optimized synthesis conditions were found to be; a molar regime of 1 Al_2O_3 : 56.80 Na_2O : 16.62 SiO_2 : 954.05 H_2O at a hydrothermal synthesis temperature of 80 ºC for 24 hours. The intergrown disc-like nano platelets created micro-/mesoporous materials that presented a greatly enhanced mesoporosity in the 3 – 11 nm range which is highly desirable for various catalytic applications to avoid diffusional constraints. The identified synthesis route that led to the crystallization of this hierarchical zeolite X from South African class F fly ash, without requiring the use of additional ingredients or post synthesis treatment, is advantageous compared to the complicated procedures that are reported in the literature.

The findings from the study on the formation mechanism of zeolite A and X from South African class F fly ash using the in-situ ultrasonic monitoring system together with the complementing ex-situ techniques supported the hypothesis that zeolite A formation from coal fly ash follows both the solution and solid-phase mediated mechanisms depending on ageing procedures. The in-

situ ultrasonic monitoring further elucidated the formation process of the novel morphology (hierarchical) zeolite X from fly ash and supported the solution-mediated model. Zeolite A was found to crystallize much faster than zeolite X as shown by comparison of the time of crystallization from the generated attenuation signals for the formation of zeolite A or zeolite X. The use of in situ ultrasonic monitoring system also provided sufficient data points which enabled closer estimation of the time of transition from nucleation to crystal growth step during the monitoring of formation mechanism of both zeolite A and X. Since in-situ investigation of formation zeolites from fly ash had not been previously conducted under real reaction conditions, the study demonstrated that the in-situ ultrasonic diagnostic technique contributed to an improved understanding of the formation mechanisms of zeolite A and X from South African fly ash. The in-depth investigation of the formation mechanism of zeolite A and X from fly ash conducted in this study using ultrasonic monitoring could be helpful in controlling and predicting the best conditions for synthesis.

The study further demonstrated that application of 10 minutes of sonication of the fused but unaged reaction mixture prior to the conventional hydrothermal synthesis step led to halving of the hydrothermal synthesis time. Similar effects of ultrasound assisted ageing of the reaction mixture were also observed when pure water was substituted with mine waters as synthesis solvent. The study also showed that zeolites could be synthesized directly from South African fly ash without prior fusion or aging by direct application of ultrasound. This novel synthesis route led to the production of a single phase hydroxy-cancrinite zeolite after only 30 minutes of sonication. The new ultrasonic assisted route was used to avoid the fusion and ageing required in conventional transformation of fly ash to zeolite precursors. The invention is advantageous and can play a significant role in the transfer of technology to industry while addressing the shortcomings of the laborious conventional hydrothermal synthetic approaches.

Overall, the research conducted in this study has not only identified and customized the synthesis conditions for producing pure phase, high value industrial zeolites A and X from South African fly ash, but has also resulted in the discovery of a simple route for producing hierarchical zeolites from South African fly ash at a low cost. The application of the in-situ ultrasonic technique to monitor the formation process of these zeolites has enabled investigation of mechanism of

formation by correlating speciation phenomenon with ex-situ analytical techniques. The study also proved that mine waters obtained from coal mines that are located close to the coal power plants could be used as a solvent to substitute pure water during the synthesis of both zeolite A and X. From an environmental and economic point of view, the process of utilizing both fly ash and mine water wastes in the synthesis of zeolites will not only reduce the environmental burden associated with these wastes but could also offer extra income generated from the sale of the synthesized zeolites as established in this study. The novel processes developed in this study have the potential to contribute towards a goal of zero waste discharge in coal mining and coal combustion industries.

KEYWORDS

Coal

Fly ash

Hydrothermal synthesis

Fused fly ash

In situ

Cancrinite

Hierarchical zeolite X

Zeolite A

Zeolite X

Ultrasound

Mine water

Major and trace elements

DECLARATION

I declare that "**Zeolite A, X and Cancrinite from South African coal fly ash: mechanism of crystallization, routes to rapid synthesis and new morphology**" is my own work, that it has not been submitted for any degree or examination in any other university, and that all the resources I have used or quoted have been indicated and acknowledged by complete references.

Nicholas Mulei Musyoka May 2012

Signed…….

ACKNOWLEDGEMENTS

I am greatly indebted and grateful to my main supervisor, Prof. Leslie Petrik, for her guidance, encouragement, invaluable advice and opportunities that I have had through the Environmental and Nano Sciences research group (ENS). My gratitude also goes to my co-supervisor, Dr. Eric Hums, for insightful contributions to my PhD work and also for the hospitality during my stay in Erlangen.

I acknowledge and thank the National Research Foundation (NRF) and Eskom for the financial support that made this study possible. I am also grateful to the German Academic Exchange Service (DAAD) for the short research scholarship that enabled me to spend four months at the University of Erlangen - Nürnberg, Germany. I specifically owe special gratitude to Prof. Wilhelm Schwieger for hosting me in his laboratory at the Institute of Chemical Reaction Engineering of the University of Erlangen –Nurnberg during this period. It was through his kindness and also help from my co-supervisor, Dr. Eric Hums, that I was able to conduct research that resulted in chapter 6 of this thesis. I also cannot forget to thank Prof. Martin Hartmann for allowing me to use the FTIR instrument in his laboratory.

I sincerely appreciate the support and the many helping hands during the journey of my doctoral studies. In particular, I would like to thank Prof. Basil Julies, Dr. Subelia Botha and Adrian Josephs (electron microscopy unit, University of the Western Cape) for the help in carrying out the SEM and HRTEM imaging. I also express my appreciation to Ilse Wells, the ENS laboratory manager, for the timely assistance in ordering equipment and also for ICP analysis. Many thanks also go to Miranda Waldron for the countless hours spent at the electron microscopy unit at the University of Cape Town. I also give further thanks to the students at the Institute of Chemical Reaction Engineering of the University/Erlangen-Nurnberg for the assistance in analyzing some samples and also for the help in the use of various instruments during my time in Germany. I particularly want to thank Hasan Baser (in-situ ultrasonic monitoring set-up), Andreas Kuhnt (XRD), Albert Machoke (SEM), Alexandra Inayat (SEM and BET analysis), Dieter Himsl (FTIR) and Regina Müller (ICP analysis). I cannot fail to mention the friendliness, welcoming

nature and stimulating discussions I had with the students and staff in Prof. Wilhelm Schwieger's and Prof. Martin Hartmann's research groups, especially those I worked alongside.

To my current and former colleagues and teachers at the Environmental and Nano Sciences research (ENS) Group, I highly appreciate the companionship, joy and all other interactions that made my doctoral journey interesting. I am especially grateful to Dr. Gillian Balfour, Dr. Wilson Gitari, and Dr. Patrick Ndungu for their various insights during the initial period of my studies. Many thanks also go Averil Abbott and Vanessa Kellerman for making my life comfortable while doing the research work. Appreciation also goes to Nkatha Murungi, Roland Missengue, Guillaume Ndayambaje, Dr. Olenrewau Fatoba and Dr. Omotola Babajide for agreeing to proof read some sections of my thesis. To my friends Eugene Tendwa, Victoria Adipo, Gertrude Kitongo and Maurine Tendwa, I cannot forget the role you have all played in my journey and I appreciate your being part of my life. A special word of mentioning and appreciation goes to the Hargrave family, (Meredith Higgins, Tom Hargraves, Anna Hargraves) and Betty Hopkins, who have been like my second family. Prof. Lydia Njenga, Beth and Jason Gierch, Paul Nasrani and Chris young, thank you for your various contributions in my journey of becoming who I am today.

Lastly, but not the least, I am very grateful to my parents and family members for their constant encouragement, unconditional love, understanding and prayers that kept me going even when times were tough. Above all, and the most needed, many thanks to the omnipresent God for the strength, mercies and blessings throughout the whole journey.

TABLE OF CONTENTS

CHAPTER 2: LITERATURE REVIEW

CHAPTER 5: IDENTIFICATION AND OPTIMIZATION OF HYDROTHERMAL SYNTHESIS CONDITIONS FOR ZEOLITE X FROM SOUTH AFRICAN FLY ASH

LIST OF FIGURES

LIST OF TABLES

LIST OF ABBREVIATION

AMD = Acid mine drainage

BET = Brunauer Emmett Teller

BJH = Barrett-Joiner-Halenda method

CCP = Coal combustion products

CEC = Cation exchange capacity

CMW = Circumneutral mine water

CTL = Coal-to-liquid technologies

DTA Differential Thermal Analysis

EC = Electrical Conductivity

ENS = Environmental and Nano Sciences research group

FBC = Fluidized bed combustion

FGD = Flue gas desulphurization

FTIR = Fourier transform infrared spectroscopy

H = Hematite

HRTEM = High resolution transmission electron microscopy

HS = Hydroxy-sodalite

ICP-AES = Inductively coupled plasma atomic emission spectrometry

ICP-MS = Inductively coupled plasma mass spectrometry

IZA = International Zeolite Association

JCPDS = Joint Committee on Powder Diffraction Standards

LOI = Loss on ignition

M = mullite

Mag = Magnetite

Mt/y = Million tonnes per year

N/A = Not detected

NMR = Nuclear magnetic Resonance

NOx = Nitrogen oxides

P = Zeolite Na-P1

PPM = Parts per million

Q = Quartz

RT = Room temperature

SAED = Selected area electron diffraction

SBU = Secondary building blocks

SDA = Spray dryer absorption

SEM = Scanning electron microscopy

SOx = Sulphur oxides

STD = standard

Stdev = Standard deviation

T – atoms = Si and Al (Silicon and Aluminium)

TDS = Total dissolved solids

TGA = Thermogravimetric analysis

Wt = weight

XRD = X-ray diffraction Spectroscopy

XRF = X-ray Fluorescent Spectroscopy

ZSM = Zeolite Socony Mobil

ACADEMIC OUTPUTS OF RESEARCH REPORTED IN THIS THESIS

Patent applications

N. M. Musyoka, L. F. Petrik, E. Hums. United Kingdom patent application number 1113768.4, filed on 10th August, 2011: Applicants: Eskom Holdings SOC ltd and University of the Western Cape, **File reference PA154022/P.**

L. F. Petrik, N. M. Musyoka, E. Hums. South African provisional patent application. Application number 2012/02206 filed on 27th March 2012: Applicant: University of the Western Cape. **File reference PA155039/P.**

Published papers

Nicholas M. Musyoka, Leslie F. Petrik, Eric Hums, Hasan Baser, Wilhelm Schwieger, In situ ultrasonic monitoring of zeolite A crystallization from coal fly ash, ***Catalysis Today,*** (2012*)* 190, pp. 38-46.

Nicholas M. Musyoka, Leslie F. Petrik, Eric Hums, Synthesis of zeolite A, X and P from a South African coal fly ash, ***Advanced Materials Research***, Vols. 512-515 (2012) pp 1757-1762.

Omotola Babajide, Nicholas Musyoka, Leslie Petrik, Farouk Ameer, Novel zeolite Na-X synthesized from fly ash as a heterogeneous catalyst in biodiesel production,
Catalysis Today, (2012) 190, pp. 54-60.

Peer reviewed conference paper

Nicholas M. Musyoka, Leslie F. Petrik, Eric Hums (2011): Ultrasonic assisted synthesis of zeolite A from coal fly ash using mine waters (acid mine drainage and circumneutral mine water) as a substitute for ultra-pure water. – In: Rüde, R. T., Freund, A. & Wolkersdorfer, Ch.: Mine Water – Managing the Challenges. p. 423 – 427; Aachen, Germany.

Oral presentations

N. M. Musyoka, L. F. Petrik, E. Hums, W. Schwieger. In-situ ultrasonic monitoring of zeolite A crystallization from coal fly ash. 4th International conference on Nanoscience and Nanotechnology, University of Free State, **Bloemfontein, South Africa** on 1 - 4 April 2012.

N. M. Musyoka, L. F. Petrik, E. Hums. Ultrasonic assisted synthesis of zeolite A from coal fly ash using mine waters (acid mine drainage and circumneutral mine water) as a substitute for ultra-pure water. 11th International Mine Water Association (IMWA) Congress, **Aachen, Germany** on 4-11 September 2011.

N. M. Musyoka, L. F. Petrik, E. Hums. Synthesis of zeolites from coal fly ash: Ultrasonic assisted ageing process. 40th SACI convention and the 3rd FASC meeting, University of the Witwatersrand, **Johannesburg, South Africa,** 16-21 January 2011.

N. M. Musyoka, L. F. Petrik, E. Hums. Ultrasonic assisted synthesis of zeolites from fly ash. Nanosciences Young Researcher Symposium (NYRS) held at the **University of the Western Cape, South Africa**, 18th September 2010.

Poster presentations

N. M. Musyoka, L. F. Petrik, R. Akinyeye, G. Madzivire, E. Hums. Synthesis of zeolites from coal fly ash using mine waters (circumneutral and acid mine drainage) as a substitute for pure water. 5th International Federation of European Zeolite Associations Conference (FEZA), **Valencia, Spain,** 3- 7 July 201.

N. M. Musyoka, L. F. Petrik, E. Hums. Characterization of zeolite A synthesized from coal fly ash using mine waters. 9th International Symposium on the Characterization of Porous Solids - COPS 9, **Dresden, Germany** 5 – 8 June 2011.

N. M. Musyoka, L. F. Petrik, K. Molapo, G. Balfour, E. Hums. Synthesis of zeolites from fly ashes sourced from different South African coal fired power stations" Analitika 2010, **Stellenbosch, South Africa**, 5 - 9 December, 2010.

CHAPTER 1

INTRODUCTION

This chapter briefly introduces the scope of this research by highlighting key areas that will be explored in the other chapters. Firstly, a brief background on coal and fly ash in South Africa is presented. The use of fly ash in zeolite synthesis is further explored while highlighting some of the key research gaps that have been identified from previous studies. The motivation and objectives of the research is thereafter presented and finally the thesis delimitations and structure is highlighted.

1 Introduction

Coal combustion is heavily relied upon in the production of electricity worldwide. In South Africa, almost 90 % of electricity is derived from coal combustion (Eskom, 2011). According to the World Coal Association, the abundance of coal reserves and the guarantee of continued supply is expected to sustain the existing coal power stations for many years to come as well as to prompt construction of new power stations especially in the developing countries (WCA, 2005). The major coal deposits in South Africa occur in the Waterberg, Witbank, and Highveld coalfields, as well as lesser amounts in the Ermelo, Free State and Springbok Flats coalfields (Jeffrey, 2005). The prospect of continued use of coal as a viable long-term energy source creates a challenge to find beneficial ways of utilizing coal combustion by-products (Pengthamkeerati *et al.*, 2008). It has been reported that about 5-20 % of the coal mass after combustion remains as fly ash and bottom ash (Molina and Poole, 2004; Yaping *et al.*, 2009). Fly ash, the major combustion residue produced during the combustion of pulverized coal, is a fine-grained, inorganic, spherical, non-opaque, glassy, particulate, powdery residue which is derived from the inorganic minerals included in coal during the coal formation process (Ahmaruzzaman, 2010).

It is estimated that about 500 million tonnes of fly ash are produced worldwide per year from coal combustion (Ahmaruzzaman, 2010) and the amount is expected to increase in future due to the pressing need for generation of sufficient energy for the ever increasing industrial and domestic energy demand. China is the largest producer of fly ash, producing about 160-185 Mt/y (Koukouzas *et al.*, 2006). Fernández-Jiménez and Palomo (2005) and Álvarez-Ayuso *et al.*, (2008) had earlier reported that of the total fly ash produced worldwide, only a small percentage

(20 – 30%) is properly utilized. In South Africa, 36.22 million tonnes of fly ash was produced in 2011 alone and only about 5.5% was recycled with the rest being disposed in ash dams and dumps located near to the coal-fired power stations (Eskom, 2011). The reason for the high fly ash quantity is related to the low grade coal that is burnt in the South African coal-fired power plants which has a high inorganic content of up to 40 % (Eskom, 2011). The disposal of these huge amounts of fly ash raises concerns because of contamination of ground water due to leaching of toxic elements, potential risk of air pollution, and rendering large tracks of land unusable (Adriano *et al*., 1980; Eary *et al*., 1990).

In recent years, a considerable amount of research on the utilization of fly ash has been conducted. Some of the proposed applications of fly ash include; (i) as an additive in the manufacturing of cement and in road construction materials (Molina and Poole 2004; Yaping *et al*., 2008), as a feedstock in zeolite synthesis (Holler and Wirsching, 1985; Shigemoto *et al.*, 1993; Hollman *et al.*, 1999, Woolard *et al.*, 2000; Querol *et al.*, 2001; Somerset *et al.*, 2004); Musyoka, 2009), and use in the neutralisation and treatment of acid mine drainage (Petrik *et al.*, 2005; Gitari, 2006). All these applications are geared towards beneficial fly ash utilization in order to minimize disposal costs, reap financial gains generated from the sale of products obtained, and replace some expensive and scarce natural resources with fly ash. Research has indicated that all the aforementioned applications of fly ash have their own advantages and disadvantages. For example, on the positive side of the utilization of fly ash in the cement industry, fly ash acts as an inexpensive replacement for lime in Portland cement, but the inherent transport cost for the relatively low value use makes it difficult for fly ash to compete with the conventional raw materials. Even though zeolite synthesis from fly ash is one of the high end applications, the applications of fly ash in this case has not been of high volume due to technical problems associated with scaling up the synthesis processes as well as due to the production of low value zeolites (impure zeolitic phases) that often fail to excite significant interest in the zeolite market.

Since the coal combustion power plants in South Africa rely on bituminous coal, the fly ash produced is reported to contain more than 70 wt% of SiO_2, Al_2O_3, Fe_2O_3 and has a low content of lime (Somerset *et al.*, 2004; Gitari, 2006; Musyoka, 2009). According to the American Society

for Testing Materials standards (ASTM C618, 2005), this fly ash falls under class F classification categories of fly ashes. This compositional content of South African fly ash makes it a good candidate for producing zeolites that can overcome transport cost barriers which in turn can stimulate increased consumption of significant quantities of fly ash during the zeolite synthesis process.

1.1 Synthesis of zeolites from coal fly ash

Zeolite science is a very topical field with many future prospects such as in applications such as catalysis, adsorption and water treatment, among others (Byrappa and Masahiro Yoshimura, 2001). In most cases, zeolites are formed by a framework of $[SiO_4]^{-4}$ and $[AlO_4]^{-5}$ which are tetrahedra linked to each other at the corners by sharing their oxygen atoms (Szostak, 1989; Weitkamp and Puppe, 1999; Nagy *et al*., 1998). The tetrahedral arrangement extends to form a three-dimensional network containing group I or II elements as counter ions. The structural properties of zeolites enable them to have a wide range of industrial applications such as; ion exchange, gas and water adsorption, catalysis and separation (Pfenninger, 1999; Bayati *et al.,* 2008). Zeolites have traditionally been synthesized from conventional aluminosilicate gels prepared from pure chemicals (Breck, 1974: Barrer, 1982) Over recent years, unconventional starting material such as metakaolin (Chandrasekhar *et al*., 2008), cupola slag and aluminum sludge (Anuwattan and Khummobgkol, 2009), municipal solid waste ash (Sallam, 2006), chrysotile and rice husk (Petkowicz *et al*., 2008) and coal fly ash (Querol, *et al*., 2002) among many others have also been used to synthesize zeolite.

The initial interest in the use of fly ash as a feedstock for zeolite synthesis was triggered by the discovery of the compositional similarity of fly ash to some volcanic materials, precursor of natural zeolites (Holler and Wirsching, 1985). Since then numerous researchers have synthesized many different types of zeolites from fly ash (Querol, *et al*., 2002). Owing to the high content of aluminosilicate glass, mullite ($Al_6Si_2O_{13}$) and quartz (SiO_2) that provides a rich source for Al and Si, fly ash is well suited as a raw material for zeolite synthesis. Different conversion routes of fly ash to zeolites have been reviewed and summarised by Querol *et al*., (2002). By applying different synthesis methods, many researchers have synthesized various types of zeolites such as zeolite A (Murayama *et al.,* 2002, Rayalu *et al.,* 2001), zeolite Na–P1 (Inada *et al.,* 2005), and

zeolite ZSM-5 (Chareonpanich *et al.*, 2004) mainly from class C type of coal fly ashes. Few studies exist on conversion of class F fly ash into zeolites (Derkowski *et al.*, 2006, 2007; Grutzek and Siemer, 1997; Koukouzas *et al.*, 2010; Wojciech, 2012). According to the American Society for Testing Materials standards (ASTM C618), the difference between class C and class F fly ashes lies in their differing total contents of SiO_2, Al_2O_3, Fe_2O_3 and CaO. Fly ash containing more than 70 wt% of SiO_2, Al_2O_3, Fe_2O_3 and having a low content of lime is classified as class F, while class C is defined for fly ash whose total content of SiO_2 Al_2O_3 and Fe_2O_3 lies between 50 and 70 wt% and with high lime content. Since each zeolite type requires unique molar composition for the specific phase to form and is dependent on synthesis conditions applied, the optimised synthesis conditions and composition for a particular zeolite phase to form from a specific coal fly ash source cannot be predicted accurately for a new source of fly ash, due to the variability of fly ash composition.

The use of coal fly ash as a raw material in zeolite synthesis stands out as the most environmentally friendly way of recycling the coal fly ash. By utilizing fly ash in the synthesis of zeolite products, potential environmental burdens associated with fly ash disposal can be mitigated. In addition, the zeolitic products produced can be sold to generate extra income for the power plant. The major potential applications of zeolites synthesized from fly ash include; ion exchangers in industrial waste water treatment (Holler and Wirsching, 1985), soil decontamination (Singer and Berkgaut, 1995), catalysis (Babajide *et al.*, 2012), and removal of post combustion gases such such as SO_x and NO_x (Querol *et al.*, 2002). Having established that the cost of synthesizing zeolites from fly ash is one fifth of the commercial zeolite production cost (Ojha *et al*., 2004), the fly ash zeolitization process can be a competitive way of producing zeolites to satisfy the new emerging applications of zeolites, especially if high value zeolite phases can be prepared.

1.2 Some issues with the current techniques for conversion of fly ash to zeolites

In this section, the issues that limit current knowledge on converson of fly ash to zeolites are identified. Even though the conversion of zeolites to fly has been studied for close to three decades, there are quite a number of challenges that have been experienced that have hindered

large scale production of zeolites from fly ash. Some of these challenges that motivated this study included:

1.2.1 Fly ash compositional variability

Owing to the compositional and mineralogical variability of fly ashes sourced from different countries or coal-fired power plants (Eary *et al*., 1990; Ural, 2005; Bhanarkar *et al.,* 2008), conditions optimized for one type/source of fly ash cannot be applied to others without adaptation (Chang and Shih, 2000; Querol *et al*., 2002). This challenge is well evident in the existing literature because it is rare to find 'standard synthesis conditions' or cases where different researchers rely on the same set of reaction conditions. Attempting to directly apply some of the reported synthesis conditions often leads to the production of mixed phase zeolite, instead of single phase or even zeolitic materials with residual fly ash phases. A good example is a study conducted by Querol *et al* (2001) who investigated synthesis of zeolites from fly ash at a pilot scale using various Spanish fly ashes and concluded that the synthesis conditions for each type of fly ash have to be identified and optimized due to differences in their mineralogical and chemical compositions. It was further confirmed that even when two fly ashes with similar SiO_2/Al_2O_3 bulk ratios, but different quartz-mullite/glass proportions are used under the same activation conditions, there is a high likelihood that different zeolites phases will be produced (Querol *et al.,* 2002).

In the case of application of South African fly ashes in zeolite synthesis, very limited research has been conducted to identify the synthesis conditions for high value zeolites. Most of the procedures identified elsewhere for producing single phase zeolites were mainly conducted using class C fly ash whose composition is different from the class F fly ash that is produced in South Africa. Despite the fact that the South African class F fly ash is reportedly a good candidate for producing zeolites due to its high aluminosilicate content (Kruger, 1997; Woodlard *et al*, 2000; Somerset *et al*., 2004), studies conducted by Woodlard *et al*. 2000), Somerset *et al*. (2004, 2008), Hendrick (2005) and Vadapalli *et al*. (2010) were mostly unsuccessful to get single phase zeolites because the studies resulted in preparation of mixed phase zeolitic products which mainly have low end applications. These impure zeolite phases have been applied in different applications such as in treatment of industrial waste waters (brine solutions and mine waters) and

have shown to lead to relatively low efficiencies of removal of toxic metal contaminants, as reported by Hendrick (2005) and Sonqishe (2008). It is on this basis that the best conditions for the synthesis of single phase zeolites with high end applications have firstly to be identified and then customised to the South African class F fly ash.

1.2.2 Limited in-depth understanding of the mechanism of zeolite formation from fly ash

One of the major challenges facing most zeolite researchers is the limited understanding and lack of ability to rationally control the synthesis process due to the limited understanding of the zeolite formation mechanism and the heterogeneity coal fly ash. This challenge also extends to the optimization and scale up process. Sankar and co-workers (2009) suggested that rational design of the synthesis process can be achieved when the zeolite crystallization mechanism is well understood. Even though many attempts have been made to understand the formation mechanisms of zeolite synthesis from fly ash (Murayama *et al*., 2002; Fernández-Jiménez and Palomo, 2005; Fernández-Jiménez *et al*., 2005; Inada *et al*., 2005), these studies have not succeeded in studying the zeolite formation process under real reaction conditions. The aforementioned researchers mostly relied on ex-situ characterization techniques which often rely on the reaction history of the zeolite formation process. The risk of using these techniques to unmask the complex processes taking place during the transformations of fly ash to zeolites lies in the artefacts that may arise during the quenching of the samples. Some of the 'true states' of the reacting species are compromised hence missing important information that could help in capturing a true or complete picture of what is happening during the conversion process.

Recently, in-situ monitoring methods have been applied by different researcher (Shih *et al*., 1996; Miladinović *et al*., 2007) to understand the formation of zeolites starting from pure chemicals. These different in-situ methods have been recently reviewed by Pienack and Bensch (2011) who classified them as follows: in-situ scattering techniqies, in-situ spectroscopy, in-situ mass spectrometry, in-situ transmission electron microscopy, and combination method. In addition to the list, the contribution of little known in-situ ultrasonic technique reported first by Toufar *et al*., (1998) and Schmachtl *et al.*, (2000) has elicited great interest for the understanding of the complexity of the zeolite formation process. Basing on the absence of studies on investigation of zeolite formation processes from fly ash under reaction conditions, a section of

the current study aimed at applying the in-situ ultrasonic monitoring system to further the knowledge for zeolite formation from fly ash. A deeper understanding of the formation mechanism should not only help in controlling and predicting the best conditions for synthesis but should also unmask the cooperative phenomena dictating chemical-structure-physical properties' relationships. The findings from this study could prove useful during scale up of the zeolite synthesis process.

1.2.3 Shortcoming of the conventional hydrothermal synthesis process

A review of the synthesis of zeolites from fly ash done by Querol and co-workers have confirmed that the production of zeolites by treating fly ash with alkaline solution is the most well-known process (Querol *et al.,* 2002). This classical alkaline conversion of fly ash route is based on the combination of different activation solution/fly ash ratios, with specific conditions of temperature, pressure and reaction time applied to obtain different zeolite types (Querol *et al*., 2001). Several other researcher have recommended improvements to this synthesis route such as; introduction of an alkaline fusion stage to monomerize the Si feedstock prior to conventional zeolite synthesis procedures (Shigemoto *et al*., 1993), application of microwave heating conditions to the synthesis procedure which resulted in the reduction of the overall reaction time to around 30 minutes under the specified conditions (Querol *et al.,* 1997; Kim *et al*., 2004; Inada *et al.,* 2005), introduction of a two way stage synthesis procedure to produce pure zeolite products from high silica containing solutions (Hollman *et al.,* 1999), use of a dry or molten-salt method (Park *et al.,* 2000), introduction of a desilification step after an alkali fusion step during conventional synthesis which improved the solubility of the Al and Si content of the fly ash (Yaping *et al*., 2008) and also the modification of the Si/Al ratio during the synthesis process which resulted in a wide variety of the synthesized zeolites with improved properties (Walek *et al.,* 2008). All these improvements were aimed at addressing the challenges associated with the conventional synthesis approach such as high consumption of energy and prolonged synthesis time.

The limited or lack of the existence of large scale production of zeolites from fly ash could imply that the synthesis of zeolites from fly ash is not yet competitive enough compared to the production of zeolites from pure chemicals. One of the reasons for the low competitiveness

could be due to limitations of the current limitations of known synthesis techniques hence calling for a need for further research in exploring other synthesis routes. A section of this research endeavoured to investigate ways of improving on the existing synthesis routes by the use of ultrasound. Ultrasonic enhanced crystallization is known to accelerate nucleation and crystallization rates (Dolores *et al*., 2007, Luque de Castro and Priego-Capote, 2007) and hence leads to improvement of the yield and particle size distribution. Studies of the effects of ultrasound on the synthesis of zeolite A from the conventional starting feedstock (pure chemicals) conducted by Andaç *et al.* (2005) concluded that it was possible to obtain highly crystalline zeolite A on application of ultrasound. Application of ultrasound to fly ash has shown that ultrasound enhanced fly ash dissolution (Feng *et al.* (2004) and could lead to formation of semi-crystalline to crystalline phases during the geopolymerisation reactions. A recent study by Belviso *et al.* (2010) demonstrated that the application of ultrasonic treatment prior to hydrothermal synthesis of zeolites from fly ash led to reduction of synthesis temperature. Up to date there are no reports on the direct synthesis of zeolites from fly ash by direct sonication of fly ash slurries.

Furthermore, coal mines and coal combustion power plants are mostly found in close proximity to each other in South Africa. However there is no research that has been conducted to investigate the viability of synthesis of zeolites from fly ash using the coal mine waste waters. Ever since the initial studies that were reported by Holler and Wirsching (1986), many different types of zeolites have been synthesized from fly ash by varying the synthesis conditions (Querol *et al*., 2002). Most of these studies utilized pure water during the synthesis process with just a few that have concentrated on the use of seawater (Lee *et al*., 2001; Belviso *et al*., 2010) and waste industrial brine solutions (Musyoka *et al*., 2011). Other studies have also shown the potential of using co-disposal solids, generated from the active treatment of acid mine drainage with coal fly ash, as a feedstock for zeolite synthesis (Somerset *et al*., 2008; Vadapalli *et al*., 2010) even though pure water was used during the synthesis procedure. A section of this study seeks to investigate the direct use of different types of mine waters as a solvent to synthesize different types of zeolites. In this regard, the use of these two wastes (fly ash and mine waters) in zeolite synthesis will not only offer a potential capital savings option for disposal of these wastes but will also be advantageous to the coal mines and power stations since it will enable

constructive use of the large volumes of waste effluents that they generate. The motivation for this objective was mainly inspired by the need for complete industrial waste re-use to achieve zero discharge goals.

1.3 Importance of the current research (Motivation)

Having no doubt that the worldwide reliance on coal for energy production will continue, with further prospects of an increase in future, the volume of generated waste will continue to grow in direct proportion to the increasing demand for industrial and domestic energy. Due to the vast coal reserves in South Africa, large pulverised coal-fired power plants are in daily operation to provide the much needed energy to support the South African economy. The consequence of this operation is that the rate of fly ash production exceeds the rate of fly ash re-use significantly. This necessitates the need for more innovative ways to deal with the waste fly ash in order to reduce the environmental burden and the concomitant disposal cost. The current low end strategies for the utilization of fly ash have led to low uses of fly ash in South Africa. This is confirmed by a survey of the state of reuse of South African fly ash conducted by Kruger (1997) who reported that the value of fly ash as a resource is yet to be fully utilized and its value remains underestimated. There is therefore the need for more value-added, high technology utilization of fly ash such as zeolite synthesis to overcome this barrier. Although the conversion of fly ash to zeolites is not a new concept, the variability of fly ash composition from country to country or from one power plant to another, as well as the logistical problems such as high transportation cost and less efficient synthesis processes have compounded the failure and/or limited the large scale production of zeolites from fly ash. It is on this basis that this study aims to treat the South African class F fly ash as the starting feedstock for preparing high value zeolites. To overcome challenges that have been experienced by previous researchers such as inability to make single phase zeolites with high industrial attractiveness under less attractive conditions, the current study seeks to develop high value zeolites from South African class F fly ash with properties that are in current demand, while concurrently developing efficient and cost effective synthesis routes. By coming up with zeolites with improved properties, made in an efficient way, the use of South African class F fly ash as a synthesis feedstock will be able to compete with other conventional pure raw materials.

1.4 Objectives of the study

The overall objectives of this study was to identify and customize synthesis conditions for producing high value zeolites such as zeolite A and X from South African fly ash, and study their formation mechanism. Further objectives were to improve routes to prepare zeolites and characterize the product quality as well as investigate the potential for a rapid ultrasonic synthesis route to produce zeolites directly from fly ash. In summary, the fourfold interrelated objectives are outlined below.

1. To identify, customize and optimize the synthesis conditions for producing zeolite A and X from South African class F fly ash.

2. To comparatively explore the use of lower quality waters (mine waters) as a substitute for pure water during the synthesis of zeolite A and X from South African class F fly ash.

3. To study the formation mechanism of zeolites from South African class F fly ash using in situ ultrasonic monitoring process.

4. To apply ultrasound as a substitute to the conventional ageing step as well as a replacement for the overall hydrothermal synthesis process.

The emphasis on finding routes for preparing high phase purity zeolite A and X from fly ash was due to the already well-established industrial uses for pure phases made from pure chemicals. These two zeolites were targeted by other researchers who used South African class F fly ash but they were not successful in producing them as single phases. This was mainly because there has been insufficient experimentation on the specific identification of conditions that would lead to enhanced quality of the zeolites formed. Since very limited research has been conducted on the use of different South African fly ashes, the findings from this research would lay a foundation for large scale conversion of the fly ash to zeolites with specific commercial applications. It is also intended that the experiments conducted during the investigation of the zeolite crystallization mechanism would contribute greatly to the understanding of the formation process

of zeolites from fly ash, which is still unclear. The study further looks at potential areas for future research in the successful synthesis of other high value zeolites.

1.5 Research questions

This study aims to address the following research questions.

1) What are the synthesis conditions for producing high quality single phase zeolite A and X from south African fly ash?
2) Can specific or new morphologies of zeolite X or A be produced from fly ash without the need for the use of additional structure-directing agents or post synthesis treatment?
3) Can mine waters be used to produce single phase zeolite A and X from South African fly ash?
4) Is it possible to study the formation process of zeolite A and X under real reaction conditions using the in-situ ultrasonic monitoring system?
5) To what extend can the application of ultrasound improve the synthesis conditions for producing zeolite A from South African fly ash?
6) Is it possible to synthesize zeolites by direct application of ultrasound?

1.6 Research approach

In the interest of achieving the above mentioned objectives, the research was designed in a sequential manner so that the preceding results could act as a platform for the attainment of the next objective. Extensive review of zeolite synthesis techniques was carried out and aspects of the appropriate synthesis methodology were adopted. The experimental programme draws on a five-tiered methodological approach. The first phase involved searching for the necessary conditions for synthesis of single phase zeolite A and X by adapting and optimizing the known synthesis conditions to the characteristics of South African class F fly ash. Initially, the variables that were most likely to affect the respective synthesis product quality were identified. Thereafter, the experimental protocol that entailed adjusting parameters by the one-step-at-a-time technique was chosen. In this case, at each step, a single factor was changed while other factors remained constant. Once the effect of one factor had been determined, the effect of the next parameter was investigated whilst keeping all the other factors constant. The sequential nature of the experiments created an opportunity for adopting the new results that emerged from the

previous stage. This made it possible to apply the best parameter in studying the effect of the next factor.

The second phase involved the substitution of pure water with mine waters that were collected from Middleburg and Navigation coal mines that are located in the Mpumalanga province of South Africa. Phase three of the study targeted the production new morphologies of zeolite X which has not been synthesized before using fly ash using a clear extract with a specific molar composition, and the products were characterized and compared with those of standard commercial zeolite X which has the typical octahedral morphology. The fourth phase of the study dealt with the use of in-situ ultrasonic monitoring of the formation process of both zeolite A and X from fly ash. The synthesis conditions that had been optimized in the first stage of the study were used in this case. The final phase involved the direct sonication of fly ash slurries to yield zeolitic phases directly and also the use of ultrasonic assisted aging of synthesis precursor mixture of zeolite A to reduce the hydrothermal crystallization time.

Fly ash which is discharged from a coal fired power plant (Eskom's Arnot fly ash) in South Africa was used as the starting material for the zeolites synthesis process. Other South African fly ashes were also analysed and compared to Arnot fly ash in order to give an indication of their potential to act as synthesis feedstock.

1.7 Scope and delimitations of the thesis

Owing to the topical nature and wide scope of the science of coal and fly ash, only those aspects that seemed important to the conversion of fly ash to zeolites were identified and highlighted. The literature review further considered the topical nature of zeolite science and only focused on overviewing general aspects of zeolites in terms of description, types and classification, synthesis and mechanism of formation with the main emphasis on conversion of fly ash to zeolites. Most of the information which was of less relevance to the study has been left out or only briefly described. The choice of characterization techniques that were used was mainly focused on the need to acquire the most important information with regard to the quality and phase purity of the synthesized zeolites which could later be fully characterized by other researchers interested in their applications. Although a detailed investigation of the formation mechanism is presented in

this thesis, only the formation process of two zeolite types was considered which acts as a representation of the fly ash zeolitization process. Two types of mine waters of different qualities (acidic and near-neutral/circumneutral nature) were used to give indications and compare how these substitute mine waters may affect the crystallization outcomes of the already proven procedures of zeolite formation when pure water is used. Since the main focus of this research was on improving conditions for conversion of fly ash to zeolites, only bench scale studies were conducted.

1.8 Thesis structure

This thesis is organized into eight chapters (including this one) and is structured as follows:

Chapter one: Introduction

This introductory chapter presents the background information upon which the research work was developed. The main aspects relating to the scope of the dissertation are briefly highlighted in order provide an outline of the focus of the study. The motivation of the study is also set out. The research approach, delimitations of the thesis and a brief outline of each chapter of the thesis are also presented.

Chapter two: Literature review

This chapter presents a literature survey of the relevant aspects of coal and fly ash, general aspects of zeolite science, and use of fly ash in zeolite synthesis. The different synthesis routes for zeolites synthesis from fly ash are brief highlighted. Other items such the previously proposed mechanisms of formation of zeolites from fly ash are also reviewed. Towards the end, focus is directed to a brief overview of some of the zeolite with high industrial applications that have been synthesized from fly ash.

Chapter three: **Experimental and analytical techniques**

This chapter presents a short description of the research design, detailed description of the experimental procedures and instrumental setups used in the present research work. The chemicals, materials and characterization procedures are also detailed. A brief rationale behind

the selection of the procedures followed is also highlighted and the research instruments used are also presented as well as set up conditions and sample preparation details.

Chapter four: Identification and customization of synthesis conditions of zeolite A from South African fly ash: synthesis from pure and mine waters.

This chapter sets the stage for the other chapters; results from the characterization of the fly ash, as the raw material, are presented in order to provide useful information on the appropriate mineralogical and physicochemical composition for their application in zeolite synthesis. The chapter further presents the results of the identification and customization of the synthesis procedure for zeolite A. The presentation of the results is followed by a discussion of the main trends. The discussion connects results with the literature survey and highlights any correlations that have emerged in the data. The results obtained from the use of mine water as a replacement of pure water during synthesis of zeolite A are also presented. A comparison is also drawn to investigate the quality of mine water–fly ash derived zeolites in relation to zeolites produced when pure water was used as the synthesis solvent.

Chapter five: Identification of synthesis conditions of zeolite X from South African fly ash: synthesis from pure and mine waters.

Results and discussion of the identification and customization of synthesis conditions for zeolite X from South African fly ash are presented. Results obtained when mine waters are used during the synthesis of zeolite X as a replacement of pure water during synthesis of zeolite A are also presented.

Chapter six: In-situ ultrasonic monitoring of the crystallization of zeolite A and X from fly ash.

This chapter presents results obtained from in-situ ultrasonic monitoring of the formation process of zeolite A and X from fly ash. The findings are compared with the existing mechanisms that have been reported in literature both for synthesis starting from conventional (pure chemicals) feedstock and also fly ash.

Chapter seven: **Direct and ultrasonic assisted synthesis of zeolites**

This chapter reports the results of studies focussed on the use of ultrasound to assist in zeolite formation. The results from ultrasonic assisted aging processes prior to the conventional hydrothermal crystallization step of zeolite A are firstly presented before the findings for a novel direct ultrasonic synthesis route for producing zeolites is discussed.

Chapter eight: Conclusions and Recommendations

This chapter presents a summary of the findings and conclusions of the work performed in this study. The novelty of the research is further highlighted together with the contributions of the current research to the body of the existing literature. Lastly, an outline of aspects that need further research is presented and draws attention to recommendations for future research.

CHAPTER 2

LITERATURE REVIEW

This chapter presents an overview of coal and coal fly ash since they are parent materials for the zeolites synthesized in this study. Thereafter, the general aspects of zeolites are broadly discussed with respect to classification, structures, properties and formation process, prior to an in-depth discussion of the conversion of fly ash to zeolites. Different synthesis procedures are then highlighted, followed by an overview of applications of zeolites from coal fly ash.

2 Introduction

2.1 Coal and fly ash

2.1.1 Coal

Coal is a solid, brittle and combustible carbonaceous material formed over a geological time scale. It comprises of both organic and inorganic matter (Sheng and Li, 2008). The process of coal formation involves the decomposition and alteration of distinct organic and inorganic entities by compaction caused by high pressure and temperature resulting from movement of the earth's crust, or by wind and water erosion (Speight, 2005). The organic components are mainly derived from decaying vegetation, that is, often moss and other low plant forms. However, in some cases woody precursors play a significant role during coal formation (Crelling *et al*., 2010). Investigation of the shale and sandstone sediments that often overlie coal deposits gives information of the type of plants that contributed to its carboniferous nature. The non-combustible substances of coal are made up of inorganic ions which are bound organically, as well as mineral matter present as crystals or fragments of true minerals (McLennan *et al.*, 2000). A coal deposit is usually stratified and the strata can range from fractions of an inch to hundreds of feet in thickness. The coal stratum is identifiable from its colour which varies from brown to black.

Coal is classified depending on its properties which depend on the origin of the coal and geological age (Goodarzi, 2002). The nature of the coal matrix determines its unique physical and chemical properties and this in turn directs the overall behaviour of a given coal sample (Krevelen, 1993). Compositional analysis of the ash in coal is often useful in the total description

of the quality of the coal (Speight, 2005). For commercial purposes, different ways of classifying coal have been adopted (Krevelen, 1993; Crelling *et al*., 2010). These are: i) coal type, based on original plant or maceral composition, ii) coal rank, which is based on the degree of maturity or metamorphism and is often referred to as the degree of coalification, iii) coal grade, depending on the amount of impurities such as ash or sulphur, and iv) Other industrial properties such as coking or agglomeration. According to ATSM standard D388 (Ahmaruzzaman, 2010), coal is classified into four classes: anthracite, bituminous, subbituminous and lignite coal. This classification is further subdivided into 13 groups on the basis of fixed carbon and volatile matter content, calorific value, and agglomerating character (Crelling *et al*., 2010). Anthracite, often referred to as hard coal is hard, brittle, and lustrous black and contains a high percentage of fixed carbon and a low percentage of volatile matter. It is the highest rank of coal. Bituminous coal can either occur as a black or dark brown dense coal, often with well-defined bands of bright and dull material, and is used primarily as fuel in coal fired power plants. Subbituminous coal may be dull, dark brown to black, and is soft and crumbly at the lower end of the range, or bright, black, hard, and relatively strong at the upper end and is used primarily as fuel for steam-electric power generation. Lignite *is* brownish black in colour and is often referred to as brown coal and is the lowest rank of coal which is used almost exclusively as fuel for steam-electric power generation (Speight, 2005).

Coal deposits are found on every continent with the world coal reserves estimated to exceed 1 trillion tonnes (Speight, 2005; Crelling *et al*., 2010). Major coal producing countries include United States, China, Former Soviet Union, India, Australia, South Africa, Indonesia, Poland, Germany, and Columbia, among others. United States and the former Soviet Union are each estimated to have about 23% of the world's reserves while China's share is estimated to be about 11% (Speight, 2005). South Africa is the fifth largest coal producer in the world, and coal accounts for 90% of South Africa's primary electricity generation (Eskom, 2011). South Africa's coal is classified as bituminuos and anthracite. South Africa exports its high quality coal while reserving its high ash content coal for its domestic use (Woodlard *et al*., 2000; Somerset *et al*., 2008). This relatively low calorific coal has high ash content and results in production of vast quantities of coal ash after combustion (Kruger and Krueger, 2005). As of 2005, the estimates for South Africa's coal recoverable reserves were estimated to be about 33 billion tons (Jeffrey,

2005). This coal is mostly found in 19 coalfields, mainly in KwaZulu-Natal, Mpumalanga, Limpopo, and the Free State provinces, with lesser amounts in Gauteng, the North West Province and the Eastern Cape (Jeffrey, 2005).

2.1.2 Coal mining and production of acid mine drainage

Mine water and coal fly ash are the two major waste products produced in close proximity at coal mines and coal-fired stations respectively. Studies have shown that these wastes have damaging effects on the surrounding ecosystem and act as major sources of environmental pollution. For a country that relies heavily on coal mining and coal combustion for its energy production such as South Africa, urgent measures to deal with the safe disposal and/or re-use of these wastes (fly ash and mine waters) are needed. Coal mining, which is a large-scale earth disturbance operation, leads to the exposure of fresh rocks and generation of overburden which often has sulphide-containing minerals such as pyrite and marcosite. The exposure of these minerals to air and water leads to their oxidation through a biologically catalysed reaction mediated by acidophilic bacteria (Petrik *et al*., 2003) to generate water with net acidity referred to as acid mine drainage. Although complex chemical processes contribute to the formation of acid mine drainage, a set of chemical reactions leading to the formation of the acidic water from sulphide containing minerals have been discussed by Stum and Morgan (1981) and Madzivire *et al*., 2010 and are summarized in Equation 2.1 to 2.3 as shown below:

$$2FeS_2(s) + 7O_2(g) + 2H_2O(l) = 2Fe^{2+}(aq) + 4SO_4^{2-}(aq) + 4H^+(aq) \quad \text{Equation 2.1}$$

$$4Fe^{2+}(aq) + O_2(g) + 4H^+(aq) = 4Fe^{3+}(aq) + 2H_2O(l) \quad \text{Equation 2.2}$$

$$FeS_2(s) + 14Fe^{3+}(aq) + 8H_2O(l) = 15Fe^{2+}(aq) + 2SO_4^{2-}(aq) + 16H^+(aq) \quad \text{Equation 2.3}$$

The conversion of Fe^{2+} to Fe^{3+} in Equation 2.2 has been termed as the rate determining step for the overall sequence (Stumm and Morgan 1981). However, Fe-oxidizing bacteria, primarily *Acidothiobacillus sp*, speed up this reaction hence enhancing the generation of AMD (Madzivire *et al*., 2010; Johnson and Hallberg, 2003). The generated acid mine water is mainly characterized by low pH (normally <3) and is enriched with SO_4^{2-} (Madzivire *et al*., 2010). As the water flows

through the surrounding environment, further dissolution of other minerals associated with the FeS_2 rock occurs hence lading it with heavy metals such as Fe, Cu, Pb, Zn, Cd, Co, Cr, Ni, and Hg), metalloids (As and Sb) and other elements such as Al, Mn, Si, Ca, Na, K, Mg and Ba (Lottermoser, 2007; Hammack *et al*., 2006; Petrik *et al*., 2003; Gazea *et al*., 1996). The discharge of the untreated acid mine water to the environment is often associated with severe environmental pollution to the surrounding soil, surface and ground water by decreasing pH, accumulation of SO_4^{2-} and heavy metals (Petrik *et al*., 2003; Banks *et al*., 1997) which endangers aquatic life, pollutes public drinking water and industrial water supplies.

When the acidic water flows past dolomite rock and other naturally occurring carbonates and silicates, it is partially neutralised and in the process some of the metal contaminants precipitate as their respective hydroxides, sulphates and carbonates to produce circumneutral mine waters (CMW), often referred as Ca-Mg waters. The outcome of this natural neutralization process leads to waters containing lesser SO_4^{2-} than acid mine water, and with pH around 6.5, and even lower concentration of toxic metals (Banks *et al*., 1997). South African coal mines, especially those in Mpumalanga province, produce mine waters that are acidic (pH<3) or circumneutral (pH= 6-7) (Madzivire *et al*., 2010). To avert the environmental problems associated with mine waters, these waters need to be treated before they are discharged into the environment. The treatment of these waste waters can be very costly and at times difficult due to the high costs of chemicals and storage of high volumes of sludge produced during chemical treatment (Madzivire, 2010). The major mine water treatment technologies are broadly classified as either passive or active treatment methods (Bosman *et al*., 1990). In the passive treatment systems, mine water is allowed to pass through systems that are not monitored regularly whereas in active treatment option, the treatment facilities contains machines and equipment that are constantly monitored and often maintained (Hammack *et al*., 2006).

Due to the shortage of landfill sites for the disposal of major coal combustion by-product (fly ash) which is further compounded by stricter environmental regulations, the search for innovative ways to recycle this coal combustion by-product has generated a lot of interest. Different ways of recycling this waste have been broadly discussed in section 2.2.3. An interesting co-disposal process that relies on the use of fly ash for the treatment of mine waters

(especially AMD) has been studied extensively (Gitari *et al*., 2008; Petrik *et al*., 2003; Klink, 2003) and has been found to be able to neutralize the mine water acidity as well as reduce toxic elements significantly by precipitation, co-precipitation and adsorption. The neutralization ability of fly ash has been associated to the presence of lime in fly ash (Gitari *et al*., 2006; Klink, 2003). Part of the research work conducted in this study dealt with the use of both wastes (mine waters and fly ash) to produce zeolites that can be sold to offset the disposal costs and most importantly prevent the environmental problems associated with their disposal. More on this will be discussed in chapters 4 and 5.

2.1.3 Coal combustion

Coal is combustible and is reported to be composed of more than 50 wt% carbonaceous material (Crelling *et al*., 2010). The high carbon content in coal allows it to act as a solid fuel when burnt to produce heat, as a liquid synthetic fuel though the coal-to-liquid (CTL) technology, or as a source of chemical building blocks due to its rich hydrocarbon content. The coal combustion process is considered an energy conversion process rather than a refining process because it involves almost complete oxidation of the carbon and hydrogen content with atmospheric oxygen (Crelling *et al*., 2010). The heat released is utilized either directly for room heating or indirectly via steam generation especially during electricity production. Coal properties have been reported to vary widely depending on the origin of the coal (Bhanarkar *et al.*, 2008). These properties affect both the choice of combustion equipment and the nature of the combustion process (Speight, 2005). There are three types of combustion systems namely fixed-bed, suspension fired, and fluidized bed (Lawrence, 1998). Coal combustion rates may be increased by increasing mixing rates, increasing the available oxygen levels, or reducing the particle size (Lawrence, 1998). During the combustion of coal, most of the organic material is burnt out (oxidized or decomposed) to give volatile products, whilst most of the inorganic materials are transformed due to combined effects of thermal decomposition and oxidation. This influences the composition of the resulting ash and makes it to differ from the original mineral matter in coal (Speight, 2005; Vathaluru and French, 2008; Sheng and Li, 2008).

Coal combustion is known to contribute up to about 40% of the earth's current electricity needs and based on the estimates of current technologies of coal recovery and usage, coal, as a source

of energy, projected to be depended upon for at least another 300 years of use (Speight, 2005). The guarantee of huge abundance of coal has made it possible for South Africa, among many other countries in the world, to continue using coal as a viable long term and sustainable energy source (Foner *et al.*, 1999).

2.1.4 Coal combustion by-products

Burning pulverized (powdered) coal produces what is commonly referred to as coal combustion by-products (CCPs) or a combination of non-combustible inorganic residue and incomplete combusted organics (Querol *et al*., 2002). Some of the resultant combustion by-products are wet bottom boiler slag, dry bottom ash, fly ash, flue gas desulphurization (FGD) materials (Scheetz and Earle, 1998; Kalyoncu, 2001). Depending on the nature of the mineral matter and the chemical changes that take place during the combustion process, the quantity of ash produced is proportional to the quantity of mineral matter in coal (Speight, 2005). Figure 2.1 presents a schematic representation of the coal combustion process leading to generation of CCPs.

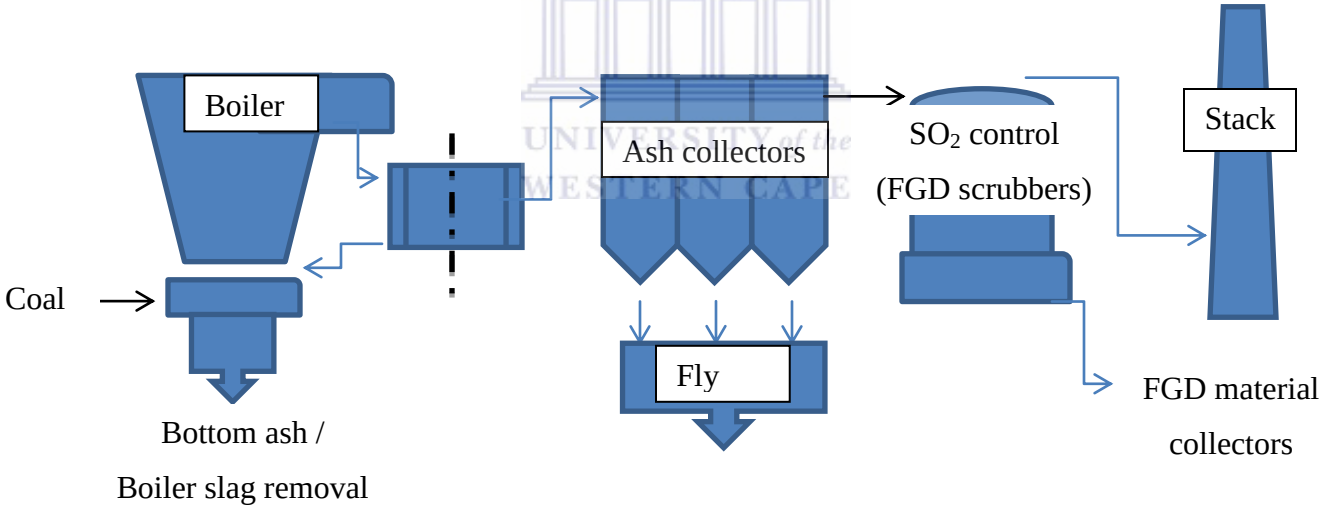

Figure 2-1: Schematic for coal combustion process (production of Coal combustion products, CCPs).

Burning coal in a dry bottom boiler, which is the most common boiler type, leads to generation of about 20% bottom ash which is a heavier, coarser and granular material. Combustion of pulverized coal also leaves about 80% fly ash, a fine powdery material which is mainly a resultant of the non-combustible coal residue, collected mainly by electrostatic precipitators,

fabric filters or by secondary scrubbers. The molten bottom ash (boiler slag) results from slag-type boilers and cyclone boilers and is made up of coarse, hard, black, dense, glassy particles which have been reported to account for about 2.5% of the total amount of CCPs produced from coal-fired power plants (Kalyoncu, 2001). Flue gas desulphurization (FGD) material results from the processes that are employed to remove SO_2 from a coal-fired boiler exhausted gas and they consist of fluidized bed combustion (FBC) ash, spray dryer absorption (SDA) products and FGD gypsum. Since the main focus of this thesis is the application of fly ash in zeolite synthesis, a discussion of fly ash, its formation process, properties and applications will be dealt with in the following section.

2.2 Coal fly ash

Coal fly ash is generated as a waste product of coal combustion. Fly ash's colour generally varies from tan to grey and even to black, and the overall appearance depends on the amount of unburned carbon in the ash. The changes in the colour of the fly ash can give an indication of the variation of fly ash properties and the composition (Speight, 2005). Fly ash is abrasive, mostly alkaline, refractory in nature. It consists of fine grains, either solid or hollow, that are made up of tiny spherical glassy particles derived from minerals included in coal and/or occurring from transformations during the coal combustion process (Kutchko and Kim, 2006; Ahmaruzzaman, 2010). The specific gravity of fly ash has been estimated to range from about 2 to 3 g/cm^3 (Ural, 2005), while its specific surface area may vary from 170 to 1000 m^2/kg (Crelling *et al.*, 2010). Fly ash is usually collected from the flue gas by means of electrostatic precipitators, bag houses, or mechanical collection devices such as cyclones as it leaves the combustion chamber. The fly ash particle size normally ranges from 0.5 to 200 microns (Scheetz and Earle, 1998) and is composed of a complex mixture of various amorphous and crystalline constituents. The primary components of fly ash include silica (SiO_2), alumina (Al_2O_3), iron oxides together with other elements such as carbon, calcium, sulphur and magnesium that occur in varying amounts (Wang *et al.*, 2006).

2.2.1 Mechanism of fly ash formation

The mechanism of reactions during coal combustion is complex because it depends on the reaction conditions and parameters such as coal chemical composition, intrinsic reactivity,

content of volatiles and coal ash contents, particle size, porosity and pore structure, mineral matter properties, among others (Crelling *et al*., 2010). The fate of an inorganic constituent during coal combustion is directed by its nature and occurrence in the coal matrix (Vuthaluru and French, 2008). In high-rank coals, inorganic constituents are mainly present as discrete minerals such as clays, quartz, carbonates and pyrites. However, low-rank coals also contain higher inorganic elements such as Na, Cl and S which may be organically associated or occur in the pore water (Vuthaluru and French, 2008). For a better understanding of the transformation of the inorganic components of the coal to ash particles, studies have involved sampling, analysis, and characterization through the entire process of combustion (Hurley and Schobert, 1991; Vuthaluru and French, 2008). Studies have also shown that during coal combustion, the materials in coal undergo a variety of complex physical and chemical changes (Helble *et al.*, 1994; Hower *et al.*, 1996) depending on their original mode of occurrence, their time-temperature history, and interactions among the constituents (Gutierrez *et al*., 1993; Hurley and Schobert, 1991). Tracing the reactions that lead to the formation of the different species in the ash is not easy but studies by Hurley and Schobert (1991) led to the proposal of two main reaction paths: those that are encountered by the inorganics present in the coal as discrete mineral particles, and those that are followed by the organically associated inorganics. Kutchko and Kim (2006) have highlighted several types of changes such as decomposition, fragmentation, agglomeration, vaporization, and condensation, which may occur in the discrete mineral matter in coal during combustion as shown in Figure 2.2.

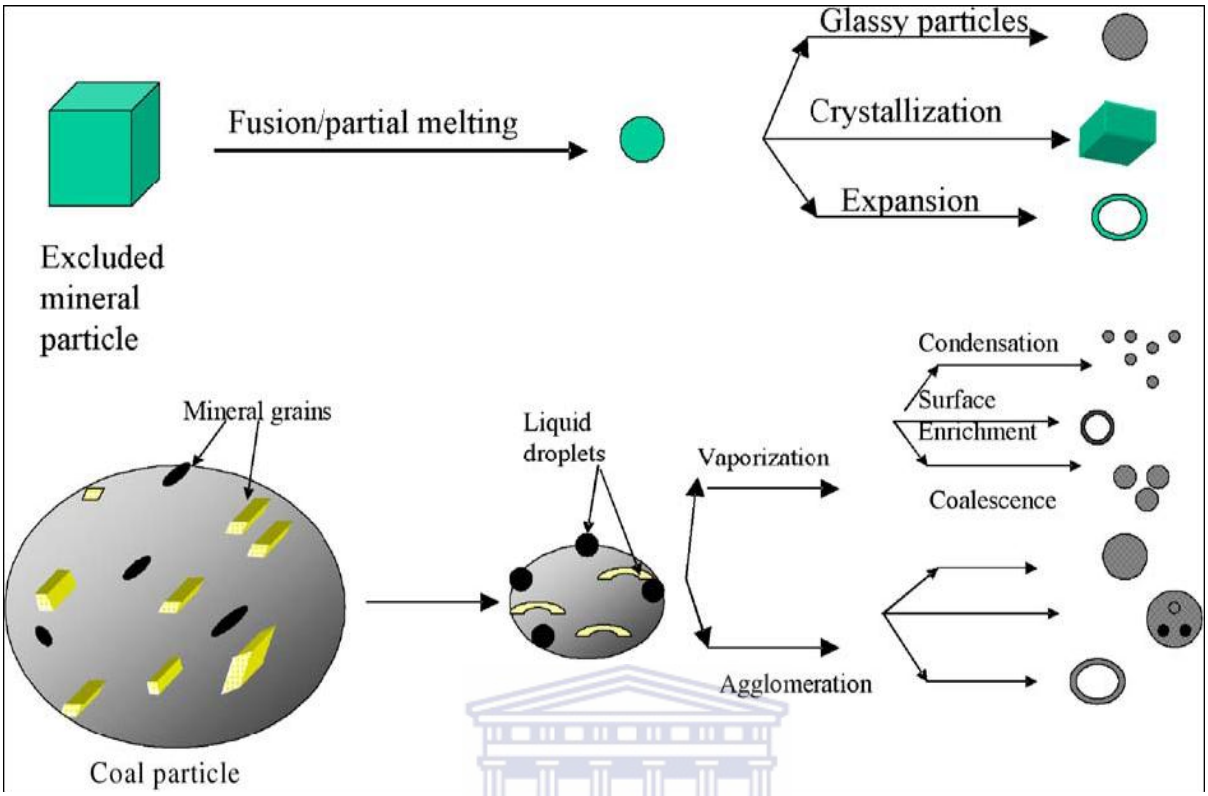

Figure 2-2: Schematic for general transformation of mineral matter in coal during combustion (From Kutchko and Kim, 2006)

For example, the transforming reaction path of some of the main minerals has been suggested to occur as follows: Kaolinite ($Al_4[Si_4O_{10}](OH)_8$) changes into metakaolinite ($Al_4[Si_4O_{10}]O_4$) at a temperature of 450–550 $^{\circ}$C, and is later converted into pseutmullite ($Al_2[SiO_4]O$) and cristobalite or vitreous body at temperatures of 950–1000 $^{\circ}$C (Liu *et al.*, 2004). The transformations of some of iron-bearing minerals during air-fired pulverized coal combustion have been suggested to occur as follows: pyrite decomposes to pyrrhotite, then oxidizes to a molten FeO–FeS phase and further oxidizes to magnetite and hematite (Sheng and Li, 2008). Studies by Bandopadhyay (2010) reported that during the coal combustion process quartz tends to pass directly to fly ash without any significant alteration whereas mullite and hematite are products of the thermal transformation of some minerals present in the coal during combustion. White and Case (1990) and Spears (2000) have reported that mullite in fly ash is formed through the decomposition of kaolinite, $Al_2Si_2O_5(OH)_4$ which is entrapped in the parent coal. Lime (CaO) presence in coal fly

ash may be due to the heat transformation of dolomite mineral or decarbonation of calcite entrained in feed stock coal (Navarro *et al*., 2009).

Morphologically, fly ash particles have a layered structure resulting from successive deposition of various chemical species, as the temperature decreases along the particle trajectory through the furnace (Kutchko and Kim, 2006). For example, the crystalline phases such as quartz and mullite remain in the core, whereas the glass phase of aluminosilicate covers the surface of the particle. Fine fly ash particles have been found to be enriched with trace elements (Bhanarkar *et al.,* 2008; Muriithi *et al.,* 2010) due to their large surface area which allows deposition and absorption of volatile elements. The extent of enrichment of specific elements in the fine particles varies with coal type, which is attributed to the differences in the mineral matter distribution in the parent coal (Akinyemi *et al.,* 2011). Several authors have described the partitioning of elements in coal combustion by-products and classified them on the basis of their relative volatility (Vories and Thogmorton, 2002) or by their relative content (Speight, 2005). The elemental content in fly ash can be classified as follows (Crelling *et al*., 2010): (1) major elements, which include aluminium, calcium, iron, and silicon, (2) minor elements, which usually include K, Mg, Na and Ti and sometimes P, Ba, Sr, B, and others, depending on the geologic area and (3) trace elements that are usually detected at the ppm down to the parts per billion (ppb) range and below. Although most nonmetallic elements are vaporised during the coal combustion process, they still leave a detectable residue in coal fly ash since they re-condense in the post combustion zone (Bhanarkar *et al.,* 2008).

2.2.2 Classification of coal fly ash: Properties of coal fly ash

The actual physical properties, chemical and mineralogical composition of a particular coal fly ash is dependent on the type of coal, composition of coal burnt, combustion system, and the coal combustion process (Eary *et al*., 1990; Ural, 2005; Bhanarkar *et al.,* 2008). In order to use fly ash in various applications, its characterization in terms of composition, mineralogy, surface chemistry and reactivity is of fundamental importance. Knowledge of fly ash chemical composition, which is mainly influenced by coal properties and the techniques used for handling and storage (Murphy *et al.,* 1984), plays an integral role in determining its potential for

recyclability. Table 2.1 compares the ranges of the chemical constituents for fly ash generated from burning different ranks of coals.

Table 2-1: Comparison of the chemical constituents ranges for fly ash produced from burning different ranks of coals (Adriano *et al*., 1980).

Component	Bituminous (mass %)	Sub-bituminous (mass %)	Lignite (mass %)
SiO_2	20-60	40-60	15-45
Al_2O_3	5-35	20-30	10-25
Fe_2O_3	10-40	4-10	4-15
CaO	1-12	5-30	15-40
MgO	0-5	1-6	3-10
SO_3	0-4	0-2	0-6
Na_2O	0-4	0-2	0-4
K_2O	0-3	0-4	0-4
LOI	0-15	0-3	0-5

Loss of ignition (LOI) is a measurement of the amount of unburned carbon remaining in fly ash (Koukouzas *et al.,* 2008) and is generally used by power plants as an indication of whether the coal is combusted completely or not and can also be used as an indicator of suitability of fly ash for use as a cement replacement in concrete. Fly ash LOI has been reported to range between 4 to 12 % (Foner *et al.,* 1999). According to the American Society for Testing Materials standards (ASTM C618), fly ash is classified according to the content of its major elements (Si, Al, Fe and Ca). The two main classifications are: class C and F. Fly ash containing more than 70 wt% of SiO_2, Al_2O_3, Fe_2O_3 and having a low content of lime is classified as class F, while class C is defined for fly ash whose total content of SiO_2 Al_2O_3 and Fe_2O_3 lies between 50 and 70 wt% and with a high lime content. Table 2.2 summarizes the classification of coal fly ash.

Table 2-2: Fly ash classification according to chemical composition (ASTM C 618 – 95) (Scheetz and Earle, 1998).

Chemical components	**Class F fly ash**	**Class C fly ash**
Silicon dioxide (SiO_2) + Aluminium oxide (Al_2O_3) + Iron oxide (Fe_2O_3), min. %	70	50
Sulphur trioxide (SO_3), max. %	5	5
Moisture content, max. %	3	3
Loss of Ignition, max, %	6	6
Available alkali (as Na_2O), max %	1.5	1.5

In addition to the above table, Class F fly ashes have also been reported to contain about 5 % CaO, while fly ashes belonging to class C contain a higher proportion of CaO which is in the range of 10–35% (Koukouzas *et al.,* 2007; Ahmaruzzaman, 2010). Class C fly ash is normally produced from the burning of low-rank coals (lignites or sub-bituminous coals) and has cementitious properties (self-hardening when it reacts with water) while Class F fly ash is commonly produced from the burning of higher-rank coals (bituminous coals or anthracites), and is pozzolanic (hardening when it reacts with $Ca(OH)_2$ and water) in nature (Adriano *et al,* 1980; Manz, 1999). Apart from the differences in the content of Si, Al, Fe and Ca, another significant difference between Class F and Class C is that the amount of alkalis (combined sodium and potassium), and sulphates (SO_4), which are generally higher in the Class C fly ash than in the Class F fly ash. Fly ash in South Africa is found to contain a relatively high concentration of SiO_2, Al_2O_3 and CaO (Somerset *et al.,* 2004).

2.2.3 Applications of coal fly ash

Fly ash can either be an industrial waste material and ecological nuisance or a valuable resource (Foner *et al.,* 1999). From the perspective of power generation, fly ash is a waste material, while from a coal utilization perspective, fly ash is a resource which is yet to be fully utilized;

producers of thermal electricity are constantly looking for ways to exploit fly ash owing to its increasing accumulation during coal burning worldwide. In the pulverized coal-fired power plants, fly ash is collected by cyclones, electric precipitators, and/or bag filters from the flue gas at the burner top (Shigemoto *et al*., 1993). It is estimated that the coal combustion activity in South Africa generates about 36.2 million tonnes of fly ash annually (Eskom, 2011) and this volume continues to grow in direct proportion to the increased consumer and industry energy demands. The prospects of continued use of coal as a long term energy source have created the challenge of finding beneficial ways of utilizing the fly ash (Wang *et al.,* 2006). Numerous fly ash utilization strategies have been proposed and implemented as presented in a recent review by Ahmaruzzaman (2010). Some of the applications of fly ash are given below.

2.2.3.1 Construction and building industries

The utilization of coal ashes in the building industry has economic and environmental advantages (Nisnevich *et al*., 2008). The economic advantages can mainly be derived from the fact that fly ash is a non-expensive waste material. The use of fly ash as a pozzolan represents substantial advantages such as savings in fuel used in cement production as well as reducing environmental pollution occurring from production of CO_2 during the calcination of lime (Foner *et al*., 1999). South African coal-fired power plants such as Matla and Lethabo have been reported to produce fly ash that has exceptional pozzolanic characteristic, hence, it is currently used to enhance the properties of concrete and other building materials (Kruger and Kruger, 2005).

2.2.3.2 Soil and/or environmental improvement

Fly ash also contains different essential elements, including both macronutrients P, K, Ca, Mg and micronutrients Zn, Fe, Cu, Mn, B, and Mo for plant growth (Truter *et al*., 2001; Gaind and Gaur, 2002). Pathan and co-worker (2003) reported that fly ash could also be used to increase the soil water-holding capacity as well as increase the soil's cation exchange capacity (CEC). However, it has been demonstrated that certain crops growing under fly ash-amended soil conditions may bioaccumulate heavy metals at concentrations greater than normal ranges (Adriano *et al*., 1980). Fly ash has also found applications in waste stabilization, whereby it is used to encase the waste in a solid block which assists in transformation of semi-liquid waste to

solid matter. A good example is shown by studies by Reynolds *et al.* (1999) who have confirmed that fly ash can be used to pasteurize microbes in waste like sewage sludge. In which case, the resulting product "SLASH" is devoid of pathogens and can either be safely disposed in landfills or preferably used as a soil ameliorant under very specific conditions because of the toxic elements content of the fly ash which may leach or bioaccumulate if wrongly applied.

2.2.3.3 Adsorbents for cleaning of flue gas

Fly ash treated with calcium hydroxide has been tested as a reactive adsorbent for SO_2 removal (Al-Shawabkeh *et al*., 1995; Davini, 1996). Lu and Do (1991) also showed that fly ash can act as an adsorbent for NOx removal from flue gases. Other gaseous organics such as toluene vapours and aromatic hydrocarbons can also be removed by the use of fly ash (Peloso *et al*. 1983; Rotenberg *et al*., 1991).

2.2.3.4 Treatment of waste water

Fly ash has been demonstrated as a low-cost adsorbent for the removal of sulphates and heavy metal from waste waters (Gitari *et al*., 2008; Madzivire *et al*., 2010). The alkaline nature of fly ash makes it a good neutralising agent which is an advantage because most metal adsorption by hydrous oxides require adjustment of the pH of waste water using lime and sodium hydroxide which is not necessary in this case. It has been proven that fly ash can be applied in beneficiation of acid mine drainage (Petrik *et al*., 2003; 2005).

2.2.3.5 Fly ash as a catalyst and catalyst support

Certain physicochemical properties of fly ash such as high thermal stability and the availability of catalytic components such as Fe_2O_3, TiO_2, CaO, MgO, K_2O, and Na_2O in its matrix makes fly ash to act as a catalyst component or a good catalyst support (Wang, 2008). The use of fly ash as a solid catalyst in the production of biodiesel was reported by Babajide *et al*. (2010).

2.2.3.6 Synthesis of useful materials – zeolites, geopolymers etc

The chemical composition of fly ash, which has a high percentage of silica and alumina, enables it to be used as a feedstock for the synthesis of zeolite and geopolymers (Querol *et al*, 2002). This application has an enormous economic benefit because fly ash acts as an inexpensive

feedstock of silicon and aluminium during zeolite synthesis and has created much interest due to the many uses of zeolites. Section 2 of this chapter will discuss in detail the general aspects of zeolite science, and later, pay special attention to fly ash derived zeolites.

To sum up the applications of fly ash, Wang and Wu (2006) presented a summary of possible applications of fly ash in different sectors based on its properties and abundance as shown in Figure 2.3.

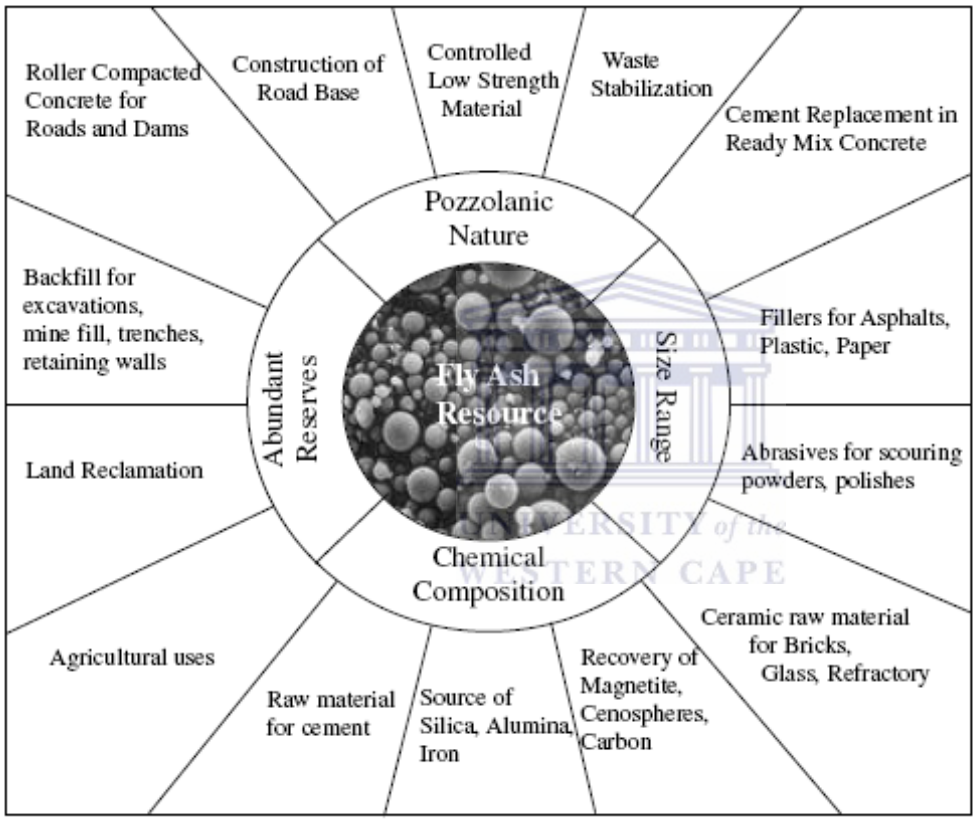

Figure 2-3: Summary of applications of fly ash based on the properties of fly ash and its abundance (From Wang and Wu, 2006).

2.2.3.7 Drawbacks of the direct use of fly ash

It had been reported that the finer particles of fly ash are enriched with toxic trace elements because of their small size and large specific surface which allows deposition or absorption of volatile elements on their surface during coal combustion process (Goodarzi *et al*., 2006; Bhanarkar *et al*., 2008). Liu *et al.* (2004) reported that the trace elements originating from coal are adsorbed on the surface of fly ash particles when the flue gas cools down. Since ash dumps

cover large tracks of land (Petrik *et al*., 2003), the presence of the toxic elements in fly ash might lead to unwanted build-up of heavy metals, salts and alkalinity in the fly ash dump sites (Liu *et al*., 2004; Akinyemi *et al.,* 2011). Elements such as Se, Cr, B, Hg, and Ba have the potential for leaching out from fly ash in ponds or landfills and may end up contaminating ground water, creating an environmental concern. The fear of potential ground water contamination by leaching of heavy elements have made Israel to forbid by law the use of fly ash as land fill or road bed material (Foner *et al.,* 1999).

The leaching of major elements from coal fly ash was extensively reviewed by Mattigod *et al*., (1990). In agriculture, when toxic elements are in high concentrations, crops such as wheat, soy beans and peanuts can highly accumulate the heavy metals in their shoots especially if they are planted in former ash dumps (Fansuri *et al*, 2008). The fine particles, which can easily be released into the atmosphere from ash dams or during transportation, have the potential of penetrating deep into the lungs of humans and animals, causing adverse health effects (Lantz and Hinton, 1984). Clarke and Sloss (1992) reported that the elements of greatest concern are As, B, Cd, Hg, Mo, Pb, and Se while elements of moderate concern are Cr, Cu, Ni, V and Zn. To summarise the environmental concern of fly ash, it is important to stress that the inclusion of toxic elements in the ash and their solubility are the primary determinants of toxicity. Concentration is not the only factor; volatility and toxicity also determine the potential for health and environmental effects (Voriers and Throgmorton, 2002).

Despite the considerable portion of fly ash used in the above mentioned applications, there is still a large portion that is directly disposed in ash dumps meaning that there is still need to find alternative ways of recycling and beneficiating fly ash.

2.3 Zeolites

Zeolite science is a topical field with many text books, patents and journal articles already published. This section serves to discuss, in brief, the key highlights of the general aspects of zeolite science. The discussion then later shifts to focus on use of fly ash in zeolites synthesis, which is the main focus area of this study.

2.3.1 General introduction to zeolites

Zeolites are defined as crystalline microporous aluminosilicates whose structure is made up of a three dimensional framework of SiO_4 and AlO_4 that are tetrahedra linked to each other at the corners by sharing their oxygens (Szostak, 1989; Weitkamp and Puppe, 1999; Nagy *et al*., 1998; Byrappa and Yoshimura, 2001; Auerbach *et al*., 2003). The tetrahedrally coordinated atoms (T-atoms, where can T is either Si or Al) make up a three-dimensional network with voids and open spaces. Upon substitution of Si (IV) by Al (III) in the tetrahedra, the +3 charge on the Al makes the framework negatively charged and hence requires the presence of extra-framework cations to counter-balance the charge to keep the overall structure neutral. The extra framework cations can be exchanged in the aqueous or solid phase to give rise to the rich ion-exchange chemistry of zeolites. The AlO_4^- tetrahedra can also be replaced by other three and four valence state ions, such as B, Ga, Fe, Ge, Ti, etc (Chester and Derouane, 2009). In all cases, the SiO_4 and AlO_4 tetrahedra combine according to Lowenstein's rule which states that two neighbouring AlO_4 tetrahedra cannot connect via an oxygen bridge in the zeolite structure because of electrostatic repulsions between the negative charges (Zhao *et al*., 1997). Figure 2.4 shows how the primary building blocks can combine to form the zeolite structure.

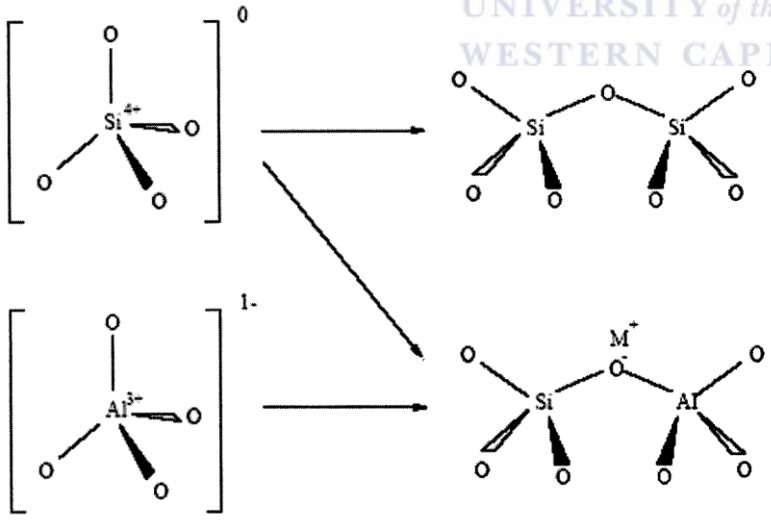

Figure 2-4: Primary building blocks of zeolites.

The framework composition of zeolites mainly depends on the composition of the synthesis mixture as well as the synthesis conditions. The general chemical composition of zeolites can be represented by the empirical formula shown in Equation 2.4 (Passaglia and Sheppard, 2001).

$M_xD_y[Al_{x+2y}Si_{n-(x+2y)}O_{2n}]\cdot mH_2O$ Equation 2.4

Where M and D = Compensating exchangeable cation (M = monovalent, D = Divalent)

m = Number of water molecules

(x+y) = Total number of tetrahedra per unit cell

The portion in square brackets represents the tetrahedral framework and is characterized by an overall negative charge (Passaglia and Sheppard, 2001). Forexample, the simplified or generalized formulae of analcime zeolite is written as $NaAlSi_2O_6\cdot H_2O$. The uniform pore openings throughout the zeolite crystal allows the ready discrimination between molecules with dimensional differences less than 1 Å which is why zeolites are referred to as molecular sieves. The water and other organic non-framework cations present during synthesis occupy the internal voids of the zeolite and when they are removed by thermal treatment or oxidation to free the intracrystalline space, it can be utilized in different applications. The uniqueness of zeolites in retaining their structural integrity upon loss of water or other organic non-framework cations makes them different from other porous hydrates. The structural complexity of zeolites is mainly attributed to the various ways in which the tetrahedral groups are linked by the common sharing of oxygen ions to form polynuclear complexes (Byrappa and Yoshimura, 2001).

2.3.2 Brief history of zeolites

The name zeolite was coined in 1756 by a Swedish mineralogist named A.F. Cronstedt after he observed that the mineral ‘zeolite’ had boiling effects due to its porous nature (Crönstedt, 1756: *cited in*, Colella and Gualtieri, 2007). The word zeolite stems from two Greek words, z*ein*, which means “to boil”, and *lithos*, which refers to “stone” hence “stones that boil” (Byrappa and Yoshimura, 2001. Upon discovery of this ‘*boiling stone’*, many other scientists further explored the unique properties of zeolites and even attempted to synthesize zeolites by imitating the natural geological conditions, although the only condition that could not be duplicated was the time factor which may cause crystallization to take a few hundred years to tens of millions of years to form, depending on the chemical environment (Breck, 1974). In the early years of the development of zeolite science, most studies were mainly based on the recrystallization of

zeolites. Efforts to synthesize zeolites artificially can be traced as far back as 1848, but it was only in the 1940s when the first synthesis of a zeolite that did not have a natural counterpart was carried out by Barrer (*cited in*, Byrappa and Yoshimura, 2001). Subsequently, many patents and publications have been produced. To date, the area of zeolite synthesis is still expanding. A good discussion on the historical perspective of zeolite science is presented by Robert Milton (Occelli and Robson, 1989).

2.3.3 Types of zeolites and their classification

Zeolites can either be of natural or synthetic origin (Nagy, 1998). Natural zeolites have been known to exist since the discovery of zeolites. These zeolites are generally associated with alkaline activation of glassy volcanic rocks (Byrappa and Yoshimura, 2001) and even though there are many existing types such as analcime, chabazite, erionite, ferrierite, heulandite, laumontite, mordenite and phillipsite, the most important and widely used natural zeolite is clinoptilolite (Wang *et al*., 2008). In the earlier days of zeolite discovery, zeolites were thought to be rare minerals, but, later, various geological studies have confirmed that they are one of the most abundant mineral phases on earth (Nagy *et al.*, 1998). Their unique properties and potential applications inspired different scientists to investigate different ways of conducting laboratory syntheses to enable greater access to a much broader range of compositions and structural types (Byrappa and Yoshimura, 2001). Many different criteria for distinguishing zeolites have been proposed, but since 1986, the IUPAC commission on zeolite nomenclature has recommended and set rules and designations consisting of the use of a three letter code for zeolites with various structures. These three letters are ‘mnemonic codes’ and the coding style consists of three capital letters that are derived from the names of the type of zeolite mineral. The code is subject to clearance by the IZA Structure Commission (Auerbach, 2003). When new structure types are reported, the commission publishes them on the World Wide Web (Byrappa and Yoshimura, 2001) in Europe: (http:// www.IZA-SC.ETHZ.CH/IZA-SC/) and on a mirror site in North America: (http://www-iza-sc.csb.yale.edu/iza-sc/). Table 2.3 gives examples of the three letter coding (the entire alphabetic list can be found in “Atlas of zeolite framework types” by Baerlocker *et al.* (2007) and also on the IZA website (Baerlocher and McCusker, 2008).

Table 2-3: Examples of the three letter coding used by IZA.

	Zeolite name
FAU	Faujasite
GIS	Gismondine
GME	Gmelinite
BOG	Boggsite
MOR	Mordenite

The three letter IZA pneumonic does not specify other properties of the zeolite such as the type of the extra framework cation, for example, the LTA framework encompasses zeolite A, as well as its ion-exchanged forms with K^+ (3A), Na^+ (4A), and Ca^{2+} (5A). From the same building units different zeolitic structures can be formed (Byrappa and Yoshimura, 2001) and a good example is how the sodalite unit can be assembled to form different zeolitic frameworks such as zeolite A (LTA), Sodalite (SOD), zeolites X/Y (FAU), and EMT (Auerbach, 2003) as shown in Figure 2.5 below.

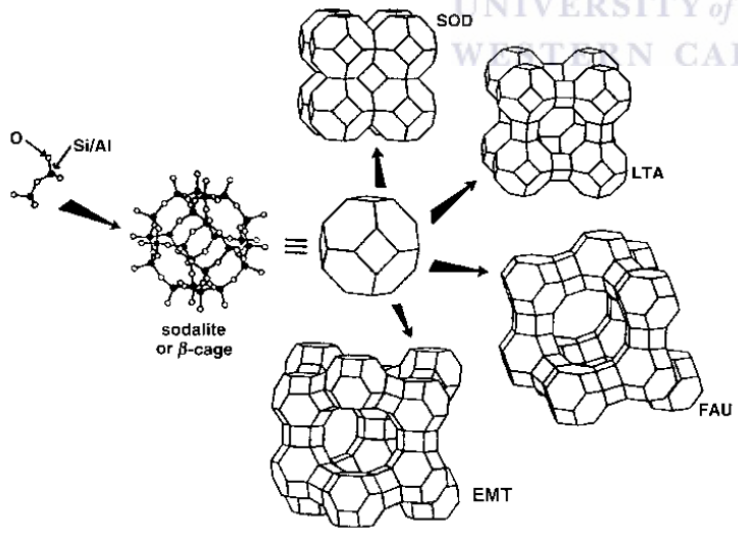

Figure 2-5: Formation of four different zeolite frameworks from sodalite (β cage) (From Auerbach *et al.*, 2003).

Another way of describing the different zeolitic framework according to the criteria cited in Baerlocker *et al*. (2007) is based on framework density (FD), secondary building blocks (SBU) and pore structure. The maximum framework density for a zeolite is reported to range from 19 to over 21 T-atoms per 1000Å^3, whereas for non-zeolitic framework structures, the values tend to be range from 20 to 21 T/1000Å^3 (Baerlocker *et al*., 2007). When classifying zeolites according to their smaller subunits (secondary building units), the zeolites can be thought to consist of finite or infinite secondary building units with each containing up to 16 T atoms (Baerlocker *et al*., 2007) as shown in Figure 2.6. Based on pore structure classification, zeolites porosity can be sub-grouped as folows:

i. Small pore zeolites: pore apertures consist of six, eight or nine membered rings such as zeolite A with pore sizes mainly ranging between 3.5–5 Å.
ii. Medium pore zeolites: pores have ten membered rings such as ZSM-5, offretite and ferrierite with pore sizes mainly between 5–6.5 Å.
iii. Large pore zeolites: they have pore sizes ranging between 6.5 and 8 Å such as faujasite and can admit large molecules like alkylaromatics.

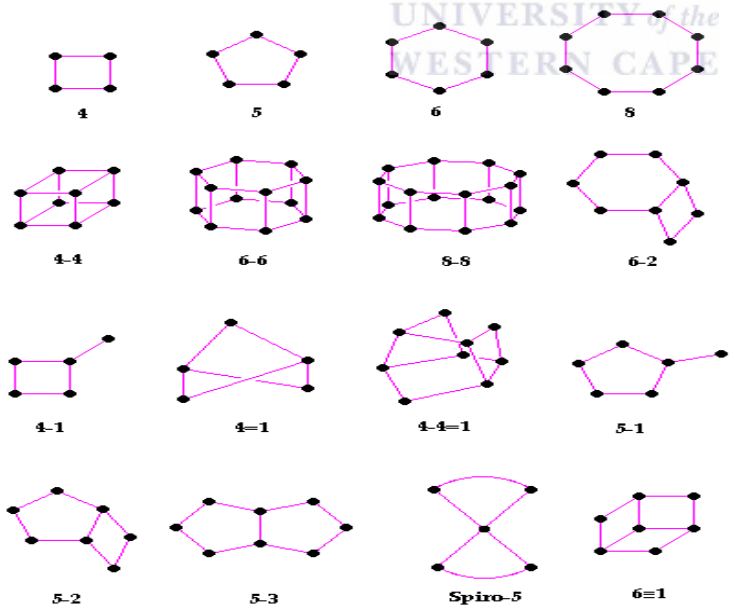

Figure 2-6: Secondary building units: the corners of the polyhedra represent tetrahedral atoms (Meier *et al.*, 1996; Nagy *et al*., 1998)

As of 2011, about 197 zeolite framework types and 22 disordered zeolite framework structures had officially been recognized by the Structure Commission of the International Zeolite Association (Baerlocher and McCusker, 2011). These zeolites have framework topologies with pore systems differing by their dimensionality or the channel aperture dimensions (Baerlocher and McCusker, 2008). There still exists an infinite number of ways in which the building units can be connected to form distinct three dimentional (3D) framework structures which could be identifiable as distinct zeolitic frameworks as has been shown by computer predictions by Dyer who reported that up 6 million zeolites can be formed (Nagy *et al*., 1998).

2.3.4 Properties of zeolites

Pure state natural zeolites are colourless but the presence of alkali or alkaline earth cations as well as other small amount of impurities account for the different colours of these minerals (Breck, 1974). The crystal hardness of zeolites has been reported to range from 4 - 5 on the mohr scale with the density reported to range from about 2 to 2.3 g/cc (Breck, 1974), although exchange with other heavy ions may increase the density. Zeolites are also known to exhibit electrical conductivity which arises from the movement of ions through the framework (Breck, 1974; Nagy *et al.*, 1998). Because of the unique pore system which penetrates the zeolite in one, two or three directions and which also vary in size and shape, zeolites exhibit interesting properties such as size-selective inclusion and sieving, reversible hydration, and ion exchanging ability. These framework voids, containing alkali metal cations and water molecules which are free to move around, allow zeolites to act as hydrating and dehydrating agents. Zeolites can take up other liquids such as ammonia or alcohol, and exchange charge compensating cations with ease. The pore size, which generally ranges between 3 and 10 Å in diameter, is the main reason that makes zeolites act as molecular sieves (Nagy, 1998; Pfenninger, 1999) enabling them to be able to sieve ions and molecules below a given size while excluding the larger molecules. Among the many properties of zeolites, ion-exchange and their ability to adsorb different molecules play a very important role in modern industrial applications (Auerbach *et al*., 2003). The ion exchange capacity of zeolites arises due to the loosely-bound nature of charge balancing extra-framework cationic species which can be readily exchanged for other types of metal cations when in an aqueous solution. Adsorption property of zeolites plays a big role in applications such as separation of gases and liquid mixtures and molecular sieving of water,

especially in the removal of water from gases and liquids and also for general drying (Pfenninger, 1999).

2.3.5 Application of zeolites

The current wave of discoveries of many different types and modifications of zeolites has triggered many new applications of zeolites. Some of the well-known and other new applications are as follows:

2.3.5.1 Ion exchangers

Ion exchange capacity is among the most important properties of microporous materials. Some of the applications of zeolites based on the ion exchange properties include wastewater treatment (Rios *et al*., 2008; Petrik *et al*., 2003; Hendricks, 2005), applications in fertilizer industries (Fansuri *et al*., 2008), and treatment of radioactive waste (Dyer, 1988). The ion exchange capability of zeolites has been exploited in the applications of zeolites in the detergent industries (Nagy *et al.*, 1998; Hui and Chao, 2006) as water softening agents. Pressure from environmentalists led to the phasing out of phosphate detergents and their replacement in detergents with zeolites (Nagy *et al*., 1998). The most commonly used zeolites are such as Zeolite A, P and X, which are characterized by high aluminium content making them to have high ion exchange capacity.

2.3.5.2 Catalysis

Synthetic zeolites are known for their use as solid acid catalysts (Breck, 1974). The presence of Brönsted acid sites together with other unique characteristics such as high thermal stability, ability to be modified by isomorphous replacement of Al with elements such as Fe, B, Ga and Ti, their porosity and ion exchange property has led to an upsurge in the consumption of zeolites for catalytic purposes and for zeolites to act as a replacement for mineral acids in catalysis (Bekkum *et al.*, 1991; Nagy, 1998). The first use of a zeolite as a catalyst was tested using zeolite Y by researchers of Union Carbide Corp. in 1959 (Dyer, 1988). The attractiveness of zeolites to act as solid acid catalysts, especially in the refining and petrochemical industries, has seen zeolites gain applications in catalytic cracking, hydrocracking, hydroisomerization and/or in other processes such as dewaxing, aromatization and aromatic conversions (Nagy et a., 1998; Roland and

Kleinschmit, 2005; Martínez and Pérez-Pariente, 2011). Zeolites have also been reported to act as bifunctional catalysts (Karge and Weitkamp, 1989). A review by Weitkamp (2000) discusses some of the fundamental properties governing the applications of zeolite in catalysis. The development of an industrial heterogeneous catalyst has been reported to be a rather complex process which involves several different steps requiring multi-disciplinary knowledge (Martínez and Pérez-Pariente, 2011). The ability of zeolites to have Brønsted and Lewis acidity is the key driver for their use as solid acids (Roland and Kleinschmit, 2005). Zeolites can be transformed into the hydrogen form to create Brønsted acid sites. Calcination of the hydrogen form causes decomposition of the acidic hydroxyl groups with liberation of water to create Lewis acid sites (Barzetti *et al*., 1996) as shown in Figure 2.7

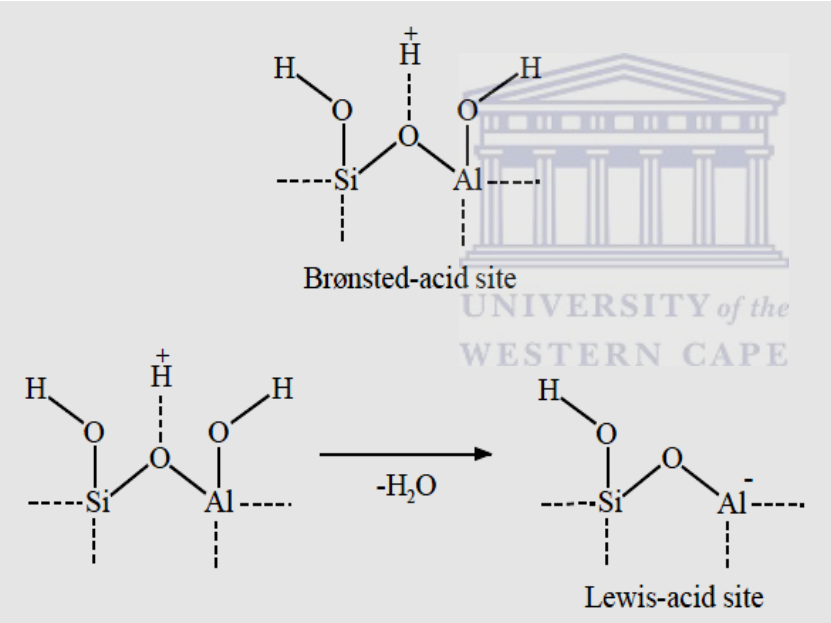

Figure 2-7: Schematic for generation of Brønsted-acid hydroxyl and Lewis-acid sites formed by dehydroxylation from Brønsted-acid sites (Barzetti *et al*., 1996).

2.3.5.3 Adsorption

Zeolites can be used in adsorption applications both in gas and liquid phases (Roland and Kleinschmit, 2005). Their adsorption ability is mainly derived from properties such as their molecular-sieving ability and the presence of regular pores with definite aperture sizes. The dimensions of zeolite channels and their ability to adsorb gases and water have made zeolite

molecular sieves suitable for a number of applications such as in processes for drying, purification, and separation of components, as well as in insulated glass windows and pressure swing absorption/vacuum swing absorption (PSA/VSA) processes for the generation of high-purity gases (Pfenninger, 1999).

2.3.5.4 Other miscellaneous and emerging applications of zeolites

An excellent semi review paper that discussed the emerging applications of zeolites was contributed by Gilson and co-authors in a monograph edited by Martínez and Pérez-Pariente (2011). These emerging applications are in fields such as processing of renewable and synthetic feedstocks to produce cleaner energy and chemicals, post-treatment of pollutants generated by stationary and mobile sources and on the unconventional uses of zeolites related to energy savings based on zeolite films and layers for membrane and sensing applications.

2.3.6 Characterization of zeolites

The first analysis of the crystal structure of a zeolite, analcime, was reported by Tayler in 1930 (cited in Breck, 1974). Since then many techniques have been developed and are used to characterize zeolites to understand their phase, formation process and properties. Some of the most commonly used techniques include X-ray diffraction spectroscopy **(**XRD), Scanning Electron Microscopy (SEM), Nuclear Magnetic Resonance (NMR), Infrared spectroscopy (IR), Thermal, Raman analysis, particle size and pore size distribution, and so on. A brief discussion of some of the main characterization techniques is highlighted below.

2.3.6.1 X-ray diffraction spectroscopy

X-ray diffraction (XRD) analysis plays an essential role in the identification and characterization of zeolite structures during and after the synthesis process (Cundy and Cox, 2005; Burton, 2010). XRD allows the examination of long-range atomic structure of crystalline materials, and thus, helps in the authentication of the identity and purity of the phase(s) obtained during zeolite synthesis (Subotic and Bronic, 2003). The most significant information obtained using the XRD technique (Szostak, 1989) enable the determination of the success or failure of formation of a crystalline material. A typical powder diffraction pattern is collected in the form of scattered intensity, as a numerical function of the Bragg angle (Pecharsky, 2005). Since each XRD

diffraction pattern gives a unique fingerprint of each mineral phase present, zeolite researchers are able to follow crystallization mechanisms, modification processes, molecular sieve properties and catalytic behaviour. After the collection of powder diffraction data, the diffraction pattern is used for the identification of known structures by comparing with standard patterns (Burton, 2010). The most complete and commonly used powder diffraction database is the Powder Diffraction File (PDF), which is maintained and periodically updated by the International Centre for Diffraction Data (ICDD') and is available on the internet at http://www.icdd.com.

By applying the Scherrer equation (Equation 2.5), which relates the diffraction peak width to the average (by mass or volume) crystallite dimension, researchers can obtain relevant interpretation of zeolites properties, especially those related to crystallite dimensions.

$$\beta_s\,(2\theta) = \frac{K\lambda}{T\cos\theta}$$

Equation 2.5

Where; β_s = crystallite size contribution to the integral peak width in radians,

K = crystal shape constant near unity, and

T = average thickness of the crystal in a direction normal to the diffracting plane hkl.

Quantitative phase analysis is used to determine the concentration of various phases that are present in a mixture after the identity of every phase has been established. Several different methods of quantitative analysis have been developed and extensively tested and the most commonly used approaches are Rietveld refinement, the absorption-diffraction method, the method of standard additions, the internal standard method, the reference intensity ratio method and full pattern decomposition. A description of each method has been discussed in depth by Pecharsky (2005). A less accurate example of quantitative measurement of the crystallinity of a zeolite (Szostak, 1989) was made using the summed heights of approximately eight peaks in the X-ray diffraction pattern.

2.3.6.2 Structural analysis: Vibrational spectroscopy

Infrared and Raman spectroscopy are vibrational spectroscopic techniques that are useful for obtaining information on zeolites, zeolite surfaces, molecules being adsorbed in the zeolite

cavities and channels, and catalytic reactions within zeolites (Liu, 2009). Both infrared and Raman spectroscopy give rise to a set of absorption or scattering peaks as a function of energy, forming a vibrational spectrum. A brief description of each technique is presented below.

Infrared Spectroscopy

Vibrational spectroscopy obtainable by Infrared spectroscopy (IR) is one of the most widely used techniques in zeolite chemistry and catalysis and is widely divided into three categories (Liu, 2009) based on the instrumental designs: near-IR (>3,000 cm^{-1}), mid-IR (4,000–400 cm^{-1}) and far-IR (<300 cm^{-1}). Near-IR spectroscopy deals with overtones of fundamental vibrations and provides information on adsorbed species such as water, organic molecules and small gas molecules, etc. in zeolite cavities or channels. Mid-infrared region of the spectrum is useful in the deduction of the structural information since it contains fundamental vibrations of the framework TO4 tetrahedra and also provides information on surface OH groups, adsorbed molecules and framework vibrations. Far-IR spectroscopy has been used to study framework oxygen and charge-balancing cations in zeolite structures. Each zeolite type exhibits typical characteristic infra-red spectra (Flanigen, 1971; Nagy 1998). The infra-red spectra can be grouped into two classes named: (1) internal vibrations of the framework TO4, which are insensitive to structural variations; and (2) vibrations related to the external linkage of the TO4 units in the structure (Szostak, 1989). Flanigen (1971), Weitkamp and Puppe, (1999) and Breck, (1974) have summarized the mid infra-red vibrations observations for most of the early-synthesized zeolites and proposed the general assignments for the IR bands shown in Table 2.4.

Table 2-4: Overview of mid-Infrared vibrations of zeolites (Flanigen, 1971).

Internal tetrahedra	Asym. stretch	1250 – 950 cm^{-1}
	Sym. stretch	720 – 650 cm^{-1}
	T-O bend	500 – 420 cm^{-1}
External tetrahedra	Double rings	650 – 500 cm^{-1}
	Pore opening	420 – 300 cm^{-1}
	Sym. stretch	750 – 820 cm^{-1}
	Asym. stretch	1150 – 1050 cm^{-1}

There are several sampling techniques in IR spectroscopy (Liu, 2009) such as KBr wafer technique, attenuation total reflection (ATR), diffuse reflectance and coupled techniques such as photoacoustic IR spectroscopy.

Raman Spectroscopy

The Raman spectroscopy technique gives vibrational information that is complementary to infrared (Cubillas and Anderson, 2010). The apparent relationship between zeolite frame work structures and raman spectra has been found to be profound for different zeolites types (Knight *et al.*, 1989). Raman spectroscopy has been reported to be a suitable technique for in-situ studies of zeolite formation as long as the synthesis set up allows.

2.3.6.3 Zeolite Morphologies: Electron Microscopy and Imaging

Since zeolites are well-ordered, different zeolite types have been known to have different morphologies such as plate-like (Iwasaki *et al*. 1998; Subotić and Bronić, 2003), cube shaped, (Cubillas and Anderson, 2010), agglomerated (Petrik *et al*., 1995) among other morphologies. The use of electrons as a microscopic illumination source in the field of electron optical instrumentation improved materials' characterization by overcoming the limitations set by the wavelength of light (~400 nm), that was used earlier in optical microscopy. Use of Transmission Electron Microscopy (TEM) and Scanning Electron Microscopy (SEM) in conjunction with scanning microprobe analysis in zeolite research has yielded a great deal of information on zeolite microstructure (Szostak, 1989).

Scanning Electron Microscopy (SEM)

Useful microstructural information can be obtained by use of SEM since zeolites typically crystallize as micron-sized aggregates in powder form (Cubillas and Anderson, 2010). An electron probe is used to scan the surface of a specimen using deflection coils in the Scanning Electron Microscope (SEM). An image of the surface is formed when the primary beam interacts with the specimen. The key advantage of SEM in relation to TEM is that it requires less stringent specimen preparation (Kliewer, 2009). In most cases, a thin coating of the crushed material is dusted onto a piece of double sided carbon tape that has been affixed to a standard SEM mount. In other instances, the zeolite powder may need to be sonicated in a non-interacting solvent (e.g.,

isopropyl alcohol, ethanol etc.) to disperse the zeolite particles. Thereafter a few drops of the dispersed zeolite particles can be pipetted onto the SEM mount and allowed to air dry before the sample is transferred into the SEM machine for analysis. In some cases, a conducting surface layer is required to ensure sufficient electrical conductivity of the sample so as to prevent the build-up of a surface charge which could lead to distorted images. In this case, samples are usually covered with a thin spluttered film of gold or carbon to help dissipate the sample charging effects. Coated specimens need to be imaged in the electron microscope as soon as possible to avoid agglomeration of 'small islands' over time. In order to characterize the general features of the zeolite crystal such as shape and size, lower accelerating voltages of SEM (<~5 kV) are typically desirable (Kliewer, 2009) to minimize creation of back-scattered electrons that are generated deeper within the crystallite, and which can mask surface details when back scattered.

Transmission Electron Microscopy (TEM)

Transmission Electron Microscopy (TEM) analysis offers a better resolution of up to about 3Å at a magnification of approximately 10^6 which enables probing of the zeolite unit cell. Unlike SEM, TEM requires difficult sample preparation since specimens should be ~100 nm or less in thickness (Kliewer, 2009). High resolution microscopy can provide information on structural defects within molecular sieve crystals and also generate information on the arrangement of channels and pores within the zeolite when enhanced with computer imaging (Szostak, 1989). It is important to be careful when carrying out analyses of zeolites using High resolution TEM (HRTEM) images because the electron beam can also damage the zeolite's microstructure which, when one is not careful, could give misleading information. The scanning transmission electron microscopy (STEM) imaging has been reported to reduce electron beam damage relative to the continuous, static illumination used during HRTEM imaging. The use of Energy Dispersive Spectrometry (EDS) in both SEM- and TEM-based studies provides a very general level of information regarding the elements present within the zeolitic material.

2.3.6.4 Nuclear magnetic resonance (NMR)

Nuclear magnetic resonance (NMR) is an analytical tool with a high sensitivity for chemical bonds in the local structure of the resonating nuclei, such as of framework atoms, extra-

framework species, surface sites, and adsorbate complexes in zeolites (Hunger, 2009). Solid-state NMR spectroscopy is complementary to diffraction methods which are widely used for investigation of the long-range order of a crystal (Cubillas and Anderson, 2010). Many aspects of the zeolite properties such as incorporation, coordination, and local structure of framework atoms in zeolites; and distribution, location, and coordination of extra-framework species; concentration, nature and the chemical behaviour of surface OH groups in dehydrated zeolites (Hunger, 2009) can be studied using NMR technique.

2.3.6.5 Elemental composition by X-Ray fluorescence spectroscopy

The X-ray Fluorescent Spectroscopy (XRF) technique is useful for both qualitative and quantitative elemental analysis (Somerset *et al.* 2004). This is because X-ray fluorescence radiation is characteristic for the emitting atom (Bekkum *et al*., 1991). XRF has both advantage and disadvantages. The advantages are derived from it being non-destructive, multi-elemental, fast and cost-effective whereas the disadvantages are based on its limitation on analysis of elements that are only heavier than fluorine and the need for a large sample (Kalnicky and Singhvi 2001). The X-ray fluorescence radiation is characteristic for the emitting atom and that makes the technique useful for qualitative and quantitative elemental analysis (Bekkum *et al*., 1991). The XRF has its limitation since it is a bulk technique thus it is impossible to distinguish framework aluminium and non-framework aluminium in the zeolite product. There is therefore need for use of other complementary techniques such as NMR.

2.3.6.6 Thermal analysis

Thermal Analysis (TA) enables the investigation of the relationship between a sample property and its temperature as the sample is heated or cooled in a controlled manner (Brown and Gallagher, 2008). The most widely used thermal analytical techniques include thermogravimetry (TG), differential thermal analysis (DTA) and differential scanning calorimetry (DSC). These techniques can be used to elucidate temperature-induced phase changes and reactions such as dehydration, dehydroxylation, and decarbonisation, occurring in zeolites. Thermal analysis techniques can also give information on the amount of organic templating molecules which are occluded in the cavities and pores of zeolites during the synthesis process. Most of these techniques are either used by themselves or can be combined with other techniques such as TG-

DSC, calorimetry-volumetry, DSC chromatography, DSC-MS among others (Auroux, 1994). Other recent techniques that have elicited interest in in-situ studies of effects of temperature on zeolites are techniques such as heating stage X-ray diffraction, heating stage scanning electron microscopy, heating stage transmission electron microscopy and heating stage X-ray photoelectron spectroscopy, heating stage Raman spectroscopy and infrared emission spectroscopy (Brown and Gallagher, 2008). In catalysis, thermal analysis is an important technique that helps in understanding the decomposition of catalyst precursors or for desorption studies involving poisoned catalysts.

2.3.6.7 Cation exchange capacity

Cation Exchange Capacity (CEC) results from the presence of loosely bound cations in the zeolite structure, mainly alkali or alkaline earth elements that are often exchangeable (Kitsopoulos, 1999). Most procedures for determining cation exchange capacity are developed for soil analysis and cannot be applied directly without optimization due to the diffusional constraints in zeolites (Ndayambaje, 2011). The ion exchange property of zeolites has commonly been used for metal loading zeolite catalysts (Haber *et al*., 1995). One of the most successful methods of compositional adjustment is the use of ion exchange to completely or partially replace the cation(s) with others which have been selected to fit the specific application (Martínez and Pérez-Pariente, 2011).

2.3.6.8 Other techniques

Characterization of transition metals, complex ions or radicals present in the zeolite can be studied using Ultraviolet –Visible Spectroscopy. Selected Area Electron Diffraction (SAED) is another important diffraction method that acts as a source of structural information that enables identification of individual microscopic sized crystallites and also attempts to identify an unknown material using its interplanar spacing or diffraction geometry (Goodhew, 2001). Computational methodologies are currently being used to study zeolite properties that cannot or are very difficult to be addressed by experimental techniques (Martínez and Pérez-Pariente, 2011).

2.3.7 Synthetic zeolites

The understanding of the hydrothermal conditions that led to the formation process of natural zeolites inspired laboratory studies of the synthesis of zeolites in the 1930s by attempting to mimic the natural conditions required to form natural zeolites. The first zeolite synthesis with reliable characterization by chemical analysis, optical properties and XRD were reported by R. M. Barrer in the 1940s (cited in Breck, 1974). The success of the laboratory synthesis triggered a huge interest in systematic studies of zeolite synthesis which later led to the production of many zeolite structures. In most cases, synthetic zeolites are synthesized from sodium alumino-silicate gels prepared from pure sodium aluminate, sodium silicate, and sodium hydroxide solutions. Even though there are many zeolites types that have been synthesized, Table 2.5 presents a few examples of zeolites that have been known to have commercial interest.

Table 2-5: Examples of zeolites with commercial interest (Mosca, 2006).

Framework code	**Zeolite type**	**Si/Al ratio**	**Application**
FAU	Zeolite X	1 – 1.5	Gas drying in industries Removal of CO_2 from industrial flue gases
	Zeolite Y	1.5 – 5.6	As an acid catalyst in fluid catalytic cracking
LTA	Zeolite A	1 – 1.7	Softeners in detergent industrial gas drying
MFI	ZSM-5	> 10	As acid catalyst for fluid catalytic cracking Use in $DeSO_x$ and $DeNO_x$ processes
GIS	Zeolite P	2-8	Waste water treatment Softeners in detergent industrial

The ability to influence and control the quality and properties of synthetic zeolites has been a great success factor because the lack of purity for many natural zeolites had excluded them from gaining high-end applications such as in catalysis and adsorption (Colella *et al.,* 1999). These synthetic zeolites have gained diverse applications and even expanded to some of the applications that were reserved for natural zeolites. The major applications of natural zeolites

have mainly been confined to waste water treatment, as building materials and in agriculture as animal supplements and soil improvement (Nagy *et al*., 1998).

Since this work is concerned with the synthesis of zeolite from fly ash, it will be important to explore the general understanding of zeolites in terms of their synthesis procedures and mechanisms of crystallization before a brief description of zeolites of interest. Subsequently, the synthesis of zeolites from fly ash is discussed. The following sub-sections focus on the general aspects of synthesis and mechanism of formation of zeolites.

2.3.8 Zeolite synthesis

The zeolite synthesis process corresponds to the conversion of a mixture of silicate and aluminium compounds, alkaline metal cations and water via an alkaline solution to form the porous zeolitic structures (Barrer, 1982). A typical hydrothermal crystallization of zeolites has been reported to follow the following sequence: (a) formation of an aluminosilicate solution and/or precipitation of an amorphous aluminosilicate precursor (gel), when alkaline aluminate and silicate solutions are mixed either with or without additives such as inorganic salts, organic templates, etc. (b) presynthesis treatment of the synthesis mixture by homogenization, aging, seeding, etc and (c) eventual crystallization of zeolite(s) by subjecting the reaction mixture (clear aluminosilicate solution, or particles of precipitated gel dispersed in supernatant) to elevated temperature and pressure in some cases (Szostak, 1989; Barrer, 1982: Cubillas and Anderson, 2010). A review by Di Renzo (1998) classified parameters influencing zeolite crystallization as follows; a) crystallization conditions which include; temperature, stirring, seeding and gel aging. b) composition-dependent parameters which are dependent on alkalinity, dilution, ratio between Si and other tetrahedronforming elements, template concentration, ionic strength, presence of crystallization poisons. Subtle changes in these preparation conditions could determine which zeolite phase crystallizes from the mixture (Kerr, 1968; Martínez and Pérez-Pariente, 2011). A brief discussion of the contribution of these parameters is presented below.

2.3.8.1 Physical parameters

The variation in temperature is known to influence the nature of the zeolite phase formed and also the crystallization kinetics (Szostak, 1989). Heating, in most cases, can be done by placing

the autoclave in an oven or surrounding the autoclaves with a heating mantle, or placing it in oil, sand, or a water bath, or a microwave. The heat rate through the reaction vessel is dependent upon the material which it is made of and if not checked well, inhomogeneous heating may result in the formation of denser phases due to the higher temperatures in certain zones. The microwave and ultrasonic systems are known to lead to very rapid synthesis (Kim *et al*., 2004). The time of synthesis plays a crucial role in the crystallization kinetics and can also determine which phase crystallizes since metastable products can undergo further dissolution leading to the formation of more stable species following the Ostwald's law of successive transformation (Nagy *et al*., 1998; Byrappa and Yoshimura, 2001).

Ageing of the synthesis mixture has been shown to influence the course of zeolite crystallization significantly by shortening the induction time, acceleration of the crystallization process, and lowering the crystal size (Subotić and Bronić, 2003). The control of synthesis pressure is not thought to be a major parameter in zeolite synthesis since most syntheses are normally conducted under autogeneous pressure (Weitkamp and Puppe, 1999). However, the presence of volatile reagents such as ammonia and methane might affect both the pH and/or concentration of dissolved species (Nagy *et al*., 1998) which in turn affect the chemical parameters. The main influence of stirring is attributed to enabling reagent dissolution, maintenance of the homogenous gel, assisting with structure break-up, maintaining a uniform temperature across the reactor, transferring "nutrients" to growing crystals and modifying the local concentration of the reagents by producing synthesis mixtures with a more uniform concentration of reagents through the mixture (Nagy *et al*., 1998). This physical parameter can lead to a change in the attributes of the synthesis gel and also affect the outcome of the zeolite synthesis process (Weitkamp and Puppe, 1999). Therefore, optimization of reaction conditions needs to be carefully considered to minimize the production of other phases while also minimising the time needed to obtain the desired crystalline phase.

2.3.8.2 Chemical parameters

In the conventional hydrothermal synthesis, zeolites are mostly synthesized in aqueous media from various silicon and aluminium feedstocks. The variation of the chemical parameters mostly determines the properties of the resulting material, such as the zeolites' structure, morphology,

particle sizes, particle size distribution, homogeneity of elements within the crystallites and others (Nagy *et al*., 1998). The chemical composition range can be specific, narrow or broad depending on the type of zeolite to be formed and the starting feedstock material. The synthesis composition influences the nature of the crystalline phases obtained, the framework composition, Si and Al distribution in the lattice, the crystal size and morphology, and the nucleation and crystallisation kinetics (Breck, 1974). The chemical composition of a particular zeolite is usually expressed in terms of molar ratios of oxides (Feijen *et al*., 1994; Weitkamp and Puppe, 1999). The effects of changing SiO_2/Al_2O_3 ratio on the physical properties of a zeolite are summarised by Szostak (1989). The SiO_2/Al_2O_3 ratio in the synthesis gel can place a constraint on the framework composition of the zeolite produced (Basaldella *et al.*, 1997). Sodalite is the only zeolitic phase that is known to crystallize in the full compositional range Si/Al = 1 to infinity (Barrer, 1982).

The type of cation/anion combination can influence the rate of formation, the crystal structure and the catalytic activity of the targeted zeolitic product (Petrik *et al*., 2009; Szostak, 1989). Depending on the targeted zeolite type, these cations can be divided into either structure making (Na^+ and Li^+) and structure-breaking (NH_4^+, K^+ and Rb^+) types (Feijen *et al*., 1994; Subotić and Bronić, 2003). The presence of water during the synthesis process helps with the dissolution of the silica and aluminium sources and also stabilises the porous oxide frame work by filling the micropore system as a guest molecule (Feijen *et al*., 1994). Other non-aqueous media such as alcohols, pyridine and sulfolane have also been used during zeolite synthesis (Weitkamp and Puppe, 1999; Criado, 2007). Depending on the type of the solvent, the solubility of certain compounds can be compromised, and hence, inhibiting the formation of other zeolite frameworks (Bekkum *et al*., 1991). For example, fluoride ion can prevent the polycondensation mechanism when it is in high concentration. The type and strength (concentration) of the mineralising agent influences the concentration of dissolved silico-aluminate species, their nature (i.e either monomeric or polymeric) and also the rate of hydrolysis of solid and liquid phases (Nagy *et al*., 1998).

2.3.9 General aspects of mechanism of zeolite formation

The mechanism of zeolite formation is a very complex process due to the plethora of chemical reactions, equilibria, and solubility variations that occur during the crystallization process (Byrappa and Yoshimura, 2001). The first possible mechanism for zeolite synthesis was proposed by Barrer in 1959 (Martínez and Pérez-Pariente, 2011). Even though the formation process of zeolites has been extensively studied by other researchers (Weitkamp and Puppe, 1999; Cundy and Cox, 2005), the exact crystallization mechanism of zeolites still remains elusive (Cubillas and Anderson, 2010). The first attempts to elucidate the mechanism of zeolite crystallization were conducted during the early year of the development of zeolite science and was based on the proposal that the crystallizing system is driven by the formation of soluble aluminosilicate species, which are precursors for nucleation and crystal growth of zeolites (Barrer, 1982; Breck, 1974). Two extremes of the mechanisms of zeolite formation have been proposed (*i)* the solution-mediated transport mechanism, and *(ii)* the solid-phase transformation mechanism. These mechanisms are discussed in detail by Cundy and Cox (2005) as well as by Byrappa and Yoshimura (2001). In order to fundamentally understand zeolite nucleation and growth mechanism, it is advisable to have an understanding of the roles played by the different mechanisms taking place during the induction, nucleation and crystal growth period as shown in the schematic presented in Figure 2.8.

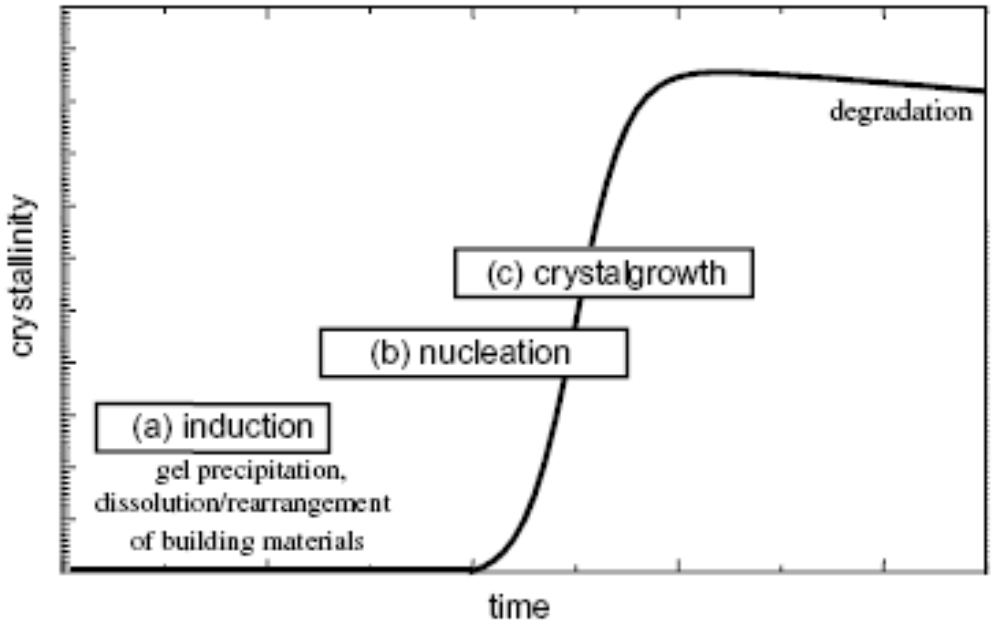

Figure 2-8: Schematic presenting the different stages involved in the development of zeolite crystallinity (From Herrmann *et al*., 2005).

2.3.9.1 Induction period

The techniques that can be used to probe the early stages of zeolite formation are still limited and this stage is often elusive (Schüth *et al*., 2001; Pienack and Bensch, 2011). In a semi-review article by Schüth *et al*. (2001), different techniques for analyzing the early stages of crystallization reaction were discussed. According to Herrmann *et al*. (2005), this initial stage involves gel precipitation, dissolution and/or rearrangement of building material. Spectroscopic analyses of the liquid phase during crystallization of different types of zeolites have shown that the liquid phase contains $Al(OH)_4^-$ monomers and different low molecular weight silicate and aluminosilicate anions (Barrer, 1982; Szostak, 1989; Subotić and Bronić, 2003). The application of UV-Raman spectroscopic analysis of the liquid phase of the synthesis system conducted by Guang *et al*., (2001) indicated that the polymeric silicate species are depolymerized into monomeric silicate species during the early stage of zeolite formation and $Al(OH)^{4-}$ species are incorporated into the silicate species. This leads to the formation of an infinitely extended three dimensional network of AlO_4 and SiO_4 tetrahedra linked to each other by sharing of oxygen atoms. In the initial stages of the formation of precursor species, the reaction is thought to be initiated via hydrolysis in order to get reactive M-OH groups (Jansen *et al.*, 1994). Condensation

then occurs and leads to the formation of metal–oxygen– metal bonds. The problem is then to make the Si-O-Al bonds in the molecular precursor and keep them during the whole hydrolysis process (Jansen *et al.,* 1994). This is because a large number of oligomeric species are formed simultaneously and they are in rapid exchange equilibria and it is not obvious which one would nucleate during the solid phase. The two main mechanisms of condensation are known as olation and oxolation (Jansen *et al.,* 1994). These processes lead to the formation of polynuclear species via the elimination of water molecules from the precursors containing at least one M-OH group. Olation corresponds to the nucleophilic addition of a negatively charged OH group onto a positively charged hydrated metal cation as shown in Equation 2.6.

$$M\text{-}OH^{\partial-} + M^{\partial+}\text{-}OH_2 \rightarrow M\text{-}OH\text{-}M^{\partial+}\text{-}OH_2^{\partial+} \rightarrow M\text{-}OH\text{-}M + H_2O \qquad \text{Equation 2.6}$$

The formation of a bridging $H_3O_2^-$ ligand is thought to play a fundamental role in the structure of these primary hydrolysis products. Oxolation involves the condensation of two OH groups to form one water molecule which is then removed to give rise to an 'oxo' bridge as shown in Equation 2.7.

$$M\text{-}OH + HO\text{-}M \rightarrow M\text{-}O\text{-}M + H_2O \qquad \text{Equation 2.7}$$

This reaction is normally described as dehydration of olated species. Oxolation is usually a slower process than olation. It is important to briefly highlight the condensation behaviour of both the Al^{3+} and Si^{4+} cations. The aqueous chemistry of tetravalent silicon cations is dominated by the fact that they remain tetrahedrally coordinated over the whole pH range. The monomeric silica anions released into the solution upon dissolution of the Si feedstock further copolymerize into higher oligomeric species which are negatively charged. The condensation rate of silica oligomers with aluminate anions increases with increasing silica ratio i.e. with an increasing oligomerization of the various silicates. The silicate and aluminosilicates polyanion chemistry is extremely complex. Therefore, various techniques such as ^{27}Al NMR spectroscopy have contributed to the identification of the silicate and aluminosilicates polyanion structures (Barrer, 1982). The condensed phases are formed by corner sharing $[SiO_4]^{4-}$ tetrahedra in order to minimize electrostatic repulsion between cations. The trivalent aluminium cation gives aquo-cations $[Al(OH)_6]^{3+}$ at the low pH. It follows an olation mechanism via nucleophilic addition of

negatively charged OH groups onto positively charged metal cations (Jansen *et al.*, 1994). This later leads to the departure of the coordinated water molecules and the formation of 'ol' bridges.

2.3.9.2 Nucleation

Nucleation has been described as 'the processes by which the atoms or molecules of a reactant phase rearrange into a cluster of the product phase that is large enough to have the ability to grow irreversibly to a macroscopically larger size' (Cubillas and Anderson, 2010). The nucleation of zeolites has been reported to either occur directly from a clear synthesis solution or via the formation of an amorphous or random structure that is transformed into a crystalline framework (Barrer, 1982; Cubillas and Anderson, 2010). Different arguments have been put forth to describe the mode under which nucleation takes place. One school of thought argues that nucleation occurs mainly in a gel phase, specifically at the solution–gel interface (Kosanovic *et al*., 2008) where the nutrient concentration gradients are probably the highest, while the other proposes that nucleation actually takes place inside the colloid-sized gel particles (Mintova and Valtchev, 1999). A schematic representing the two prominent theories (sol-mechanism and gel-mechanism) of nucleation is shown in Figure 2.9.

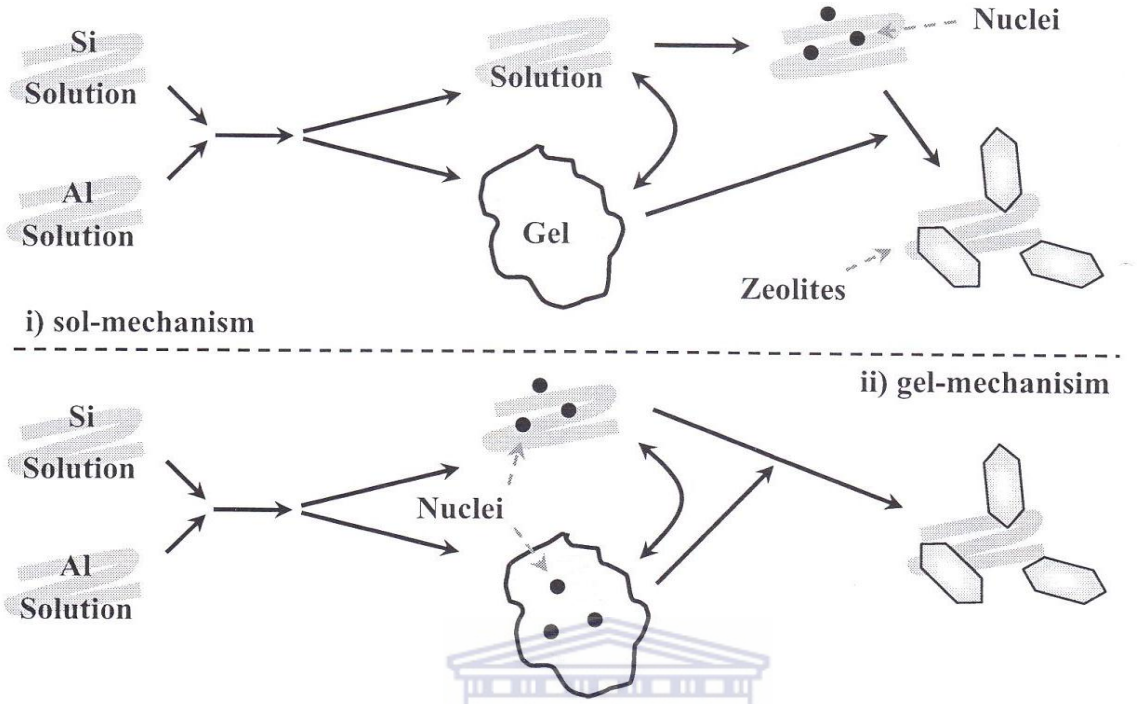

Figure 2-9: Schematic illustrating i) sol-mechanism and ii) gel-mechanism theories of the nucleation and crystal growth (From Fansuri *et al.*, 2008).

During the period preceding the formation of viable nuclei, different kinds of 'germ' nuclei form by chemical aggregation of the aluminosilicates precursor species and disappear again through polymerization. Due to these kinds of fluctuations, the 'germ' nuclei grow in time and form to become viable nuclei on which crystal growth occurs spontaneously (Barrer, 1982). It is difficult to pinpoint the exact time of transition from nucleation to crystallization; therefore, in order to obtain the nucleation time correctly, sufficient data points are essential (Hu and Lee, 1990). In summary, the lag seen in the initial step of the zeolite crystallization process presented in Figure 2.8 has been associated with the time needed for the germ nuclei to reach the critical size required for further growth to occur spontaneously. It could also be due to other explanations such as time needed for gel particles to form, formation of nuclei in the gel particles and the eventual release of the nuclei from the gel particles during their dissolution.

2.3.9.3 Crystal Growth

Crystal growth has been defined as 'the processes by which an atom or a molecule is incorporated into the surface of a crystal, causing an increase in size' (Cubillas and Anderson, 2010). Crystal growth succeeds nucleation and the nuclei have been reported to grow either by addition or condensation of precursor species towards full-grown crystals (Byrappa and Yoshimura, 2001). The rate of crystallization, types of products formed, and their particulate properties (habit, morphology, and crystal size distribution) depend on a large number of parameters (Barrer, 1982). These parameters encompass the crystallization conditions such as temperature, stirring, seeding, and gel aging as well as composition-dependent parameters such as pH, water content, and the ratio between framework-forming elements, template concentration, and ionic strength (Szostak, 1989; Barrer, 1982; Cubillas and Anderson, 2010). The rate of crystal growth is reported to decrease at the end of the crystallization (Herrmann *et al*., 2005) and at this stage the crystals have attained their maximum (final) size and all the amorphous aluminosilicate, often observed in the initial parts of the process, are completely consumed and are absent. As the time of crystallization is extended, degradation occurs since metastable products can undergo further dissolution leading to the formation of more stable species following the Ostwald's law of successive transformation (Nagy *et al*., 1998). Various studies to identify the different species in liquid, gel or solid phases during the crystallisation process have also been conducted to understand the crystallisation kinetics that characterise zeolite synthesis (Dyer, 1988; Weitkamp and Puppe, 1999).

These steps involved in zeolite crystallization can be well defined or difficult to differentiate. This is due to either the overlapping of the various steps or difficulty encountered in generating experimental proof (Cundy and Cox, 2005). The schematic presented in Figure 2.10 shows how the overlapping of the various step involved in zeolite formation can occur.

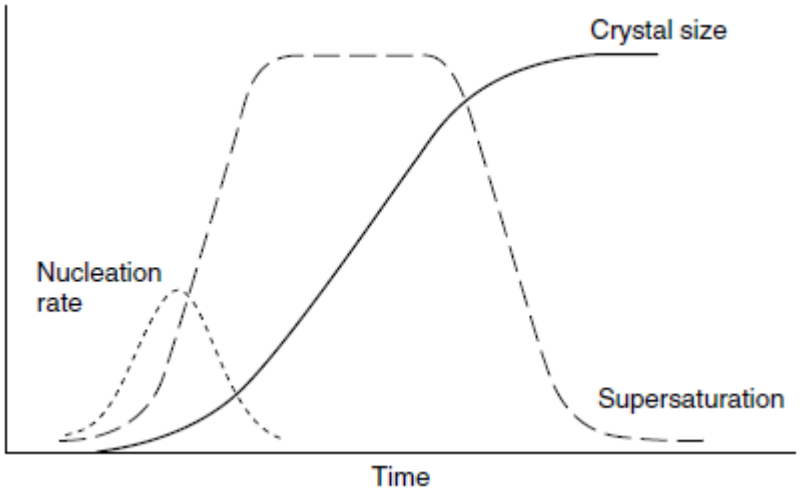

Figure 2-10: Schematic representation of the zeolite synthesis process showing the evolution of nucleation and growth rates, as well as supersaturation, as a function of time (From Cubillas and Anderson, 2010).

An excellent review discussing the principal of different proposed mechanisms of zeolite formation has been presented by Cundy and Cox (2005).

2.3.10 In-situ monitoring of zeolite crystallization

One of the challenges facing most zeolite researchers is the lack of ability to rationally control the synthesis process due to the limited understanding of the zeolite formation mechanism. This challenge also extends to the optimization and scale up process. Sankar and co-workers (2009) suggested that the rational design of the synthesis process can be achieved when the zeolite crystallization mechanism is well understood. An in-depth understanding of the formation mechanism will not only help in controlling and predicting the best conditions for synthesis, but it will also unmask the cooperative phenomena dictating chemical-structure-physical properties relationship. Many attempts to comprehend the zeolite formation process have been based on the use of ex-situ monitoring techniques (Shi *et al*., 1996; Miladinović *et al*., 2007). These techniques rely on periodic quenching of the reaction mixture i.e. separating the solid and the liquid phases prior to independent analysis. The challenge with this approach is that it is not so reliable since there could be artefacts caused by the quenching process. Recently, in-situ monitoring methods have been applied by different researchers (Shi *et al*., 1996; Schüth *et al*.,

2001; Miladinović *et al*., 2007) and most of these developments are captured in a recent review by Pienack and Bensch (2011) who have classified the different in-situ methods as: i) in-situ scattering techniques, ii) in-situ spectroscopy, iii) in-situ mass spectrometry, iv) in-situ transmission electron microscopy, and vi) combination method. In addition to the list, the in-situ ultrasonic technique, reported first by Toufar *et al*., (1998) and Schmachtl *et al*, (2000), has also elicited great interest as it also contributes to the understanding of the complexity of the zeolite formation process.

The in-situ ultrasonic monitoring technique is an indirect, non-invasive, phase insensitive method that is based on investigating the degree of interaction of ultrasonic wave transport properties with the zeolitic precursor species as it travels through the synthesis mixture. The use of in-situ ultrasound diagnostic of zeolite crystallization had been reported (Schmachtl *et al*., 2000; Herrmann *et al*., 2005; Baser and Schwieger, 2008) to successfully enable monitoring of the complex formation process of zeolites from pure analytical grade sources of Si and Al. The use of ultrasonic attenuation as an investigation tool (Baser *et al*., 2007) was an improvement of the earlier use of ultrasound velocity and amplitude (Schmachtl *et al*., 2000; Herrmann *et al*., 2005; Baser and Schwieger, 2008). This improvement was necessitated by the challenges encountered due to scattering from the solid products which made it difficult to correlate ultrasound phase and amplitude with the increasing zeolites crystallinity during the crystal growth step (Baser *et al*., 2007).

2.3.11 Kinetic analysis of zeolite crystallization

Many different approaches have been used to study the crystallization kinetics of zeolites (Zhdanov, 1971). Zeolite crystallization rates are quite often analyzed by means of a crystallization curve (Ouden and Thompson, 1992). These curves can be generated from data based on the zeolite yield or the percentage of zeolite in the solid phase as a function of the crystallization time (Ouden and Thompson, 1992). The slopes of crystallization curves, especially those generated from reaction systems that are carried out at different temperatures, can be used to rationalize the relative crystallization rates hence enabling calculation of crystallization kinetics and activation energies. Understanding the mechanism of reactions, reaction kinetic, as well as factors controlling the crystallization process is of great importance in

industrial crystallization (Kim *et al*., 2007). This knowledge has been shown to influence the control of important properties such as crystal size distribution and morphology which in return can help in customizing the synthesis products to meet specific applications (Subotić and Bronić, 2003). Different theories of the crystallization process have been proposed but there exist discrepancies between the theories and the experiment due to the over-simplification of model concepts. Avrami-Eroféev, Jander and Toufar kinetic models are among the many models that have been widely used by researchers to generate information on the kinetics and mechanism of many solid crystallization processes (Ciric, 1968; Toufar *et al*., 1995 and Avrami, 1939.

2.4 Zeolites from coal fly ash

Since the initial study by Holler and Wirschin (1985), different hydrothermal synthesis methods have been applied during the synthesis of zeolites from coal fly ash. These techniques are mostly based on the activation of fly ash by the use of an alkaline solution such as a NaOH and KOH to promote dissolution of Si-Al bearing mineral phase and also enhance the subsequent crystallization of the zeolitic phase (Moreno *et al*., 2001).

2.4.1 Methods of zeolite synthesis from fly ash

Most of the synthesis methods reported in the literature are based on the conventional hydrothermal alkaline conversion. This hydrothermal synthesis method is based on the combination of different synthesis variables such as temperature, alkaline solution, pressure, ageing time and temperature among others to obtain different types of zeolites. The alkaline solution not only acts as an activator but it also generates cations such as Na which stabilize the sub-building units during the initial stages of the formation of the zeolite framework (Ojha *et al*., 2004). The main source of aluminium and silica during fly ash zeolitization process are the crystalline phases (quartz, mullite, hematite etc.) as well as the amorphous material. Different researchers have investigated the effects of independent synthesis parameters. Just to mention a few, Shih and Chang (1996) investigated the effects of curing temperature and chemical composition during the synthesis of zeolite A and faujasite from Class F fly ash. Querol and co-workers (1997) investigated the effects of the use of either KOH or NaOH as activators and found that NaOH had higher conversion efficiency compared to KOH solutions. Wang *et al.* (2008) studied the influences of variation of NaOH concentration and found that higher

concentration of NaOH accelerated the crystallization step of zeolite A. Relatively high temperatures (125–200 ˚C) were reported by Querol *et al* (2002) to lead to high dissolution of Si and Al from the fly ash particles which in effect reduces the synthesis time and can lead to crystallization of larger pore zeolites.

Even though the conventional hydrothermal synthesis of zeolites is the most widely used synthesis technique, it faces a number of drawbacks such as: i) the need for longer synthesis time and temperature in order to dissolve the Si-Al containing phases of fly ash during the zeolite formation, ii) lower yields because of incomplete conversion of fly ash to zeolites and iii) lack of reproducibility due to the fact that different types of fly ashes may dissolve significantly differently under the same synthesis conditions. In order to overcome these challenges, different modifications of the classical hydrothermal synthesis process have been conducted and reported to lead to improvement of the entire synthesis procedure. Some of these modifications are discussed below.

2.4.1.1 Introduction of a fusion step prior to conventional hydrothermal synthesis process

Shigemoto *et al. (*1993) introduced a fusion step before the hydrothermal treatment method which facilitated the formation of highly active Na-aluminate and silicate species which were more readily soluble in water and consequently enhanced zeolite formation. The fusion process involves the mixing of fly ash with NaOH powder in varying ratio (but mostly fly ash/NaOH = 1.1.2) which is followed by heating the mixture in an oven (mostly at 450 ºC for periods ranging from one to three hours). After the fly ash has been fused with NaOH, the resulting powder is ground and mixed with water and can be optionally followed by ageing or taken through the hydrothermal crystallization step. Even though this process may solve some of the main shortcomings of the conventional hydrothermal synthesis, the process may present additional challenges when it comes to large scale industrial production of zeolites due to the requirement of extra energy for fusion and also the cost of equipment. A desilification step, after an alkali fusion step, was also introduced by Yaping *et al*., (2008) during the conventional synthesis and led to the improvement of the solubility of the Al and Si from the fly ash.

2.4.1.2 Introduction of two-step synthesis process: before the conventional hydrothermal process

The two-way step synthesis procedure was developed by Hollman *et al.*, (1999) and was found to enable the production of pure zeolite products from high silicon containing solutions. The process involves an extraction of the amorphous Si and Al elements of fly ash by the use of an alkaline solution followed by subsequent hydrothermal crystallization of the extracted solution. Even though the two-step synthesis process can lead to production of purer zeolites from fly ash, the process still requires longer synthesis times which may discourage large scale synthesis (Musyoka, 2009).

2.4.1.3 Introduction of two-step synthesis procedure: with "step-change of synthesis temperature"

The step-change of synthesis temperature was introduced by Hui and Chao (2005) to reduce the total synthesis time when synthesizing pure zeolites from fly ash. Because of the fact that the rates of zeolite nucleation and crystal growth are influenced by temperature, the developed process extended the work of Hollman *et al*., (1999) and was able to reduce the synthesis time to between 3.5 – 9.5 hours. Unfortunately, the application of step change procedure may complicate the zeolite scale up process.

2.4.1.4 Use of the microwave assisted method during synthesis

Although the use of the microwave to synthesize zeolite starting from pure sources of Si and Al had earlier been reported (Jansen *et al*., 1992), the microwave-assisted method for zeolite synthesis from coal fly ash was introduced by Querol *et al.* (1997). The method was reported to lead to the production of zeolites within extremely shorter synthesis times (from between 24 and 48 hours to 30 minutes). Microwave energy is based upon electromagnetic radiation with wavelengths ranging from 1 m to 1 mm with corresponding frequencies ranging between 300 MHz to 300 GHz. Microwave irradiation is relatively efficient in transferring thermal energy when compared to conventional heat transfer such as convection or conduction. The challenge with this approach is that the zeolites produced were small pore zeolites (such as: hydroxysodalite, cancrinite, analcine, zeolite Na-P1, and kalsilite) which have limited industrial applications.

2.4.1.5 Introduction of Molten salt synthesis approach

The synthesis of zeolites under molten conditions that did not require any addition of water was pioneered by Park and co-workers (2000). This innovative process is environmentally friendly because it avoids the generation of waste water which often requires further treatment before discharge. Even though this method seems to be attractive, it has its own disadvantages. First, the irregular morphology of the zeolites produced, and secondly, the synthesized zeolites are usually of sodalite and cancrinite types, with low cation exchange capacity (CEC) values. Therefore, the zeolites produced through this method will have limited applications.

2.4.1.6 Ultrasonic assisted synthesis of zeolites

The use of ultrasound has been shown to lead to improved reaction rates, yields and product properties of a variety of synthesis processes (Wang *et al*., 2008; Mason, 1997; Eldik and Hubbard, 1997). Studies to compare the effects of ultrasound and mechanical agitation on a reacting solid-liquid system were conducted by Hagenson and Doraiswamy (1998). They found that the use of ultrasound led to significant enhancements both in homogeneous and heterogeneous reactions even in cases when the two methods had similar power consumption (Ratoarinoro *et al*., 1995). A recent review article by Bang and Suslick (2010) discussed the application of ultrasound-assisted synthetic methods in the synthesis of nanostructured materials and also pointed out some of the fundamental principles of sonosynthesis. Unlike conventional energy sources, application of ultrasound has been found to provide rather unusual reaction conditions (a short duration of extremely high temperatures and pressures in liquids) that cannot be realized by other methods (Mason, 1997; Bang and Suslick, 2010). When ultrasound is applied to a system, there is no direct molecular-level interaction between ultrasound and the chemical species but instead acoustic cavitation, defined as the formation, growth, and implosive collapse of bubbles in liquids, is known to drive both the mechanical and chemical effects of ultrasound (Suslick and Doktycz, 1990). The chemical effects of ultrasound are due to the implosion of microbubbles, generating free-radicals whereas mechanical effects are caused by shock waves formed during symmetric cavitation, or by microjets formed during asymmetric cavitation (Hagenson and Doraiswamy, 1998).

Direct application of ultrasound to crystallize zeolite A from metakaolinite without the conventional hydrothermal treatment step was reported by Kim *et al.*, 2010. The authors reported that zeolite A started to crystallize after 30 minutes of direct sonication, with fully crystalline zeolite A formed after only 120 minutes. Other studies conducted by Andaç *et al*., (2005) also reported use of ultrasonic energy during the synthesis of zeolite A from a 'clear-to-the-eye' sodium aluminosilicate solution prepared from pure chemicals. The authors showed that the rate of crystallization as well as the yield of zeolite A was increased significantly when sonication was applied. A different study by the same authors (Andaç *et al*., 2006) also reported that sonication allowed the preparation of thinner and continuous zeolite A coatings on stainless steel substrates within shorter synthesis times. The application of ultrasonic ageing procedures prior to conventional heating during the synthesis of zeolites has been found to result in gradual reduction of the induction period and even shortened the crystallization time (Abrishamkar *et al*., 2011). Ultrasound-assisted ageing was also reported to lead to alteration of morphologies of the product particles in a study by Azizi and Yousefpour (2010) as well as decrease the amount of hexamethyleneimine (HMI) used for the syntheses of MCM-49 (Wu *et al*., 2006]) and MCM-22 (Wang *et al*., 2008). During fly ash zeolitization process, a study conducted by Belviso *et al*. (2010) applied ultrasound to age the fly ash based synthesis mixture and reported that ultrasound enabled formation of zeolites at a lower-temperature than when the synthesis was not preceded by sonication. A recent review article by Askaris *et al.*, (2012), discusses the latest studies focusing on applications of ultrasound during the synthesis of zeolites. Up to date, there are no studies that have reported the synthesis of zeolites by direct sonication of fly ash.

2.4.1.7 Other miscellaneous modifications

Other researchers have introduced slight modifications to the well-known classical hydrothermal synthesis. Most of these studies utilized pure water during the synthesis process apart from a few studies that have concentrated on the use of seawater (Lee *et al*., 2001; Belviso *et al*., 2010), brine solution (Musyoka *et al*., 2011) and the use of structure directing agents (Chareopanich *et al*., 2004) to produce larger pore zeolites such as ZSM-5. Pre-treatment of fly ash with HCl was also adopted by Sutarno and Arryanto (2007) to increase dissolution of fly ash as well as to decrease the metal impurities in the fly ash sample. A section of this thesis deals with the production of zeolites using mine waters as a substitute for pure water. This is a novel process

for producing valuable products from two wastes (fly ash and mine waters) that are found in close proximity to each other.

2.4.2 Mechanism of zeolite formation from coal fly ash

The zeolite formation process from fly ash has been studied by different researchers using a combination of different ex-situ analytical techniques (Shigemoto *et al.*, 1995). Understanding the formation mechanism of the fly ash zeolitization process is expected to enable a rational design of the synthesis process that can lead to the production of predetermined zeolite types with intended properties. Murayama *et al*. (2002) also suggested that understanding the reaction mechanism of zeolites from fly ash would enable a proper design of the manufacturing equipment at the scaled up level. The complexity of fly ash composition as the starting material makes it difficult to directly relate the formation process to that of zeolites from pure analytical grade sources of Si and Al. Murayama *et al*. (2002) studied the mechanism of zeolite synthesis from coal fly ash by following the hydrothermal reaction taking place. In their study, they reported that during the zeolite formation process, there exist three distinct steps: dissolution step of Si and Al from coal fly ash, condensation step of silicate and aluminate ions in alkali solution to make aluminosilicate gel, and finally the crystallization step of aluminosilicate gel to make the zeolite crystal. The schematic shown in Figure 2.11 presents a general outlook of the fly ash zeolitization process.

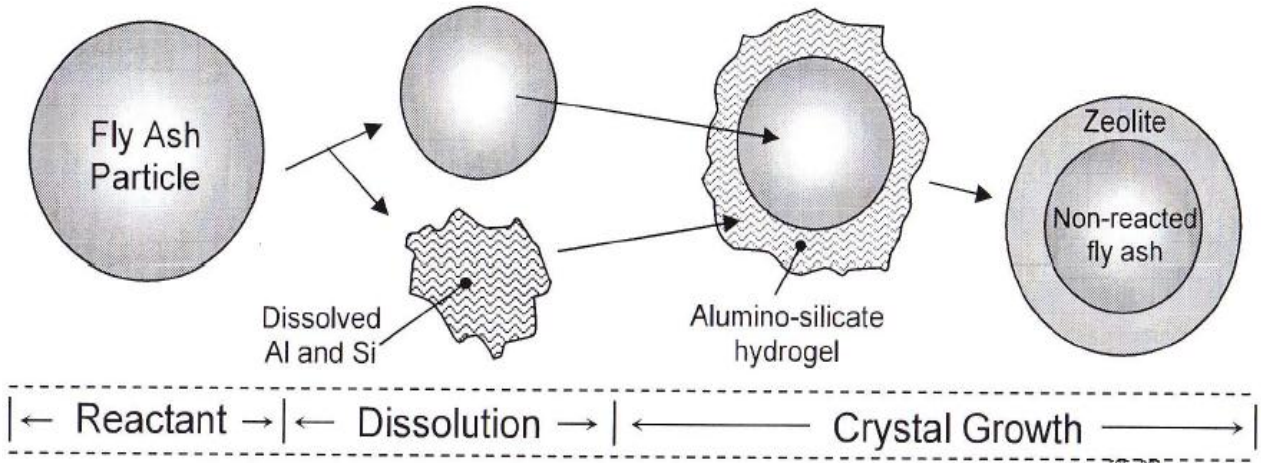

Figure 2-11: Schematic showing the proposed process for fly ash zeolitization (Fansuri *et al*., 2008).

During the early stages of synthesis, higher concentrations of Al ions than that of Si in the alkaline medium were also observed by Fernández-Jiménez and Palomo (2005), which they attributed to the fact that the Al–O bonds are weaker than the Si–O bonds, and therefore more easily broken. But the trend changes with time because fly ash has larger quantities of Si than that of Al. Murayama *et al* (2002) observed that the Si bearing material in the coal fly ash dissolved linearly in relation to dissolution time during the initial temperature rising stage. They further observed that the extracted aluminate and silicate ions condensed to form an aluminosilicate gel which is a precursor of the zeolite crystallization step. Since their synthesis solution still contained the undissolved fly ash particles, they observed that the zeolite crystals formed at the interface between the particle and the alkali solution. They postulated that further dissolution did not take place since the particle surface was covered with the deposited zeolitic phase, hence the aluminate and silicate ions that remained in the alkali solution was completely consumed, and was not replenished. As a result, the zeolite crystallization step became slower as the dissolved aluminate and silicate ion were slowly exhausted.

Studies by Shigemoto *et al*. (1995) employed infrared spectroscopy (IR), magic angle spinning nuclear magnetic resonance (MAS NMR), X-ray photoelectron (XPS) and Auger electron (AES) spectroscopy and thermogravimetric (TG) analysis to characterize zeolites and their amorphous precursors in order to elucidate the crystallization processes of zeolite from fly ash. Fernández-Jiménez and Palomo (2005) and Rayelu *et al*., (2005) employed the use of FTIR to gain a deeper understanding of mid-range order in the zeolite precursor formed after alkali activation of fly ash. They found that the X-ray amorphous precursor had a three-dimensional structure and long-range and mid-range disorder. A correlation between the vibrational spectra and the reaction product formed in the alkali activation of fly ash after different curing periods was observed. The presence of T-O vibrations (T = Al, Si) of diverse origin, in the initial ash, zeolite precursor and the final crystalline zeolites, yielded overlapping spectral bands whose correct interpretation was difficult because all these materials are composed of tetrahedral SiO_4 and AlO_4 whose main difference is their degree of structural order. Rayalu *et al*. (2005) used IR spectroscopic technique to calculate the percentage crystallinity of fly ash-based zeolite A and concluded that it was in good agreement with the XRD analysis**.**

Since most of the studies investigating the zeolite formation process from coal fly ash relied solely on the use of ex-situ analytical techniques as well as from slurries that still had the unreacted particles in them, the study presented in Chapter 6 aimed to investigate the crystallization mechanism from both the clear solution extract as well as from unseparated slurry using both in-situ ultrasonic monitoring system as well as complementing ex-situ analytical techniques.

2.4.3 Selected zeolites synthesized from fly ash

Even though many different types of zeolites have been synthesized from fly ash (Querol *et al*., 2002), the discussion below only focuses on a few of the zeolites that have been widely synthesized from fly ash due to their industrial applications.

2.4.3.1 Gismondine type zeolites (GIS)

Gismondine zeolites belong to the zeolite group comprised of four double-connected 4-ring building units consisting of $(Si,Al)O_4^-$ tetrahedra (Meier *et al.*, 1996). The four 2-ring units form "crankshaft" chains around a screw tetrad, to build up the three-dimensional framework. According to Gottardi and Galli (1985), the highest topological symmetry of gismondinetype zeolite framework is tetragonal (see Figure 2.7). The Gismondine (GIS) framework topology is shared by the following natural zeolites; amicite, gobbinsite, and garronite and also by the synthetic zeolite P (Betti *et al*., 2007).

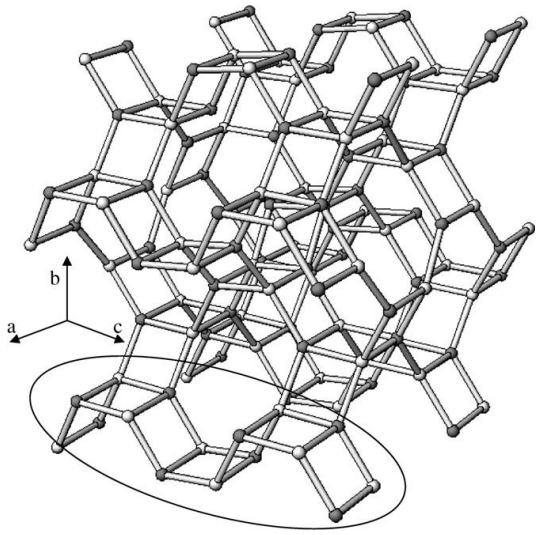

Figure 2-12: Stick-and-ball drawing of Gismondine framework "'double crankshaft'', where white balls = Si, gray balls = Al (Betti *et al*., 2007).

Zeolite P class includes a series of synthetic zeolite phases namely: High silica variety of NaP ($Na_{3.6}Al_{3.6}Si_{12.4}O_{32}.14H_2O$), Low silica NaP ($Na_8Al_8Si_8O_{32}.xH_2O$), NaP1 ($Na_6Al_6Si_{10}0_{32}.12H_2O$), NaP2 ($Na_4Al_4Si_{12}O_{32}.14H_2O$). The interesting properties of zeolite P are associated with the significant flexibility of its framework. For example, dehydration of NaP zeolite results in a reversible 20 % decrease in unit cell volume (Zholobenko *et al.*, 1998). Even though Zeolite P may be limited in its applications as catalysts, it has been found to have significant potential in applications such as the removal of toxic elements during the waste water treatment (Hendricks, 2005; Petrik *et al*., 2007), use as a geosynthetic liner and in ground water remediation (Czurdo *et al.,* 2002). Studies by Elliot (2006) have also shown that zeolite Na-P1 can be used in the fertilizer industries. Other scientists who have been interested in zeolite Na-P1 have reported that it is a common product of fly ash hydrothermal transformation under alkaline conditions (Catalfamo *et al*., 1993; Berkgaut and Singer, 1996; Hollman *et al*., 1999; Scott *et al*., 2001; Querol *et al*., 1997, 2001; Musyoka *et al.,* 2012). Only a few studies have been conducted to produce zeolite P from South African fly ash (Woolard *et al*., 2000; Hendrick, 2005; Vadapalli *et al*., 2010; Musyoka *et al.,* 2012).

2.4.3.2 Linde Type A (LTA)

Zeolite type A, denoted by the International Zeolite Association (IZA) code system as Linde Type A (LTA) (Baerlocher *et al*., 2007), is of great commercial importance due to its molecular sieving and ion exchange properties (Breck, 1974). The structure of zeolite A consists of sodalite (SOD) cages linked via four rings, and has a Si/Al ratio of 1. These sodalite units join together to produce an α-cage (see Figure 2.5), the large cavity in the centre of the structure, with a diameter of 11.4 Å and two channel systems which are connected to allow movement of the Na^+ ions and water molecules (Cubillas and Anderson, 2010). Zeolite A is classified into three subgroups based on the type of exchangeable cations present in its structure. These subgrouping include; potassium exchanged form, K-LTA or Linde 3A, sodium exchanged form, Na- LTA or Linde 4A and calcium exchanged form, Ca- LTA (Linde 5A), (Montanari and Busca 2006). Zeolite A synthesized in sodium form has pore opening of 0.34 nm, when ion exchanged with potassium its pore reduces to 0.30 nm whereas when exchanged with calcium the pore increases to 0.43 nm (Pfenninger, 1999). These seemingly small differences in pore openings play a significant role when it comes to determining the best application for zeolite A. Synthesis of zeolite A from fly ash has been conducted by many authors as shown in Table 2.6. The list is not exhaustive.

Table 2-6: Some studies on production of zeolite A from fly ash sources from different countries.

Fly ash source	Synthesis temperature and time	Reference
Japanese and Australian	100 °C, 6 hours	Shigemoto *et al*., 1993
USA	2 days at rm, 38 °C for 3 days	Shih *et al*., 1996
USA	80 °C, 1-7 days	Grutzeck *et al*., 1997
Dutch	90 °C, 72 hours	Hollman *et al*., 1999
USA	60 °C, 3 days	Chang *et al*., 2000
Spanish	90 °C, 10 hours	Querol et a., 2002
Japanese	85 °C, 24 hours	Tanaka *et al*., 2002
Chinese	90 °C, 1.5 hours then 95 °C, 2.5 hours	Hui and Chao, 2006

2.4.3.3 Faujasite type zeolites (FAU)

Faujasite zeolites (X and Y) have wide applications and since their discovery they have elicited a lot of industrial and research interests. Because zeolites X and Y have a similar XRD pattern, it is often difficult to distinguish the two zeolitic phases based on their XRD patterns (Chang and Chih, 2000). To differentiate the two phases, Breck (1974) suggested the use of their compositional variation (SiO_2/Al_2O_3 mole ratio ranges). In this case, the relatively higher aluminous species having a $SiO_2/A1_2O_3$ ratio ranging between 2 and 3 is designated as type X whereas the siliceous species with a $SiO_2/A1_20_3$ ranging between 3 and 6 is labeled as type Y. Zeolite Na-X (the Na form of zeolite X) has a general unit cell formular Na_{86} $[(AlO_2)_{86}$ $(SiO_2)_{106}]$ mH_2O where m is the number of water molecules (Akbar *et al.,* 2005) and has a pore size of 0.74 nm (Pfenninger, 1999). The building units of zeolite X are formed when Si and Al tetrahedra are coupled to form a sodalite unit, which has the shape of a truncated octahedron having square and hexagonal faces. The sodalite units are then interconnected to four other sodalite cages via hexagonal prisms on their hexagonal faces (see Figure 2.5). Entrances to the sodalite cages of zeolite X are composed of six tetrahedral (6 rings) which have a pore diameter of 2.5 Å whereas the supercages are made up of larger rings having 12 tetraheda with an internal diameter ranging between 8-9 Å (Jain *et al.,*1990; Oslon, 1970). For zeolite Na-X, 82% of component Na ions are located in the supercages whilst the rest of the Na is located in the smaller sodalite cages (Oslon, 1970).

Although zeolite X has numerous applications, its main uses are in catalysis, purification and separation of gases and organic components, cation exchange and adsorption. Due to the numerous industrial applications of zeolite Na-X, this zeolite has become an important target for synthesis from many unconventional starting materials such as rice husk ash, metakaolin, oil shale ash, coal fly ash among other Si-Al containing feedstocks. Although synthesis of hierarchical zeolite X from pure grade analytical chemicals was recently reported by Inayat *et al* (2012), all the studies focusing on producing zeolite X from fly ash (Mondragon *et al*., 1990; Shigemoto *et al*., 1993; Amrhein *et al*., 1996; Hollman *et al*., 1999; Srinivan *et al*., 1999; Chang *et al*., 2000; Scott *et al*., 2001; Querol *et al*., 2002; Tanaka *et al*., 2004; Molina *et al*., 2004 and Somerset *et al*., 2008) have only managed to generate the well-known pyramidal octahedral-shaped crystals of zeolites X. Alkali fusion of fly ash prior to the conventional hydrothermal

crystallization, even though it is energy intensive, is often preferred when synthesizing zeolite X from fly ash because it enables synthesis of zeolite X from fly ashes with different compositions (Shigemoto *et al.*,1993).

2.4.4 Applications of fly ash derived zeolites

The use of coal fly ash in the synthesis of zeolites with high end industrial applications is expected not only to provide a new source of revenue for the coal combustion companies, but may also offset expenses associated with fly ash disposal. From the environmental point of view, intensifying the use of zeolites that are derived from fly ash will indirectly reduce the need for additional landfill space, reduce the energy consumption during transportation of ash to disposal sites, and eventually conserve natural resources. Owing to the large amounts of fly ash produced in South Africa on a yearly basis, it can be estimated that the available fly ash can provide enough zeolite feedstock to satisfy the current South African zeolite market. Some of the known applications of zeolites synthesized from fly ash include:

2.4.4.1 Treatment of waste waters

Many studies (Hui and Chao, 2005; Sonqishe *et al*., 2009; Sommerset *et al*., 2008; Vadapalli *et al*., 2010) have shown that fly ash-derived zeolites can be used to remove toxic metals from waste waters. For example, Moreno *et al*., (2001) reported that use of zeolites increased the pH of the mine waters which caused the metal-bearing solid phases to precipitate leading to enhancement of the efficiency of the decontamination process. The attractive ion-exchange capacity or uptake ability of zeolites has been reported to be 2-4 times higher than that of coal fly ash (Hui and Chao, 2008). Musyoka *et al*. (2011) reported that it was possible to synthesize zeolites from waste industrial brine solutions instead of ultrapure water.

2.4.4.2 Use of zeolites in detergent industries

On the realization of the devastating effects, such as eutrophication (decaying of lakes), of the use of phosphate builders in detergents, scientists decided to employ zeolites as a substitute. Initially, zeolite P had been used but later studies showed that zeolite A was more effective (Nagy, 1998). Studies by Rayalu *et al*., (2001) suggested that zeolite A, produced from coal fly ash, could act as a substitute for the commercially produced zeolite A whose starting material is

pure grade industrial sources of Si and Al. In order to prove that fly ash-derived zeolite A could be used in the detergent industries, Hui and Chao (2006) conducted leaching tests of fly ash based zeolites and showed that fly ash based zeolite A leached the same elements (Sb, As, Se and Tl) in the same order of magnitude as the commercial zeolite A. Thereby confirming that fly ash-derived zeolites do not pose serious threats to the environment when compared with their commercial counterparts.

2.4.4.3 Use of zeolites in catalysis

Studies by Sutarno and Arryanto (2007) showed that Faujasite zeolite that was synthesized from fly ash could be used in hydrocracking of petroleum distillate. Srinivasan and Grutzeck (1999) also showed that zeolites synthesized from fly ash could be used for adsorption of SO_2. Hui and Chao (2008) performed studies on the use of multi-ion-exchanged zeolite A prepared from coal fly ash in methane emissions abatement and found that fly ash derived zeolite A demonstrated similar efficiency as an alternative to the commercial adsorbent.

2.4.4.4 Other miscellaneous applications

Studies on the use of fly ash based zeolites for controlled fertilizer release and soil amendment were conducted by Fansuri *et al.* (2008) and suggested that fly ash-derived zeolite fertilizers can consume a significant percentage of waste fly ash. Recent studies by Lee and Jo (2010) have also suggested that zeolite synthesized from waste fly ash can be used for adsorption of CO_2. Other studies on the use of fly ash derived zeolites in separation were pointed out by Querol *et al*. (2002).

2.5 Chapter Summary

The relevant information concerning coal, fly ash, zeolite and more specifically the use of fly ash in the synthesis of zeolites has been presented in this chapter. Despite the fact that there exist some fly ash applications, the rate of fly ash production exceeds the rate of its reuse all over the world hence presenting a serious challenge in finding innovative ways to cope with the imbalance. Synthesis of zeolites from fly ash stands out as one of the most attractive ways of beneficiating fly ash but since the synthesis methodologies that are reported in the literature are mainly developed for fly ashes sourced from Europe, United States and some other countries in

Asia, customization or even development of new synthetic protocol for producing high value zeolites from South African fly ashes is an area that needs more attention. Furthermore, it was also noted that the mechanism of formation of zeolites from fly ash is still not well understood meaning that there was a need for further work in that direction.

In view of the gaps identified in the literature review, the research presented in this thesis aims at identifying the best synthesis condition for producing some industrially important zeolites (A and X) from South African fly ash, studying their formation mechanism, exploring the potential for use of mine waters during the synthesis process as well as developing new or efficient synthetic protocols by the use of ultrasound.

The next chapter presents the experimental materials, set-up and sample preparation together with a description of the procedures that were conducted to achieve the research objectives set for this thesis.

CHAPTER 3

EXPERIMENTAL AND ANALYTICAL TECHNIQUES

This chapter presents detailed description of materials and chemicals used in the study. The research approach, experimental procedures, equipment set ups and characterization techniques used in the present research work are also detailed. A schematic highlighting the experimental design and procedure that was followed in the respective chapters is laid out as a guide to the sequential nature of the research approach.

3 Experimental approach overview

In the interest of achieving the research objectives set forth in chapter one of this thesis, the experimental approach was designed in such a way to provide the answers to the predetermined research questions. The schematic diagram presented in Figure 3.1 highlights the four sub-sections that represent the respective results and discussion chapters.

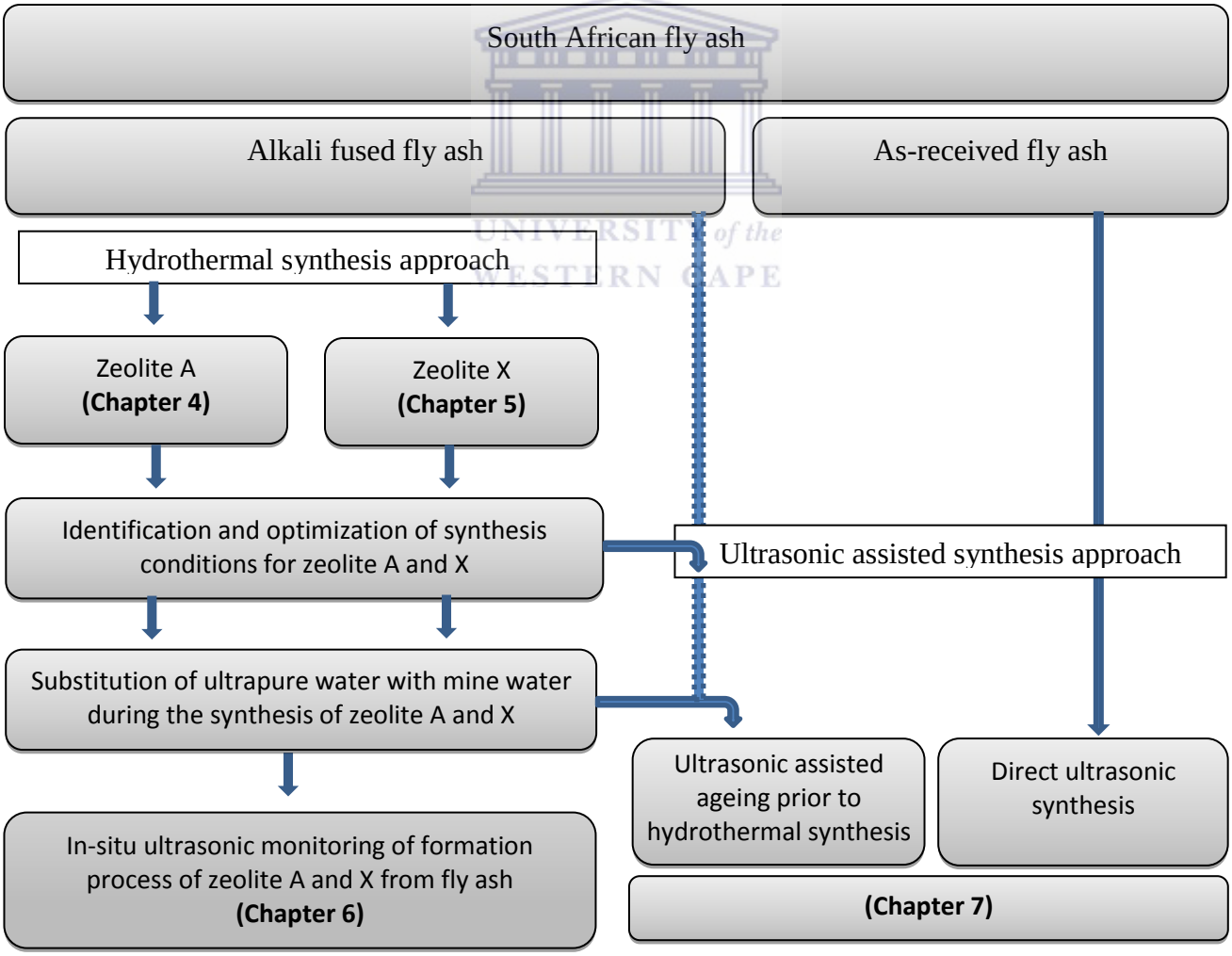

Figure 3-1: Schematic diagram of the research approach followed in this thesis.

CHAPTER 3

3.1 Materials and chemicals

Since two main waste materials (fly ash and mine waters) were used in this study, the details of their sources, sampling procedures together with the list of the chemicals used in this study are given in this section.

3.1.1 Fly ash source, sampling and handling procedure

Seven coal fly ash samples were collected from seven different South African coal-fired power plants (Arnot, Duvha, Hendrina, Kriel, Matla, Lethabo and Tutuka) which are all located in Mpumalanga and Gauteng provinces of South Africa as shown in Figure 3.2. The collected bulk fly ash samples were mixed to achieve homogeneity and stored in sealed containers. The storage was in a dark environment and away from fluctuating temperature in order to preserve their compositional integrity. This was because upon exposure to the atmosphere many of the metastable assemblies of minerals phases in fly ash, which are initially formed at high temperatures during coal combustion, can alter to form thermodynamically stable minerals which might alter the overall initial composition of fly ash (Klink, 2003; Sonqishe, 2008). The same batch of fly ash was used during the synthesis process to avoid complications which could be caused by the fly ash source or batch variability.

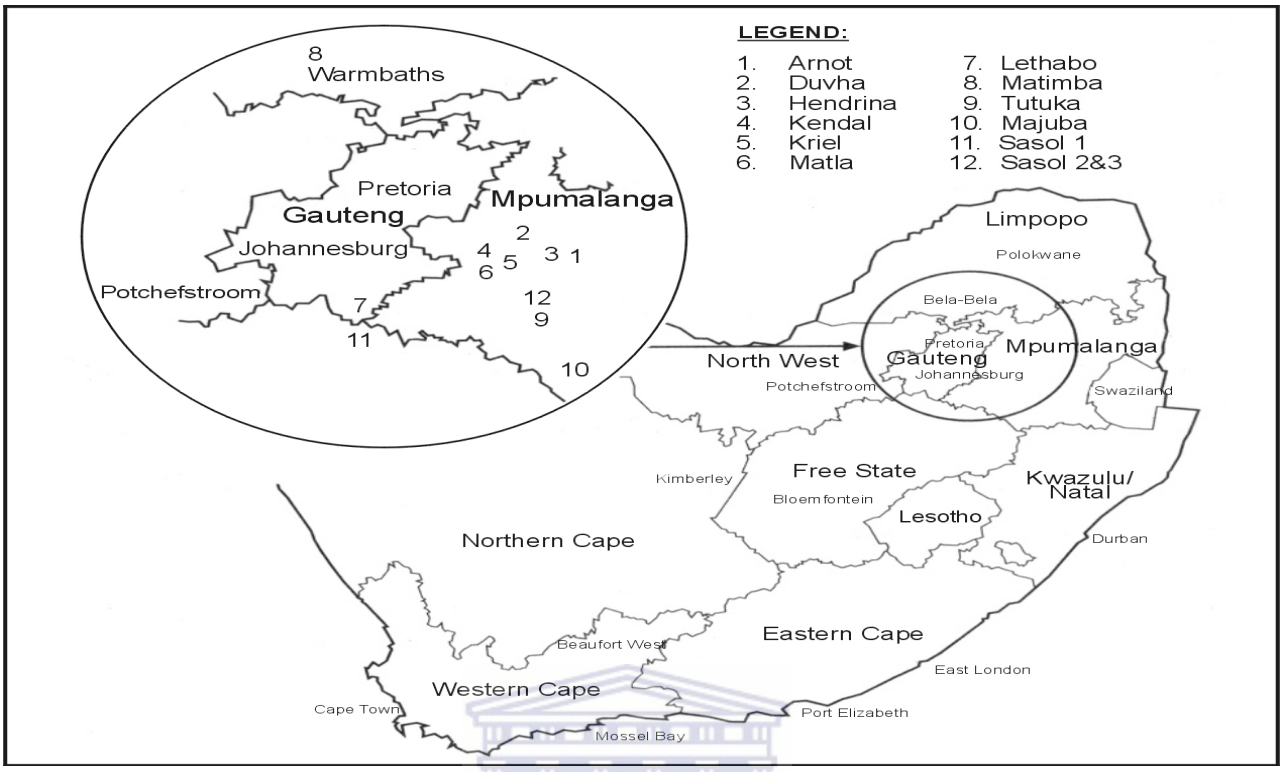

Figure 3-2: Location of important pulverized coal-fired thermal power stations in the Republic of South Africa (Krüger, 2003).

3.1.2 Mine water source, sampling and handling procedure

The representative circumneutral and acid drainage mine waters that were used in the study were collected from Middleburg and Navigation coal mine respectively. These coal mines are located in the Mpumalanga province of South Africa as shown in Figure 3.3. Since most of the power stations in the South Africa are located in close proximity to the coal mines, the use of mine waters and fly ash in zeolite synthesis makes logistical sense since their use can not only act as a way of beneficiating these waste products but also help in moving towards zero effluent discharge from these industries. Studies on the synthesis of zeolites using both fly ash and mine waters have not been done before.

The collected mine waters were filtered during the collection process and kept in a cold environment (refrigerator) to preserve their compositional integrity after collection. Before use, a portion of the mine water was further filtered through a 0.45 μm pore membrane filter paper and the filtered sample was further divided into two portions in order to conduct cationic and anionic

compositional analysis. For cationic analysis, the samples were preserved with 3 drops of concentrated HNO_3 for approximately 100 ml of sample in order to make the cationic species labile.

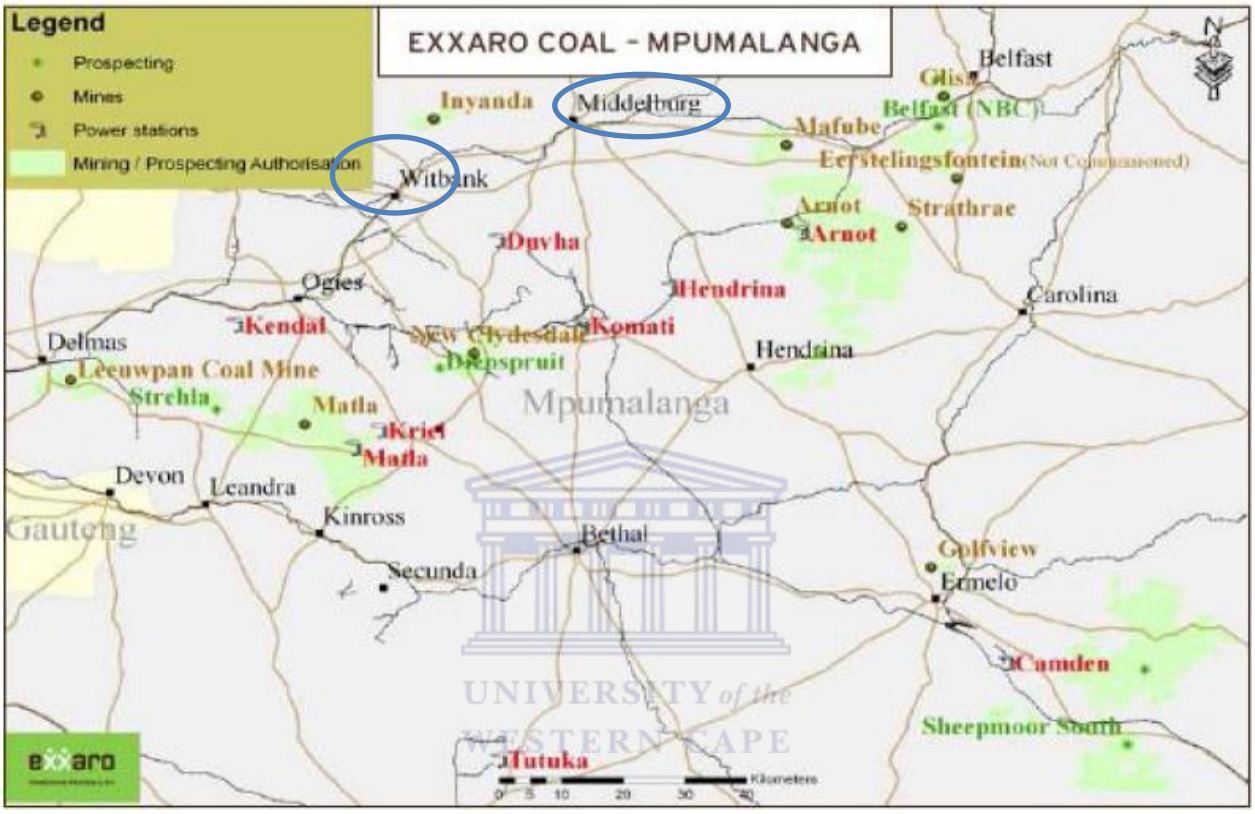

Figure 3-3: Location of coal mines (in South Africa) where the mine waters were collected (Exarro, 2003).

3.1.3 Chemicals

The list of chemicals used in this study together with their source and purity are presented in Table 3.1.

Table 3-1: List of chemical reagents used in the study.

Chemical	Source	Purity
Sodium hydroxide pellets	Merck	99.8 %
Sodium aluminate	Riedel-de Haën	54 % Al_2O_3, 41 % Na_2O
Sodium silicate	Riedel-de Haën	28 % SiO_2, 27 % Na_2O,
Nitric acid	Merck	Min. 65 %
Hydrofluoric acid	Saarchem	Min. 55 %
Hydrochloric acid	Merck	Min. 37 %

3.2 Experimental procedures for synthesis of A and X from South African fly ash: Identification and optimization of synthesis condition

The specific procedures, conditions, parameter variations and experimental setups that were followed are presented in the following sub-sections, for the respective chapters as was shown in the schematic presented in Figure 3.1. In both the synthesis of zeolite A and X, the as-received fly ash was firstly fused with sodium hydroxide to convert the insoluble fly ash mineral phase to soluble sodium aluminosilicate phases.

3.2.1 Preparation of Alkali fused fly ash

During the fusion process, 1:1.2 mass ratio of Arnot fly ash to NaOH powder was initially ground together using a laboratory scale ball mill grinder for 10 minutes to achieve a homogenous mixture. The resulting fly ash-NaOH powdered mixture was poured in a porcelain crucible and transferred a muffle furnance and left to fuse for 1.5 hours at 550 ˚C. After the 1.5 hours stay in the oven, the fused material was removed and allowed to cool to room temperature. The cooled fused material was ground using using a laboratory scale ball mill grinder for another 10 minutes to a achieve fine powder that was used during the synthesis of both zeolite A and X. For the sake of reference, the generated heated fly ash-NaOH powder is referred to as fused fly ash in this study.

3.2.2 Synthesis of zeolite A

After the analysis of the seven fly ashes sourced from different South African coal-fired stations listed in section 3.1.1, fly ash sourced from Arnot coal-fired power plant was chosen as a representative fly ash to use during the identification and optimization of synthesis conditions for producing zeolite A. Zeolite A was prepared using either unseparated fused fly ash slurry or a clear extract of the fused fly ash.

3.2.2.1 Synthesis of zeolite A starting from the unseparated fused fly ash slurry

In the case where zeolite A was prepared using unseparated fused fly ash slurry, four variables were identified and investigated to determine the best synthesis conditions for producing zeolite A from South African fly ash. These variables were grouped as either chemical or physical parameters. The chemical parameters were; variations of the Si/Al ratio by adding different amounts of Na-AlO_2 and variations of water content during synthesis. The physical parameters investigated were; variation of hydrothermal synthesis temperature and time. A one-step-at-a-time optimization process was chosen in which each parameter was varied independently to identify its optimum before investigating the effect of the next parameter. The levels of variation of the parameters that were investigated, together with those paraneters that were held constant, are shown in Figure 3.2.

Table 3-2: Levels of variations of the parameters investigated during the search for the synthesis conditions for producing zeolite A from unseparated fused fly ash slurry (based on preparation of 70 mL reaction mixture).

<table>
<tr><td>Parameter under investigation</td><td colspan="4" rowspan="2">Level of variation</td></tr>
<tr><td>1. Effect of additional Al (Na-aluminate solution)

Mass (g) ratio Na-AlO_2:NaOH:H_2O</td></tr>
<tr><td></td><td>0 : 0 : 0</td><td>0.6 :1.2 : 20</td><td>1.2 : 2.4 : 20</td><td>3.6 : 7.2 : 20</td></tr>
<tr><td>Variables held constant</td><td colspan="4">Fused fly ash slurry: 50 mL pure water + 10 g of fused fly ash
Hydrothermal synthesis temperature: 100 °C
Hydrothermal synthesis time: 2 hours</td></tr>
<tr><td>2. Effect of reduction of water content during preparation of fused fly ash slurry</td><td colspan="2">50 mL water + 20 g of fused fly ash</td><td colspan="2">50 mL water + 10 g of fused fly ash</td></tr>
<tr><td>Variables held constant</td><td colspan="4">Na-aluminate solution: 20 mL pure water+0.6 g Na-AlO_2+1.2 g NaOH
Hydrothermal synthesis temperature: 100 °C
Hydrothermal synthesis time: 2 hours</td></tr>
<tr><td>3. Effect of variation of hydrothermal temperature and time</td><td colspan="4">Level of variation</td></tr>
<tr><td>Syntheis temperature</td><td>80 °C</td><td>90 °C</td><td colspan="2">100 °C</td></tr>
<tr><td>Synthesis time</td><td>0.67, 1, 1.5, 2, 2.5, 3, 4, and 6 hours</td><td>0.67, 1, 1.5, 2, 2.5, 3, 4, 6 and 6 hours</td><td colspan="2">0.67, 1, 1.5, 2, 2.5, 3, 4, and 6 hours</td></tr>
<tr><td>Variables held constant</td><td colspan="4">Fused fly ash slurry: 50 mL pure water + 10 g of fused fly ash
Na-aluminate solution: 20 mL pure water+0.6 g Na-AlO_2+1.2 g NaOH</td></tr>
</table>

3. Effect of extended hydrothermal synthesis period.	Hydrothermal synthesis time: 3 days	Hydrothermal synthesis time: 6 days
Variables held constant	Fused fly ash slurry: 50 mL water +10 g of fused fly ash Na-aluminate solution: 20 mL water+0.6 g Na-AlO_2+1.2 g NaOH Hydrothermal synthesis temperature: 100 ℃	

In all the studies listed in Table 3.2, the hydrothermal treatment was conducted by pouring the reaction mixture (obtained by mixing the 50 mL fused fly ash slurry with the 20 mL Na-aluminate solution) into different 23 mL Teflon cups of the Parr Bombs (Figure 3.4). The filled Teflon cups (60 % of the total volume) were put in their respective steel Parr casings and sealed tightly. The filled and sealed Parr Bombs were placed into a Memmert hot air oven where the temperature of synthesis was controlled as specified in Table 3.2.

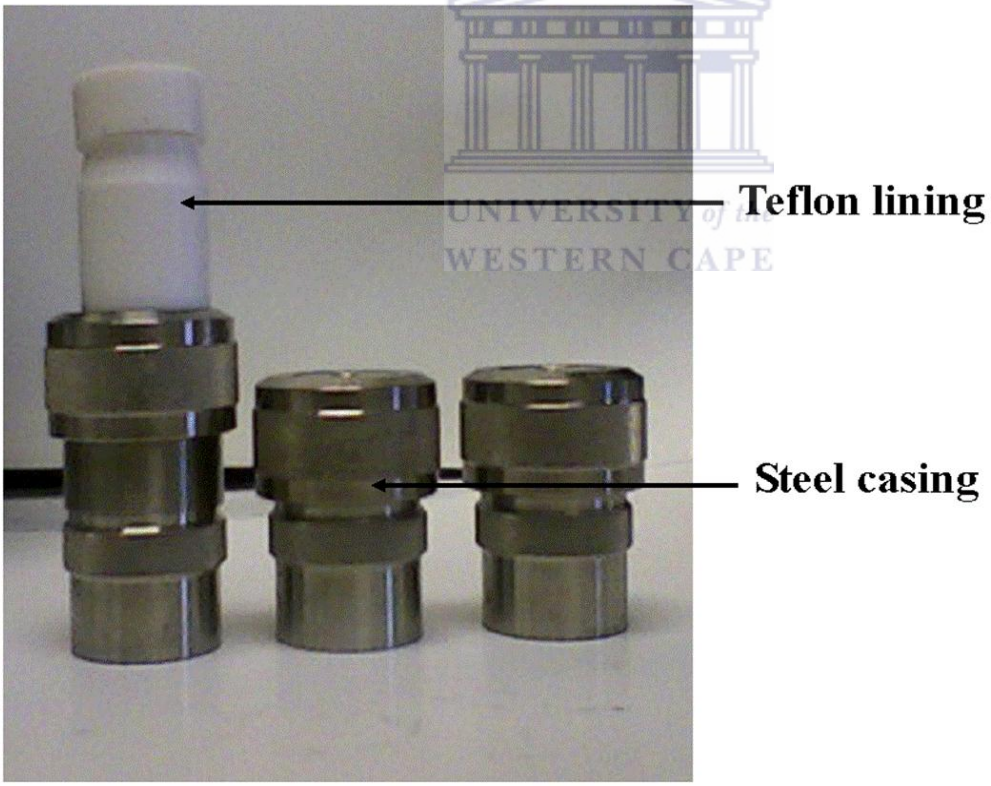

Figure 3-4: Parr bombs and Teflon lining (cup) used during the hydrothermal treatment process.

3.2.2.2 Synthesis of zeolite A starting from the from clear extract of fused fly ash

After identifying that the sythesis mixture having a molar regime of 1 Al_2O_3 : 5.39 Na_2O : 2.75 SiO_2 : 111.82 H_2O led to the crystallization of a single phase-high crystalline zeolite A at a hydrothermal temperature of 100 °C for 2 hours (from the experiments conducted in section 3.2.2), a clear extract of fused fly ash slurry that was obtained by filtering the fused fly ash slurry (see Figure 3.5) was used as the synthesis feedstock.

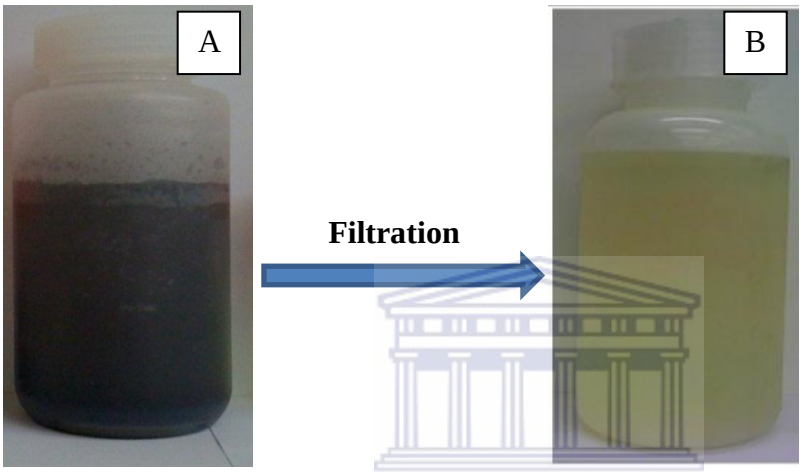

Figure 3-5: Images of a) unseparated fused fly ash slurry b) clear solution extracted from fused fly ash slurry by filtration.

To the 50 mL of the obtained clear extract of the fused fly ash, 20 ml of additional Na-aluminate solution prepared as per instructions presented in Table 3.2 was added to generate 70 mL synthesis mixture that had a molar ratio of 1 Al_2O_3 : 30.84 Na_2O : 4 SiO_2 : 414.42 H_2O. The resulting reaction mixture was hydrothermally treated at 100 °C for 2 hours.

A schematic for the steps followed in the synthesis process for zeolite A from either unseparated fused fly ash slurry or clear solution extracted from fused fly ash is shown in Figure 3.6.

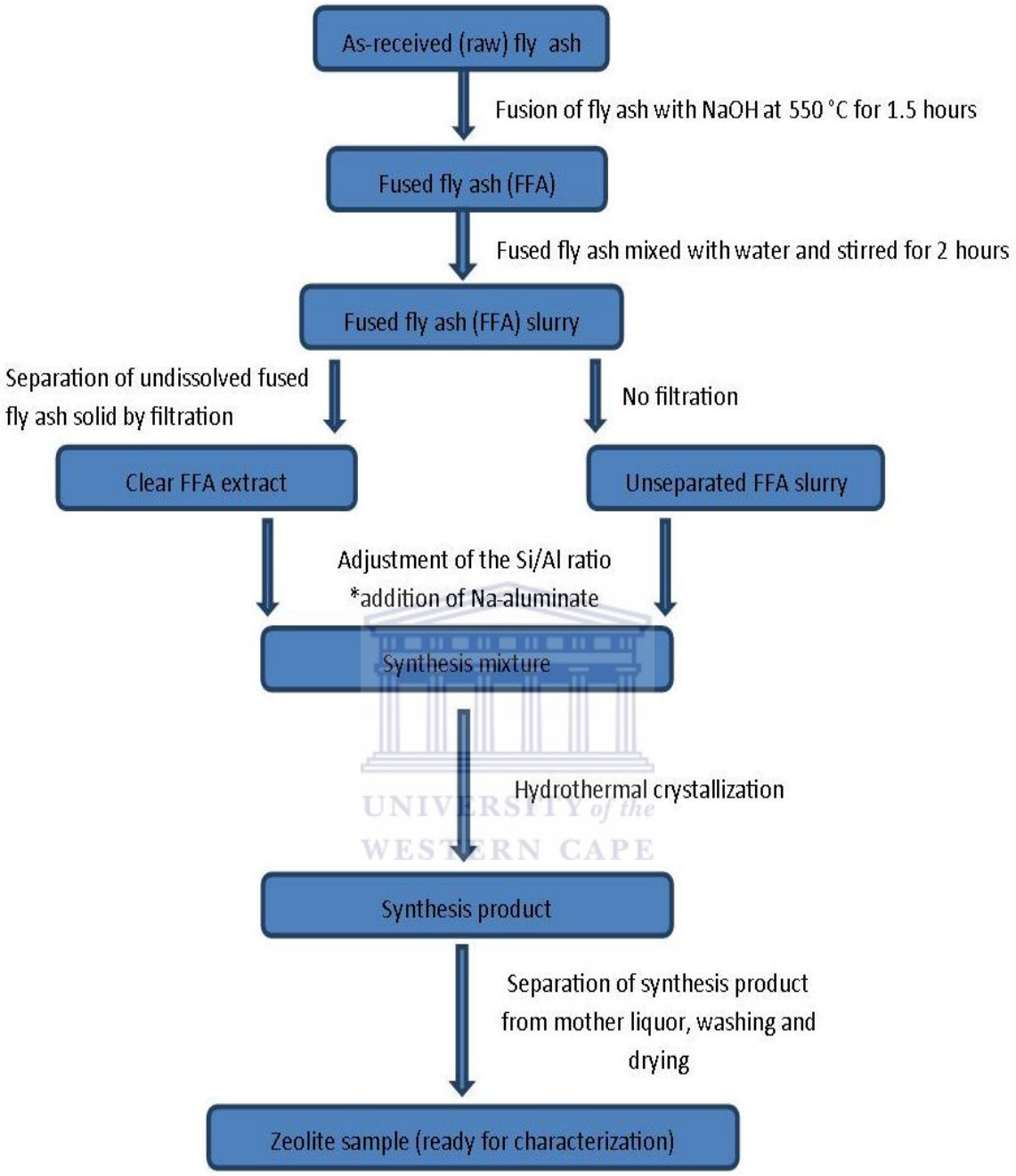

Figure 3-6: Schematic for the steps followed in the synthesis process for zeolite A from South African fly ash (FFA = Fused fly ash).

3.2.2.3 Synthesis of zeolite A starting from the unseparated fused fly ash using mine waters as a substitute for pure water

The effect of different types of mine waters (circumneutral (near-neutral) and acid drainage mine waters) as a substitute for pure water during the synthesis of zeolite A from unseparated fused fly ash slurry was also investigated. The preparation of sythesis mixtures as well as the syntheis conditions applied is presented in Table 3.3.

Table 3-3: Synthesis conditions for preparation of zeolite A starting from unseparated fused fly ash using mine waters as a substitute for pure water (based on preparation of 70 mL reaction mixture).

Effect of use of mine waters as a substuture of pure water during synthesis of zeolite A	Circumneutral mine water	Acid drainage mine water
Fused fly ash slurry: + Aluminate solution:	10 g fused fly ash + 50 mL of circumneutral mine water + 20 mL circumneutral mine water +0.6 g Na-AlO_2+1.2 g NaOH	10 g fused fly ash + 50 mL of acid drainage mine water + 20 mL acid drainage mine water +0.6 g Na-AlO_2+1.2 g NaOH
Molar regime of the resulting synthesis mixture	1 Al_2O_3 : 5.56 Na_2O : 2.50 SiO_2 : 110.86 H_2O	1 Al_2O_3 : 5.10 Na_2O : 2.69 SiO_2 : 107.66 H_2O
Variables held constant	Hydrothermal synthesis temperature: 100 °C Hydrothermal synthesis time: 2 hours	

It is important to point out that even though the same amount of Na-aluminate was used, as that used when the synthesis was conducted using pure water, the presence of extra Si and Al in the mine waters (see Chapter 4, Table 4.8) led to a new molar regime of the synthesis mixture when either circumneutral or acid drainage mine waters were used as a substitute for pure water. After the crystallization step, the solid crystals obtained were separated from the liquid supernatant, thoroughly washed and dried at 90 ˚C for 12 hours. Various characterization techniques such as;

powder X-ray diffractometry (XRD), X-ray refractive spectrometer (XRF), infrared (IR) spectroscopy, were employed to explore the physicochemical properties of the synthesis product.

3.2.3 Synthesis of zeolite X

The objective of this section was to identify and optimize the synthesis conditions for producing zeolite X from a South African coal fly ash sourced from Arnot power plant starting from either unseparated fused fly ash slurry or its clear solution extract. Just as in the procedure for the synthesis of zeolite A, the as-received Arnot fly ash was first fused with sodium hydroxide in the ratio of 1:2 at 550 °C for 1.5 hours as discussed in section 3.2. It is important to point out that unlike in the case for synthesis of zeolite A, there was no addition of extra Al to the reaction mixture during the synthesis of zeolite X either from unseparared fused fly ash slurry or clear extract of fused fly ash.

3.2.3.1 Synthesis of zeolite X starting from unseparated fused fly ash slurry

In the case where zeolite X was to be synthesized from unseparated fused fly ash slurry, the fused fly ash solids were mixed with pure water in a solid-to-liquid ratio of 1:5. The resulting mixture was stirred for 2 hour prior to static hydrothermal crystallization. The experimental runs conducted during the search for the best conditions for synthesis of zeolite X from South African fly ash are presented in Table 3.4.

Table 3-4: Levels of variations of the parameters investigated during the search for the synthesis conditions for producing zeolite X from unseparated fused fly ash slurry (based on preparation of 50 mL reaction mixture).

1. Effect of hydrothermal synthesis temperature	80 °C		90 °C		100 °C	
Variables held constant	10 g fused fly ash + 50 mL of pure water Hydrothermal synthesis time: 12 hours					
2. Effect of hydrothermal synthesis time	4 hours	6 hours	9 hours	12 hours	24 hours	48 hours
Variables held constant	10 g fused fly ash + 50 mL of pure water Hydrothermal synthesis temperature: 80 °C					
3. Effect of use of mine waters as a substuture of pure water during synthesis of zeolite X	Circumneutral mine water			Acid drainage mine waters		
Fused fly ash slurry:	10 g fused fly ash + 50 mL of circumneutral mine water			10 g fused fly ash + 50 mL of acid drainage mine waters		
Molar regime of the resulting synthesis mixture	1 Al_2O_3 : 4.95 Na_2O : 3.77 SiO_2 : 118.12 H_2O			1 Al_2O_3 : 5.43 Na_2O : 3.50 SiO_2 : 120.65 H_2O		
Variables held constant	Hydrothermal synthesis temperature: 80 °C Hydrothermal synthesis time: 9 hours					

During hydrothermal crystallization (under static conditions), the synthesis mixture was poured into the Teflon cups of Parr bombs (Figure 3.4) and put into a Memmert hot air oven where temperature was controlled as per the experimental protocol presented in Table 3.4. The molar regime of the optimized synthesis mixture prepared using pure water in step 2 from the experiments conducted in Table 3.4 was 1 Al_2O_3 : 4.90 Na_2O : 3.63 SiO_2 : 115.92 H_2O. The schematic of steps followed during the synthesis process of zeolite X from South African fly ash is presented in Figure 3.8.

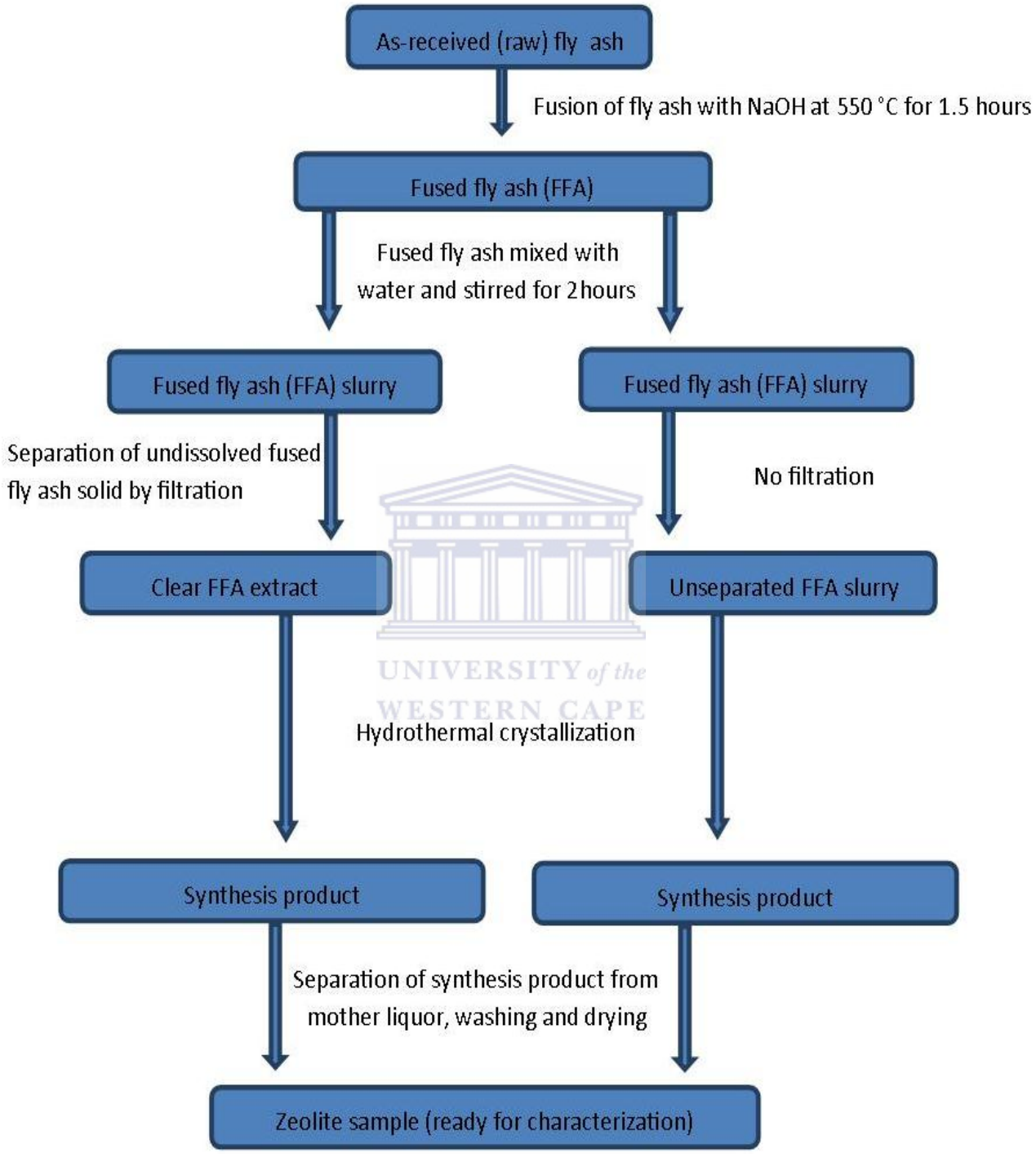

Figure 3-7: Schematic for the steps followed in the synthesis process for zeolite X from South African fly ash (FFA = Fused fly ash).

3.2.3.2 Synthesis of zeolite X from the clear extract of fused fly ash slurry

In the case when zeolite X was synthesized starting from a clear extract of fused fly ash, the experimental runs conducted during the search for best synthesis conditions are presented in Table 3.5.

Table 3-5: Levels of variations of the parameters investigated during the search for the synthesis conditions for producing zeolite X from clear extract of fused fly ash (based on preparation of 50 mL reaction mixture).

1. Effect of hydrothermal synthesis temperature	60 °C	70 °C	80 °C	90 °C	94 °C
Sample code	Con X60	Con X70	Con X80	Con X90	Con X94
Variables held constant	20 g fused fly ash + 50 mL of pure water Hydrothermal synthesis time: 24 hours				
2. Effect of variation of water used the during extraction of clear extract of fused fly ash	40 g fused fly ash + 50 mL of pure water			10 g fused fly ash + 50 mL of pure water	
Variables held constant	Hydrothermal synthesis temperature: 80 °C Hydrothermal synthesis time: 24 hours				
2. Effect of ageing the synthesis mixture	Synthesis mixture left to aged at room temperatute under stirred conditions (100 rpm) for 12 hours				
Variables held constant	20 g fused fly ash + 50 mL of pure water Hydrotherrmal synthesis temperature: 80 °C Hydrotherrmal synthesis time: 24 hours				

It is important to point out that unlike the synthesis of zeolite X from unseparated fused fly ash slurry, hydrothermal crystallization of zeolite X from clear extract of fused fly ash was conducted under stirred conditions. Once the synthesis mixture had been prepared as per the details set in Table 3.5, the synthesis mixture was transferred into a 100 mL plastic bottle, a magnetic stirring bar was inserted in the mixture and the bottle containing the mixture was

placed in a thermostated oil bath having a thermocouple that allowed temperature control. Figure 3.7 shows the set up of the hydrothermal crystallization process for producing zeolite X from clear extract of fused fly ash.

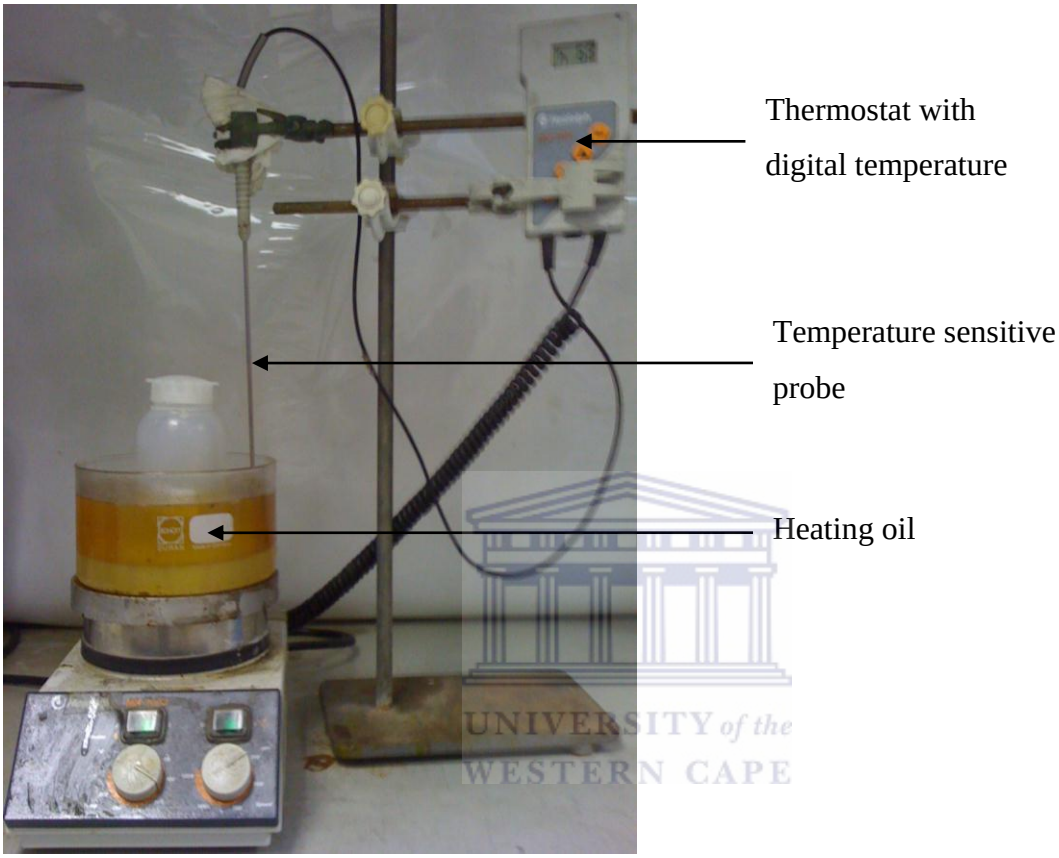

Figure 3-8: Set up for the hydrothermal crystallization process for producing zeolite X from clear extract of fused fly ash

After the crystallization step, the obtained solid crystals were separated from the mother liquor, thoroughly washed and then dried at 90 ˚C for 12 hours prior to characterization.

3.3 In-situ ultrasonic monitoring of formation of zeolite A and X from fly ash

3.3.1 Experimental set up and materials

The diagram presented in Figure 3.9 shows the connections of all parts of the in-situ ultrasonic monitoring system that was used in the assemply for the set up shown in Figures 3.10 and 3.11. The monitoring of the formation process of zeolite A and X from fly ash was done under real reaction conditions. These set of experiements were conducted at the Institute of Chemical

Reaction Engineering of the University/Erlangen-Nurnberg (Prof. Wilhelm Schwieger's laboratory).

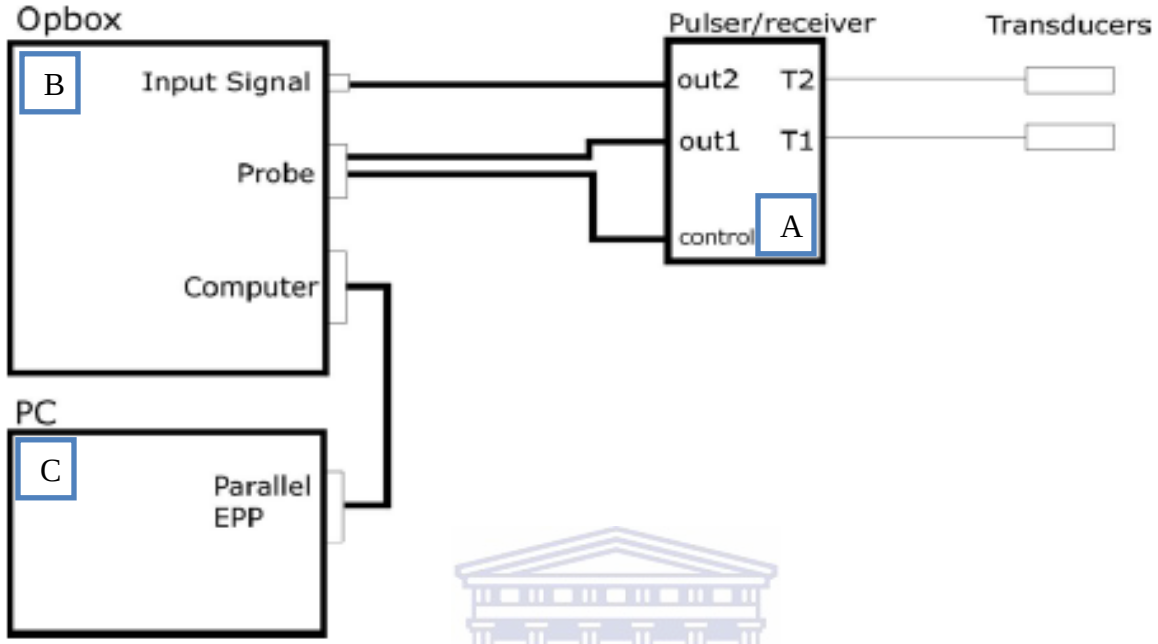

Figure 3-9: Diagram of connections for the in-situ ultrasonic monitoring system a) Pulser/receiver box b) OPbox ultrasonic testing device c) computer (Optel, 2010).

The PC-card, OPbox ultrasonic testing box, pulser and receivers are manufactured by PBP Optel Ltd. In the pulser/receiver box presented in Figure 3.12, only the connection ports "T1" and "out1" of the ultrasonic 'pulser and receiver' box (Figure 3.9) were used in the studies conducted in this section since it coud allow one-transducer mode. The ultrasonic transducer (10 mm Ø, PIC 155, central frequency: 2 MHz) which was able to transmit and receive ultrasound waves via the pulse-echo mode method was supplied by PI Ceramic, Germany. In order to capture the ultrasonic measurements data (time of flight, signal velocity and attenuation) PBP Optel software (Ver. 4.1/2004) was used.

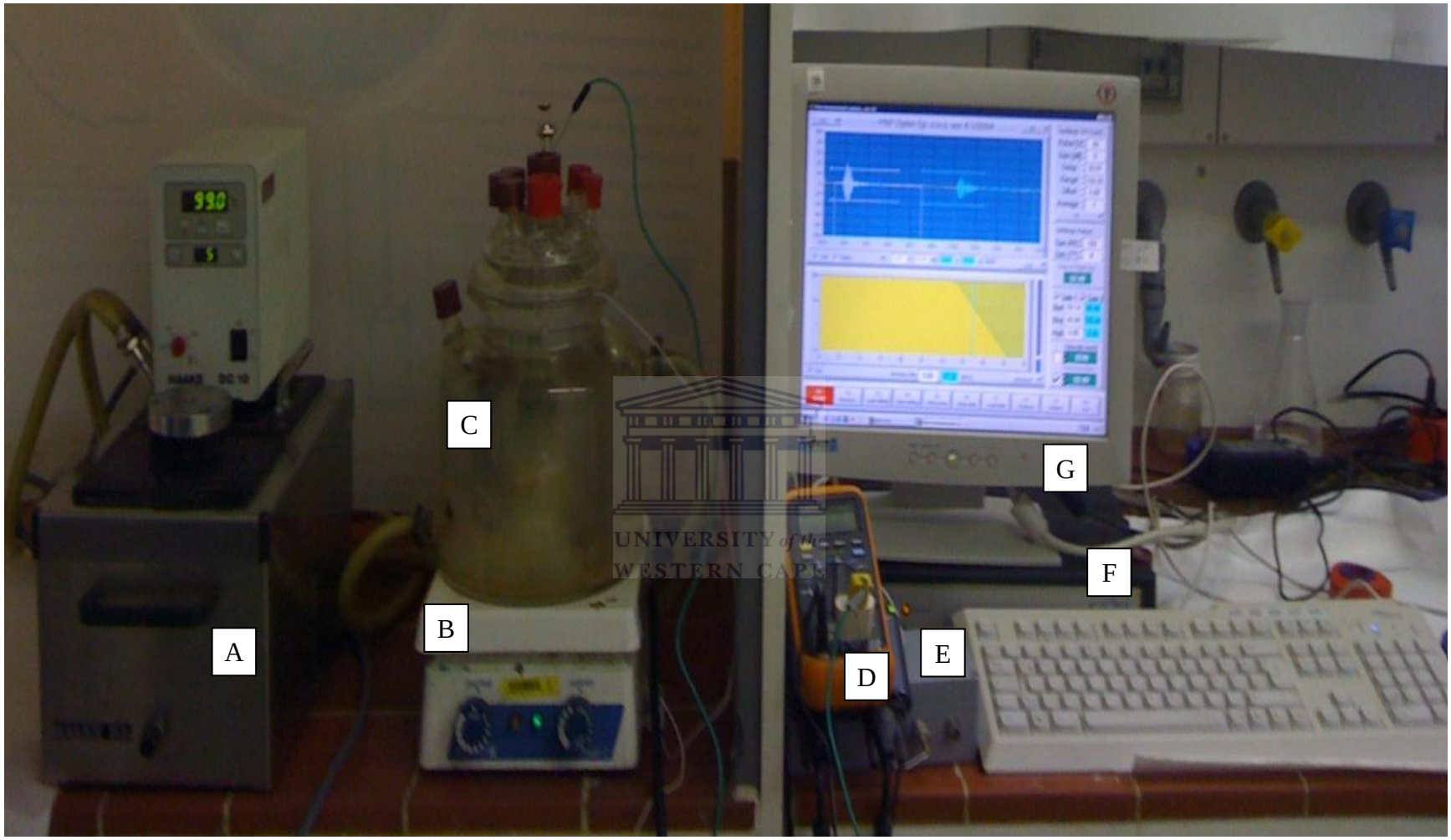

Figure 3-10: The experimental set up showing A) water bath B) magnetic stirrer C) double walled reaction container D) online temperature monitoing system E) ultrasonic pulser/receiver F) Optel box Opbox 01/100 G) computer.

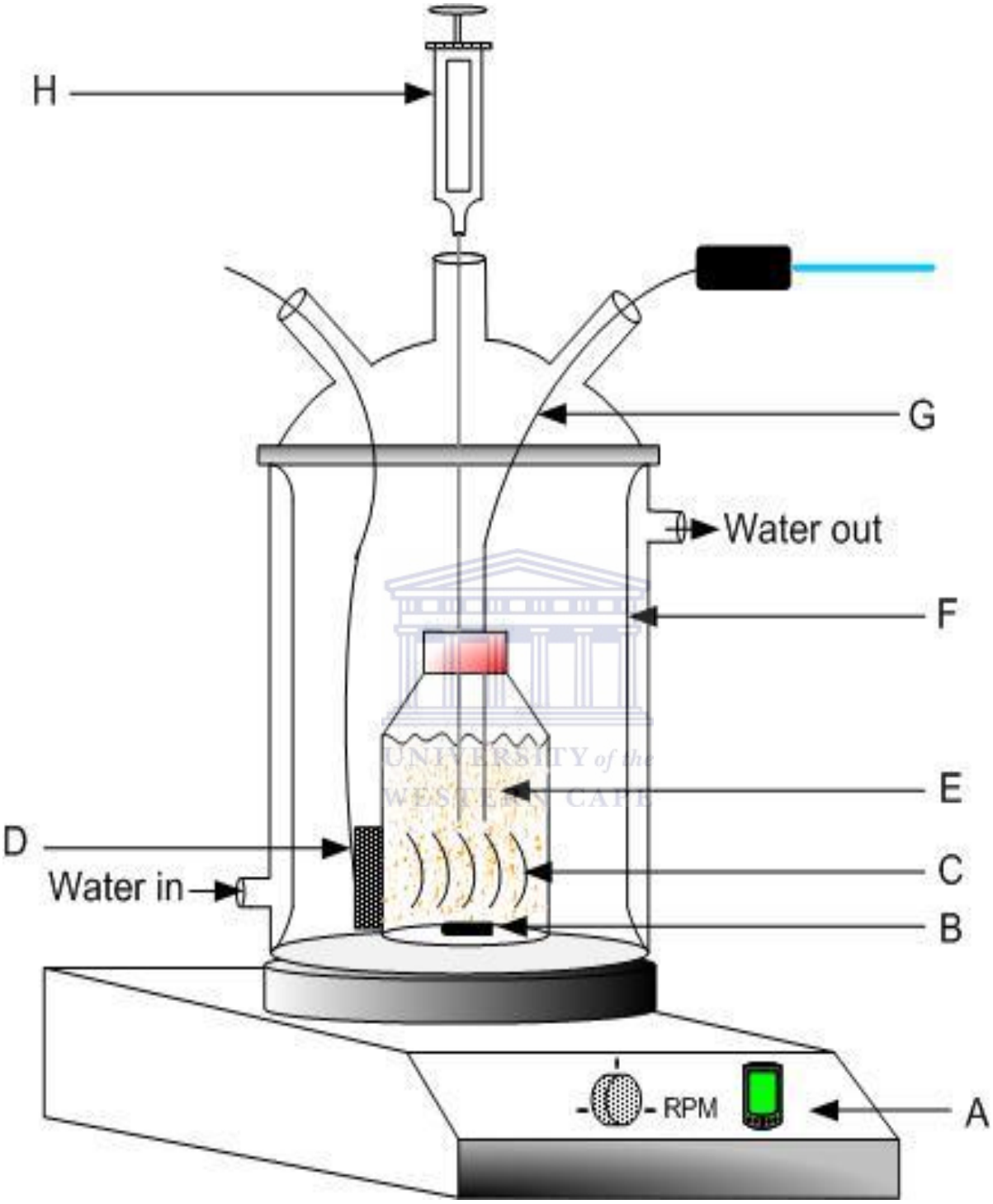

Figure 3-11: The schematic of the section of the in-situ ultrasonic monitoring set-up that housed the synthesis mixture (part c, Figure 3.10); A) magnetic stirrer, B) magnetic stirring rod, C) ultrasonic waves, D) ultrasonic transducer, E) synthesis mixture, F) thermostated double walled glass container, G) thermocouple, H) syringe.

As shown in Figure 3.11, the glass container containing the synthesis mixture had an ultrasonic transducer attached on the outer wall of the glass container. The ultrasonic signal pathway was 52 mm. The smooth surface of the glass opposite the side to which the transducer was attached acted as the reflecting surface. A syringe was inserted in the glass container and the tip was about 3 cm above the pathway of the ultrasound to enable collection of samples during the in-situ monitoring process. A thermocouple was also attached to the glass container for online temperature monitoring. The ultrasonic glass container was transferred into a double-walled glass reactor which was heated by circulating water (see Figure 3.10). Attenuation of the ultrasound signal travelling through the synthesis mixture was captured by PBP Optel software (Ver. 4.1/2004) using a Opbox 01/100 manufactured by Optel Ltd. Changes of ultrasonic attenuation were recorded after every 1 minute. The synthesis mixture was stirred during the entire in-situ monitoring process to enhance homogenization and avoid sedimentation.

3.3.2 In-situ ultrasonic monitoring of formation process of zeolite A from fly ash

3.3.2.1 Baseline study

The study began by conducting in-situ ultrasonic monitoring of blank demineralized water and NaOH (6 M) solution. The heating rate was about 0.5 ºC/min up to the final predetermined temperature of 80 ºC. These blank background experiments were to enable decoupling of the interferences caused by effect of heating on the ultrasonic attenuation. Once established, investigations of the formation mechanism of zeolite A were conducted.

3.3.2.2 Procedure for preparing zeolite A for in-situ ultrasonic monitoring

As discussed earlier in section 3.2.1, zeolite A was synthesized starting from either clear extract of fused fly ash or unseparated fused fly ash slurry. The fusion of the fly ash was conducted following the procedure reported in section 3.2.1. Since 100 mL of the precursor solution was required for the in-situ ultrasonic monitoring glass container, the amounts of feedstock material were scaled up in order to generate 100 ml of the synthesis mixture, while maintain the same molar regimes as identified in Section 3.2.2.

For the synthesis starting from the clear extract of fused fly ash slurry, fused fly ash was mixed with demineralized water in a ratio of 1:5, stirred for 2 h and the liquid phase of the resulting fused fly ash slurry was separated from the undissolved solid mater by filtration after centrifuging. 72 mL of the recovered clear solution was used as the source of Al and Si. The aluminate solution (28 mL) that provided the additional Al for crystallization of zeolite A from fly ash was prepared by mixing (1.38 g) commercial sodium aluminate solid (Riedel-de Haën) and (2.76 g) sodium hydroxide (Merck) in water (28 mL). The resulting precursor mixtures (100 mL) obtained by mixing the clear extract of fused fly ash with the aluminate solution had a molar ratio of 1 Al_2O_3 : 30.84 Na_2O : 4 SiO_2 : 414.42 H_2O. For the synthesis starting from unseparated fused fly ash slurry, 72 mL of the unseparated fused slurry was mixed with the 28 mL to generate the required volume (100 mL). The molar regime of the resulting synthesis mixture was; 1 Al_2O_3 : 5.39 Na_2O : 2.75 SiO_2 : 111.82 H_2O. On different experimental runs, the mixtures prepared starting from either clear extract or unseparated fused fly ash were transferred into the in-situ ultrasonic monitoring glass container (Figure 3.11). The heating rate was around 0.5 $^{\circ}$C/min and for the initial investigation, the final reaction temperature for hydrothermal synthesis in each case was set at 80 $^{\circ}$C for 360 minutes.

3.3.2.3 Effect of simulation of fly ash molar regime

In order to compare the mechanism of zeolite A formation from fly ash feedstock with that from the chemical species prepared using the commercially available Si, Al and Na, the fly ash based molar composition of the synthesis mixture obtained by use of clear extract of fused fly ash (1 Al_2O_3 : 30.84 Na_2O : 4 SiO_2 : 414.42 H_2O) was simulated using pure analytical grade sources of silica (waterglass (27.34 % SiO_2, 8.37 % Na_2O, 64.29 % H_2O), sodium aluminate (28.04 % Al_2O_3, 27.40 % Na_2O, 44.56 % H_2O) and Sodium hydroxide (77.48 % Na_2O, 22.52 % H_2O). The calculations for simulation are presented in Figure A3. The actual amounts used were 5.10 g sodium aluminate, 12.33 g waterglass, 31.48 g sodium hydroxide and 87.45 g demineralised water.

3.3.2.4 Effect of ageing the synthesis mixture

To study the effect of ageing of the precursor species prepared starting from the clear extract of fused fly ash, the reaction mixture was placed in the in-situ ultrasonic monitoring glass container

to age at room temperature for different periods (360, 720 and 1050 min) before heating was commenced. The heating rate was around 0.5 ˚C/min and the final reaction temperature for hydrothermal synthesis was set at 80 ˚C for 360 min.

3.3.2.5 Effect of variation of hydrothermal crystallization temperature

In order to study the effect of temperature during the in-situ ultrasonic monitoring of formation process of zeolite A starting from either clear extract of fused fly ash or unseparated fused fly ash ash slurry, three hydrothermal crystallization temperatures were investigated i.e 80, 90 and 94 ºC. In all these experiments the heating rate was still at around 0.5 ˚C/minutes. The higher temperature was limited to 94 ºC because the heating system was based on thermostated circulating water and it had been found that the synthesis lasting up to 20 hours could be conducted without requiring additional water to be added to the thermostated system that had been lost due to evaporation.

3.3.3 Complementary ex-situ monitoring of zeolite A formation process

Small well mixed aliquots (4 ml) were extracted using a syringe (Figure 3.11) at predetermined times (0, 30, 60, 90, 120, 150, 200, 210, 220, 240 and 360 minutes) from the reaction mixture prepared using clear extact of fused fly ash as presented in section 3.3.2.2. The sampling was done using a syringe which did not disturb the ongoing in-situ ultrasonic monitoring process. Extracted samples were used for complementary ex-situ characterization. In each case, the extracted samples were separated by filtration after centrifuging the sample. The recovered solids were further washed using demineralized water and dried overnight at 110 ˚C prior to ex-situ analysis. The concentration of Si and Al in the liquid phase was determined using Inductively Coupled Plasma Atomic Emission Spectrometry (ICP-AES, Perkin-Elmer). Crystallinity and mineral phase content of the solid samples were measured using a Philips X-pert pro MPD X-ray diffractometer. Morphological analysis of the solid samples was conducted using a scanning electron microscope (ULTRA55 (Carl Zeiss MST AG)). Structural analysis of the solid samples was conducted using a Fourier Transform Infra-red spectrometer (JASCO FT/IR-4100).

3.3.4 In-situ ultrasonic monitoring of zeolite X formation from fly ash

The procedure for in-situ monitoring of zeolite X was based on the use of only the clear solution extracted from fused fly ash. The fused fly ash solid-to-water mass ratio used during the extraction process was 1:2.5. The same setup that was used for ultrasonic monitoring of formation process for zeolite A was used for monitoring zeolite X formation (see Figures 3.10 and 3.11). The initial experiments were conducted using a reaction mixture with a molar regime of 1 Al_2O_3 : 56.80 Na_2O : 16.62 SiO_2 : 954.05 H_2O at hydrothermal synthesis conditions of 80 ºC for 6 hours. Furthermore, in order to evaluate the effect of temperature on the resulting in-situ attenuation signal, two higher temperatures (90 and 94 ºC) were also investigated. The heating rate was about 0.5 ºC/min up to each of the final predetermined temperatures. As mentioned in Section 3.2, the main difference between the procedures for synthesis of zeolite X compared with that of zeolite A was that the procedure for producing zeolite X required no additional Al to be added to the synthesis mixture. It should be noted that unlike the procedure used when synthesizing zeolite X from unseparated slurry under static hydrothermal conditions which was reported in Section 3.2.2.1, the ultrasonic monitoring of the crystallization process was performed on a magnetically stirred system to avoid settling of the product as it was being formed, which if left to sediment, would have interfered with the monitoring process.

3.4 Direct and ultrasonic assisted synthesis of zeolites from fly ash

The main purpose for conducting experiments in this Section were; i) to improve the hydrothermal synthesis conditions for producing zeolite A, identified in Section 3.2.2, by using ultrasound to accelerate the crystallization process and ii) investigate the possibility of using ultrasound to synthesize zeolites directly from as-received fly ash which would enable elimination of the alkali fusion step as well as the hydrothermal step altogether.

3.4.1.1 Equipment used for direct and ultrasonic assisted synthesis

An Omni Sonic Ruptor 400 Ultrasonic Homogenizer (400 Watt maximum Power, 20 kHz system) was used in this study (Figure 3.12). The instrument has the capability of processing samples ranging from 0.25 to 1000 mL. It is important to highlight that the instrument has the following features; variable power supply, auto-tuning for optimal processing efficiency, power-

emitted display for accuracy and repeatability, 0-15 minute timer, tips compatible with most 20 kHz systems and pulse mode option. For all the experiements conducted in this study, the power was adjusted to 100% and the pulse control was set to read 100%.

Figure 3-12: Omni Sonic Ruptor 400 ultrasonic homogeniser.

3.4.2 Ultrasonic assisted ageing process prior to hydrothermal crystallization of zeolites

This Section builds on the experiments conducted in Section 3.2.2. The aim was to apply ultrasound prior to the hydrothermal crystalization step in order to accelerate the crystallization process. In this case, instead of subjecting the reaction mixture directly to the heated hydrothermal crystallization step at 100 °C for 2 hours (as had been done in Section 3.2.1.1 and 3.2.1.2), the reaction mixture that was derived from either unseparated fused fly ash slurry or from clear extract of fused fly ash was sonicated for 10 minutes before being transferred to the heated hydrothermal crystallization step at 100 °C for 1 hour. The details for the experiments conducted using pure water are presented in Table 3.6.

Table 3-6: Experimental details for ultrasonic assisted synthesis of zeolite A from either clear extract of fused fly ahs or fused fly ash slurry using our water (based on preparation of 100 mL reaction mixture).

	Synthesis from clear extract of fused fly ash slurry	Synthesis from unseparated fused fly ash slurry
Preparation of fused fly ash slurry/clear extract	Alkali fusion of fly ash (refer to Section 3.2.1) For each case, 16 g fused fly ash+80 mL water+stirring for 2 hours either filterd (clear extract) or used as unseparated slurry	
Volume of fused slurry or clear extract + Volume of Na-aluminate solution	72 mL of the recovered clear solution 28 mL water+1.38 g Na-AlO_2+2.76 g NaOH	72 mL of fused fly ash slurry 28 mL water+1.38 g Na-AlO_2+2.76 g NaOH
Resulting molar regime	1 Al_2O_3 : 30.84 Na_2O : 4 SiO_2 : 414.42 H_2O	1 Al_2O_3 : 5.39 Na_2O : 2.75 SiO_2 : 111.82 H_2O
Sonication time	10 minutes	10 minutes
Hydrothermal synthesis temperature and time	100 ˚C for 1 hour	100 ˚C for 1 hour

In order to investigate the effect of sonication when mine waters were used as a substitute for pure, circumneutral mine water and acid drainage mine water were independently used as a substitute for pure water in every stage of the synthesis process for zeolite A shown in Table 3.7.

Table 3-7: Synthesis conditions for preparation of zeolite A starting from 'clear' extract of fused fly ash using mine waters as a substitute for pure water (based on preparation of 100 mL reaction mixture).

Effect of use of mine waters as a substuture of pure water during synthesis of zeolite A	Circumneutral mine water	Acid drainage mine waters
Extract of fused fly ash (using mine waters):	72 mL extract of fused fly ash using circumneutral mine water	72 mL extract of fused fly ash using acid drainage mine waters
+		
Aluminate solution:	28 mL circumneutral mine water +1.38 g Na-AlO_2+2.76 g NaOH	28 mL acid drainage mine waters +1.38 g Na-AlO_2+2.76 g NaOH
Molar regime of the resulting synthesis mixture	1 Al_2O_3 : 28.75 Na_2O : 3.06 SiO_2 : 380.16 H_2O	1 Al_2O_3 : 23.32 Na_2O : 2.82 SiO_2 : 315.60 H_2O
Sonication time	10 minutes	
Hydrothermal synthesis temperature and time	100 ˚C for 1 hour	

For sonication experiements shown in Table 3.6, the resulting 100 mL of the was poured into a 100 mL plastic beaker and was placed on the sample platform of the Omni Sonic Ruptor 400 ultrasonic homogenizer and approximately 3 cm of the standard processing tip (3/4'') was inserted in the solution (as shown in Figure 3.13) before sonication (10 minutes) commenced.

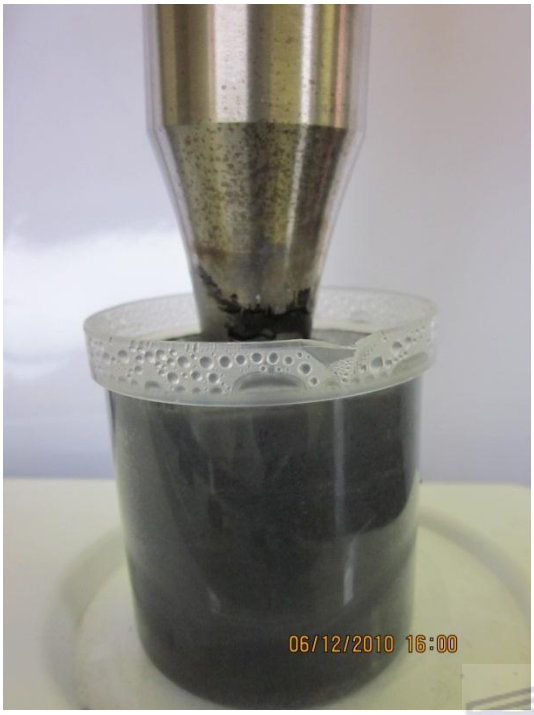

Figure 3-13: Standard ultrasonic processing tip (3/4'') inserted in the synthesis mixture.

For all the experiements listed in Table 3.6 and 3.7, hydrothermal treatment was conducted by pouring the reaction mixture into different 23 mL Teflon cups of the Parr Bombs (Figure 3.4). The filled Teflon cups were inserted in their respective steel Parr casings and sealed tightly. The filled and sealed Parr Bombs were placed into a Memmert hot air oven where the temperature was st at 100 ˚C from 1 hour.

3.4.3 Direct synthesis of zeolites without the need for hydrothermal crystallization step

This Section of the study was aimed at investigating the possibility of applying ultrasonic energy to generate zeolites directly from the as-received South African fly ash sourced from Arnot power plant. The source of the Ultrasonic energy was the Omni Sonic Ruptor 400 ultrasonic homogenizer presented in Figure 3.12. The power setting of the Omni Sonic Ruptor 400 ultrasonic homogenizer was set at its maximum (100 %) and the pulse control also set to read 100 %.

In the intial phase of this study, it was of interest to understand the reactivity of fly ash in terms of dissolution behaviour of Si and Al upon application of ultrasound so as to explain some of the

observations noted after the sonication process. The variables investigated included the effects of varying NaOH concentration, sonication time, stirring and fly ash particle size**.** Studies on the respective variations of parameters under investigation are reported in the subsections below.

3.4.3.1 Effect of variation of NaOH concentration on the dissolution behaviour of sonicated fly ash without a fusion step

During the investigation of the effect of the NaOH concentration on the dissolution behaviour of the as-received South African class F fly ash, four NaOH concentrations (1 M, 3 M, 4 M and 7 M) were studied. In each experimental run, the fly ash-NaOH slurry was prepared by mixing 20 g of the as-received fly ash with predetermined weights of NaOH pellets. 100 mL of water was added to each of the respective fly ash-NaOH mixtures to generate about 100 mL of the final ash slurry that was ready to be sonicated. The resulting ash slurry was poured into a 100 mL graduated plastic beaker (see Figure 3.13) and was placed on the sample platform of the Omni Sonic Ruptor 400 ultrasonic homogenizer. Approximately 3 cm of the standard processing tip (3/4'') was inserted in the solution, followed by sonication for 10 minutes. After sonication of each of the different variations of fly ash-NaOH slurries, the solid and liquid supernatant was separated by filtration and the dissolution of the fly ash was monitored by analysing the resulting liquid supernatant for Si and Al using ICP-AES.

3.4.3.2 Effect of sonication time on the dissolution behaviour of the as-received fly ash

The effect of sonication time on the dissolution behaviour of the as-received South African class F fly ash was investigated by fixing NaOH concentration at 5 M. The as-received fly ash-NaOH slurry was prepared by mixing 20 g of the as-received fly ash with 20g of NaOH pellets with addition of 100 mL water in a 100 mL graduated plastic beaker (as shown in Figure 3.15). The choice of the 5 M NaOH concentration was guided by the results of the experiments run in Section 3.4.3.1. The sonication time was varied as follows 5, 10, 15 and 30 minutes. The dissolution trend was monitored by extracting aliquots after the specified sonication time and after filtering out the solids, analysis of Si and Al content in the solution was done by using ICP-AES.

3.4.3.3 Effect of stirring during sonication on the dissolution behaviour of the as-received fly ash

The effect of stirring the fly ash-NaOH-water mixture during sonication was investigated at a NaOH concentration and sonication time of 5 M and 10 minutes respectively. The as-received fly ash-NaOH slurry was prepared as detailed in Section 3.4.3.2 and instead of placing the sample on the sonicator's sample platform, the sample was placed on a magnetic stirrer and a magnetic stirring bar was placed in the slurry. The magnetic stirring was conducted whilst sonication continued. The dissolution trend was monitored by determining levels of Si and Al in the filtered aliquots sampled at the end of the set time period.

3.4.3.4 Effect of fly ash particle size on the dissolution behaviour of the as-received fly ash

In order to study the effect of fly ash particle size, the as-received South African fly ash was sieved through 90 µm, 150 µm and 212 µm mesh sieves. Each experimental run, based on a different fly ash particle distribution, was studied at a NaOH concentration of 5 M and sonication time of 10 minutes. The dissolution trend was monitored by determining the levels of Si and Al in the filtered aliquots sampled at the end of the 10 minutes sonication.

3.4.3.5 Effect of hydrothermal treatment of the already sonicated as-receiced fly ash.

After the as-received South African fly ash was sonication for 10 minutes as detailed in Section 3.4.3.2, about 10 mL of the resulting product was transferred into a 23 mL Parr bomb (Figure 3.4). Crystallisation of the feedstock was achieved by placing the mixture in sealed Parr bombs in a thermostated Memmert hot air oven set at 140 °C for 48 hours. After the hydrothermal treatment step, the Parr bombs were removed from the oven and allowed to cool down to room temperature. The liquid phase was separated from the resulting synthesis product by filtration and then the solid product was washed with deionised water until a filtrate pH of 9 -10 was obtained. The recovered solid product was dried overnight at 90 ^{o}C and then transferred into airtight plastic containers prior to characterization.

3.5 Characterization techniques

3.5.1 pH measurements

The pH measurement of the mine water and the supernatant obtained after zeolite synthesis was measured by using a Hanna HI 991301 pH meter with portable pH/EC/TDS/Temperature probe. The pH meter was calibrated before use with buffer solution of pH 4.01, 7.01 and 10. Duplicate samples measurements were conducted at room temperature to ensure replicability of the results.

3.5.2 Elemental analysis

3.5.2.1 X-ray Fluorescence Spectroscopy analysis

The X-ray Flourescence spectroscopy (XRF) was used to carry out multi-element analysis of the starting feedstock fly ash and the synthesized zeolitic materials. The samples were prepared by mixing 9 g of fly ash or zeolitic material with 2 g of a binder (which was made up of 10 % C-wax binder and 90 % EMU powder. The mixture was then thoroughly shaken, poured into the mould and pelletized at a pressure of 15 tons for about 1 minute using a Dickie and Stockler manual pelletizer. Loss on ignition (LOI) was measured by placing the samples in a furnace at 1000 °C for at least 45 minutes. Analyses were done on a Philips PW 1480 X-ray fluorescence spectrometer. The spectrometer was fitted with a Chromium tube, five analyzing crystals namely LIF 200, LIF 220, GE, PE and PX and the detectors were a combination of gas-flow proportional counter and a scintillation detector. The gas-flow proportional counter uses P10 gas, which is a mixture of 90 % argon and 10 % methane. Major elements were analysed on a fused glass bead at 40 kV and 50 mA tube operating conditions and trace elements were analyzed on a powder briquette at 50 kV and 40 mA tube operating conditions. Matrix effects in the samples were corrected for by applying theoretical alpha factors and measured line overlap factors to the raw intensities measured with the SuperQ Philips software. To assess replicability of the XRF results, the analysis was conducted in triplicate.

3.5.2.2 Inductively Coupled Plasma (Atomic Emission and Mass) Spectroscopy

The concentrations of ionic species in the zeolite post-synthesis aqueous supernatant solution as well as mine waters, inductively coupled plasma atomic emission (ICP-AES) and mass spectrometry technique (ICP-MS) were used. The instrument used for the majors was a Varian

Radial ICP-AES, while traces were done on an Agilent 7500ce ICP-MS, using a High Matrix Introduction (HMI) accessory and He as collision gas. For both instruments, external calibration was performed daily, and results of a quality control standard to verify accuracy was included with every batch of samples analyzed. For ICP-MS analysis, internal standards were used to correct for matrix effects and instrument drift. Samples were diluted 20 times for majors and traces, with data corrected for dilution factors. Analysis was done in triplicate.

3.5.3 *Mineralogical characterization by X-ray Diffraction Spectroscopy*

3.5.3.1 Qualitative XRD analysis

The mineralogy of the as-received fly ash, fused fly ash and synthesized zeolitic samples was analyzed using a Philips X-pert pro MPD X-ray diffractometer with Cu-K radiation at 40 kV and 40 mA. In order to collect the spectral data, the raw materials (raw and fused fly ash) and zeolitic samples were ground to a fine powder and mounted onto sample holders and were scanned over a range of 4˚ to 60˚ 2θ. Crystalline phases were identified with the help of Highscore Xpert software by comparing spectra with the standard line patterns from the powder diffraction file database supplied by International Centre for Diffraction Data (ICDD).

3.5.3.2 Quantification of mineral and amorphous phases in fly ash

After addition of 20 % Si (Aldrich 99 % pure) for determination of the amorphous content and milling in a McCrone micronizing mill, the samples were prepared for XRD analysis using a back loading preparation method. Samples were analysed with a PANalytical X'Pert Pro powder diffractometer with X'Celerator detector and variable divergence- and receiving slits with Fe filtered Co-Kα radiation. The phases were identified using X'Pert Highscore plus software. The relative phase amounts (weight %) was estimated using the Rietveld method (Autoquan Program).

3.5.4 *Physical characterization by morphological analysis*

3.5.4.1 Scanning Electron Microscopy

The morphology of the starting materials (as-received and fused fly ash) and the synthesized zeolitic products was investigated by use of ultra high resolution FESEM, (Carl Zeiss MST AG) ULTRA 55 (University of Erlangen). Due to limitations to access of the ULTRA55 instrument,

other samples were analysed using Nova NanoSEM 230 (University of Cape Town) and Hitachi X-650 Scanning electron microanalysser (University of Western Cape) equiped with a CDU – lead detector at 25 Kv. Details for the operating conditions for analysis conducted using ULTRA 55 and Nova NanoSEM 230 instruments are captured in each of their respectice SEM micrographs. For all the morphological analysis, the already ground samples (dried powdery starting material or zeolite powder) were dusted onto aluminium stubs that had been lined using a double-sided adhesive carbon discs. The specimens were then observed under the SEM microscope under different magnifications. For Energy dispersive spectroscopic (EDS) analysis, the same samples were used.

3.5.4.2 Transmission Electron Microscopy

For TEM analysis, samples were analyszed using a Tecnai G2 F20 X-Twin MAT high resolution transmission electron microscope (HRTEM) with Field Emission gun lens 1 with spotsize 3, at 200 kV. The samples were prepared by diluting a suspension of the synthesis products in ethanol, ultrasonicating it for 5 minutes and depositing a drop onto S147-4 Holey carbon film 400 mesh Cu grids. Samples were thereafter mounted in a sample holder, which was introduced directly into the shaft of the microscope.

3.5.5 *Structural analysis: Fourier Transform Infrared Spectroscopy*

Fourier Transform Infrared spectroscopy **(**FT-IR) was used to provide information about molecular structure of the starting material (as-received and alkali fused fly ash) and also monitor evolution of crystallinity during the synthesis process. Attenuated total reflectance (ATR) FT-IR is less complicated than using KBr pellets and requires virtually no sample preparation, is fast and a very small amount of the sample is needed. In this case, approximately 15 mg of the sample was placed on the Attenuated Total Reflectance (ATR) sample holder; a force was applied to the sample before the collection of the spectrum, baseline was corrected and the spectra smoothened. Two models of the FT-IR instrument models were used. For the FT-IR results presented in chapter 6, a JASCO FT/IR-4100 (University of Erlangen) was used. An improvised circular plastic gadget was used to contain Argon gas during analysis as shown in Figure 3.16. This improvisation was done to prevent absorption of moisture during the sample analysis in order to avoid the masking of important details in the spectra that can be obscured by

the water bands. The Perkin Elmer spectrum 100 FT-IR spectrometer was used for the FTIR analysis presented in the other chapters (4, 5 and 7). Though the spectra were recorded in the range of 4000-400 cm^{-1}, in transmission mode, only regions of most interest were highlighted in the results and discussion.

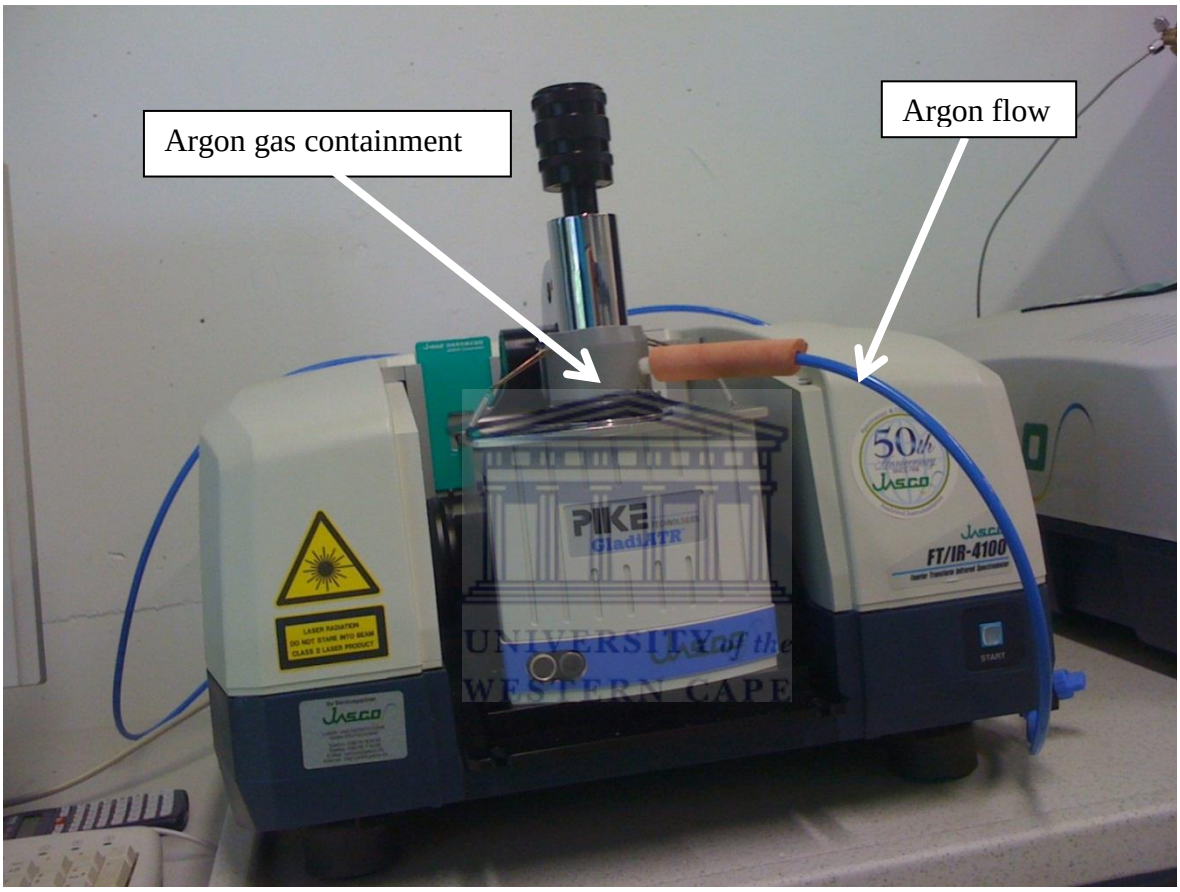

Figure 3-14: JASCO FT/IR-4100 with an improvised flow of Argon gas during analysis.

3.5.6 *Surface area and pore size determination*

Physical analysis of the synthesized zeolitic products to determine surface area and pore size distribution was conducted by nitrogen adsorption using the Brunauer-Emmett-Teller (N_2-BET) surface analysis technique. The sample to be analysed (0.35 – 0.5 g) was outgassed at 250 °C on the Flow Prep 060 using helium gas. Micromeritics Tristar instrument was used with nitrogen as the analysis gas based on a 5 point with 30 adsorption and 30 desorption points, together with a total surface area measurement.

3.5.7 *Thermal stability analysis of the zeolitic product synthesized from fly ash*

3.5.7.1 Temperature programmed XRD analysis

Temperature-induced phase transition or possible structural collapse of the zeolitic samples were studied using automated temperature controlled X-ray analysis studies. PANalytical X'Pert Pro powder diffractometer with X'Celerator detector and variable divergence and fixed receiving slits with Fe filtered Co-Kα radiation was used. Mineralogical temperature-induced phase transition investigations were carried out by attachment of Anton Paar HTK 16 High-Temperature Chambers where the sample was directly heated with a heating strip. The mineral phases were identified using X'Pert Highscore plus software.

3.5.7.2 Thermogravimetric analysis

The synthesized zeolitic products were analyzed for thermal stability and volatile content by SDT 2960 Simultaneous DSC-TGA from TA Instruments (University of Erlangen) between 25 and 900 °C using a heating rate of 10 °C min^{-1} under flowing air. Approximately 25 to 30 mg of sample was ground and directly filled into the platinum crucible and TG testing initialized.

CHAPTER 4

IDENTIFICATION AND OPTIMIZATION OF SYNTHESIS CONDITIONS FOR ZEOLITE A FROM SOUTH AFRICAN FLY ASH

This chapter starts by presenting a brief motivation for conducting studies on identification and customization of the synthesis conditions for zeolite A from South African fly ashes. The physicochemical and mineralogical properties of the fly ash source used are presented. The step-wise optimization process for the synthesis conditions for zeolite A is presented based on the XRD analysis, as the main optimization guide for zeolite phase quality. Upon identifying the best conditions for formation of a single phase zeolite A, results from other complementing and confirmatory characterization techniques are presented and discussed. The results for replacement of pure water with mine waters during synthesis is also presented and discussed.

4 Introduction

It has been widely reported and established that synthesis conditions for a specific zeolite type from a particular fly ash cannot be applied directly to a different type/source of fly ash to obtain the same type and quality of zeolitic product (Querol *et al*., 2002). This is mainly because of the variability of fly ash composition and properties that depend on the coal source, type of coal burnt, boiler type and its operating conditions and the processes undergone by coal before the combustion process (Scheetz and Earle, 1998; Querol *et al.*, 2001, Iyer and Scott, 2001; Inada *et al*., 2005; Vassilev and Vassileva, 2007). Bearing in mind that South Africa utilizes low grade coal that has a high ash content to generate electricity, the fly ash produced is reportedly a good candidate for producing zeolites due to its high aluminosilicate content (Kruger, 1997; Woolard *et al*, 2000; Somerset *et al*., 2004). Despite the potential for the use of the South African fly ashes in zeolite synthesis, only a few studies have concentrated on producing zeolites from South African fly ash (Woolard *et al*, 2000; Pretorius and Woolard, 2003; Hendricks, 2005; Somerset *et al.*, 2008; Vadapalli *et al.*, 2010; Musyoka *et al.*, 2012). It is important to mention that most of the aforementioned studies either yielded mixed phase zeolites that do not attract high end industrial applications or the synthesis conditions applied were not attractive from a scale up point of view because they either took longer crystallization periods or required high activation temperatures. It is on this basis and understanding that studies presented in this chapter sought to identify, optimise and customize the synthesis conditions for producing a high phase purity of zeolite A using reasonable synthesis conditions from class F fly ashes sourced from South

African coal fired power plants. Once the conditions were identified and optimised, they served as a basis for investigating the possibility of using the mine waters as a substitute for pure water during the synthesis process. The identified conditions further built a platform for an in-depth study aimed at understanding the formation mechanism for zeolite A from fly ash (to be presented in Chapter 6). Out of the many known zeolite types that have been synthesized from fly ash, as presented in review by Querol *et al*. (2002), the main reason for identifying zeolite A as the synthesis target was based on its huge commercial importance in applications such as in catalysis, separation, water treatment, use in the detergents industries and sequestration of CO_2 among other applications (Nagy *et al*., 1998; Hui and Chao, 2006; Cubillas and Anderson, 2010).

4.1 Characterization of the starting material (Fly ash)

Understanding the physicochemical and mineralogical characteristics of the fly ash feedstock helps in predicting the types of zeolites that can possibly be made from it. This section starts by presenting results from the chemical, mineralogical and morphological analysis of fly ash sourced from Arnot power plant in Mpumalanga, South Africa. Thereafter, other South African fly ashes were analyzed to predict their potential use as a feedstock for the synthesis of zeolite A.

4.1.1 Chemical analysis of Arnot fly ash

X-ray fluorescence technique (XRF) is one of the most useful methods for bulk qualitative and quantitative analysis of fly ash because it is relatively fast, widely available, economical and does not require complicated sample preparation steps (Fatoba, 2011). In the fly ash zeolitization studies, fly ash composition is reported as one of the crucial factors influencing the zeolite synthesis process (Inada *et al.*, 2005). The XRF results presented in Table 4.1 and 4.2 give the respective major and trace elements present in fly ash sourced from Arnot coal fired power station. The analysis was conducted in triplicate (i.e. sample A, B and C – taken from different parts of the storage container) to reduce errors. Apart from showing the results from each analysis, Table 4.1 and 4.2 also present the average mass percentage together with the relative standard deviation for both major and trace elements.

Table 4-1: XRF chemical analysis of Arnot fly ash: Major elements

	Mass %				
Element (oxide)	Arnot A	Arnot B	Arnot C	Average	Std. Dev.
SiO_2	51.45	51.54	51.57	51.52	0.06
Al_2O_3	27.42	27.53	27.61	27.52	0.10
CaO	6.67	6.61	6.57	6.62	0.05
Fe_2O_3	5.02	4.95	4.92	4.96	0.05
MgO	1.97	1.96	1.95	1.96	0.01
TiO_2	1.06	1.06	1.06	1.06	0.00
K_2O	0.58	0.58	0.57	0.57	0.01
P_2O_5	0.27	0.27	0.26	0.27	0.00
Na_2O	0.09	0.08	0.09	0.09	0.00
MnO	0.05	0.05	0.05	0.05	0.00
SO_3	0.07	0.07	0.06	0.06	0.00
LOI	5.70	5.70	5.70	5.70	0.00
Sum	100.35	100.39	100.42	100.39	0.04
SiO_2/Al_2O_3	1.88	1.87	1.87	1.87	

From Table 4.1, the Arnot fly ash was found to contain primarily SiO_2, Al_2O_3 and Fe_2O_3 and these elements accounted for over 70 % of the total mass although many other elements were present in relatively lower concentration (Table 4.2). This analysis is in good agreement with a study by Koukouzas *et al*. (2007) who reported that fly ash contains most elements found in the periodical table. According to the specification of ASTM C618-84, this fly ash can be classified as class F type because the total weight percent of silicon oxide, alumina, and iron oxide is larger than 70 wt %. This class of fly ash is reported to result from the burning of the harder, older anthracite and bituminous coal (Vassilev and Vassileva, 2007). The average SiO_2/Al_2O_3 ratio of the Arnot fly ash was found to be 1.87 and was thus suitable for the synthesis of mostly low

silica zeolites. This ratio is also known to influence the final Si/Al ratio of the synthesis product (Szostak, 1998). The degree of reactivity of fly ash towards zeolite formation has been reported to be directly dependent on the SiO_2/Al_2O_3 ratio, Fe_2O_3 and CaO content (Rayalu *et al*., 2001). Based on the analysis presented in Table 1, it was possible to predict that this fly ash would require less additional sodium aluminate which would end up reducing the cost of producing of zeolite A compared to other sources of fly ash (Rayalu *et al*., 2001).

The fly ash was also noted to have a relatively low CaO and MgO content. Ca^{2+} and Mg^{2+} together with Na^{+} can act as competing counter ions during the crystallization of zeolites. Fly ashes with very high Ca-bearing phases such as calcium silicate are reported to be unfavorable for zeolite synthesis firstly because they are hard to dissolve (Juan *et al*., 2007; Ríos *et al*., 2009) and secondly because the high amount of Ca^{2+} is associated with the structure breaking properties which lead to suppression of the zeolite crystallization process (Catalfamo *et al*., 1997). The relatively lower Fe content in the fly ash could give an indication that the fly ash contained less Fe-bearing minerals which also tend to be difficult to demineralize (Juan *et al*., 2007). The Fe and Ti that could be present in the synthesis mixture have been reported to isomorphously substitute Al in the zeolitic framework (Nagy 1998). The measurement of Loss-On-Ignition (LOI) which is a combined effect emanating from the loss of weight occurring due to the presence of carbonates, free carbon and water when fly ash is burned (Alonso and Wesche, 2005), could also help in predicting the potential for producing quality zeolites from fly ash. Rayalu *et al*. (2001) pointed out that large amounts of unburnt carbon could interfere with the fusion step which impacts on the quality of the fused product.

The distribution and types of trace elements present in Arnot fly ash are presented in Table 4.2. The concentration of elements was presented in ascending order of magnitude so as to simplify comparison. The presence or absence of these trace elements in fly ash is not only known to influence the eventual application of fly ash but can also help predicting the potential quality of the synthesized zeolitic product (Liu *et al*., 2004).

Table 4-2: XRF chemical analysis of Arnot fly ash: Trace elements

Element (ppm)	Arnot A	Arnot B	Arnot C	Average	Std. Dev.
Sr	1365.28	1363.11	1379.12	1369.17	8.68
Zr	638.14	637.99	642.23	639.45	2.41
Ba	418.25	389.90	391.18	399.78	16.01
Cr	235.68	233.45	230.75	233.29	2.47
Ce	228.23	216.54	212.59	219.12	8.13
Ni	111.87	107.76	98.56	106.06	6.82
Cu	100.79	105.31	137.15	114.42	19.82
Y	92.09	95.21	94.04	93.78	1.58
Zn	88.73	83.25	112.65	94.88	15.64
Pb	83.32	84.90	96.48	88.23	7.19
V	76.68	83.64	85.50	81.94	4.65
Rb	60.63	60.41	59.36	60.13	0.68
Th	43.36	42.52	42.78	42.89	0.43
Nb	40.86	39.23	38.68	39.59	1.13
U	35.53	36.80	17.80	30.04	10.62
Co	27.73	26.59	22.02	25.45	3.02
Mo	2.23	2.22	2.24	2.23	0.01

From Table 4.2, it was noted that apart from relatively high levels of Sr, Zr, Ba, Cr, and Ce ranging between 219 – 1369 ppm, the concentration of most trace elements was found to be less than 200 ppm. Certain elements such as Cd, Cr and Ni have been reported as carcinogens, their quantities and mobility from fly ash is an important topic in the current literature (Segun, 2011; Fatoba, 2011). The distribution of trace elements in fly ash, just like the major elements, can be related to the coal sources and also on the coal combustion technology used (Querol *et al*., 2001).

Different researchers have reported that trace elements in fly ash are found to be heavily concentrated in the finer particles of fly ash (Muriithi *et al*., 2011). As reported by Goodarzi (2006), the concentrations of elements such as Pb, Ga, Ca, Cu, Mo, S, Sb, Se, TI and Zn were found to increase as the fly ash particle size decreased. Other studies have reported that most of these elements are not fully bound to the fly ash particles and are able to leach out from fly ash at varying degree depending on the prevailing conditions (Querol *et al*., 2001; Akinyemi, 2011; Fatoba, 2011).

4.1.2 Mineralogical analysis of Arnot fly ash

Figure 4.1 compared the mineralogy of the as-received and alkali fused South African Arnot fly ash as determined by the XRD technique following the procedure described in Chapter 3, Section 3.5.3.1. The alkali fusion of the fly ash involved mixing the as-received fly ash with NaOH in a mass ratio of 1:1.2 and heating it in an oven at 550 ºC for 1.5 hours as described in the experimental section detailed in Chapter 3, Section 3.2. The knowledge of mineralogical variability of different fly ashes, well in advance, could help in assessing the potential of a particular fly ash to act as a feedstock for zeolite synthesis (Querol *et al*., 2002).

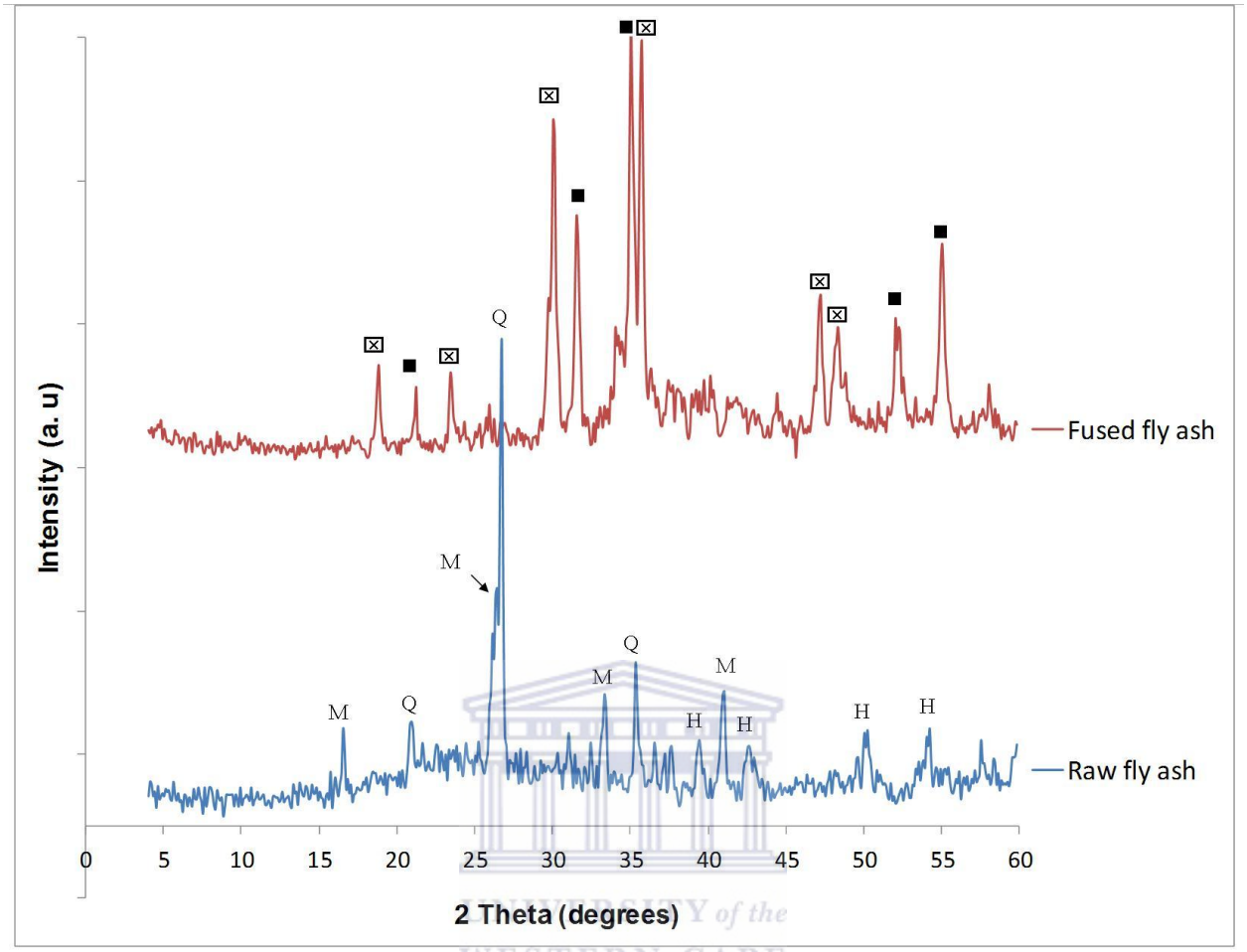

Figure 4-1: Mineralogy of the as-received (raw) and alkali fused South African fly ash (Q = Quartz, M = Mullite, H = Hematite, Mag = Magnetite, ☒ = Na_2SiO_3, ■= Na_2AlO_2).

From the X-ray diffraction pattern presented in Figure 4.1, the major crystalline phases in the Arnot fly ash were found to be Quartz (SiO_2), Mullite ($3Al_2O_3.SiO_2$), Magnetite and Hematite. The glassy amorphous material was identified as the broad hump in the XRD spectra which was observed to occur between 20 and 40° 2θ. This hump was also identified by other researchers (Inada *et al*., 2005a; Criado *et al*., 2007; Ríos *et al*., 2009). In the XRD pattern of the fused fly ash, the main mineral phases were Na-aluminate and Na-silicate as shown in Figure 4.1 and no presence of Quartz, Hematite and Mullite remained. These new mineral phases were formed from transformation that occurred during the solid-state reactions of the as-received fly ash with the NaOH in the presence of heat as illustrated in Equation 4.1 (Ojha *et al*., 2004).

$$NaOH + xAl_2O_3.ySiO_2 \xrightarrow{\text{Fusion}} Na_2SiO_3 + Na_2AlO_2 \qquad \text{Equation 4.1}$$

Quantitative XRD analysis was performed as per the procedure detailed in Chapter 3, Section 3.5.3.1 and the relative weight percent of the minerals and amorphous phases present in the as-received Arnot fly ash are presented in Figure 4.2.

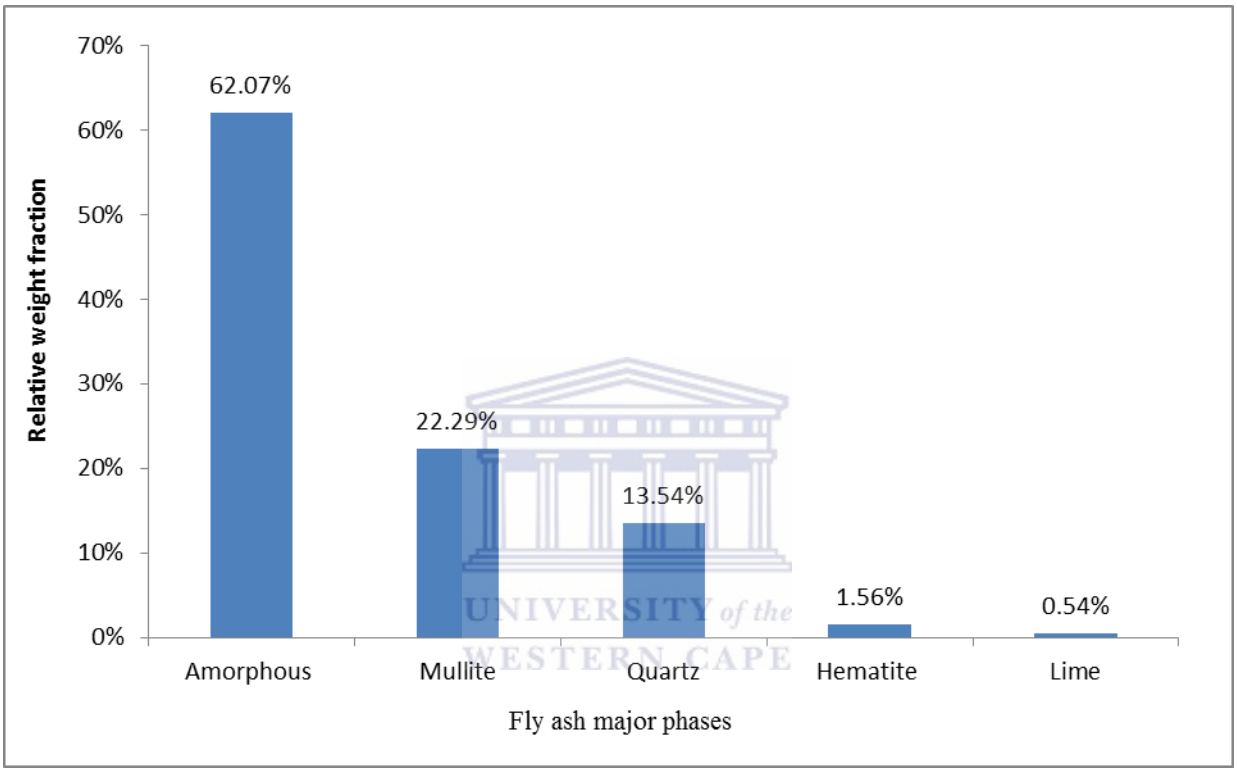

Figure 4-2: Relative XRD quantification of major mineral phases in the as-received Arnot fly ash.

The overall quantitative XRD analysis confirmed that Arnot fly ash was composed of phases that had been observed through qualitative XRD analysis presented in Figure 4.1 (i.e. Quartz, Mullite, Amorphous phase, Magnetite and Hematite). The relative mass % of the different phases was found to be in the following order: Amorphous (62.07 %) > Mullite (22.29 %) > Quartz (13.54 %) > Hematite (1.56 %) > Lime (0.54 %). The amorphous glassy phase is the most reactive phase and plays a significant role in determining the type and composition of the resulting zeolites. Fly ashes with higher weight % of glassy amorphous phase are known to lead to higher yield of zeolite (Querol *et al.*, 2001). Of the four phases, Mullite is the least reactive

(Berkgaut and Singer, 1996; Catalfamo *et al*., 1993; Mondragon *et al*., 1990) with lower quantities of Mullite known to favour zeolite crystallization (Moreno *et al*., 2002; Rayalu *et al*., 2001) and the alkali fusion process successfully decomposed this mineral phase as can be seen in Figure 4.1.. Other Fe-bearing minerals, such as Magnetite are reportedly known to be difficult to demineralize in NaOH solution (Juan *et al*., 2007). Querol *et al*. (1997) reported an increase in fly ash conversion efficiency when Magnetite was magnetically removed from fly ash before zeolite synthesis.

4.1.3 Morphological analysis of raw and fused fly ash

As mentioned by Vassilev and Vassileva (2007), SEM analysis falls in the category of technique that are highly recommended and mostly used for chemical and physical characterization of fly ash. Figure 4.3 presents the SEM micrographs that were obtained for (a) as-received Arnot fly ash (b) fused fly ash (prepared by heating a mixture of fly ash and NaOH (in a mass ratio of 1:1.2) at 550 °C for 1.5 hours).

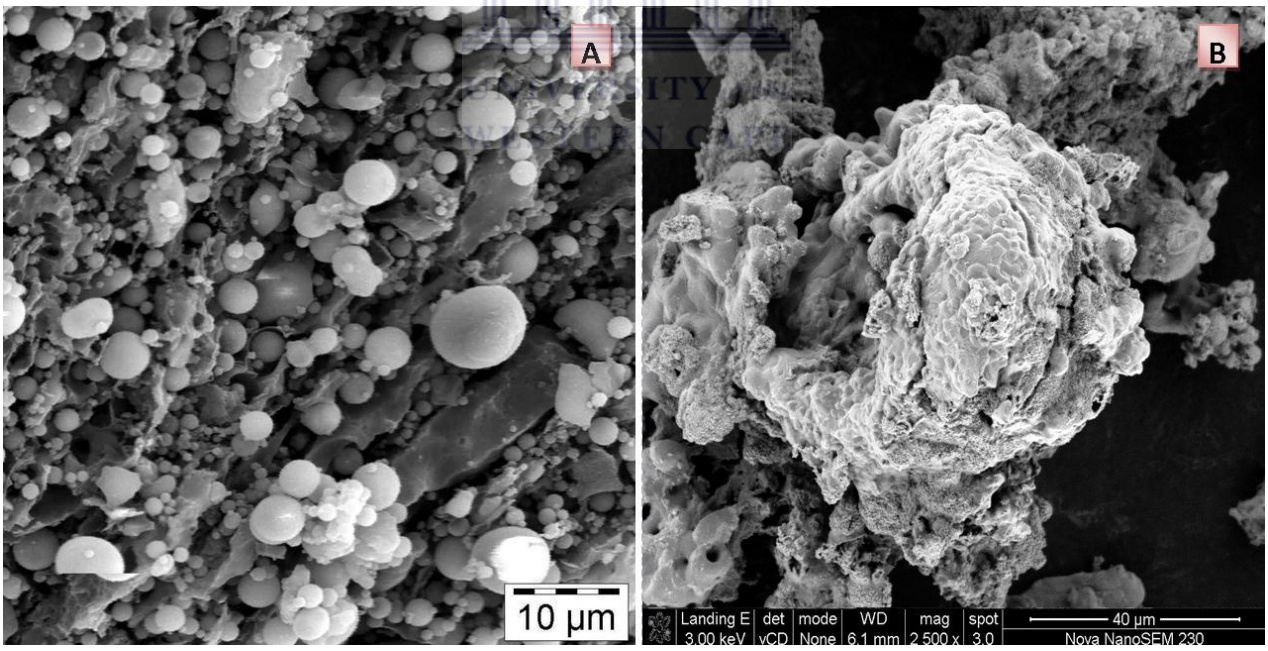

Figure 4-3: SEM micrographs of (a) as-received Arnot fly ash (b) fused fly ash (prepared by heating a mixture of fly ash and NaOH (in a mass ratio of 1:1.2) at 550 °C for 1.5 hours).

The majority of the as-received Arnot fly ash particles shown in Figure 4.3 (a) were observed to be generally spherical in shape. The spherical shaped particles are mostly related to the cooling effect since the fly ash particles solidify while suspended in the flue gases (Li *et al*., 2003; Kutchko and Kim, 2006). Their smooth surface are attributed to the fact that these particles are covered with an amorphous glass phase (Inada *et al*., 2005b). Even though the diameter of the most spherical fly ash particles is seen to be less than 10 μm, other agglomerated and bigger irregularly shaped particles can be observed in Figure 4.3 (a). The identity of the different mineralogical phases reported in Section 4.2 could not be established from the SEM analysis because the crystalline components in fly ash have been reported to be too small and too intimately inter-grown in the glass to the extent that their definitive mineral identification from micrographs would not be possible (Ward and French, 2005).

From the morphological analysis of fused fly ash, presented as SEM micrograph in Figure 3 (b), the predominant spherical particles that had been observed in the SEM micrograph of the as-received fly ash (Figure 3 (a)), had been transformed into an agglomerated porous mass after fusion. This resulting material, identified as a Na-aluminosilicate phase from XRD, was laurel-green in colour and was easy to grind. The solid-state reactions that occurred during the fusion of fly ash (heating fly ash with NaOH (ratio of 1:1.2) at 550 °C for 1.5 hours) were the main reason for the observed morphological transform. In comparison to an earlier study (Musyoka, 2009), the fused fly ash was found to be more readily soluble in both water and alkali solution which further confirmed the results reported by Shigemoto *et al*. (1993). The use of NaOH during the fly ash fusion process acts as an extra source of Na^+ cation which are known to stabilizes the sub-building units of the zeolite framework during the fly ash zeolitization process (Ojha *et al*., 2004). The OH^- from NaOH acts as a mineralizing agent to depolymerize Si content in minerals in fly ash to monomeric species.

4.1.4 Structural analysis (infra-red) of the as-received and alkali fused Arnot fly ash

The FT-IR spectra of the as-received and alkali fused South African Arnot fly ash which were obtained following the experimental procedure outlined in Chapter 3, Section 3.5.5, is presented in Figure 4.4.

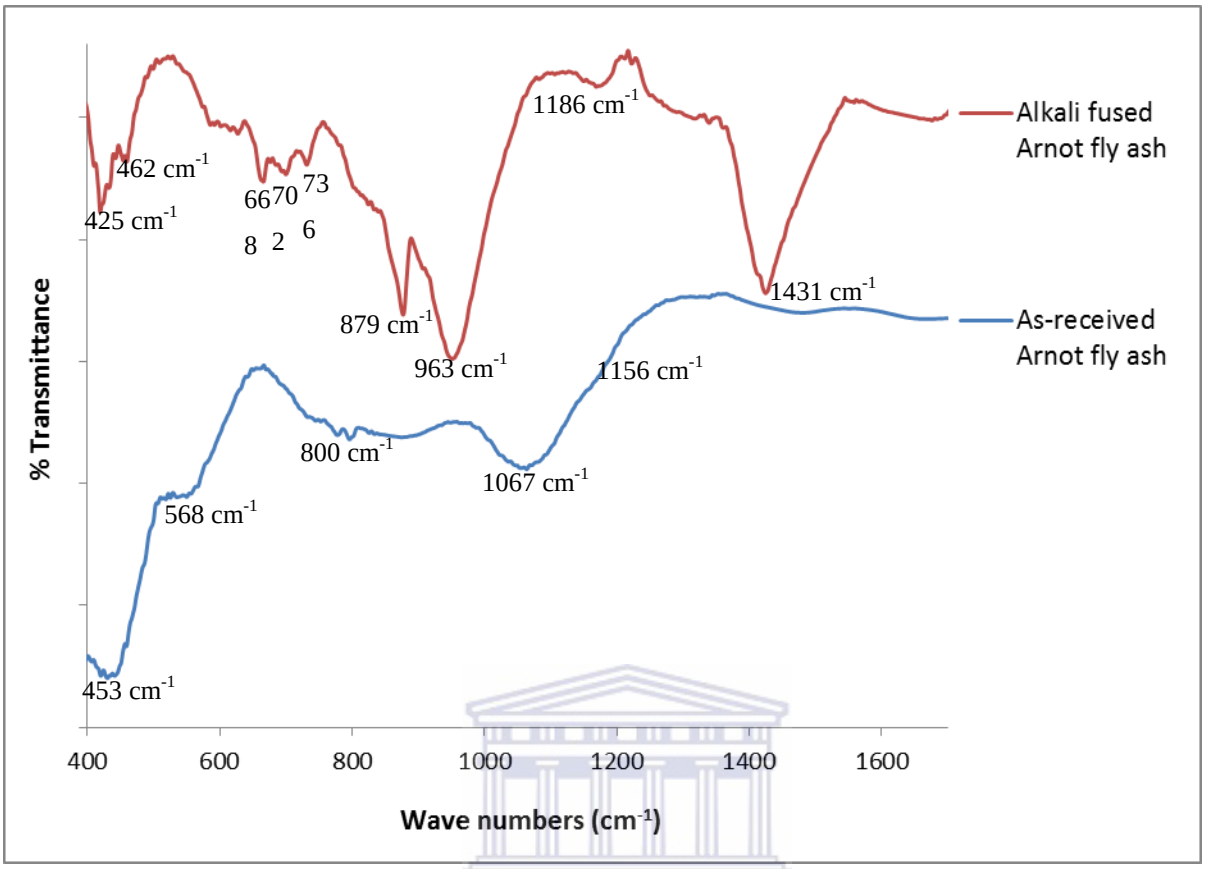

Figure 4-4: FTIR of the as-received and alkali fused South African Arnot fly ash

In the as-received Arnot fly ash shown in Figure 4.4, three wide bands characteristic of aluminosilicates were identified. These vibrational bands were: the band at 453 cm^{-1} was associated with T–O bending vibrations (Fernandez-Jimenez and Palomo, 2005); the bands appearing at around 800 cm^{-1} were associated with T–O (T = Al, Si) symmetric stretching vibrations that correspond to Quartz present in the original fly ash; the band appearing at 1067 cm^{-1} was associated with T–O (T = Al, Si) asymmetric stretching vibrations. Colthup *et al*., (1964), suggested that the band at 1156 cm^{-1} is likely to be from the asymmetrical stretching vibration and symmetrical vibration of the Al–O–Si groups, respectively. Fernandez-Jimenez and Palomo (2005) also reported those bands identified at around 568 cm^{-1} are associated with octahedral aluminium present in the Mullite phase.

According to Bass and Turner (1997), the sodium silicate species are commonly observable between 700 and 1250 cm^{-1} with the glassy sodium silicates peaks appearing below 700 cm^{-1}. In

the alkali fused fly ash shown in Figure 4.4 these peaks appearing at 702 cm^{-1} , 736 cm^{-1} , and 1186 cm^{-1} whereas the strong peaks at 870 cm^{-1} and 963 cm^{-1} are associated with crystalline orthosilicates. The peak at 462 cm^{-1} can be associated with T–O bending vibrations (Fernandez-Jimenez and Palomo, 2005). Li *et al.* (2011) reports that the peak at 879 cm^{-1} could also corresponds to condensed AlO_4 tetrahedral aluminate ion whereas the peak at 1431 cm^{-1} is associated with presence of carbonates (Zheng *et al*., 1997). In the as-received fly ash, the silicate bands are reported to be broad and diffuse because of the overlapping of different types of silicate molecular vibration resulting from various silicate minerals (Mollah *et al*., 1999).

4.1.5 Characterization of other fly ashes sourced from different South African coal fired power plants.

Since the coal burnt in different South African coal-fired power plants is mined from different geographical locations, it was deemed important to analyse fly ashes sourced from different South African coal combustion power plants to see how the compositions varied. This knowledge would be useful in predicting their potential for use as starting feedstock for synthesis of zeolite A. Table 4.3 and 4.4 presents the respective average mass % of major and trace elements as analysed in fly ash obtained from several other South African coal-fired power stations.

Table 4-3: XRF analysis of other South African fly ashes (major elements).

	Average Mass %						
Element (oxide)	Tutuka fly ash	Matla fly ash	Lethabo fly ash	Kriel fly ash	Hendrina fly ash	Duvha fly ash	Arnot fly ash
SiO_2	52.63	58.44	58.32	52.00	55.52	54.92	51.52
Al_2O_3	26.49	31.25	31.36	31.44	27.30	27.27	27.52
CaO	5.33	3.21	3.16	7.32	3.37	3.69	6.62
Fe_2O_3	4.87	3.09	3.04	2.38	3.16	4.78	4.96
TiO_2	1.46	1.17	1.16	1.25	1.00	0.3	1.96
MgO	1.31	1.14	1.13	2.03	1.22	1.07	1.06
K_2O	0.82	0.54	0.54	0.57	0.51	0.66	0.57
Na_2O	0.55	0.46	0.46	0.65	0.25	0.07	0.27
P_2O_5	0.38	0.40	0.39	0.47	0.35	0.61	0.09
SO_3	0.06	0.02	0.02	0.04	0.03	1.71	0.05
MnO	0.05	0.02	0.02	0.03	0.03	0.05	0.06
LOI	6.09	0.28	0.40	1.83	7.45	4.44	5.70
Sum	100.04	100.00	100.00	100.01	100.18	99.58	100.39
SiO_2/Al_2O_3 ratio	1.99	1.87	1.86	1.65	2.03	2.01	1.87

When compared to the XRF analysis of Arnot fly ash, the distribution of major element in Table 4.4 was found to be fairly similar apart from the relatively higher SiO_2 (52.00 – 58.32 %) and Al_2O_3 (26.49 – 31.44 %) especially in Matla and Lethabo fly ashes. Fly ash sourced from Kriel power station was noted to have a relatively higher CaO content (7.32 mass %) which implied

that it would require some adjustment in the reaction conditions to take care of the structure breaking properties associated with the high amount of Ca^{2+} (Catalfamo *et al.*, 1997). Comparing the content of Fe_2O_3 in fly ashes sourced from Matla (3.21 %), Lethabo (3.16 %), Hendrina (3.37 %) and Duvha (3.69 %) with that sourced from Arnot power station (6.62 %), these fly ashes were noted to have a relatively lower Fe_2O_3 content. The average SiO_2/Al_2O_3 ratios of the fly ashes investigated were found to range between 1.65 and 2.03 and were still within the range suitable for crystallizing low-silica zeolites (Querol *et al*., 1997). As aforementioned, this ratio plays an important role during zeolite synthesis since it dictates the framework composition of the zeolite produced (Szostak, 1998). All the above South African fly ashes still fall within the class F type (according to the ASTM standard C618) because their individual SiO_2 + Al_2O_3 + Fe_2O_3 content is greater than 70 %. The big variation in Loss On Ignition (LOI) is probably due to burner conditions at different powerstations since not all are equally effective. As for the trace element analysis presented in Table 4.4, the concentration of Ba (913.11-1271.20 ppm), Th (372.72 – 920.80 ppm) and Mo (6.35 – 16.43 ppm) was higher than that identified in Arnot fly ash (Ba (399.78 ppm), Th (42.89 ppm) and Mo (2.23 ppm)). Comparing the concentration of the other trace elements (Zr, Ce, V, As, Nb, Cu, Pb, Rb, Co, Zn, Ni and U) presented in Table 4.4, these elements were found to have their concentration in the same range apart from the relatively higher concentrations of Sr (2135.95 ppm) and Th (920.80 ppm) in fly ash sourced from Kriel power plant. It is important to mention that the list of elements highlighted in Table 4.1, 4.2, 4.3 and 4.4 is not comprehensive since not all elements were analyzed to due to experimental constraints.

Table 4-4: XRF analysis of other South African fly ashes (trace elements).

Element	Average concentration (ppm)						
	Thuthuka fly ash	Matla fly ash	Lethabo fly ash	Kriel fly ash	Hendrina fly ash	Duhva fly ash	Arnot fly ash
Sr	1384.72	976.19	970.66	2135.95	1167.71	957.41	1369.17
Ba	913.11	917.53	918.23	1271.20	1154.52	n/a	399.78
Th	558.96	373.09	372.75	920.80	448.59	n/a	42.89
Zr	492.99	384.58	385.24	434.70	445.03	527.84	639.45
Ce	155.80	107.75	112.73	124.90	166.86	n/a	219.12
V	122.29	110.70	123.49	88.73	105.68	125.55	81.94
Y	98.29	71.71	73.72	88.73	92.87	76.71	93.78
As	85.70	41.09	41.09	43.38	50.99	n/a	n/a
Nb	65.92	57.66	53.05	72.21	41.21	38.54	39.59
Cu	51.43	55.71	53.85	45.59	47.32	50.88	114.42
Pb	48.83	51.81	51.71	23.48	49.66	82.61	88.23
Rb	41.01	35.77	27.57	27.95	41.08	42.14	60.13
Co	39.52	17.97	14.84	17.40	32.84	33.32	25.45
Zn	38.03	39.48	39.54	23.44	61.69	118.28	94.88
Ni	22.04	20.45	21.95	20.41	24.90	72.29	106.06
U	10.12	38.69	58.48	41.82	59.73	n/a	30.04
Mo	7.48	10.58	7.86	6.35	16.43	n/a	2.23

* n/a = not analysed.

A comparative qualitative and quantitative XRD analysis of the other South African fly ashes is presented in Figure 4.5 and 4.6 respectively. This comparison plays an important role in discerning the fly ash similarities and differences.

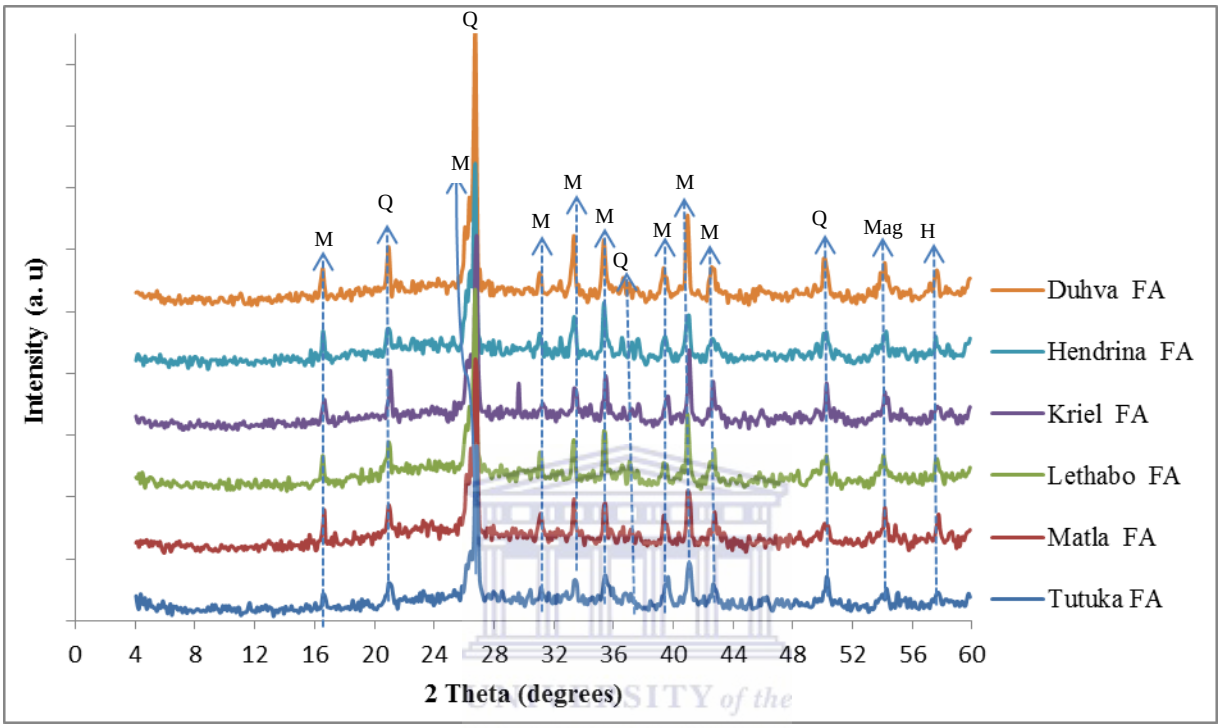

Figure 4-5: Qualitative XRD analysis of other South African fly ashes (Q = Quartz, M = Mullite, H = Hematite, Mag = Magnetite).

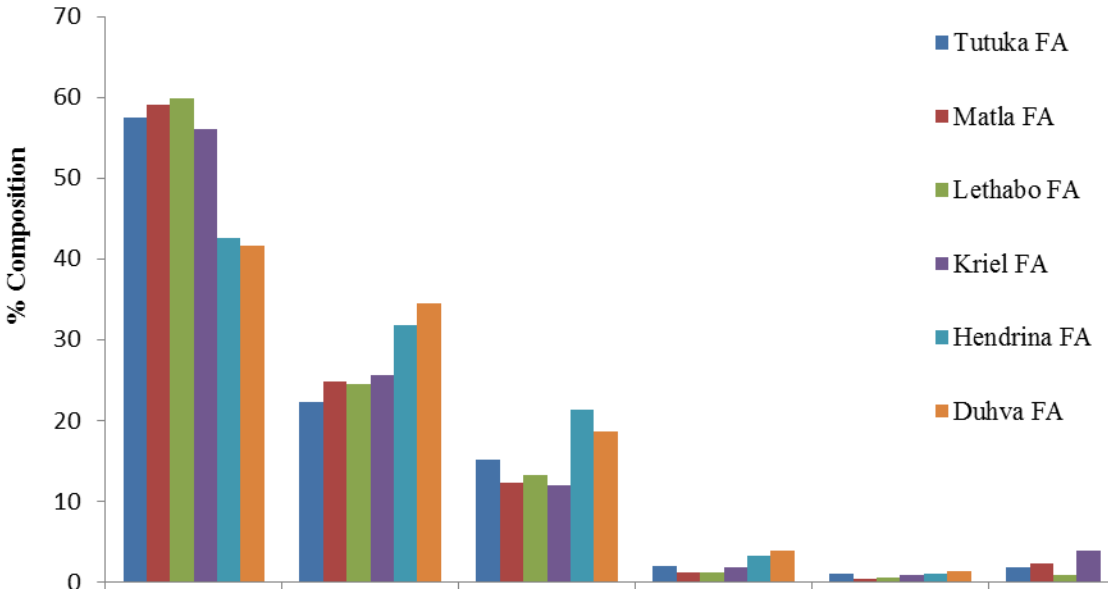

	Amorphous	Mullite	Quartz	Magnetite	Hematite	Others
Tutuka FA	57.54	22.27	15.2	2.04	1.07	1.88
Matla FA	59.06	24.84	12.33	1.13	0.42	2.22
Lethabo FA	59.79	24.49	13.27	1.14	0.5	0.81
Kriel FA	56	25.54	11.92	1.78	0.82	3.94
Hendrina FA	42.6	31.72	21.38	3.24	1.06	
Duhva FA	41.55	34.55	18.61	3.9	1.39	

Figure 4-6: Relative quantitative XRD analysis of other South African fly ashes (FA = fly ash).

Comparing the qualitative XRD analysis of the different sources of South African fly ashes shown in Figure 4.5, it can be noted that these fly ashes had the same major mineral phases but with varying relative content of specific mineral phases as shown in quantitative XRD presented in Figure 4.6. Tutuka, Matla amd Lethabo fly ashes had amorphous glassy content above 55 % whilst Hendrina and Duhva fly ash less than 45 % which would predict the trend of ease of zeolite formation from these fly ashes since the amorphous glassy phase is the main determining factor (Ward and French, 2005). This ~10% difference in amorphous content coincided with the higher Quartz (31.72 %) and Mullite 34.55 %) in Hendrina and Duhva respectively. Studies by Querol *et al.*, (2002) highlighted that even in cases where two fly ashes have similar SiO_2/Al_2O_3 bulk ratios, slight differences in the Quartz-Mullite/glass proportions can results in different zeolites under the same activation conditions. Therefore, slight composition differences in these South African fly ashes might require minor adjustments to ensure greater phase purity and reproducibility of the synthesis product.

4.2 Identification and optimization of hydrothermal conditions for zeolite A from Arnot fly ash.

After screening numerous papers that have reported synthesis conditions for producing zeolite A using fly ash obtained from different types and sources of fly ash (Shigemoto *et al*., 1993; Shih *et al*., 1996; Grutzeck *et al*., 1997; Chang *et al*., 1998; Hollman *et al*., 1999; Rayalu *et al*., 2001; Querol *et al*., 2002; Tanaka *et al*., 2004, 2008; Hui and Chao, 2006; Wang *et al*., 2008), it was deemed that the most important parameters for the identification and optimization of the synthesis conditions for zeolite A from South African fly ash would be: amount of additional Al, water quantity, hydrothermal synthesis time and temperature. Upon further scrutiny of the synthesis conditions that had been reported by the aforementioned researchers, it was noted that most of them had produced zeolite A after longer periods of crystallization (6 hours to 38 days) except for very few researchers such as Hui and Chao (2006) who had tried to reduce the time of crystallization to 4 hours by applying a step-change of synthesis temperature technique.

Hui and Chao's (2006) study acted as a good basis for comparison. Apart from aiming at generating synthesis conditions that would enable the synthesis of zeolite A from South African fly ash within a shorter synthesis, the work presented here further sought to avoid the complexity of following the temperature step-change technique that was suggested by Hui and Chao (2006). By avoiding this technique, the developed synthesis process would avoid future complications especially those associated with the synthesis scale up stage. It is important to also point out that there are no studies reported in the literature that have used South African class F fly ash to synthesized single phase zeolite A. In addition, most of the above mentioned studies applied pure water as a solvent through the entire zeolite A synthesis process. The focus of this work related to the search and customization of synthesis conditions for a single phase zeolite A from South African class F fly ash and also importantly, to investigate the potential for the use of mine waters as a synthesis solvent. Mine waters are found in close proximity to the coal combustion power stations. A one-step-at-a-time optimization process was chosen in which case each parameter was varied independently to identify its optimum before investigating the effect of the next parameter.

4.2.1 Chemical parameters optimization

In the following section, the influence of different chemical parameters on the quality of the synthesized material is described. Since most researchers who have synthesized zeolite A from fly ash have incorporated the fusion step during their procedures, it was also deemed important to start with the same route but later identify other novel synthesis ways as will be presented in Chapter 8. For the sake of clarity, each optimization parameter is described independently.

4.2.1.1 Variation of additional amount of Al

As reported in the literature, the SiO_2/Al_2O_3 ratio of the synthesis mixture plays an important role in determining the type of zeolites formed (Basaldella *et al.,* 1997). Since the amount of Si and Al in the fused South African fly ash was not enough to enable the crystallization of zeolite A, the Al content had to be adjusted, by adding varying amounts of Na-AlO_2 to the fly ash slurry, before starting the hydrothermal crystallization process, until the optimum Si/Al could be identified. The details for the procedure followed during preparing the fused fly ash, fused fly ash slurry and variation of it Al content in the fused fly ash slurry (based on the addition of varying amounts of Na-AlO_2) are described in detail in Chapter 3, Section 3.2. The hydrothermal synthesis temperature and time was initially set at 100 °C for 2 hours. Figure 4.7 presents the XRD patterns for the synthesis products obtained from the hydrothermal synthesis (at 100 °C for 2 hours) using fused fly ash slurries that had varying Na-AlO_2:NaOH:H_2O ratios.

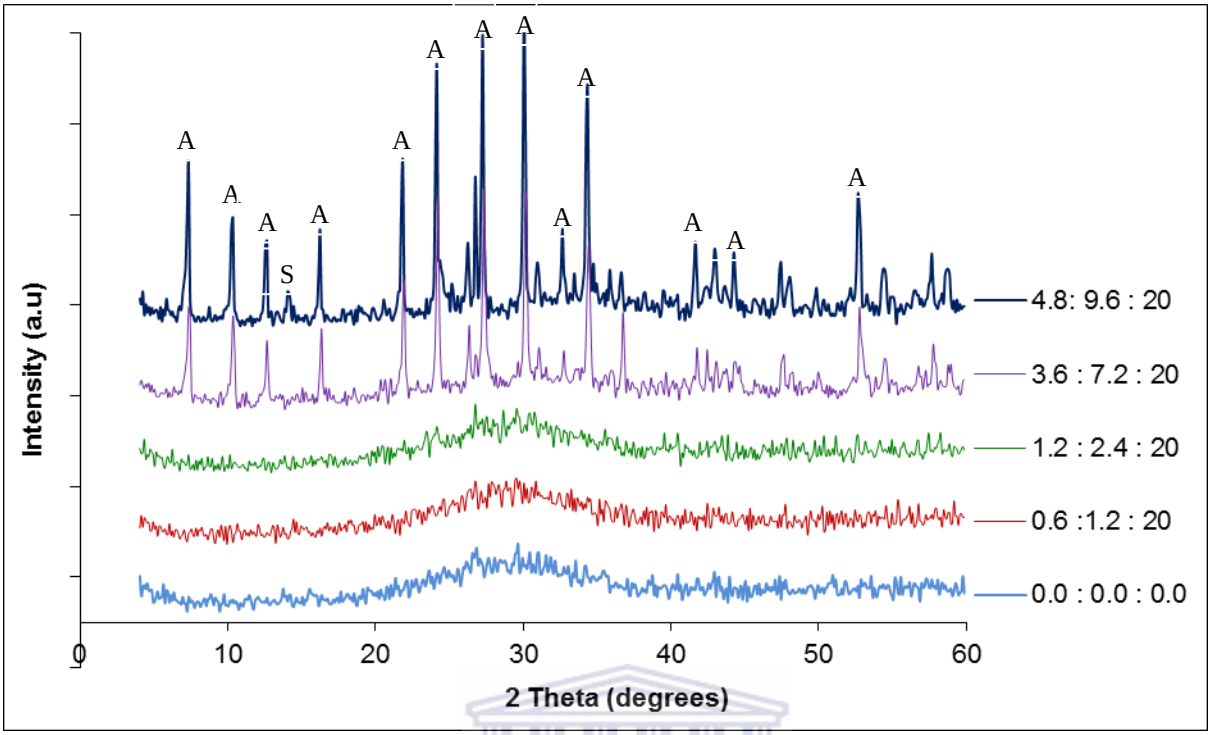

Figure 4-7: XRD patterns for synthesis products obtained after hydrothermal syntheses (100 °C for 2 hours) starting from fused fly ash slurries that had varying Na-AlO_2:NaOH:H_2O ratios (A = zeolite A, S = Hydroxy-sodalite).

From the XRD patterns in Figure 4.7, the synthesis mixture with the Na-AlO_2 : NaOH : H_2O ratio of 3.6 : 7.2 : 20 was found to result in the crystallization of a single phase zeolite A. When the synthesis mixture had a ratio of 1.2 : 2.4 : 20, or lower, only an amorphous phase could be identified after 2 hours at 100 °C. The presence of the amorphous material was confirmed by the appearance of the broad diffraction peak seen between 20 and 36° 2θ. These XRD spectra also confirm again that no Quartz or Mullite remained in the precursoe species or products. The synthesis mixture with the lowest Na-AlO_2 : NaOH : H_2O ratio (3.6 : 7.2 : 20) was found to lead to co-crystallization of zeolite A together with hydroxyl-sodalite. Since the synthesis mixture with a Na-AlO_2 : NaOH : H_2O ratio of 3.6 : 7.2 : 20 was found to give the targeted zeolite, the amount of additional Na-AlO_2 added in the synthesis mixture with this ratio was used to optimize water content in the next set of experiments, as is specified in Chapter 3, Section 3.2.2.1.

4.2.1.2 Variation of water content

In order to reduce the amount of water used during synthesis, the quantity that had been used during the optimization of the Si/Al ratio (5 mL of water per g of fused fly ash) was reduced by half (2.5 mL of water per g of fused fly ash) while the hydrothermal synthesis temperature was held at 100 °C for 2 hours. The XRD analysis for the product obtained when the water content was varied, is presented in Figure 4.8.

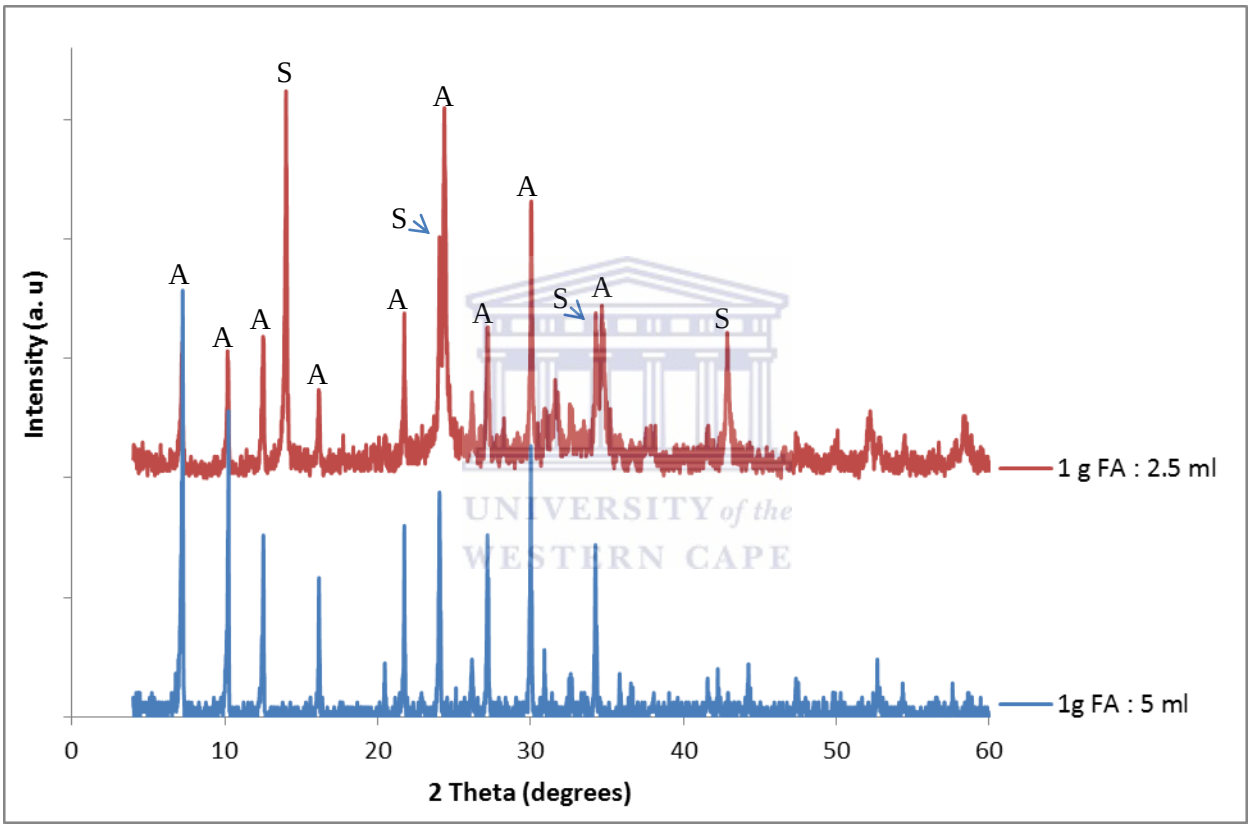

Figure 4-8: XRD analysis for product synthesized when the water content was varied (A = zeolite A, S = Hydroxy-sodalite).

From Figure 4.8, it is evident that halving of the amount of water that was used to prepare the fly ash slurry resulted in the co-crystallization of zeolite A with hydroxy-sodalite zeolite which in this case acted as a contaminant phase. Even though the optimum amount of additional Na-AlO_2 reported in Section 2.1.1 was used, less solvent may have led to changes in the amount of extracted Si and Al species, impacting on the Si/Al ratio of the fused fly ash synthesis slurry

hence resulting in a mixed phase zeolitic product. In this regard, the quantity of water used to prepare the fused fly ash slurry used for the next optimization stage was retained as 5 mL per g of fused fly ash with the same additional Al content identified in Section 4.1.1. This fused fly ash slurry had a molar ratio of 1 Al_2O_3 : 5.39 Na_2O : 2.75 SiO_2 : 111.82 H_2O.

4.2.2 Physical parameter optimization

The following section dealt with variation of selected physical parameters in order to understand their influence on the final synthesis product as well as to identify the optimum condition following a one-step-at-a-time optimization approach.

4.2.2.1 Variation of hydrothermal synthesis temperature and time

Having identified the optimum additional Al and water content (Section 2.1.1 and 4.1.2) required to generate fused fly ash slurry with a molar ratio of 1 Al_2O_3 : 5.39 Na_2O : 2.75 SiO_2 : 111.82 H_2O, the next set of experiments investigated the variation of hydrothermal crystallization temperature and its impact on synthesis time. Figures 4.9, 4.10 and 4.11 present the results obtained when the hydrothermal treatment temperature was varied from 80 °C to 100 °C showing the respective synthesis time concomitantly varied between 40 minutes to 6 hours.

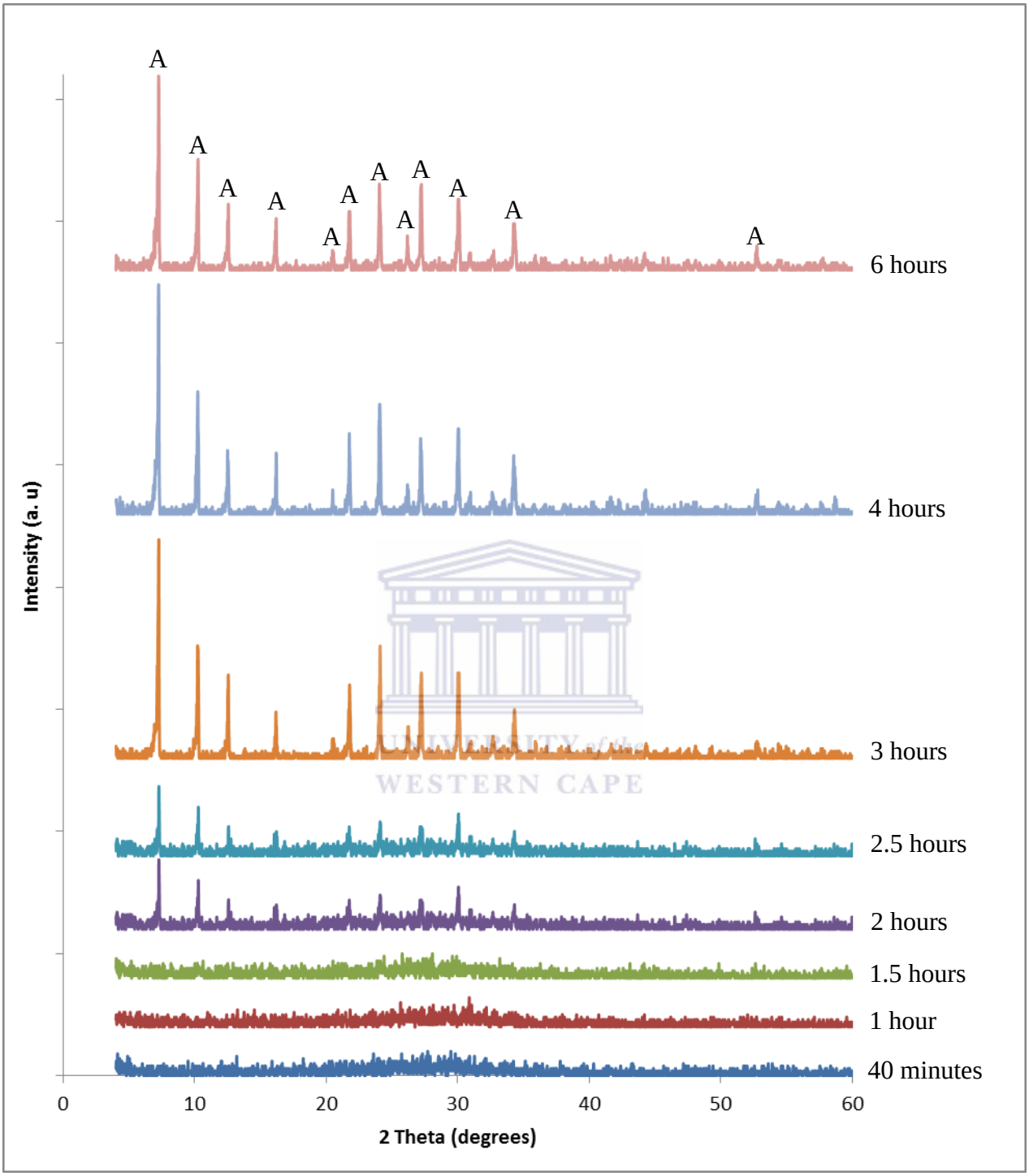

Figure 4-9: XRD patterns for product synthesized at 80 °C, the respective synthesis time was varied between 40 minutes to 6 hours using fused fly ash slurry with a molar ratio of 1 Al_2O_3 : 5.39 Na_2O : 2.75 SiO_2 : 111.82 H_2O.

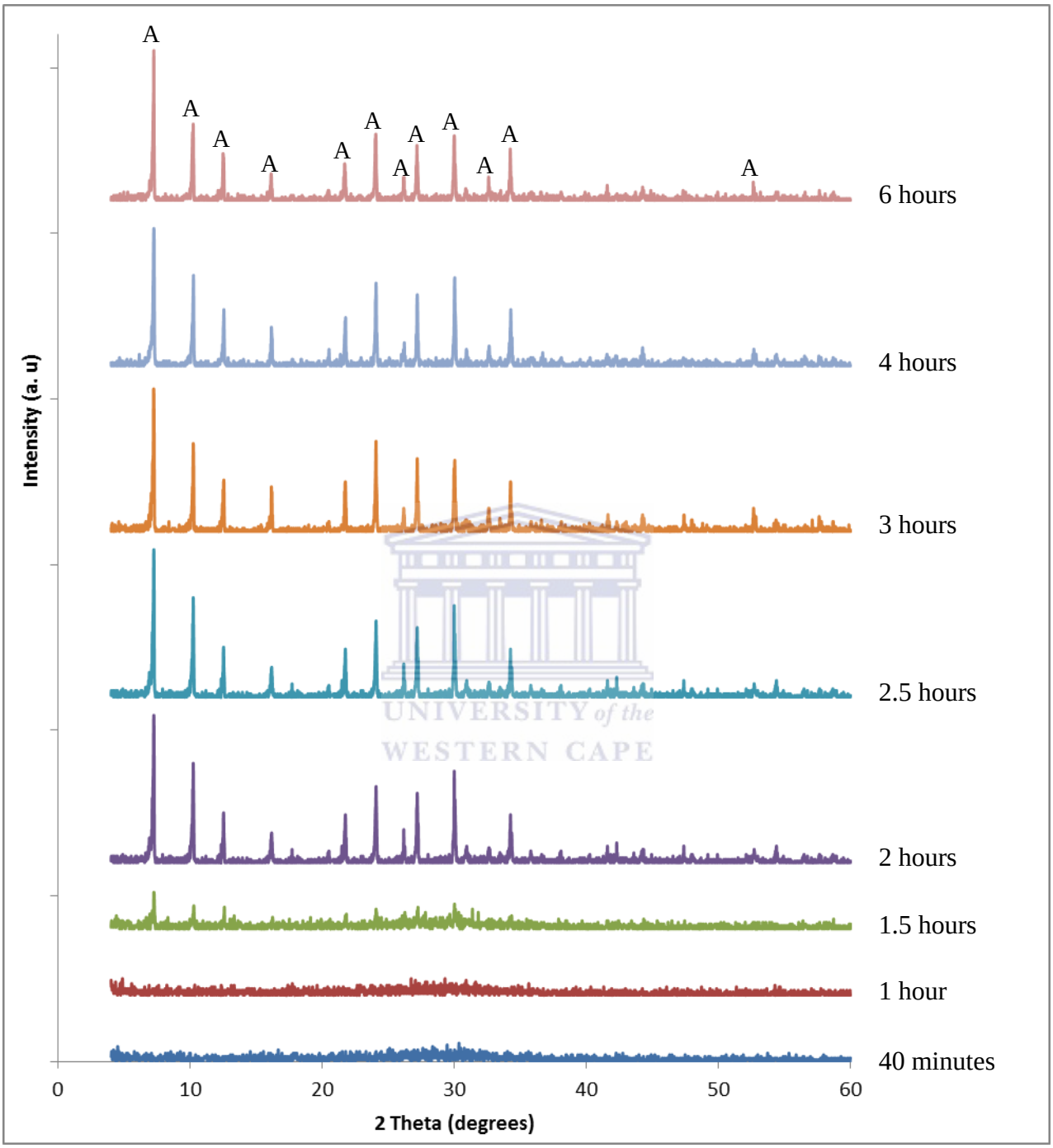

Figure 4-10: XRD patterns for product synthesized at 90 °C, the respective synthesis time was varied between 40 minutes to 6 hours using fused fly ash slurry with a molar ratio of 1 Al_2O_3 : 5.39 Na_2O : 2.75 SiO_2 : 111.82 H_2O.

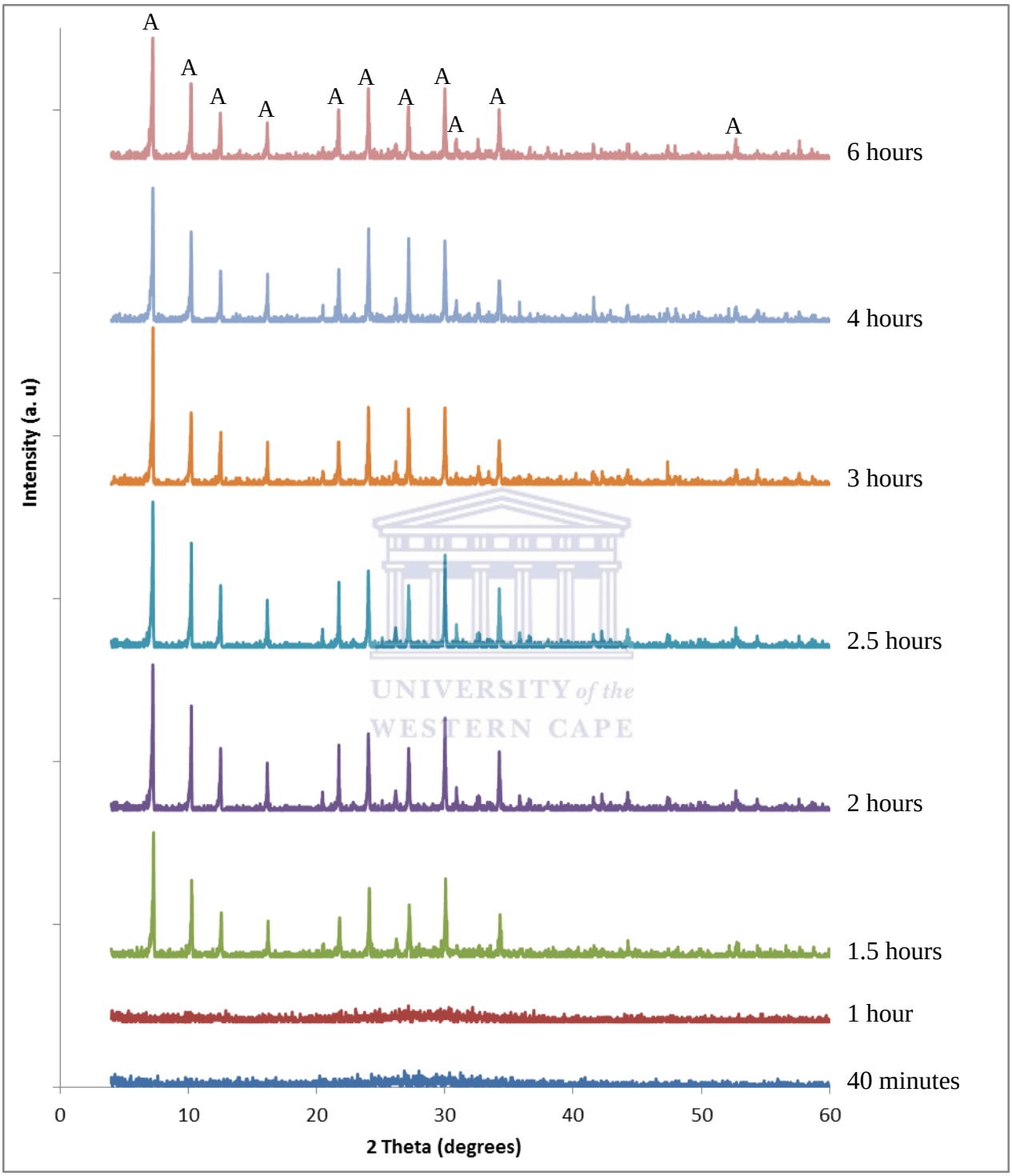

Figure 4-11: XRD patterns for product synthesized at 100 °C, the respective synthesis time was varied between 40 minutes to 6 hours using fused fly ash slurry with a molar ratio of 1 Al_2O_3 : 5.39 Na_2O : 2.75 SiO_2 : 111.82 H_2O.

As shown in Figures 4.9, 4.10 and 4.11, the XRD patterns of the synthesis products did not have any of the mineral phases that were originally in the as-received and alkali fused fly ash. Only amorphous components were observed as the broad hump between 20 and 40 ° 2θ in the earlier synthesis times (40 minutes to 1 hour) meaning that the crystalline sodium-aluminosilicate phases identified in the alkali fused fly ash (Figure 4.1) had been demineralized completely. In order to compare the rate of crystallization when zeolite A was synthesized at different temperatures (80, 90 and 100 °C), the relative percentage crystallinity was calculated and is presented in Figure 4.12. The calculation of the relative crystallinity was based on the summation of integral areas of the main diffraction peaks, and relating these areas to that of the most crystalline sample which had been assigned as 100%. This technique for calculation of relative crystallinity was also used by Ouden and Thompson, (1992).

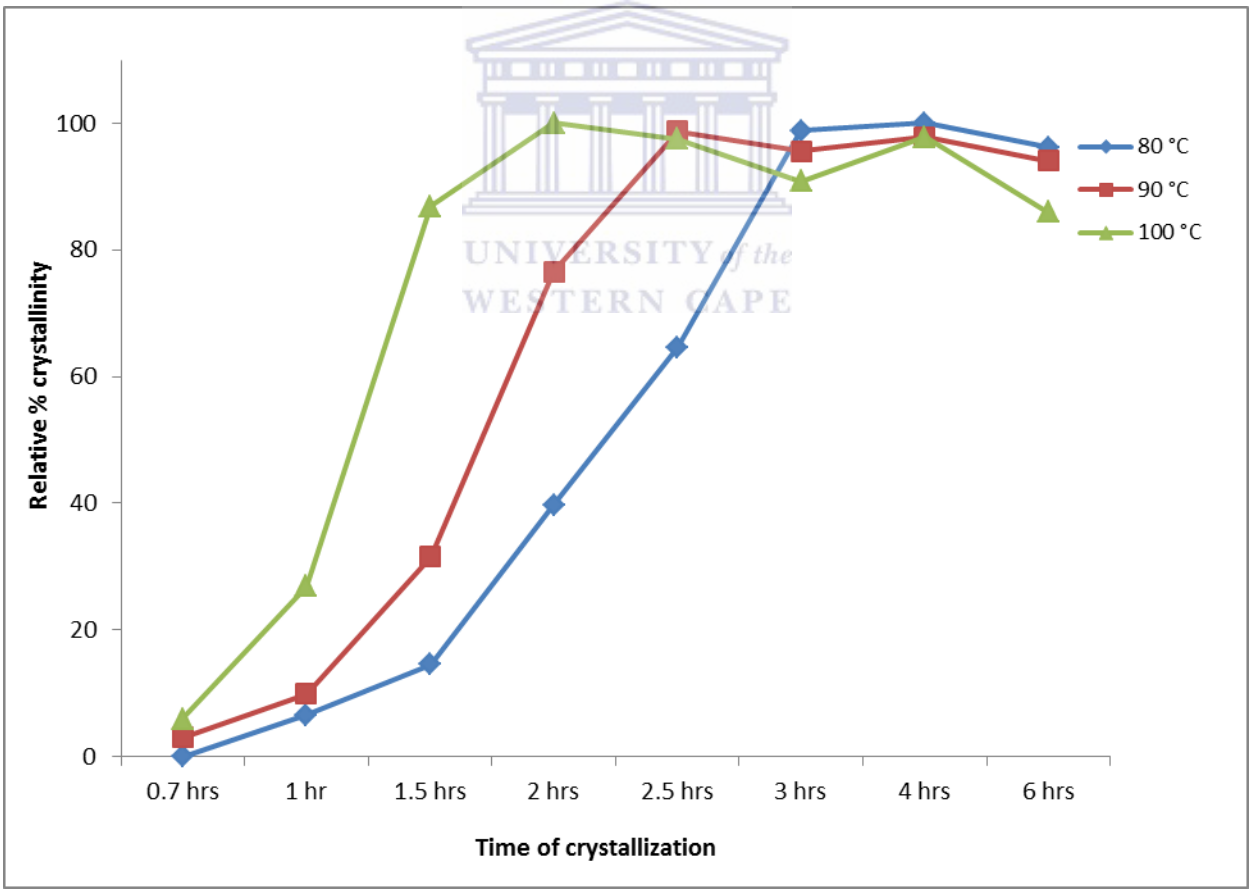

Figure 4-12: Relative % crystallinity for zeolite A synthesized at different temperatures (80 °C, 90 °C, 100 °C) using fused fly ash slurry with a molar ratio of 1 Al_2O_3 : 5.39 Na_2O : 2.75 SiO_2 : 111.82 H_2O.

From the relative percentage crystallinity of zeolite A presented in Figure 4.12, it can be seen that zeolite A crystallized faster at higher temperature (100 °C) compared to lower temperatures (80 and 90 °C). Since it took a relatively shorter time (2 hours) to crystallize zeolite A when synthesis was conducted at 100 °C, this temperature was set as the basis for the next set of experiments.

In order to determine whether the zeolite A phase purity would be compromised when an extended synthesis period was applied, the synthesis mixture was subjected to hydrothermal treatment in an oven (at 100 °C) for up to 6 days and the results are shown in Figure 4.13.

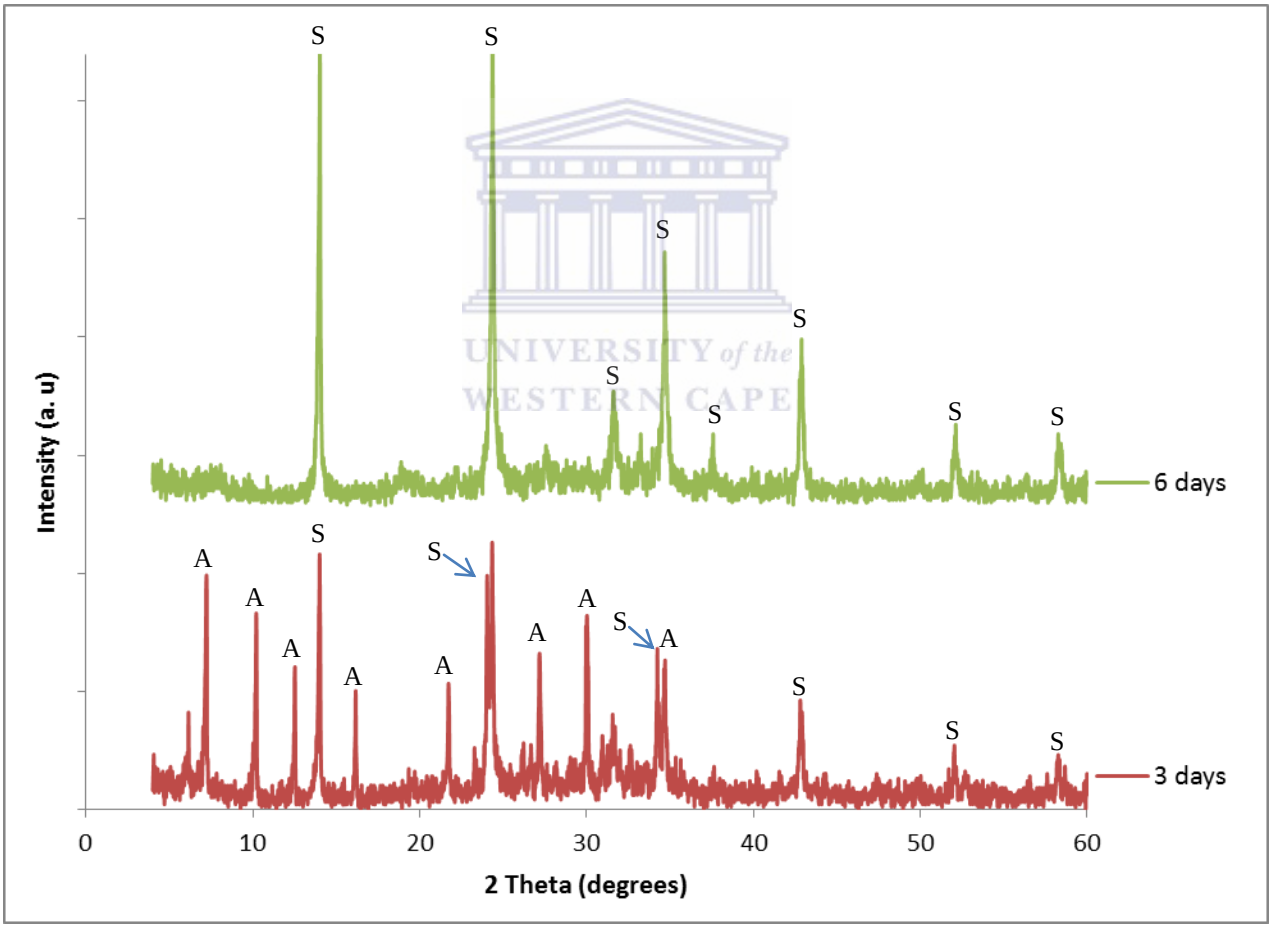

Figure 4-13: XRD analysis for product synthesized using fused fly ash slurry with a molar ratio of 1 Al_2O_3 : 5.39 Na_2O : 2.75 SiO_2 : 111.82 H_2O when hydrothermal synthesis time was varied between 3 to 6 days.

Comparing the single phase zeolite A obtained after 2 hours of hydrothermal synthesis at 100 ° C (Figure 4.11) with the XRD patterns presented in Figure 4.13, it was interesting to note that after three days of subjecting the synthesis mixture to hydrothermal synthesis at 100 °C sodalite phase transformation occurs and that zeolite A had been totally converted to hydroxy-sodalite zeolite after 6 days. Thus extending synthesis times are not useful to improve product quality. The formation of the denser hydroxy-sodalite zeolite phase could be associated with Ostwald law of successive transformation.

4.2.3 Synthesis of zeolite A from clear solution extracted from fly ash

Instead of using the unseparated fused fly ash slurry during crystallization of zeolite A, a filtered extract of fused fly ash (clear solution) prepared as described in Chapter 3, Section 3.2.1.2 was used. Filtration of the fused fly ash slurry removed the undissolved components remaining from the fused particles out of the solution. Even though the optimum amount of additional Na-AlO_2 reported in Section 4.1.1 was used, the removal of undissolved fused fly ash particles from the fused fly ash solution led to a change in the molar regime of the resulting clear solution extract. Therefore, comparing the molar regime of the fused fly ash slurry that had led to the crystallization of zeolite A (1 Al_2O_3 : 5.39 Na_2O : 2.75 SiO_2 : 111.82 H_2O) as was found in Section 4.1 with the molar regime generated after extracting the clear solution (1 Al_2O_3 : 30.84 Na_2O : 4 SiO_2 : 414.42 H_2O), the difference in the composition of these two synthesis mixtures is clearly evident. It is important to note that even though the reuse of the remaining residual had not been investigated for the synthesis of zeolites, there could be potential for their reuse and could possibly lead to generation of zeolite A as long the Si/Al is adjusted. Figure 4.14 presents a comparative XRD analysis of synthesis product obtained when the filtered extract (clear solution) and unseparated fused fly ash slurry were used to synthesize zeolite A at 100 °C for 2 hours.

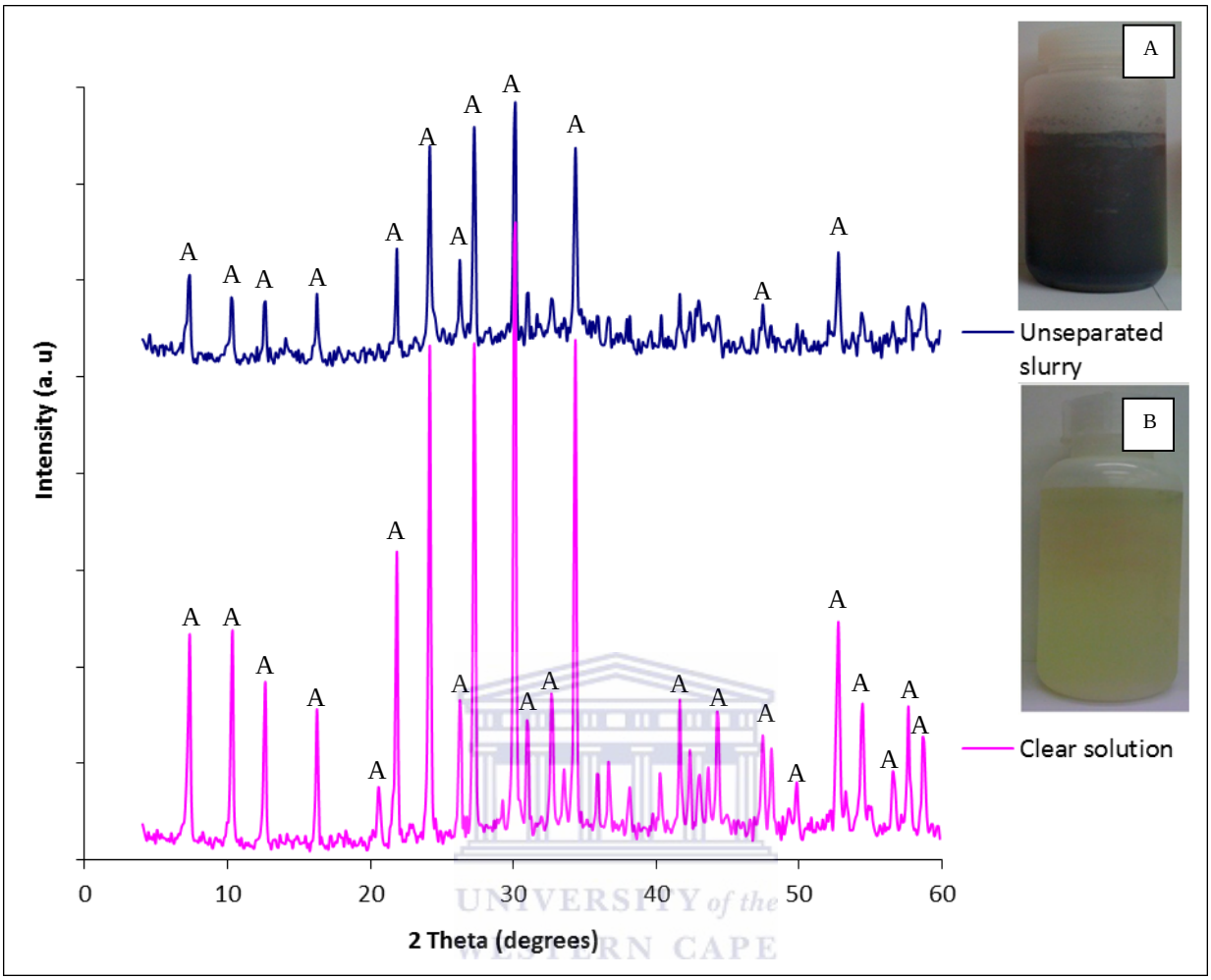

Figure 4-14: Comparative XRD analysis of synthesis product obtained when clear fused fly ash solution (image a) and unseparated fused fly ash slurry (image b) was used to synthesize zeolite A at hydrothermal synthesis of 100 °C for 2 hours.

From Figure 4.14, it can be seen that the use of the filtered extract of fused fly ash (clear solution) led to the formation of a significantly more crystalline zeolite A after 2 hours. It was interesting to note that zeolite A could still crystallize from both solutions even after establishing that they had a different molar regime (i.e. 1 Al_2O_3 : 5.39 Na_2O : 2.75 SiO_2 : 111.82 H_2O and 1 Al_2O_3 : 30.84 Na_2O : 4 SiO_2 : 414.42 H_2O). Morphological analysis was conducted by scanning electron microscope (SEM) of the two products as shown in Figure 15. Morphological analysis is a useful characterization technique that is highly valued during the investigation of crystallization process of zeolites since it can be used to examine the quality of the synthesis product.

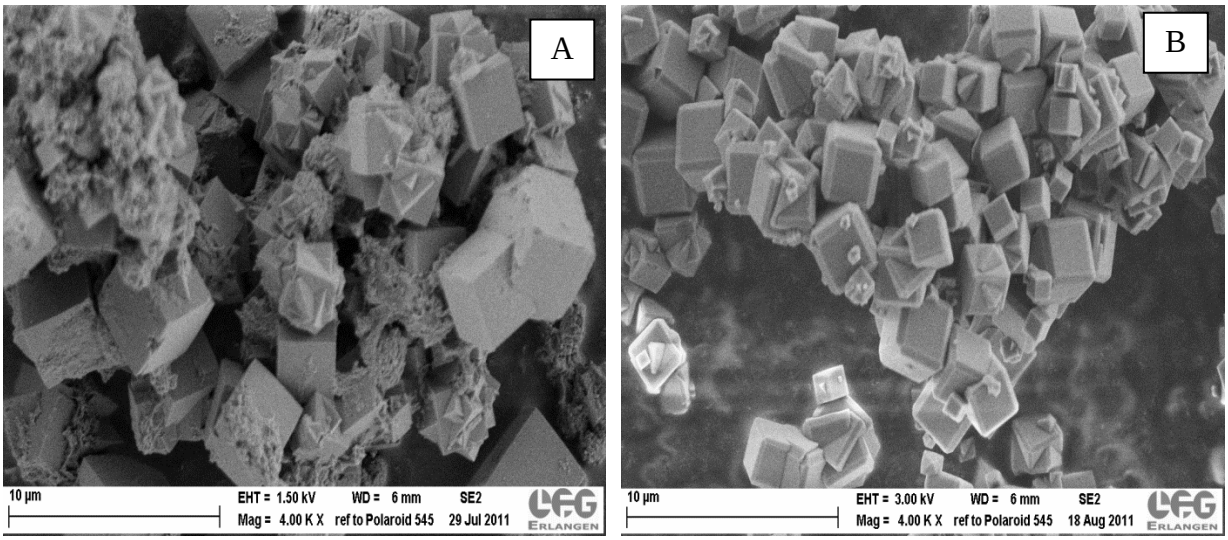

Figure 4-15: SEM micrographs of zeolite A synthesized from (a) unseparated fly ash slurry (b) filtetred fused fly ash extract (clear solution).

As shown in Figure 4.15, the use of the filtered extract of the fused fly ash (clear solution) promoted the preparation of uniform cube shaped zeolite A crystals and reduced the co-existence of zeolite A crystals with the feedstock precursor species. When the unseparated fused fly ash slurry was used the well-known sharp edged cubic crystals, which are typical of zeolite A, were formed (Figure 4.15 (a)) whereas when a clear extract of fused fly ash was used during the synthesis process, zeolite A with mostly chamfered (rounded-off corners and edges) cubic morphology was formed (Figure 4.15 (b)). The differences in the crystal morphology can be attributed to the differences in Si/Al ratio in the respective synthesis mixtures. When unseparated fly ash slurry was used as the synthesis feedstock, changes in Si/Al were expected to occur as the reaction progressed because further demineralization of the precursors from the fly ash feedstock that had been fused was expected to take place upon heating. In the case where the clear solution was used, the Si/Al ratio of the reaction mixture was expected to stay constant until the synthesis process was terminated. In as much as structural as well as chemical properties of zeolites play an important role in determining the type of application, their morphology has been reported to also play an important role (Subotić and Bronić, 2003). When zeolite A is used as a detergent builder, the sharp-edged crystal morphology shown in Figure 4.15 (a) has been reported to get entangled in textile fiber and hence this zeolite morphology is not favourable whereas when zeolite A with chamfered morphology presented in Figure 4.15 (b) is used, it has been found to

have a decreased tendency for the deposition on the textile material hence making it the preferred shape as a detergent builder (Subotić and Bronić, 2003).

Further analysis of the two zeolites with the different morphologies was conducted using the Fourier transform infrared spectrometer (FTIR) and the FTIR spectra are shown in Figure 4.16.

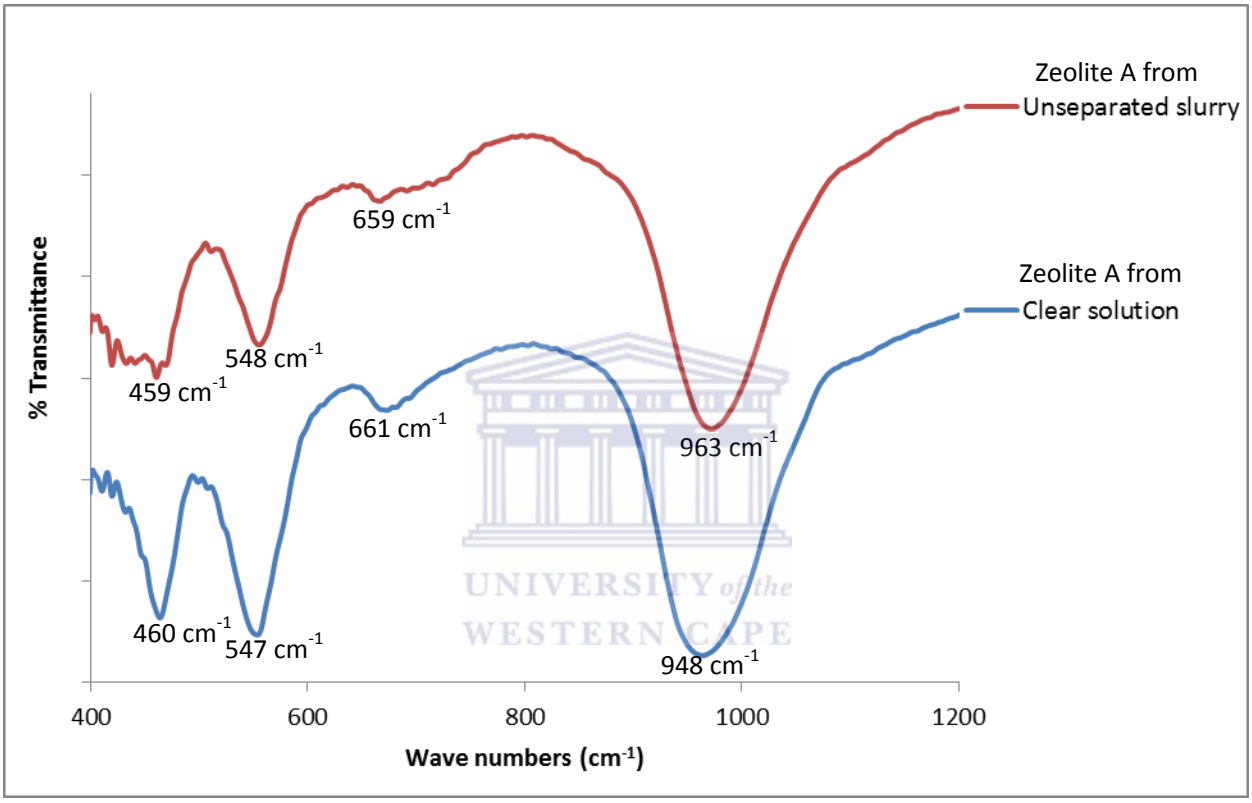

Figure 4-16: Comparative FTIR spectra of synthesis products obtained when zeolite Na-A was synthesized from filtered fused fly ash extract (clear solution) and unseparated fly ash extract.

The general vibrational bands associated with all zeolite types as reported by Flanigen (1971) were identified in both samples as shown in Figures 4.16. These vibrational bands were as follows; bands appearing between 1250 – 950 cm^{-1} and 720 – 650 cm^{-1} are assigned to asymmetric and symmetric stretch of the internal tetrahedral respectively whereas bands observed between 420 and 500 cm^{-1} are be correlated to T– O bend of the internal tetrahedra. In addition to the above general spectral bands for zeolites, a vibrational band which is normally associated with the presence of double four-ring units (D4R) in zeolite A was observed to occur

at around 540 cm^{-1} for both the samples. According to the work of Kiricsi *et al.* (1994) and Coutanceau *et al.* (1997), the position of peaks at 548, 547 cm^{-1} and are influenced by the content of Al in the zeolite framework. Flanigen (1971) further reported that the peaks at 948 cm^{-1} and 963 cm^{-1} are sensitive to the framework Si/Al ratio which could also explain the differences in the morphology of zeolite A synthesized using clear extract of fused fly ash with that using the fused fly ash slurry as shown in Figure 4.15. The increase in the wavenumber (shift to the right) of the peak at 963 cm^{-1} for the sample obtained from clear extract of fused fly ash in relation to the peak at 948 cm^{-1} for the sample obtained from unseparated fused fly ash indicated that the amount of aluminium was relatively higher in the zeolitic product obtained from clear extract of fused fly ash. This observation was in good agreement with the elemental analysis presented in Table 4.5, hence FTIR analysis gives a good indication of the Al content in the zeolites.

4.2.4 Chemical analysis of the synthesized zeolite A

The comparative X-ray Fluorescence Spectroscopy (XRF) results of the major elemental composition of synthesis product (zeolite A) that was obtained from Arnot fly ash using filtered fused fly ash extract (clear solution) and unseparated fused fly ash slurry as prepared according to the procedure set out in Chapter 3 (Section 3.5.2.1) is presented in Table 4.5. The samples were analysed in triplicate and only the average values are presented.

Table 4-5: Comparison of chemical composition (major elements) in the synthesized zeolite A using filtered extract (clear solution) and unseparated fused fly ash slurry (n = 3).

Major elements (oxide)	Product from clear solution (Average mass %)	Product from Unseparated slurry (Average mass %)
SiO_2	36.90	31.64
Al_2O_3	31.06	19.64
Na_2O	15.33	12.80
CaO	0.06	7.45
Fe_2O_3	0.10	6.48
MgO	1.19	1.82
`TiO_2	0.06	1.08
K_2O	0.18	0.14
P_2O_5	0.01	0.05
MnO	nd	0.06
SO_3	nd	0.01
LOI	14.93	16.03
H_2O	0.18	2.23
SUM	100.00	99.42
SiO_2/Al_2O_3 ratio	1.19	1.61

*nd = not detected

As shown in Table 4.5, the SiO_2/Al_2O_3 ratio for zeolite A prepared using filtered fused fly ash extract (clear solution) was found to be 1.19 whereas that of zeolite A prepared from unseparated fused fly ash slurry was 1.61. These values were less than the value identified in the raw fly ash hence signalled that there was wastage of the Si and Al feedstock especially in the case of the

zeolite prepared from unseparated fly ash slurry. In both samples but especially in the clear solution product, Na_2O was higher than in the original starting fly ash and this was because of the incorporation of Na^+ into the zeolite structure as a charge balancing cation since additional NaOH was used as the alkaline solution in the presynthesis fusion step. The relative mass % of CaO, Fe_2O_3, MgO, TiO_3, K_2O, P_2O_3 and MnO in the zeolitic sample that was prepared from unseparated fused fly ash slurry was almost similar to the content identified in the fly ash (Table 4.1) whilst the content of these elements was significantly reduced in the zeolite A sample that was prepared using filtered fused South African fly ash extract. Elements such as Na, Ca, K and Mg in the synthesized zeolite can act as charge balancing cations. It was noted that the zeolite A sample synthesized from the unseparated fused fly ash slurry had a higher Ca cation content than in from the clear extract of fused fly ash. This could be because some of the CaO in the fly ash may have reacted with CO_2 to form $CaCO_3$ during the alkali fusion process as was shown by the presence of the carbonate peak at 1431 cm^{-1} in the FTIR spectra presented in Figure 4.4. $CaCO_3$ is known to be insoluble in high pH environments (Butler, 1998) that were created when fused fly ash solid mater was mixed with water. From the XRF data in Table 4.5, it was also noted that synthesis from clear extract of fused fly ash favoured the Na-form of the zeolite whereas the synthesis from unseparated solution allowed incorporation of more of the other cations such as Ca and K in the zeolite.

Table 4.6 presents the comparative X-ray Fluorescence Spectroscopy (XRF) results of the trace element analysis of synthesis product (zeolite A) that was obtained from Arnot fly ash using filtered fused fly ash extract (clear solution) and unseparated fused fly ash slurry as prepared according to the procedure set out in Chapter 3, Section 3.5.2.1).

Table 4-6: Comparison of chemical composition (trace elements) in the synthesized zeolite A using filtered extract (clear solution) and unseparated fused fly ash slurry.

Trace elements (ppm)	Product from clear solution (Average mass %)	Product from Unseparated slurry (Average mass %)
Ba	75.89	351.11
Rb	71.07	52.45
Sr	43.14	1167.43
Zr	30.53	557.43
Cu	28.13	88.47
Ni	18.11	98.81
Pb	10.98	61.75
V	7.17	nd
Zn	7.70	85.33
Y	6.62	81.89
Co	2.58	25.45
Mo	0.67	2.05
Ce	nd	222.20
Cr	nd	107.70

*nd = not detected

Considering the concentration of trace elements in the synthesized zeolite A (Table 4.6), it is clearly evident that zeolite A prepared using filtered fused fly ash extract (clear solution) was of higher purity and quality compared to that prepared from unseparated fused fly ash slurry. This can be confirmed by the significantly lower concentrations of Cr, Co, Ni, Cu, Zn, Rb, Sr, Y, Zr, Ba, Mo, Ce and Pb in zeolite A prepared using filtered fused fly ash extract (clear solution). The relatively higher concentration of these elements in zeolite A prepared from unseparated fused

fly ash slurry further confirmed that the trace elements were associated with that portion of the fused sample that was not immediately soluble and could be filtered out (see Figure 15) which could be observed in the SEM images (Figure 4.15), showing there was the presence of residual precursor material in the synthesized zeolitic product made from the unseparated fly ash slurry. This observation shows that using clear extract is a technique that is useful to improve purity and reduce trace metal contamination of the zeolitic product.

4.2.5 Thermal stability comparison of zeolite A synthesized form clear fused extract and unseparated fused fly ash slurry.

Thermal analysis of the zeolitic products was used to provide valuable information on their dehydration processes as well as thermal stability. For applications requiring high temperatures, a zeolite that can withstand harsh conditions without collapsing to a denser phase or even turning to amorphous compounds is highly preferred (Pfenninger, 1999). There are many methods of determining the thermal stability of zeolites, but the thermal gravimetric method and high temperature in-situ XRD techniques were applied in this study. Figures 4.17 and 4.18 present the respective TGA plots of the synthesized zeolite A from clear fused extract and unseparated fused fly ash slurry determined using the method set out in Chapter 3, Section 3.5.7.1. These were compared with the commercial counterpart. A detailed discussion follows.

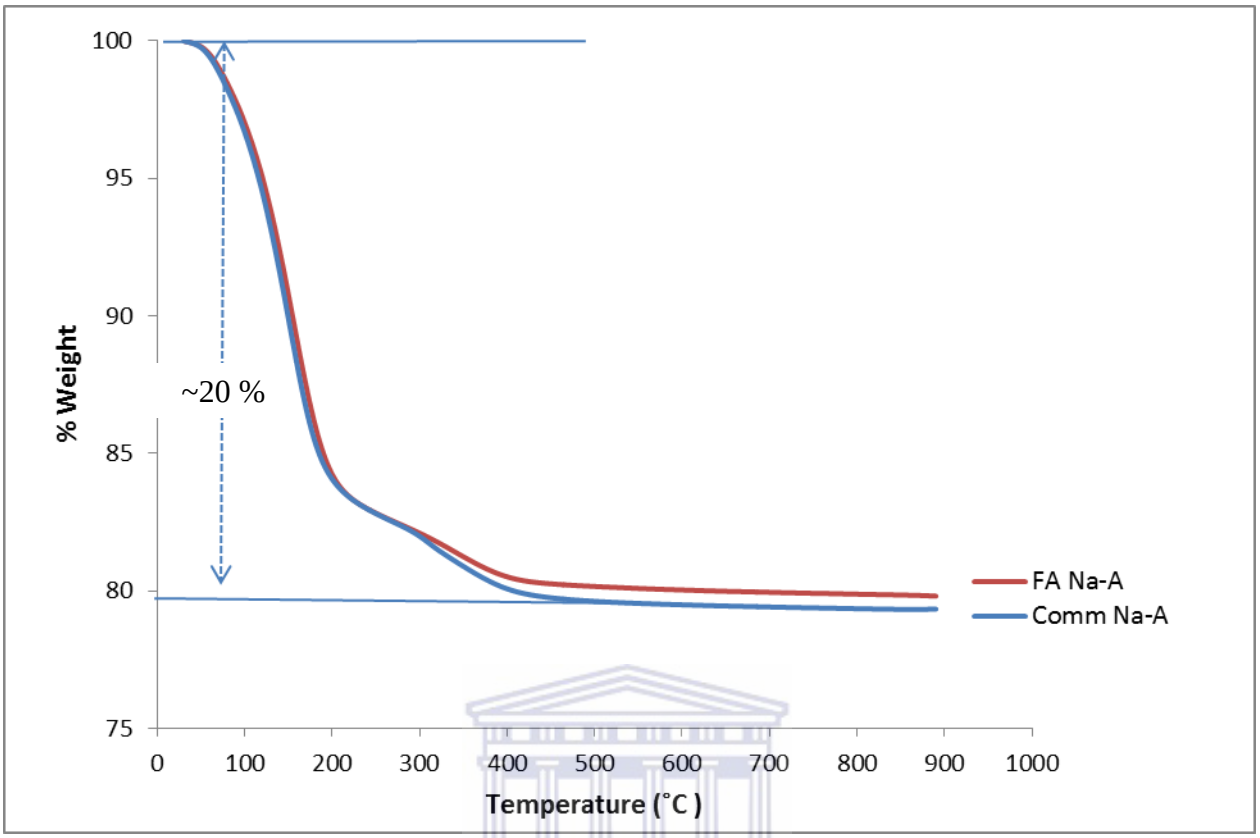

Figure 4-17: Comparison of thermograph of commercial zeolite A with that of fly ash-based zeolite A synthesized using clear fused fly ash extract.

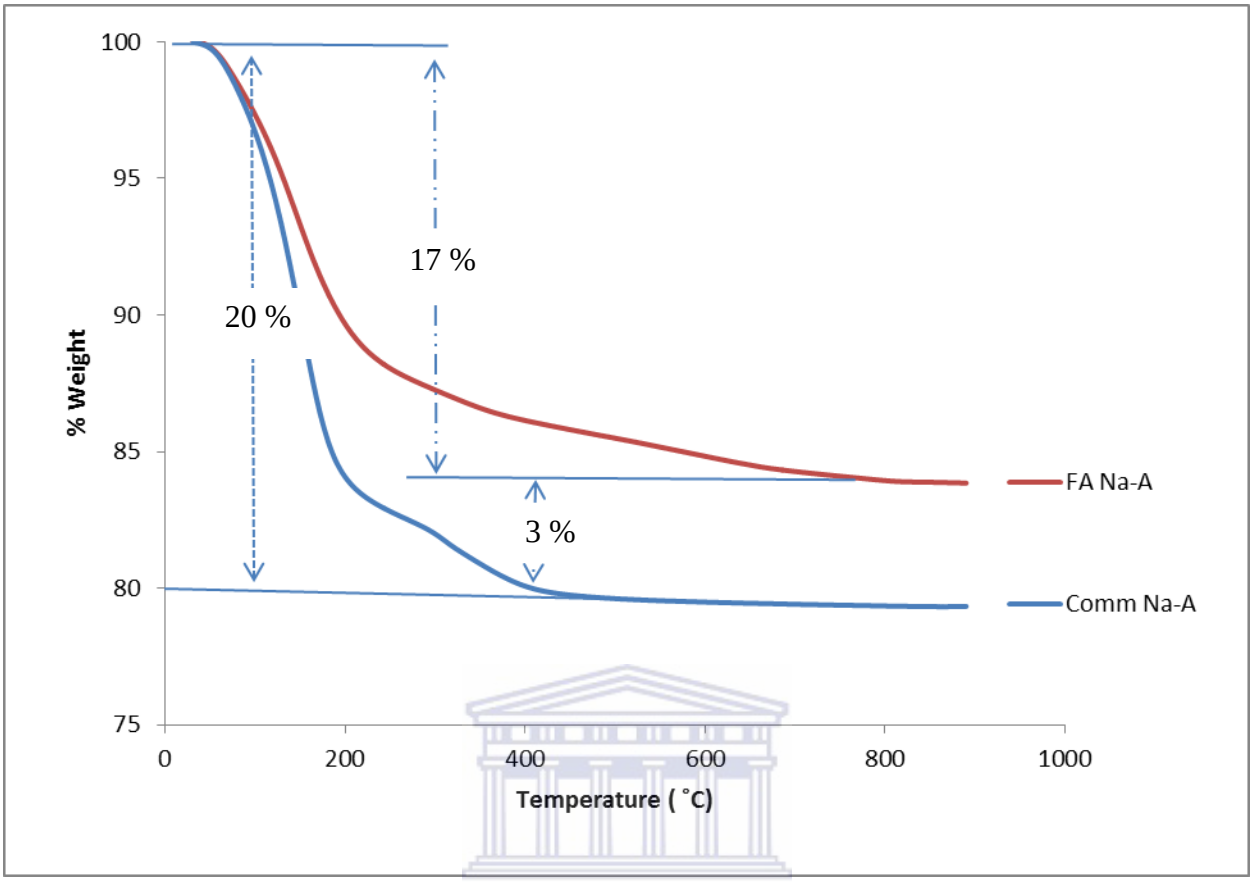

Figure 4-18: Comparison of TGA thermograph of commercial zeolite with fly ash-based zeolite A synthesized using unseparated fused fly ash slurry.

From the thermographs shown in Figures 4.17 and 4.18, it was observed that the moisture loss from both the commercial and fly ash based zeolite A started between 40 and 50 ˚C and seen to continue up to about 200 ℃. Comparing % weight loss for the thermograph obtained when fly ash based zeolite A was synthesized from clear extract of fused fly ash with that of commercial zeolite A (Figure 4.17), there was no significant difference since the observed % weight loss of moisture for both samples was about 20 % with the slight difference at the higher temperature (from 400 ˚C) attributed to the presence of other cationic species (Ca^{2+}, Mg^{2+} instead of Na^{+}) in the fly ash-based zeolite A product which may have had a zeolite pore filling effect. On the other hand, when the % weight loss of commercial zeolite A (~20 %) (Figure 4.18, part a), was compared with that of fly ash based zeolite A obtained when unseparated fused fly ash slurry was used (~17 %) (Figure 4.18, part b), the % weight loss difference of ~3% (Figure 4.18, part c) can be attributed to the presence of unconverted precursor species from the fused fly ash

feedstock that had been observed using the SEM (see Figure 4.15) which were not porous. The other explanation could also be due to the presence of larger cationic species such as Ca^{2+}, Mg^{2+} instead of Na^{+} in the zeolite product structure from unseparated slurry as had been noted in Table 4.5. The noticeable weight losses at the temperature range of 40 - 200 °C for both zeolite A samples synthesized from clear and unseparated fused fly ash slurry observed in Figure 4.17 and 4.18 could be associated with loss of free and physically adsorbed water inside the zeolite pores.

Another prominent weight loss in both Figure 4.17 and 4.18 was observed to occur between 200 and 400 ˚C and complete dehydration seems to be completed at around 800 to 900 ˚C. The weight loss occurring above 200 ˚C is thought (Usachev *et al*., 2003; Akbar *et al*., 2005) to be associated with water loss that could form hydration complexes with the exchangeable Na^{+} cations. The negligible mass loss occurring above a temperature of 400 ˚C could be due to dehydroxylation (Akbar *et al*., 2005) which leads to the expulsion of more water when hydroxyl bonds that are formed when exchangeable cations that polarize the water molecule are destroyed. The zeolitic water content has been reported to be dependent on the nature and size of the exchageable cation and also on the number of Al ions in the zeolitic structure (Usachev *et al*., 2003; Akbar *et al*., 2005). Si/Al ratio of zeolites has also been reported to have an impact on the thermal stability of zeolites whereby high thermal stability is often directly proportional to respective increase in the Si/Al ratio (Usachev *et al*., 2003). This direct proportionality is attributed to the variation of the lattice constant which is related to Al-O (1.728 Å) and Si-O (1.608 Å) bond lengths (Breck, 1974). In support of the effect of the differences in Si/Al ratio, the analysis of the two zeolite A products presented in Figure 4.18, had earlier been noted from XRF (Table 4.5) and FTIR (Figure 4.16) analysis that the Al content was different in the products.

In-situ temperature programmed XRD analysis (shown in Figure 4.19 and 4.20) was conducted to probe whether there was any temperature induced mineralogical transformations taking place in the fly ash-based zeolite A. The experimental details for the analysis are detailed in Chapter 4, Section 3.5.7.1. This analysis aimed to complement the results from thermogravimetic analysis reported above. Due to experimental contraints (temperature limitations of the heating stage of

the instrument), the temperature could not be studied above 450 ˚C but the information obtained was still valuable.

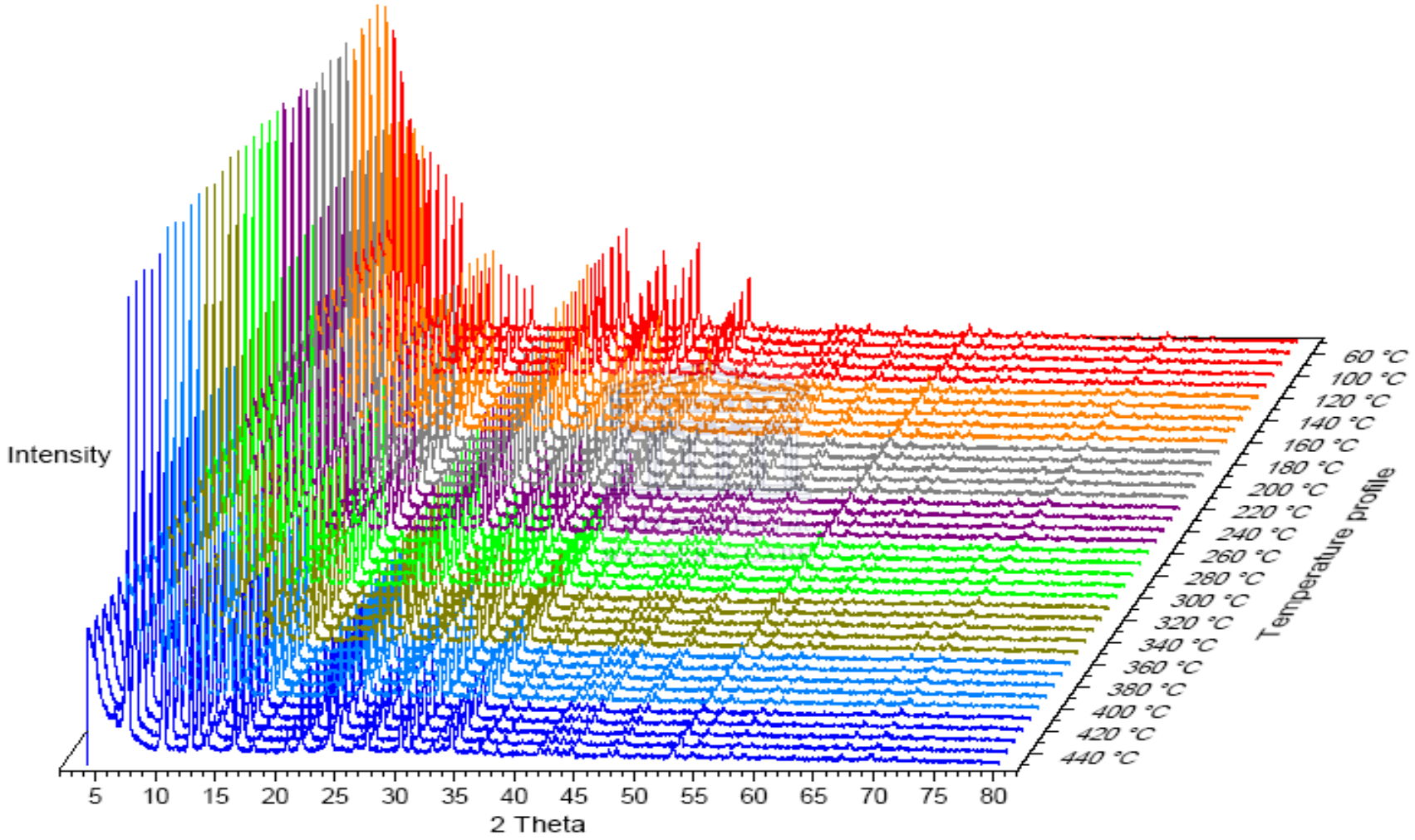

Figure 4-19: XRD patterns for in-situ thermal stability measurements for zeolite A synthesized from unseparated fused fly ash slurry.

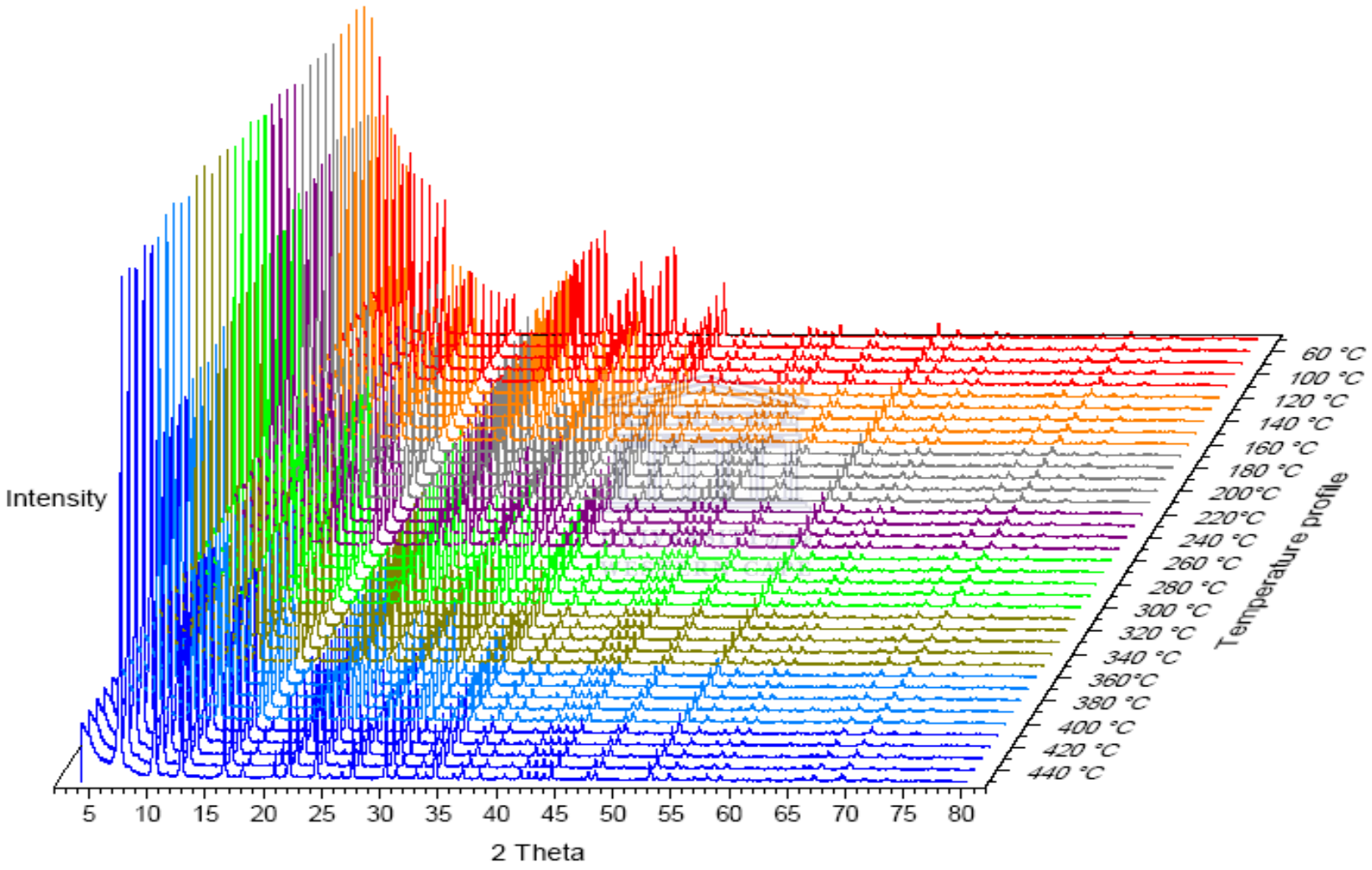

Figure 4-20: XRD patterns for in-situ thermal stability measurements for zeolite A synthesized from clear fused fly ash extract.

From the in-situ temperature programmed XRD analysis presented in Figure 4.19 and 4.20, zeolite A synthesized from either the clear extract or the unseparated slurry were found to retain their characteristic diffraction peaks up to 440 ˚C meaning that the crystal structure was still stable. Even though the XRD analysis was stopped at 440 ˚C, that does not mean that the zeolitic material became unstable thereafter since the TGA analysis did not show any structural changes up to 900˚C. The ability to retain the structural integrity upon heating and water loss together with other properies, makes these zeolites useful in processes that would require elevated temperatures or that might need heat treatment during the regeneration process

4.2.6 Comparison of surface area for zeolite A synthesized from clear fused extract and unseparated fused fly ash slurry.

Table 4.7 presents the comparative results obtained for N_2-BET surface area for the zeolite A synthesized from clear fused extract or unseparated fused fly ash slurry. The respective nitrogen adsorption/desorption isotherms are shown in Figure 4.21.The BET analysis was done on the as-sythesized zeolites product without any post synthesis modifications.

Table 4-7: N_2-BET surface area comparison for zeolite A synthesized from clear fused extract or unseparated fused fly ash slurry.

Sample from	BET surface area (m^2/g)
Clear solution	47
Unseparated slurry	42

From Table 4.7, the BET analysis showed that there was a slight improvement in the N_2-BET surface area when zeolite A was synthesized starting from a clear fused fly ash extract (47 m^2/g) compared to 42 m^2/g that was obtained when unseparated fused fly ash slurry was used. The increase in the product's surface area can be attributed to the relatively higher crystallinity obtained when using the clear extract of fused fly ash that was also observed from XRD and SEM analyses as presented in Figure 4.14 and 4.15 respectively.

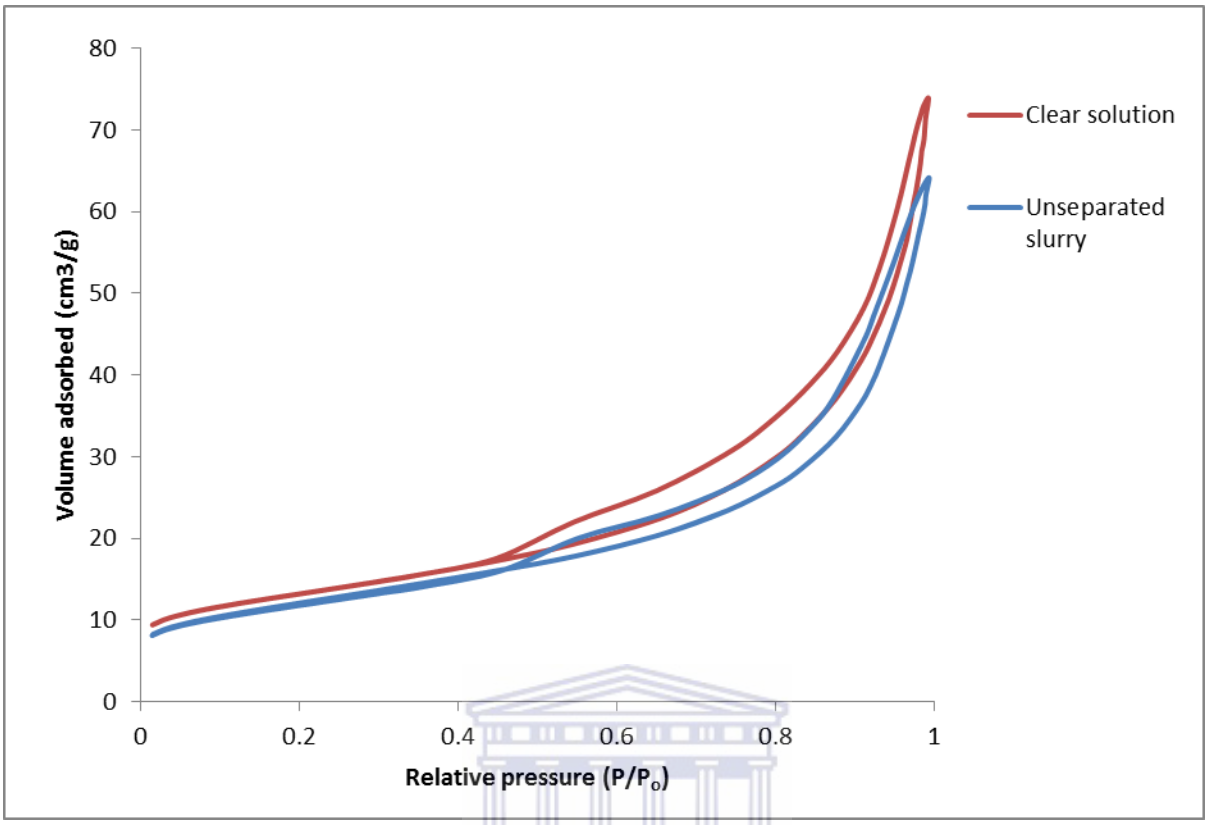

Figure 4-21: Comparison of N_2 adsorption – adsorption isotherms for zeolite A synthesized from clear fused fly ash extract and unseparated fused fly ash slurry.

It has to be mentioned that the obtained surface area can be higher than that reported in Table 4.7 if the zeolite A samples were ion exchanged to the H-form prior to starting the N_2-BET analysis. The reported surface areas are lower than expected probably because of the pore filling effects of the other bigger cations such as Ca^{2+}, K^{+} and Mg^{2+} (see Table 4.5) originating from fly ash that were present as exchangeable cations in the channels of the zeolite A samples, especially in the case of the unseparated fused fly ash slurry sample. As earlier reported (Musyoka, 2009) the BET data should be interpreted with caution and assessed in conjunction with other techniques such as XRD and CEC results to get a better picture of possible artefacts such as those related to the size of the N_2 molecule in relation to the size of the micropore that could lead to lower surface area values.

4.2.7 Synthesis of zeolite A from coal fly ash using mine waters

Since mine water and coal fly ash are the two major waste products produced in close proximity at coal mines and coal-fired stations respectively, it would be of interest to develop a holistic strategy to ameriolate these waste by-products together. Since the initial studies that were reported by Holler and Wirsching (1985), many different types of zeolites have been synthesized from fly ash by varying the synthesis conditions (Querol *et al*., 2002). Most of these studies utilized pure water during the synthesis process apart from a few studies that have concentrated on the use of seawater (Lee *et al*., 2001; Belviso *et al*., 2010). In a previous study (Musyoka *et al*., 2011), it was showed that waste industrial brine could be used during the zeolitization process and a single phase hydroxy-sodalite zeolite was obtained from South African coal fly ash. Another study conducted by Vadapalli and co-workers (2010) showed that co-disposal solids, generated from the active treatment of acid mine drainage with coal fly ash, could be used as a feedstock for zeolite synthesis even though pure water was used during the synthesis procedure.

The current study seeks to investigate the direct use of different types of mine waters as a substitute for pure water during the synthesis of zeolites A. The motivation for this work was inspired by the need for complete industrial waste re-use. In this regard, the use of these two wastes (fly ash and mine waters) in zeolite synthesis will not only offer a potentially capital savings option for disposal of these wastes but will also be advantageous to the coal mines and power stations since it will enable constructive use of the large volumes of waste that they generate.

This section begins by presenting the results of the chemical analysis of the mine waters before results for its applications in the synthesis of zeolite A are discussed.

4.2.7.1 Elemental composition of mine waters

The two types of mine waters (acid and circumneutral) used in this study were collected from Middleburg and Navigation coal mines respectively following the procedure set out in Chapter 3, Section 3.1.2. These coal mines are located in Mpumalanga province of South Africa. The average elemental composition of these mine waters is as reported in Table 4.8. Although the

generic term acid rock drainage is often used to describe mine water discharges, the pH for circumneutral water and acid mine drainage used in this study was found to be 6.5 and 2.5 respectively. The low pH of the acidic mine waters is a known characteristic of these waters (Feng *et al*., 2000). The almost neutral characteristic of the circumneutral water arises due to the partial neutralization of the acidic mine waters as it flows past dolomite rich minerals (Madzivire *et al*., 2010).

Table 4-8: Chemical analysis of circumneutral (CNW) and acid drainage (AMD) mine waters.

Cationic species	CNW (mg/l)	AMD (mg/l)
Fe	0.06	4694.00
Na	952.00	67.74
Ca	18.81	458.40
Mg	37.75	385.50
K	7.60	nd
Mn	0.01	87.75
Si	1.24	31.17
Al	nd	612.60
P	nd	0.54
B	1.02	nd
Ni	nd	2.95
Ba	0.02	nd
Co	nd	1.03
Cu	0.02	2.51
Li	nd	0.36
Pb	0.11	nd
Sr	1.02	1.09
Zn	nd	18.98

Anionic species		
SO_4^{2-}	1475.25	42862
Cl^-	24	9.8

*nd = not detected

From Table 4.8, it is evident that the acidic mine water (AMD) had a high concentration of Fe (4694 mg/L), Ca (458.40 mg/L), Mg (385 mg/L), Al (612.60 mg/L) and Mn (87.75 mg/L) as well as high concentration of SO_4^{2-} (42862 mg/L) and Cl^- (9.8 mg/L). The presence of these elements in the acidic mine water is due to the effect of sulfuric acid which dissolves and mobilizes the elements from the surrounding rocks as it flows around or beyond the mining area. The chemical composition of the generated acidic mine water has been reported to be mainly influenced by the geology of the bedrock in the coal mine (Madzivire *et al.*, 2010). Comparing the chemical compositions of the acidic mine water with that of the circumneutral mine water (CNW), it can be noted that the CNW water had a high concentration of Na (952 mg/L) as well as a comparatively lower amounts of Mg (37.75 mg/L), Ca (18.81 mg/L), K (7.60 mg/L) as well as SO_4^{2-} (1475.25 mg/L) and Cl^- (24 mg/L) content meaning. The high concentration of Na in the circumneutral mine water classifies the CNW as Na-rich mine water (Madzivire *et al.*, 2010). It was also noticeable that the acidic mine water had an orange-yellow colour because of the high concentration of Fe.

4.2.7.2 Synthesis of zeolite A using mine waters

The optimal hydrothermal synthesis conditions for producing zeolite A using pure water (100 °C for 2 hours) starting from unseparated fused fly ash slurry were applied but in this case mine waters (circumneutral and acid mine water) were used as the synthesis solvent. The initial molar ratio of (1 Al_2O_3 : 5.39 Na_2O : 2.75 SiO_2 : 111.82 H_2O) identified was slightly changed by the presence of the additional Al, Si and Na and the new molar ratio for the synthesis mixture prepared using circumneutral mine water was found to be 1 Al_2O_3 : 5.56 Na_2O : 2.50 SiO_2 : 110.86 H_2O whereas that from use of the acidic mine water was 1 Al_2O_3 : 5.10 Na_2O : 2.69 SiO_2 : 107.66 H_2O. Figure 4.22 presents comparative XRD patterns that were obtained when the three solvents (pure, circumneutral or acid mine water) were used when zeolite A was targeted as the

synthesis product. The hydrothermal synthesis temperature and time were retained as 100 °C and 2 hours respectively.

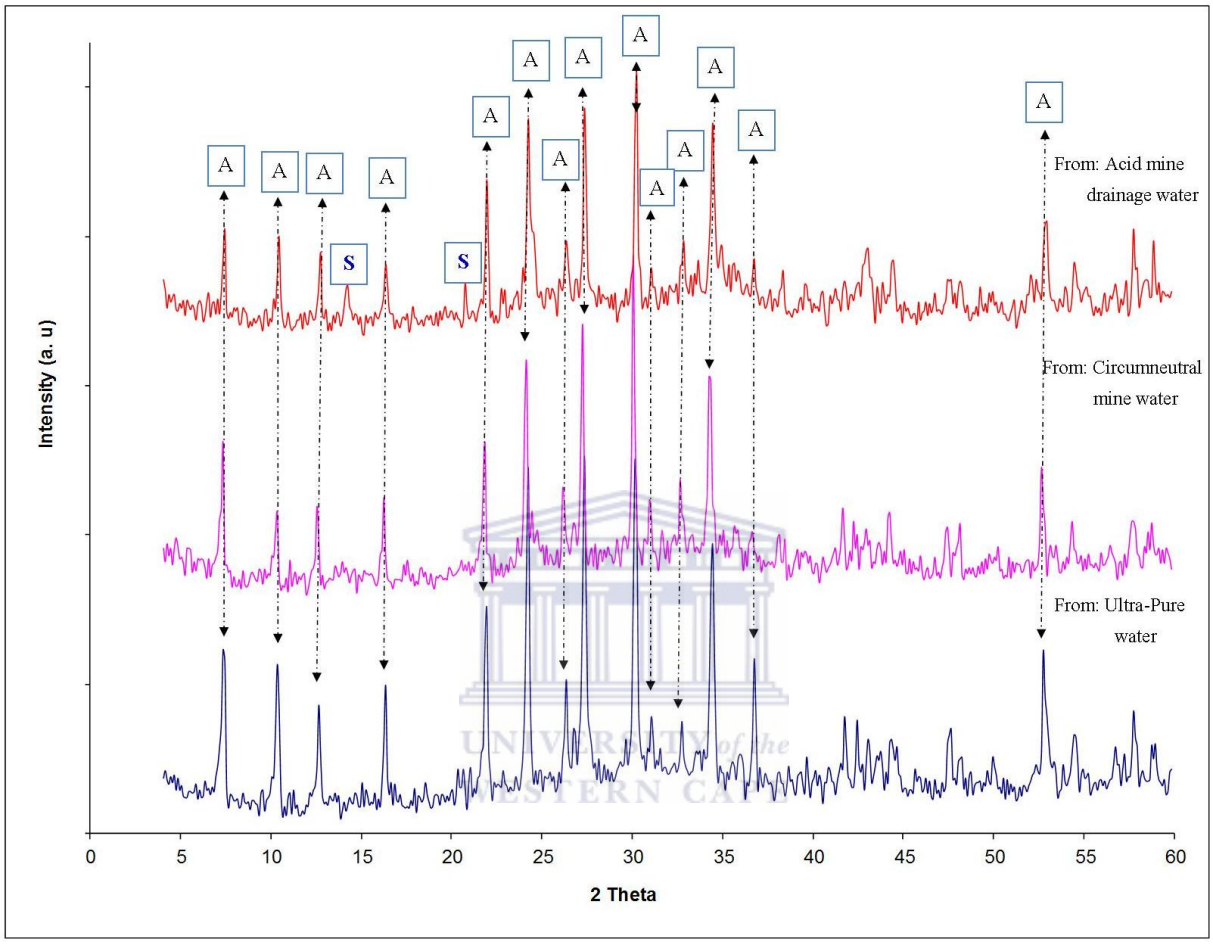

Figure 4-22: Comparative XRD analysis of synthesis products that were obtained when zeolite A was targeted using the three solvents (pure, circumneutral and acid mine water).

From Figure 4.22, when circumneutral mine water was used as the synthesis solvent a single phase zeolite A was obtained. There was not an observable difference compared to the XRD pattern obtained when pure water was used in the synthesis process. In the case when acid mine drainage was used as the synthesis solvent, zeolite A was found to co-crystallize with a 'contaminant' hydroxy-sodalite phase. The formation of single phase zeolite A using circumneutral mine water means that the extra cations in the circumneutral mine water did not have any profound effect upon the crystallization of the zeolite. The failure to obtained single

phase zeolite A in the case when acid mine drainage was used could be attributed to the presence of higher concentrations of Fe and Ca in the acid mine drainage mine water.

The SEM micrographs of the synthesis product obtained from unseparated fused fly ash slurry when circumneutral mine water or acid mine drainage water were used are presented in Figure 4.23.

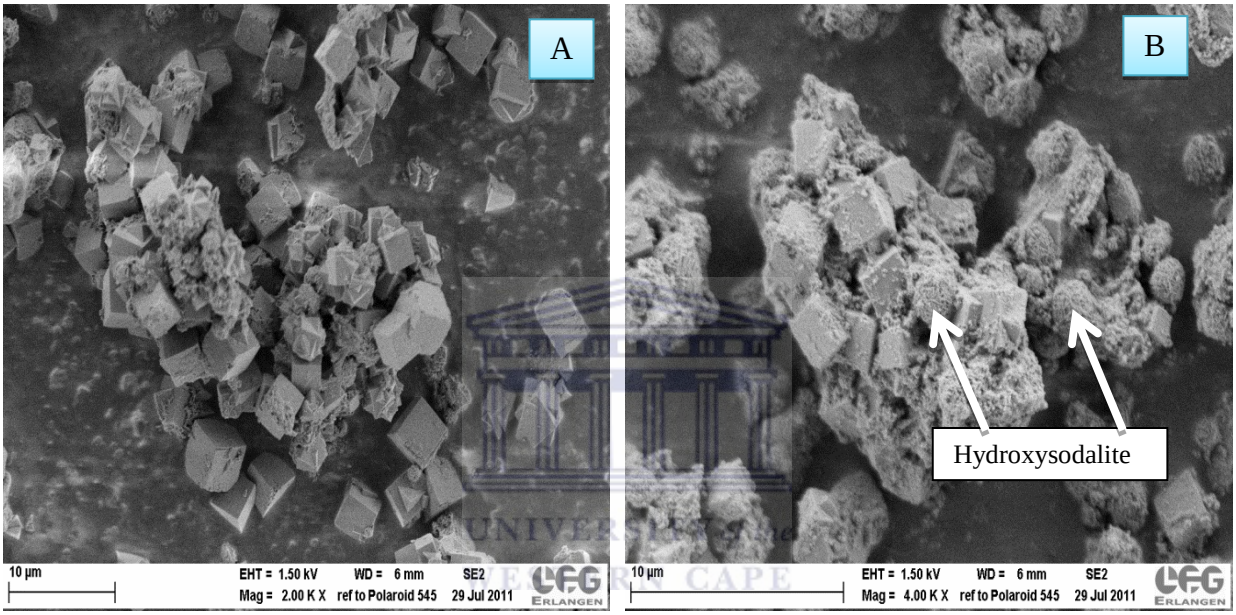

Figure 4-23: SEM micrographs of zeolite A synthesized from unseparated fused fly ash slurry using a) circumneutral mine water and b) acid mine drainage water.

The observations noted in the SEM micrographs presented in Figure 4.23 served to complement the XRD analysis. It can be seen that the well-known sharp edged cubic crystals of zeolite A were observed when circumneutral mine water (Figure 23 (a)) was used as the synthesis solvent. The morphology of the zeolite A crystals was similar to that obtained when pure water was used during synthesis as shown in Figure 4.15 (a). A mixture of the two zeolitic phases in the case of the use of acid mine drainage was confirmed by the SEM images where cubic crystals of zeolite A and small irregular crystals that correlate to hydroxysodalite zeolite were observed.

4.2.7.3 Chemical analysis of zeolitic products

The chemical analyses of zeolitic products obtained when circumneutral mine water and acid mine drainage water were used as a substitute for pure water during the synthesis of zeolite A from unseparated fused fly ash slurry are presented in Table 4.9 (major elements) and 4.10 (trace elements).

Table 4-9: Elemental analysis (major elements) of solid synthesis product obtained following the procedure for synthesis of zeolite A using pure water, circumneutral mine water (CNW) and acid mine drainage water (AMD) when unseparated fused fly ash slurry was used.

Major elements (oxide)	Pure water (Average mass %)	CNW water (Average mass %)	AMD water (Average mass %)
SiO_2	31.64	34.43	26.24
Al_2O_3	19.64	29.38	18.60
Na_2O	12.80	18.27	6.65
CaO	7.45	0.05	2.27
Fe_2O_3	6.48	0.06	34.18
MgO	1.82	0.04	1.64
TiO_2	1.08	0.05	0.06
K_2O	0.14	0.06	0.06
P_2O_5	0.05	0.01	0.06
MnO	0.06	nd	0.38
SO_3	0.01	nd	0.09
LOI	16.03	17.47	9.60
H_2O	2.23	0.17	0.15
SUM	99.42	99.99	99.99
SiO_2/ Al_2O_3	1.61	1.17	1.41

Table 4-10: Elemental analysis (trace elements) of solid synthesis product obtained following the procedure for synthesis of zeolite A using pure water, circumneutral mine water (CNW) and acid mine drainage water (AMD) when unseparated fused fly ash slurry was used.

Trace elements	Product from Pure water (Average ppm)	Product from CNW water (Average ppm)	Product from AMD water (Average ppm)
V	351.11	nd	14.31
Co	1167.43	nd	18.66
Ni	557.43	59.33	93.70
Ce	222.20	nd	161.86
Pb	107.70	15.43	nd
Zn	98.81	nd	189.01
Cu	88.47	34.48	82.76
Y	85.33	nd	57.56
Zr	81.89	30.92	30.86
Rb	61.75	61.12	nd
Cr	52.45	nd	27.17
Ba	25.45	75.52	74.66
Mo	2.05	0.64	0.76
Sr	nd	82.47	51.27
U	na	138.42	nd

*nd = not detected, na = not analyzed

A number of the elements that were originally in the fly ash (Table 4.1 and 4.2) and mine waters (Table 4.8) were also detected in all the zeolitic products as shown in Table 4.9 and 4.10. The major elements in the zeolitic products synthesized using circumneutral mine water were Si, Al, Fe, Na, Ca, Fe, Mg, Ti, K, P, Mn, and SO_3 while the trace elements were Ni, Cu, Rb, Sr, Zr, Zn,

Ba, Mo, Pb and U. Trace elements such as V, Cr, Co, Zn, Y and Ce that had been shown in the starting fly ash (Table 4.2) were not detected in the zeolitic product synthesized from circumneutral mine water. In the synthesis product obtained when acid mine drainage mine water was used, the major elements in the zeolitic products were Si, Al, Fe, Na, Ca, Fe, Mg, Ti, K, P, Mn, and SO_3 while the trace elements were V, Cr, Co, Ni, Cu, Rb, Sr, Zr, Zn, Ba, Mo and Ce. Though available in the original fly ash Rb, Pb and U were not detected in the synthesis product obtained when acid mine drainage water was used as the synthesis solvent. Comparing the concentration of both major and trace elements in both Table 4.9 and 4.10, it can be noted that the zeolitic product obtained using the circumneutral mine water had a higher concentration of some elements such as Si, Al, Na, Sr, and Ba. The elevated concentration of Na and Ba in zeolitic product obtained using the circumneutral mine water could be explained due to the higher content in the circumneutral mine water whereas the differences in concentration of Si, Al, and Sr could not be explained at this stage.

In both cases when circumneutral mine water and acid mine drainage water were used as a substitute for pure water during the synthesis of zeolite A from unseparated fused fly ash slurry, the concentration of Fe, Mg, Ca and Na was found to be higher in the zeolitic product than was found in the original fly ash. The rest of the elements had a relatively lower concentration in the product implying that the balance of the species had been released into the post-synthesis supernatant. Si and Al, being the main elemental building units of the zeolite structure, were the most abundant in the zeolitic products. Different ways of incorporation of the cations and trace elements are possible, e.g a) availability within the framework as charge balancing cation which would be the case for K, Na, Ca, Mg and possibly Rb, Sr, Cs and Ba, b) isomorphous substitution in the zeolitic framework i.e Fe and Ti and/or c) as an oxide in the zeolitic channels or pores d) as discreet adsorbed species. The concentration of Na was found to be relatively higher because it is the most prominent charge balancing cation in the zeolitic product and its quantity was promoted by the use of NaOH during the fusion step and also by the Na content in the mine waters. High percentages of incorporation of Fe could make this zeolite gain applications in processes that require Fe such as in DeNOx but would require future work to ascertain the validity of the proposal. Zeolite containing elements such as Ti, V, Fe and other transition elements are also of interest mainly because of their potential applications as catalysts

for selective oxidation (Weitkamp, 2000). Comparing the concentration of elements in the zeolite A obtained using pure water (starting from unseparated fused fly ash slurry) with the product obtained using mine waters, it was noted that product obtained using pure water and curcimneutral mine water had their elemental content in the same order of magnitude whereas acid mine water product had a completely different trend.

4.3 Chapter summary

In conclusion, the optimum conditions for preparing A single phase zeolite A from South African class F fly ash were identified. There conditions were a molar ratio of 1 Al_2O_3 : 30.84 Na_2O : 4 SiO_2 : 414.42 H_2O for synthesis conducted starting from clear fused fly ash extract whereas when the unseparated fused fly ash slurry was used, the molar ratio was 1 Al_2O_3 : 5.39 Na_2O : 2.75 SiO_2 : 111.82 H_2O; the best hydrothermal synthesis temperature and time were 100 ℃ and 2 hours respectively. Apart from identifying and optimizing the synthesis conditions for producing high phase purity of zeolite A from South African fly ash, a reduction of synthesis time was achieved. The procedure used also managed to avoid the step-change synthesis temperature that had been recommended by Hui and Chao (2006) who had reported that this route enabled faster synthesis time. The direct 2 hours synthesis was achieved by optimizing Al content, amount of water and synthesis temperature and guarantees simplicity of the synthesis procedure should the zeolite A production process go to the scale up stage. The considerable improvement in the quality of zeolite A which was shown when the clear extract of fused fly ash was used instead of starting from unseparated fused fly ash slurry is also another success because the better quality zeolite is expected to allow high end applications of the zeolite, which are often unattainable due to the presence of residual fly ash in the synthesis product as obtained by other researchers. The reduction of trace elements in zeolite A product obtained by use of the clear extract of fused fly ash also showed that filtration of the fused fly ash slurry prior to hydrothermal synthesis played a crucial role in determining the quality of the zeolitic product.

It was also found that it was possible to obtain high quality of zeolite A when circumneutral mine waters were used as a substitute for pure water during the synthesis process whereas a mixture of zeolite A and hydroxysodalite was obtained when acidic mine water was used. This

novel finding highlight that the quality of the zeolite formed is dependent on the type of mine water used. From an environmental and economic point of view, the process of using both fly ash and mine water established in this study will not only reduce the environmental burden associated with these wastes but could also offer extra income generated from the sale of the synthesized zeolites. These findings are also expected to trigger research on the synthesis of zeolite from mine waters and fly ash using the waste heat generated in the coal power plants.

The next chapter discusses results obtained during the search for the synthesis conditions for zeolite X from the same South African fly ash (Arnot). The study aimed at obtaining a better quality zeolite X from fly ash than has been reported in the literature.

CHAPTER 5

IDENTIFICATION AND OPTIMIZATION OF SYNTHESIS CONDITIONS FOR ZEOLITE X FROM SOUTH AFRICAN FLY ASH

This chapter is divided into two sections; the first section presents results of studies conducted to customize the synthesis conditions for producing the well-known octahedral morphology of zeolite X from South African fly ash so as to create a basis for investigating the potential of using mine waters as a substitute for pure water during the synthesis process. The second section presents the findings of the procedure developed to produce novel morphology (hierarchical) zeolite X from fly ash. The optimized conditions identified in this chapter will later be applied during the investigation of the formation mechanism of this zeolite from fly ash (Chapter 6). Different characterization techniques such as FTIR, SEM, HRTEM, TGA and BET were used to probe properties that are important when determining the characteristics of these zeolites.

5 Introduction

Synthesis of zeolite X from South African fly ash was targeted because it has many industrial applications and has proved to be almost equally effective as a catalysts compared to its commercial counterpart (Ojha *et al*., 2004; Sutarno and Arryanto, 2007; Hui *et al*., 2008). It is also worthwhile to mention that estimates reported by Ojha *et al*., (2004) suggested that the cost of producing zeolite X from fly ash was almost one-fifth that of producing commercial X from pure chemicals. Hence from an economic point of view the synthesis of zeolite X from South African coal fly ash feedstock could present a competitive advantage compared to the existing pure chemical feedstock used for preparing commercial zeolite X. As discussed earlier in Chapter 4, the variability in fly ash composition, in relation to fly ashes used by other researchers, requires that conditions for the synthesis of zeolite X from fly ash sourced from South African coal-fired power plants have to be identified and optimized. The study commenced by reviewing the different synthesis methods reported in the literature (Mondragon, 1990; Shigemoto *et al*., 1993; Amrhein *et al*., 1996, Srinivan *et al*., 1999, Hollman *et al*., 1999; Chang *et al*., 2000; Scott *et al*., 20001; Tanaka *et al*., 2002; Querol *et al*, 2002; Molina *et al*., 2004, Derkowski *et al.,* 2006, 2007; Wojciech, 2012). Apart from noting that most of the existing synthesis methods were diverse and customized to suite the composition and type of fly ash used, they all generated the well-known pyramidal octahedral-shaped crystals of zeolite X. This finding implied that should a route be found for the synthesis of zeolite X with unique and

improved features such as hierarchical morphology, the new morphology would excite more interest for fly ash zeolitization. The first section of this chapter is dedicated to studies on identifying and customizing the hydrothermal synthesis conditions for producing a single phase zeolite X from South African fly ash. Once these conditions had been identified, investigations on the potential to synthesize zeolite X using mine waters as a substitute for pure water were conducted. There are no studies that have reported the use of mine waters as solvent to produce zeolite X. The use of mine waters, as solvent which is an effluent produced from coal mining operation, in zeolite synthesis using fly ash would serve to beneficiate two major wastes that are found in close proximity to each other. The second section is dedicated to studies on the synthesis of a high quality zeolite X from fly ash. This section also lays the foundation for studies intended to investigate the formation mechanism of zeolite X using the in-situ ultrasonic monitoring technique which will be presented in Chapter 6.

5.1 Identification and optimization of hydrothermal conditions for zeolite X from unseparated fused fly ash slurry.

This subsection presents the results obtained from studies on identification and optimization of zeolite X (typical octahedral morphology) from South African fly ash (Arnot). Based on reports from previous studies (Shigemoto *et al*., 1993; Chang *et al*., 2000; Molina and Poole, 2004), variation of hydrothermal synthesis temperature and time were the two main parameters that would require adjustment. The chosen synthesis route followed the alkali fusion step prior to hydrothermal crystallization step mostly because it has been reported to lead to a higher probability for selective synthesis of zeolite X from fly ash. Information generated from the XRD analysis was used as a guide during the optimization process. Once the conditions for producing the best quality of zeolite X were identified, other characterization techniques such as FTIR, SEM, HRTEM, TGA and BET were applied.

5.1.1 Variation of hydrothermal synthesis temperature

The South African Arnot fly ash used during the synthesis of zeolite X was firstly fused with NaOH (mass ratios of 1:1.2) by heating in the oven at 550 ºC for 1.5 hours (see Chapter 3, Section 3.2). The solid/liquid mass ratio of fused fly ash to water was maintained at 1:5 and after

fusion, the mixture had been stirred for 2 hours at room temperature to dissolve the fused fly ash before the hydrothermal crystallization step. Unlike in the case of synthesis of zeolite A, no additional Na-aluminate was added to the fly ash based synthesis mixture. For the synthesis mixture having a molar regime of 1 Al_2O_3 : 4.90 Na_2O : 3.63 SiO_2 : 115.92 H_2O, three hydrothermal temperatures variations (80, 90 and 100 ºC) were chosen and the synthesis time was fixed at 12 hours. Figure 5.1 presents the XRD diffractograms for the synthesis products obtained at these three hydrothermal synthesis temperatures using unseparated fused fly ash slurry.

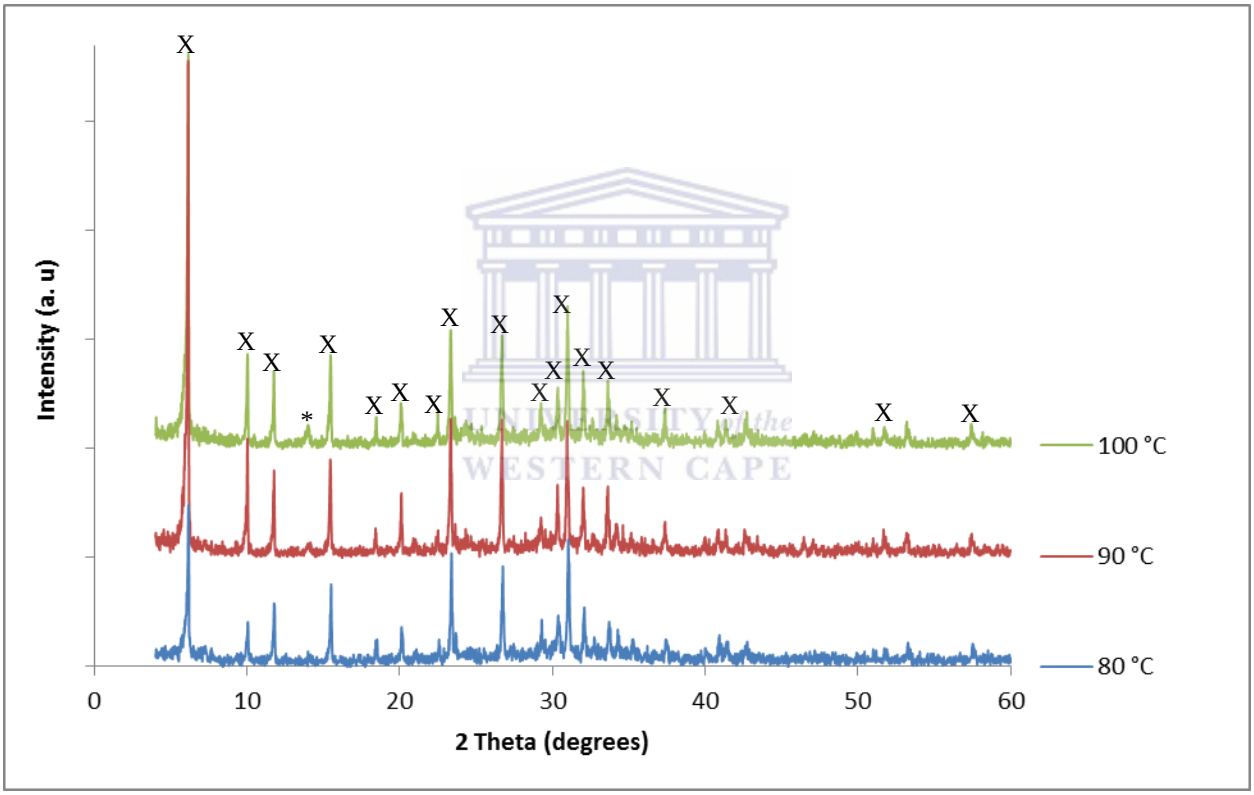

Figure 5-1: XRD diffractograms for the synthesis products obtained when unseparated fused fly ash was used in the case where the hydrothermal synthesis temperature was varied between 80, 90 and 100 ºC for the synthesis time fixed at 12 hours.

From Figure 5.1, it can be observed that a single pure phase zeolite X was obtained when hydrothermal synthesis was conducted at 80 and 90 ºC but when the temperature was raised to 100 ºC a contaminant phase (marked as *) could be observed. From a scale up point of view it

would be attractive to synthesize zeolites at lower hydrothermal temperatures, so it was deemed important to optimize the synthesis time when the hydrothermal synthesis temperature was set at 80 ºC. The discussion that follows concentrates on the optimization of hydrothermal synthesis time.

5.1.2 Variation of hydrothermal synthesis time

Following the identification of the best hydrothermal synthesis temperature (Section 5.1.1), the hydrothermal synthesis time was varied from 4 hours to 48 hours while holding the synthesis temperature constant at 80 ºC. The solid/liquid mass ratio of fused fly ash to water was still maintained at 1:5 with 2 hours stirring time at room temperature before the hydrothermal crystallization step commenced using unseparated fused fly ash. After hydrothermal crystallization, the mineralogical analysis of the resulting synthesis product is presented in Figure 5.2.

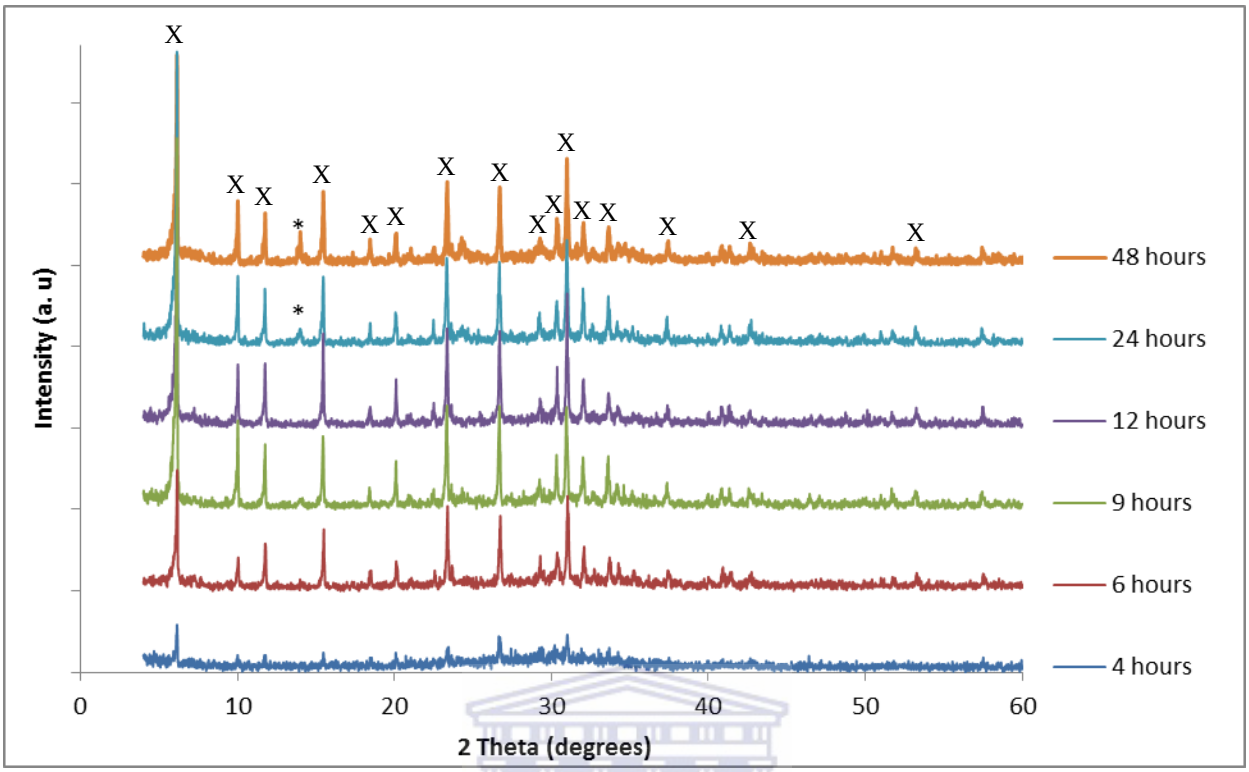

Figure 5-2: XRD patterns for the synthesis products obtained when unseparated fused fly ash was used in the case where the hydrothermal synthesis time was varied between 4 to 48 hours at a synthesis temperature of 80 ºC.

Figure 5.2 shows that at lower hydrothermal synthesis time (4 and 6 hours) traces of amorphous material, as characterized by the 'hump' between 20 and 35° in the XRD diffractograms, were still present signifying that zeolite X was not fully crystalline. When the synthesis time was increased up to 9 and 12 hours, a single phase highly crystalline zeolite X was formed. When the synthesis time was prolonged to 24 and 48 hours, an unidentified contaminant phase (marked as *) was observed to co-crystalize with zeolite X. Since synthesis at 9 and 12 hours did not show any significant difference in the quality of the synthesis product, the hydrothermal crystallization time of 9 hours at 80 ºC was chosen as the most suitable for preparing a single pure phase zeolite X.

5.1.3 Characterization of zeolite X obtained after optimization experiments

The optimized temperature and synthesis time (from subsection 5.1.1 and 5.1.2) for preparation of zeolite X from unseparated slurry mixture, having a molar regime of 1 Al_2O_3 : 4.90 Na_2O : 3.63 SiO_2 : 115.92 H_2O, was 80 ºC and 9 hours respectively. The synthesis products obtained under these conditions were further characterized using other techniques as will be discussed in the sub-sections that follow.

5.1.3.1 Morphological analysis of synthesis products prepared from unseparated fly ash slurry

Figure 5.3 compares the morphological features of the synthesized fly ash-based zeolite X with that of commercial zeolite X in its Na-form (obtained from CWK, Bad Köstritz) as analysed by Scanning Electron Microscopy (SEM) following the procedure described in Chapter 3, Section 3.5.4.1.

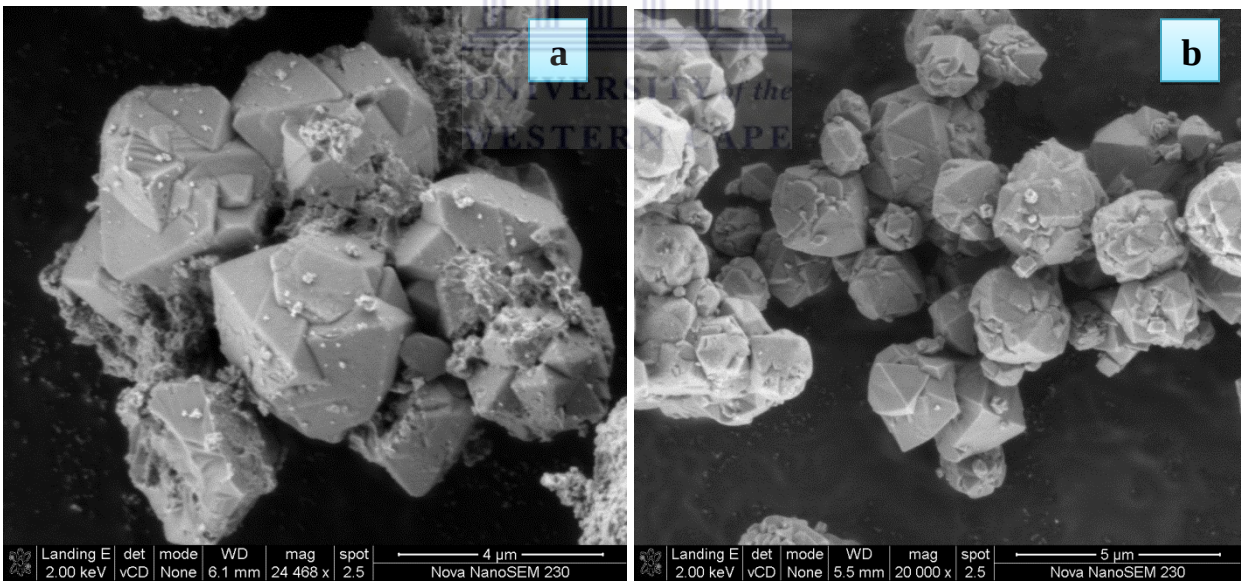

Figure 5-3: SEM micrographs of zeolite X a) synthesized from fused unseparated fly ash slurry at 80˚C for 9 hours a) Commercial zeolite Na-X.

SEM micrographs presented in Figure 5.3, showed that the well-known pyramidal octahedral-shaped crystals (though with some crystal intergrowths) of zeolite X was formed when zeolite X

was synthesized from unseparated fused fly ash slurry having a molar regime of 1 Al_2O_3 : 4.90 Na_2O : 3.63 SiO_2 : 115.92 H_2O at 80 ºC for 9 hours (Figure 3 (a)) and the morphology compared well with its commercial counterpart (Figure 3 (b)).

5.1.3.2 Structural analysis of the synthesis products

A comparison of the infra-red spectra of commercial zeolite X (Na-form) with that of the synthetic product obtained from unseparated fused fly ash at 80 ˚C for 9 hours is presented in Figure 5.4.

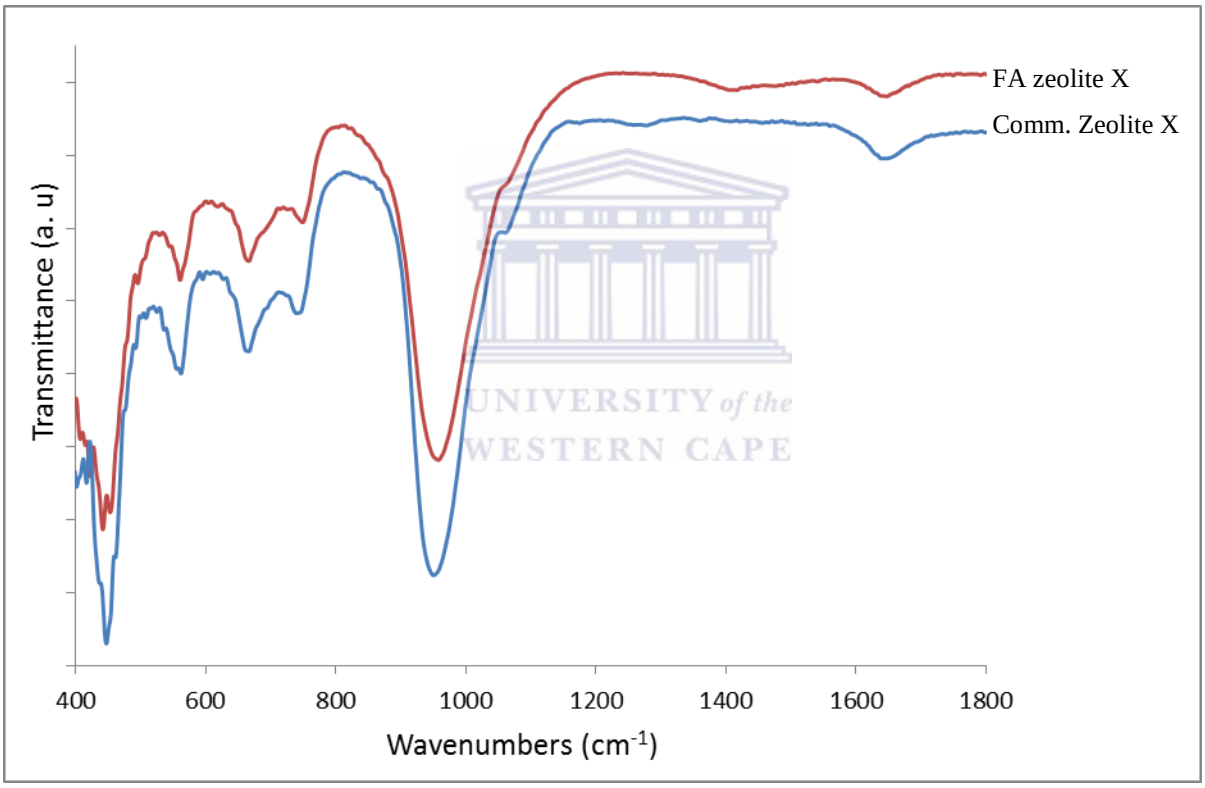

Figure 5-4: Comparative FTIR spectra of commercial zeolite X with that of fly ash (FA) based zeolite X synthesized from unseparated fused fly ash at 80 ˚C for 9 hours.

As shown in Figure 5.4, all the IR vibrational bands identified in the commercial zeolite X closely matched the bands of fly ash-based zeolite X. This close matching is indicative of the similarity of their structural units and chemical moieties. It is also important to highlight that there was close matching of IR spectral data with that reported in the literature (Flanigen, 1971)

for X type zeolites. The presence of vibrational bands between 550 and 560 cm^{-1} is a good identifier for zeolite X since this vibrational region is designated for double ring region. Zeolite X is known to have double six-ring (D6R) units in the framework structure as shown in Figure 2.2 and 2.3 (Chapter 2).

5.1.3.3 Thermal stability analysis

Thermal stability limits of the fly ash-based zeolite X were investigated by thermal gravimetric analysis (TGA) following the experimental procedure detailed in Chapter 3, Section 3.5.7.2. In order to compare the thermal stability of the fly ash-based zeolite X to its commercial counterpart, their TGA thermographs were overlaid as shown in Figure 5.5.

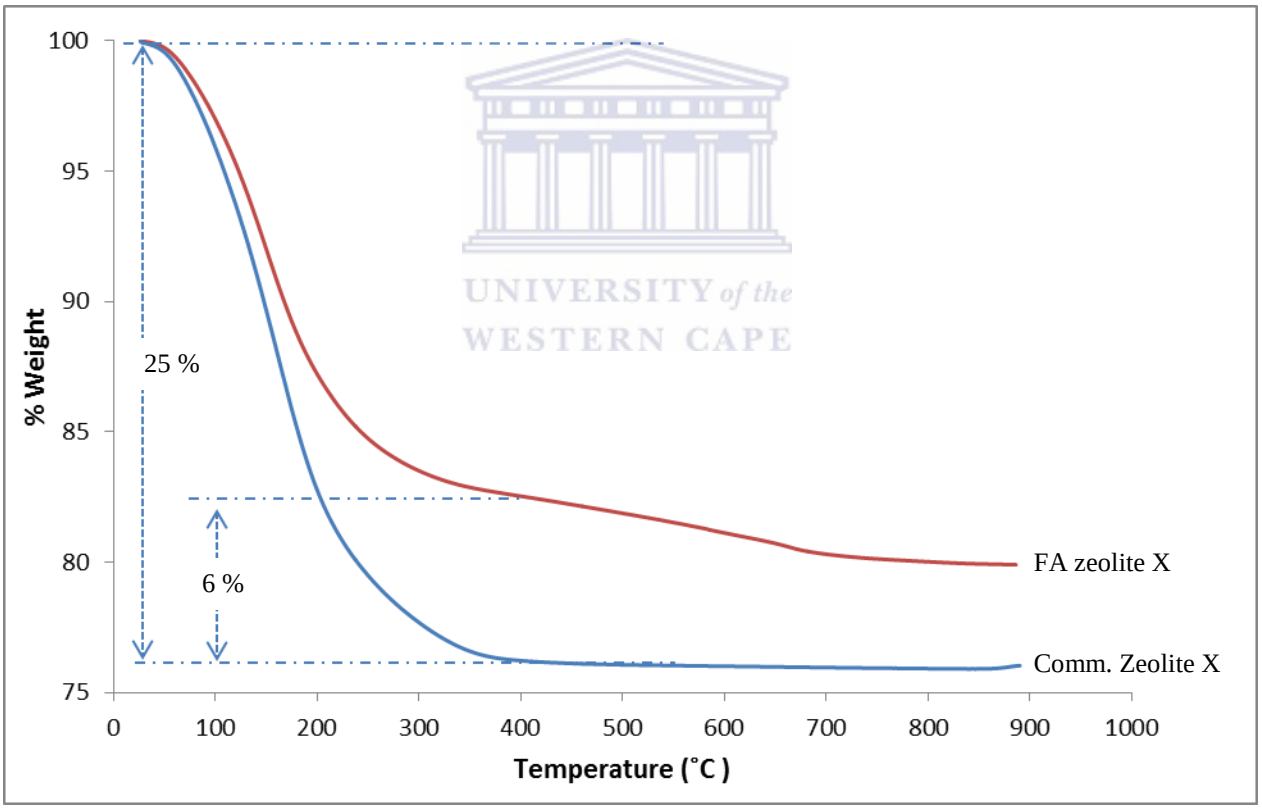

Figure 5-5: Comparative TGA thermographs of commercial zeolite X with that of fly ash (FA) based zeolite X synthesized from unseparated fused fly ash at 80 ˚C for 9 hours.

From Figure 5.5, it can be observed that the moisture loss from both the fly ash-based zeolite X and its commercial counterpart started between 40 and 50 ˚C. The weight loss observed below

100 °C is caused by desorption of physically adsorbed moisture from within the porous microstructure. Complete dehydration associated with the loss of all the free, sorbed and Na-complexed water is expected to occur between 400 – 450 ˚C which can be observed as negligible weight loss that occurred beyond this temperature range (Akbar *et al*., 2005). The difference in % weight loss (6 %) between the fly ash-based zeolite X and its commercial counterpart could be explained by the differences in their porosity as is indirectly reflected in their surface areas shown in Table 5.1. The presence of small amounts of unconverted precursor species that were seen in the SEM micrographs for the fly ash-based zeolite X (Figure 5.3 (a)) could be the main contributing factor. As is also shown in the Table 5.2, the presence of cations such as Ca^{2+}, K^{+}, and Mg^{2+} in the pores of the zeolite could act as counter ions in the zeolite X. These cations could have had a pore filling effect thus leading to a lower void volume reducing the water uptake. From the TGA thermographs, it can be concluded that the fly ash-based zeolite X was as thermally stable as its commercial counterpart and that it could serve well in applications requiring elevated temperatures.

5.1.3.4 Surface area and pore size distribution analysis of fly ash based zeolite Na-X.

The BET surface area of the South African fly ash-based zeolite X and the N_2 adsorption – desorption isotherm for fly ash based zeolite X synthesized from unseparated fused fly ash at 80 ˚C for 9 hours is shown in Table 5.1 and Figure 5.6 respectively. The details for sample preparation and procedure for analysis is described in Chapter 3, Section 3.5.6.

Table 5-1: The BET surface area of the fly ash-based zeolite X synthesized from unseparated fused fly ash at 80 ˚C for 9 hours

	Fly ash based zeolite X	Commercial zeolite X
Micropore Area (m^2/g)	303	713
External Surface Area (m^2/g)	48	33
Total BET Surface Area (m^2/g)	351	746

The obtained total BET Surface Area of the South African fly ash based Na-form zeolite X (351 m^2/g) was in the range that has been reported by other researchers such as by Ojha *et al*. (2004). The difference in the surface area when compared to commercial zeolite X can be ascribed to be due to pore blocking effect emanating from presence of cations in the fly ash based zeolite framework as shown in Table 5.2.

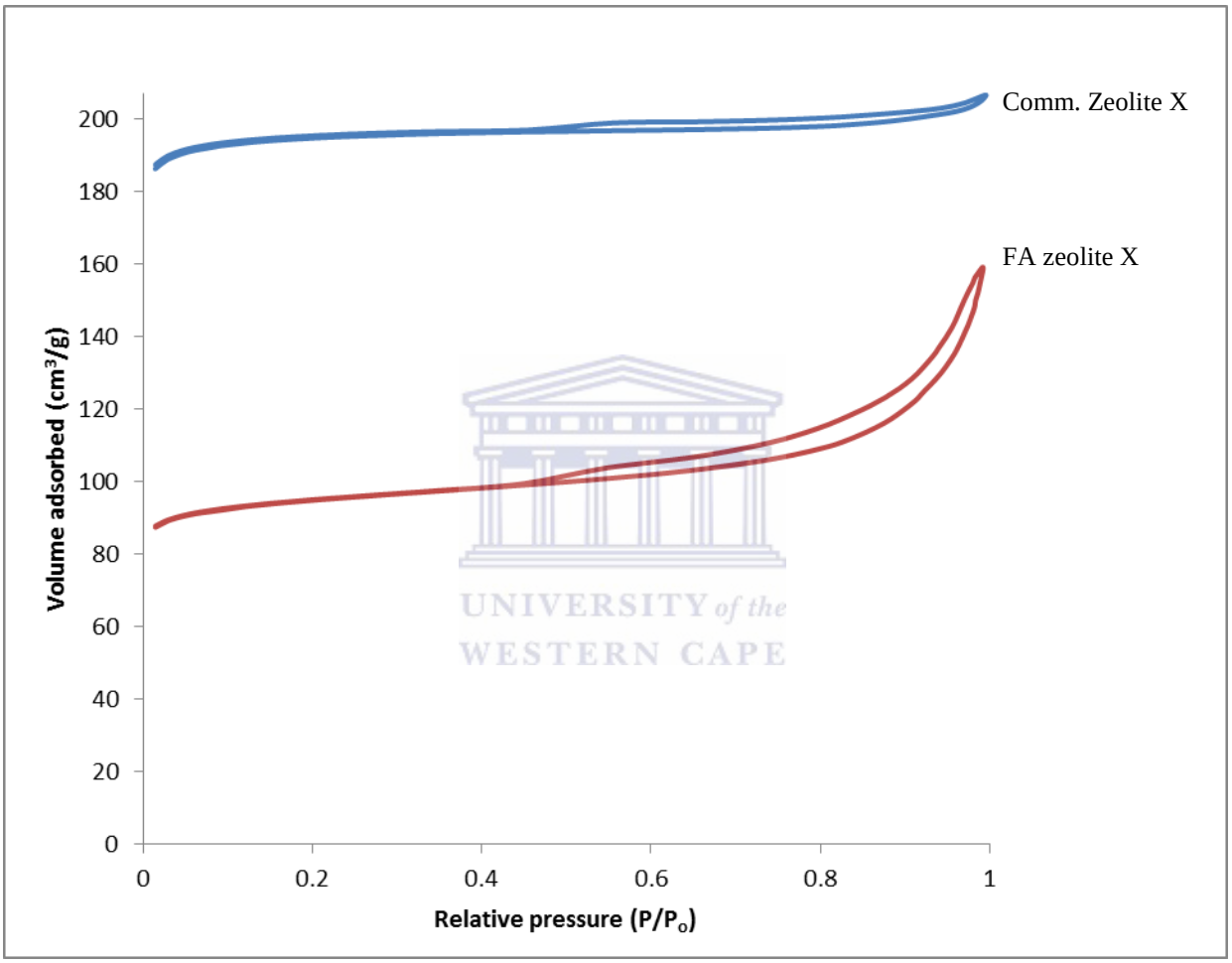

Figure 5-6: Comparative N_2 sorption isotherms for commercial zeolite X with that of fly ash (FA) based zeolite X synthesized from unseparated fused fly ash at 80 ˚C for 9 hours.

According to classification of N_2 sorption isotherms reported by Lowell *et al*. (2006), N_2 sorption isotherms for both commercial zeolite X and fly ash based zeolite X (Figure 5.6) was observed to be of type IV systems. The hysteresis loops observed in the region of higher partial pressure originates from mesopores created by the aggregated zeolite crystals.

5.1.4 Synthesis of zeolite X from South African fly ash using mine waters

These experimental details for the use of mine waters during the synthesis of zeolite X are described in Chapter 3, Section 3.2.3.1. The hydrothermal synthesis was conducted at 80 °C for 9 hours. The results of the elemental analysis of the mine waters are presented in Table 4.8 (Chapter 4). The initial molar ratio of the synthesis mixture prepared using pure water (1 Al_2O_3 : 4.90 Na_2O : 3.63 SiO_2 : 115.92 H_2O) was slightly changed by the presence of the additional Al, Si and Na in the mine waters to obtain 1 Al_2O_3 : 4.95 Na_2O : 3.77 SiO_2 : 118.12 H_2O for the mixture prepared using circumneutral mine water and 1 Al_2O_3 : 5.43 Na_2O : 3.50 SiO_2 : 120.65 H_2O when acidic mine water was used. The comparative XRD analysis of the synthesis products obtained when zeolite X was synthesized using pure water, or either circumneutral mine water or acid mine drainage mine water, is presented in Figure 5.7.

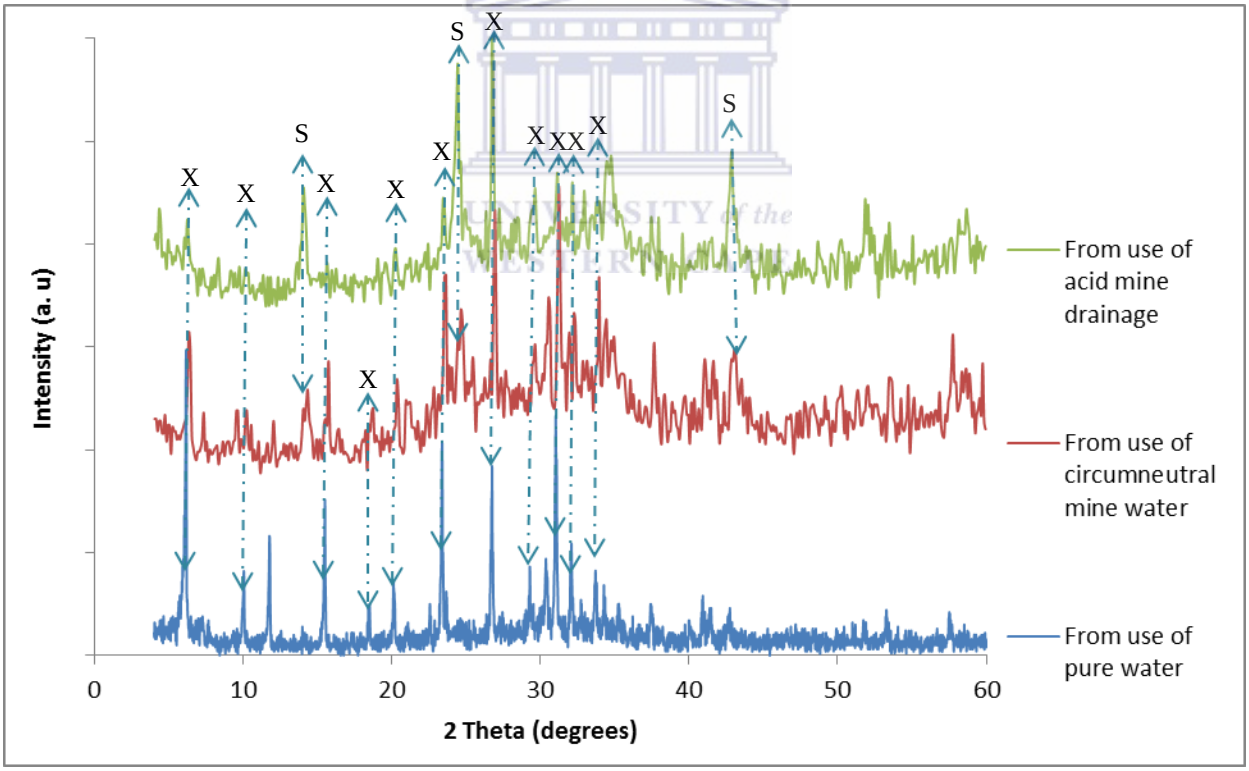

Figure 5-7: XRD analysis of synthesis products that were obtained when zeolite X was targeted using pure water, or either circumneutral mine water or acid mine drainage mine water.

As shown in Figure 5.7, when the optimized hydrothermal synthesis conditions for producing zeolite X were applied using either the circumneutral or acidic mine water as a substitute for pure water, a mixture of hydroxysodalite and zeolite X was obtained, which was unlike the single phase zeolite X obtained when pure water was used. The background hump appearing between 20 - 40 ° 2θ in the XRD spectra provides evidence for the presence of an amorphous glassy phase meaning that the fused precursor species had not been fully transformed into zeolitic material. This observation could mean that the hydrothermal synthesis conditions of 80 ℃ for 9 hours could still need further optimization in the cases of the use of mine water as the synthesis solvent. This observation was also confirmed by the respective SEM images presented in Figure 5.8.

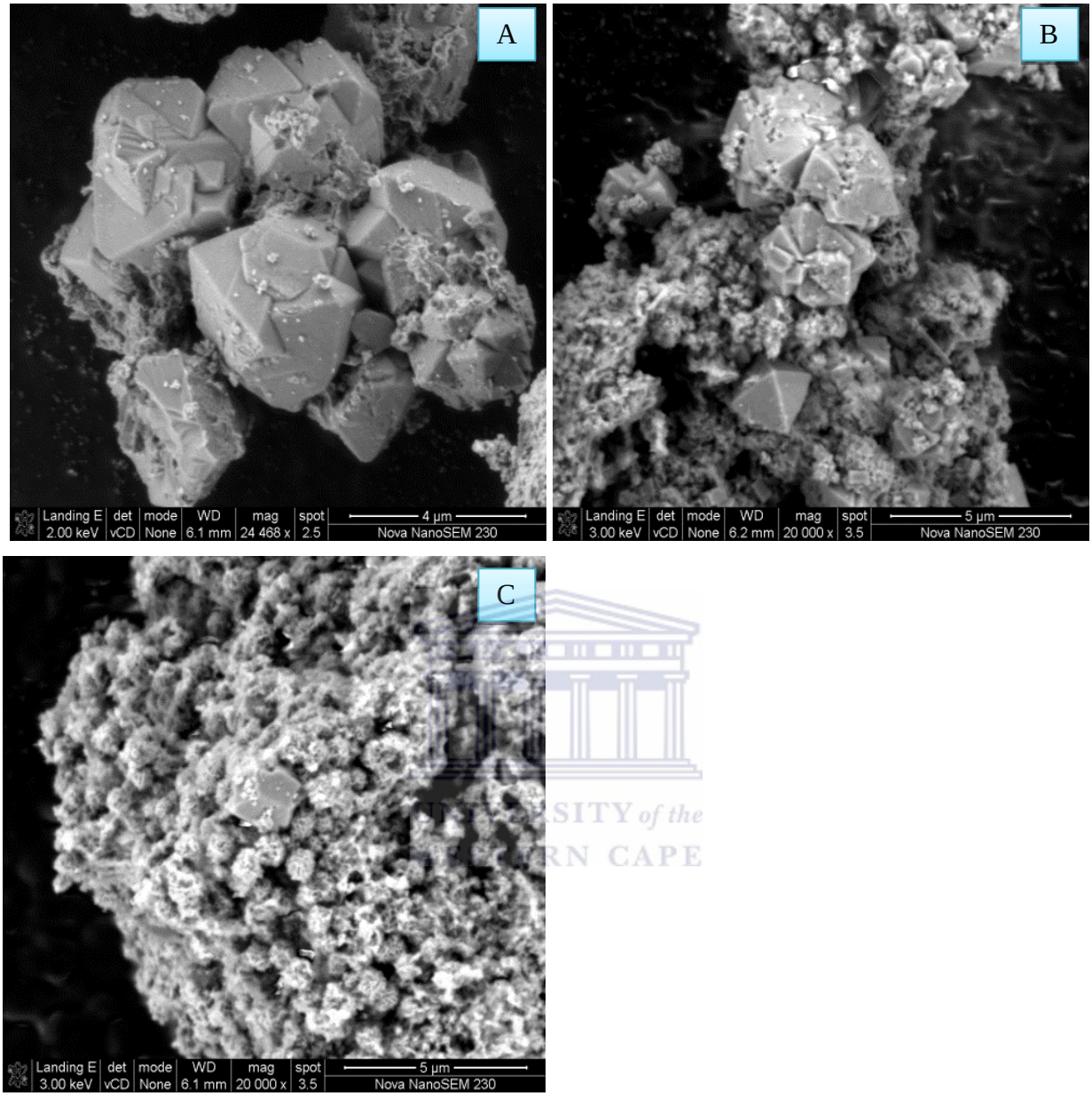

Figure 5-8: SEM micrographs of zeolite X synthesized from unseparated fused fly ash slurry using a) pure water b) circumneutral mine water and c) acid mine drainage water.

In the corresponding morphological analysis by SEM of the synthesized zeolitic products, shown in Figure 5.8, the single phase zeolite X obtained using pure water had the typical pyramidal octahedral shaped crystal morphology whereas a mixture of small globular-shaped aggregates of hydroxy-sodalite crystals and the pyramidal octahedral-shaped crystals of zeolite X could be observed when the mine waters were used. The failure to obtained single phase zeolite X, unlike

in the case when zeiolite A when mine waters were used could be attributed to the presence of higher concentrations of extra cations in the acid mine drainage mine water, of which some are known to interfere with zeolite crystallization (Ca^{2+}) or direct a specific zeolite type such as K for zeolite X or due to inadequate synthesis conditions which would need further optimization due to the changes in the molar regimes brought by the extra Al and Na in the mine waters.

5.1.4.1 Comparative chemical analysis of zeolitic products synthesized using the different solvents (pure water, circumneutral and acid mine water).

The comparative chemical analyses of synthesis products obtained when the different solvents (pure water, circumneutral and acid mine water) were used when zeolite X was targeting starting from unseparated fused fly ash slurry are presented in Tables 5.2 (major elements) and Table 5.2 (trace elements). The hydrothermal synthesis conditions were 80 °C for 9 hours. The analysis was conducted in triplicate and the average values are presented.

Table 5-2: Comparative chemical analyses (major elements) of synthesis products obtained when the different solvents (pure water, circumneutral and acid mine water) were used when zeolite X was targeting starting from unseparated fused fly ash slurry

Major elements (oxide)	Product from use of pure water (Average mass %)	Product from use of CNW water (Average mass %)	Product from use of AMD water (Average mass %)
SiO_2	34.86	38.39	36.37
Al_2O_3	19.43	22.22	19.52
Na_2O	15.56	10.21	11.43
CaO	4.96	5.30	5.35
$Fe_2O_{3;}$	3.28	3.22	9.50
MgO	1.38	1.53	1.84
TiO_2	1.23	1.39	1.17
K_2O	0.17	0.12	0.10
P_2O_5	0.07	0.03	0.03
MnO	0.04	0.06	0.13
Cr_2O_3	0.01	0.01	0.01
LOI	17.06	16.12	13.81
H_2O	1.94	1.40	0.74
SUM	100.00	100.00	100.00
SiO_2/ Al_2O_3 ratio	1.79	1.73	1.86

Table 5-3: Comparative chemical analyses (trace elements) of synthesis products obtained when the different solvents (pure water, circumneutral and acid mine water) were used when zeolite X was targeting starting from unseparated fused fly ash slurry.

Trace elements (ppm)	Product from use of pure water	Product from use of CNW water	Product from use of AMD water
Sr	779	879	741
V	141	158	168
Ce	140	154	200
Zr	341	361	312
Cr	90	86	108
Y	57	63	77
Nd	56	62	79
Ni	55	61	80
Co	39	58	77
Th	35	38	33
Zn	44	55	160
Pb	41	47	41
Nb	29	29	24
U	6	6	5
Cu	nd	105	nd
Ga	15	14	12
Rb	14	12	9

* nd = not detected

As it had earlier been observed when mine water was substituted for pure water during the synthesis of zeolite A (Chapter 4, Section 4.2.7.3), Table 5.2 and 5.3 also shows that all the major and trace elements that had been originally identified in fly ash were still present in the synthesized zeolitic products obtained using the three solvents except for Cu that was absent in the zeolitic product obtained using the acidic mine water. The differences are in their amounts. It can be noted that the relative content of Na_2O in three zeolitic samples presented in Table 5.2 was higher (15.56, 10.21, and 11.43 %) than originally in the fly ash (0.09 %) because additional NaOH had been used during the fusion of the fly ash as detailed in Chapter 3, Section 3.2.2. The extra Na in the mine waters (Table 4.8, Chapter 4) is also thought to have contributed to the elevated Na amount in the zeolitic products synthesized using mine waters. It is also noticeable that the Fe content in the synthesis product obtained when AMD was used was higher than in the original fly ash or in the synthesis product obtained when pure and circumneutral mine water had been used during the synthesis. The same trend as in zeolite A of elevated Fe was due to its high concentration in the acidic mine water as was shown in Table 4.8 (Chapter 4). The concentration of the other major element (Si, Al, Ca, Mg, K, P, Mn, and Cr) and trace elements (Sr, V, Ce, Zr, Cr, Y, Nd, Ni, Co, Th, Zn, Pb, Nb, U, Cu, Ga and Rb) were relatively lower in concentration in the synthesized zeolitic product than in the original fly ash, implying that these elements had reported to the post-synthesis supernatant. Si and Al, being the main elemental building units of the zeolite structure, had a higher concentration compared to the other elements. As highlighted earlier in Chapter 4, Section 4.2.7.3, elements such as Fe and Ti could have been isomorphously substituted in the zeolitic structure fo Al or maybe present as an oxide in the zeolitic channels (Nagy 1998) or even as discreet adsorbed particles. It was not possible to determine this due to limitations of analysis. From a quantitative perspective, the most prominent charge balancing cation was Na^+ but other elements such as Ca^{2+}, Mg^{2+} and K^+ could still be expected to compete with Na^+ for the same exchangeable sites (Barrer, 1982).

5.1.5 Summary for section one

In this section, hydrothermal synthesis conditions for producing a single phase zeolite X, with the typical octahedral crystal morphology, from South African fly ash using pure water as the synthesis solvent were identified as follows: molar regime of (1 Al_2O_3 : 4.90 Na_2O : 3.63 SiO_2 : 115.92 H_2O) at hydrothermal synthesis of 80 ºC for 9 hours respectively. It is important to point

out that the single phase zeolite X that was successfully obtained in this study had been a challenge that had troubled the other researchers who had tried to produce the faujasite zeolites from South African fly ash such as Somerset *et al*., (2005). Another interesting finding from this work was that it was proved that zeolite X could crystallize when mine water was used as a synthesis solvent but not in pure phases. The novel process of using mine water as the solvent during the synthesis of zeolite X from fly ash may need further optimization in order to fully transform the synthesis precursor species into zeolitic material.

5.2 Synthesis of zeolite X from clear extract of fused fly ash: Novel morphology

In order to obtain a higher quality zeolite X from South African fly ash, the clear solution extracted from fused fly ash by filtration was used during the hydrothermal synthesis process. The fly ash used had firstly been fused with NaOH (mass ratios of 1:1.2) by heating at 550 ºC for 1.5 hours (see Chapter 3, Section 3.2.2). The solid/liquid mass ratio of fused fly ash to water was initially set at 1:2.5. After fusion, the mixture had been stirred for 2 hours at room temperature to dissolve the fused fly ash before the resulting slurry was filtered to obtain the clear solution (clear fused fly ash extract) that was used for the hydrothermal crystallization step. The hydrothermal synthesis time had been set at 24 hours. The choice of relatively longer synthesis time, compared to the study that was conducted using unseparated fused fly ash (9 hours), was directed by a preliminary experimental run conducted at 60 ºC which resulted in a small yield of zeolite sample from the clear extract, that was not enough for XRD analysis, indicating low conversion of the clear extract feedstock and thus low yields of product at short synthesis times. The optimization process therefore began by investigation the effect of hydrothermal synthesis temperature followed by investigating the solid/liquid ratio of fused fly ash to water and lastly investigating the effects of ageing the synthesis mixture. The sub-sections that follow present the results that were obtained from the variation of the different synthesis parameters.

5.2.1 Effect of variation of hydrothermal treatment temperature

The XRD analyses of the synthesis products obtained after 24 hours at different hydrothermal synthesis temperatures (60, 70, 80, 90 and 94 ºC) are presented in Figure 5.9. The effect of

variation of the hydrothermal temperature will also be shown during the study for the mechanism of crystallization in Chapter 6.

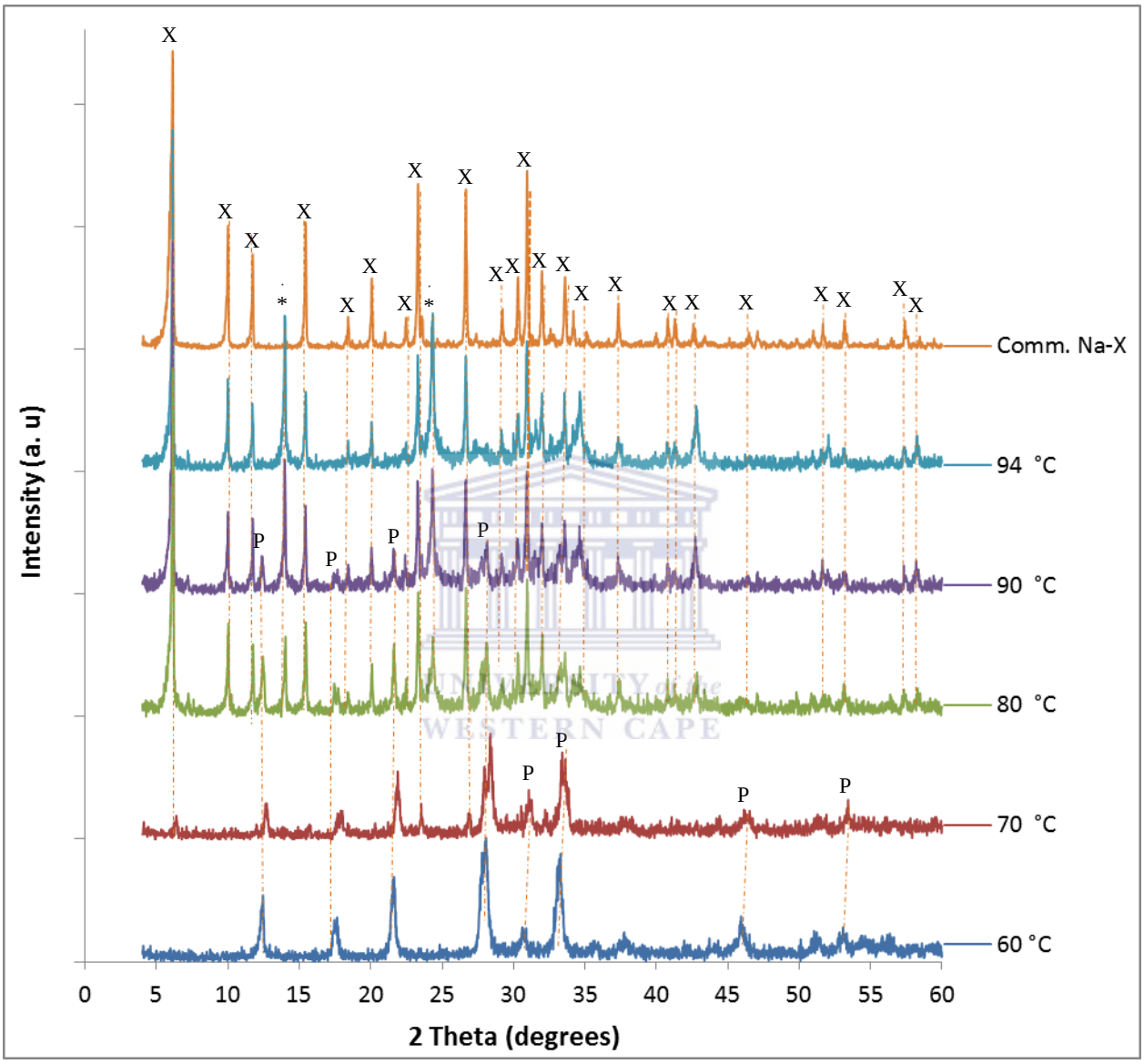

Figure 5-9:XRD patterns for the synthesis products obtained when clear fused fly ash extract was used in the case where the hydrothermal synthesis temperature was varied from 60 to 94 ºC for the synthesis time fixed at 24 hours.

From the XRD patterns presented in Figure 5.9, it can be observed that a single phase zeolite P crystallized at the lower temperature (60 °C) from the clear extract after 24 hours and as the temperature was increased to 80 °C, the diffraction peaks for zeolite X started to appear but

zeolite P peaks were visible in the XRD patterns, up to 90 °C. Since zeolites are metastable structures, the less stable phases (in this case zeolite P) can be transformed into a more stable phase (in this case zeolite X). At 94 °C, no peaks of zeolite P were identified and only diffraction peaks of zeolite X could be identified. This finding is also supported by studies by Byrappa and Yoshimura (2001). An explanation for the diffraction peaks appearing at 13.97 and 24. 31 ° 2θ (marked as *) is presented during the discussion of the morphological analysis.

In order to gain more insight into the effects of variation of hydrothermal synthesis temperature, SEM analysis of the samples was conducted and the results are presented in Figures 5.10 to 5.14. For the sake of references, the samples synthesised at the 60, 70 80 and 94 ˚C were coded as coded as Con X60, 70 80, 90 and 94 respectively.

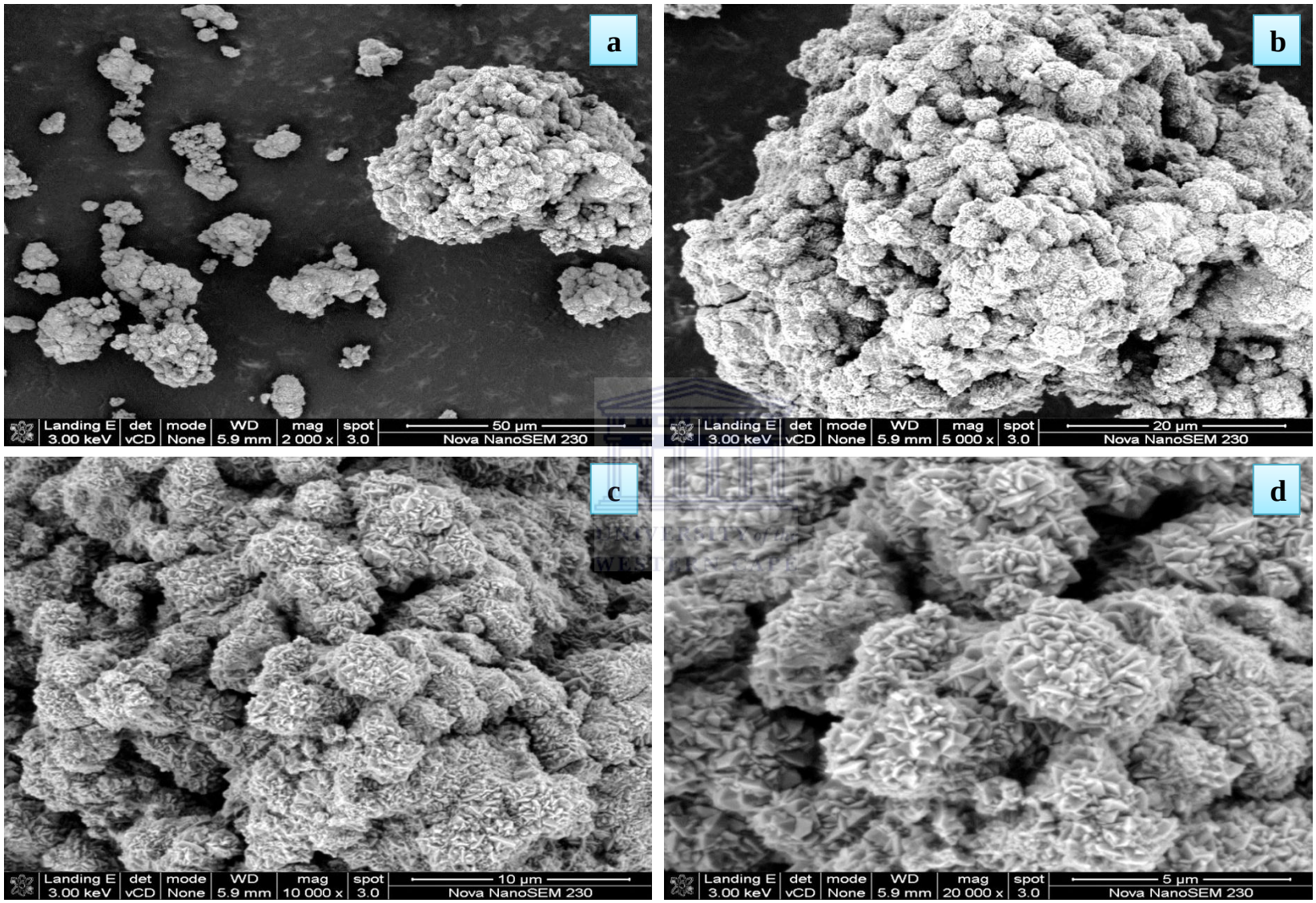

Figure 5-10: SEM micrographs of zeolite P synthesized from clear fused fly ash extract at 60˚C for 24 hours (Con X60) - shown at different magnifications a) x 2,000 b) x 5,000 c) x 10,000 and d) x 20,000.

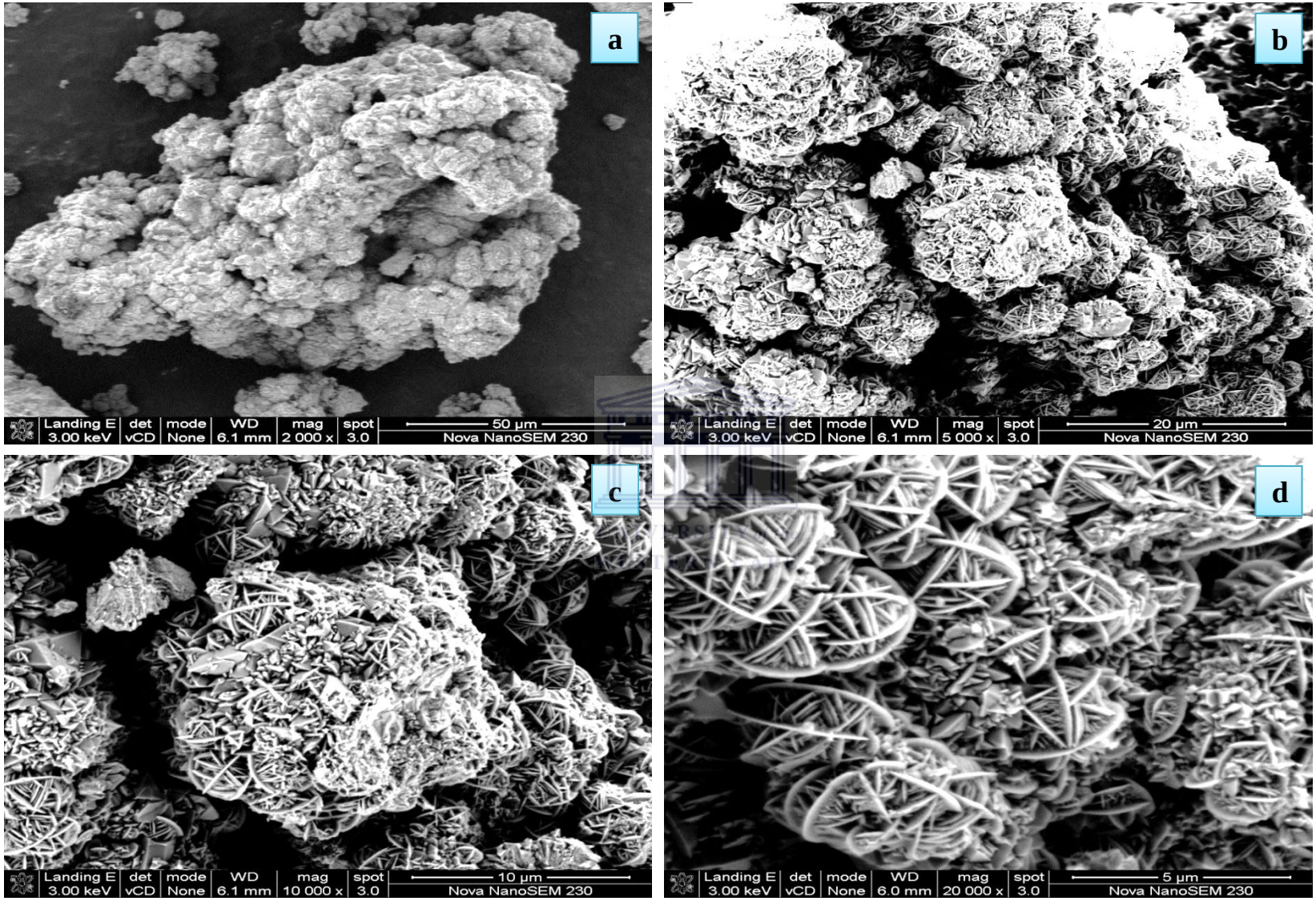

Figure 5-11: SEM micrographs of zeolite X mixed with zeolite P synthesized from clear fused fly ash extract at 70˚C for 24 hours (Con X70) - shown at different magnifications a) x 2,000 b) x 5,000 c) x 10,000 and d) x 20,000.

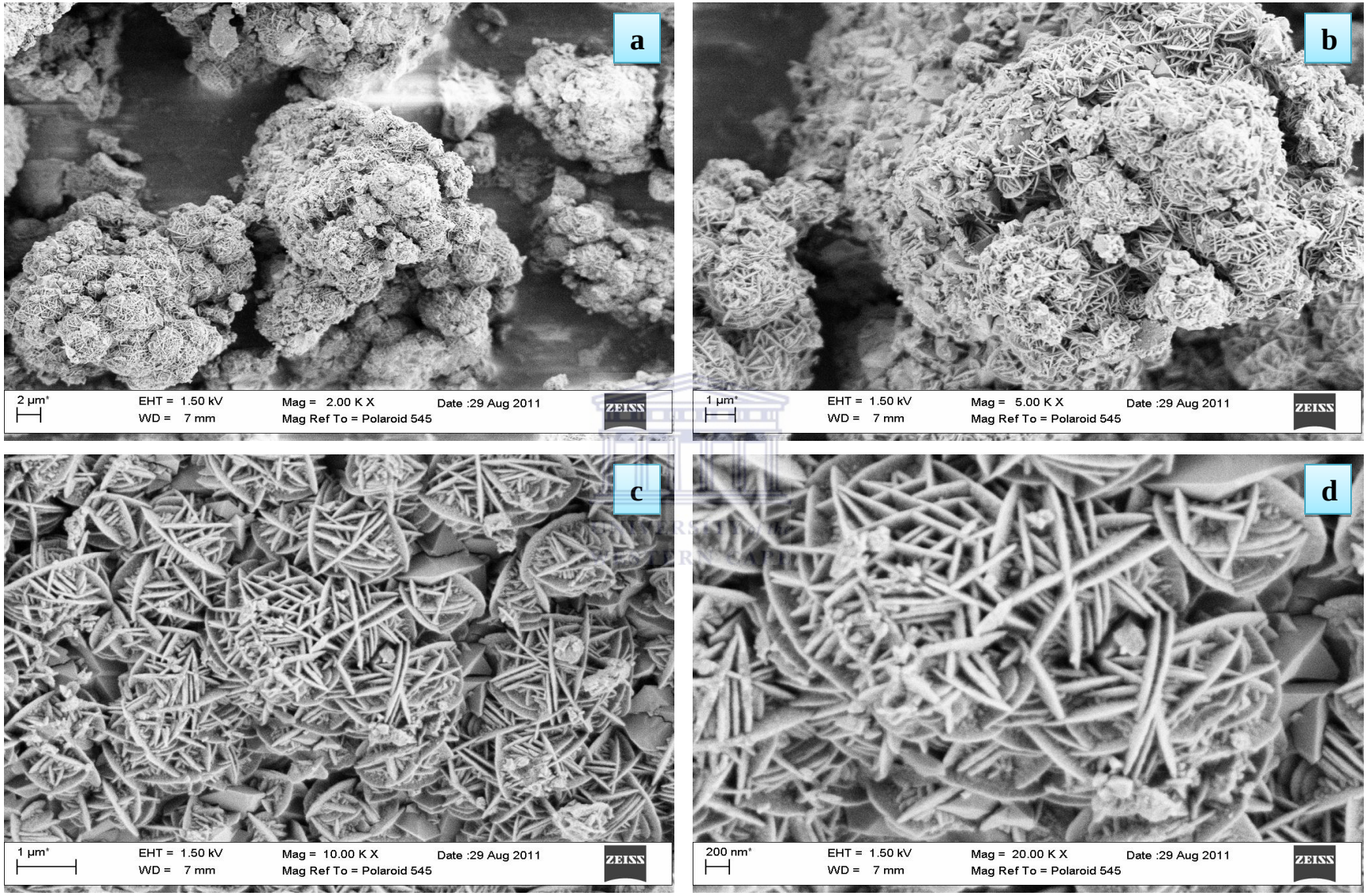

Figure 5-12: SEM micrographs of zeolite synthesized from clear fused fly ash extract at 80˚C for 24 hours (Con X80) - shown at different magnifications a) x 2,000 b) x 5,000 c) x 10,000 and d) x 20,000.

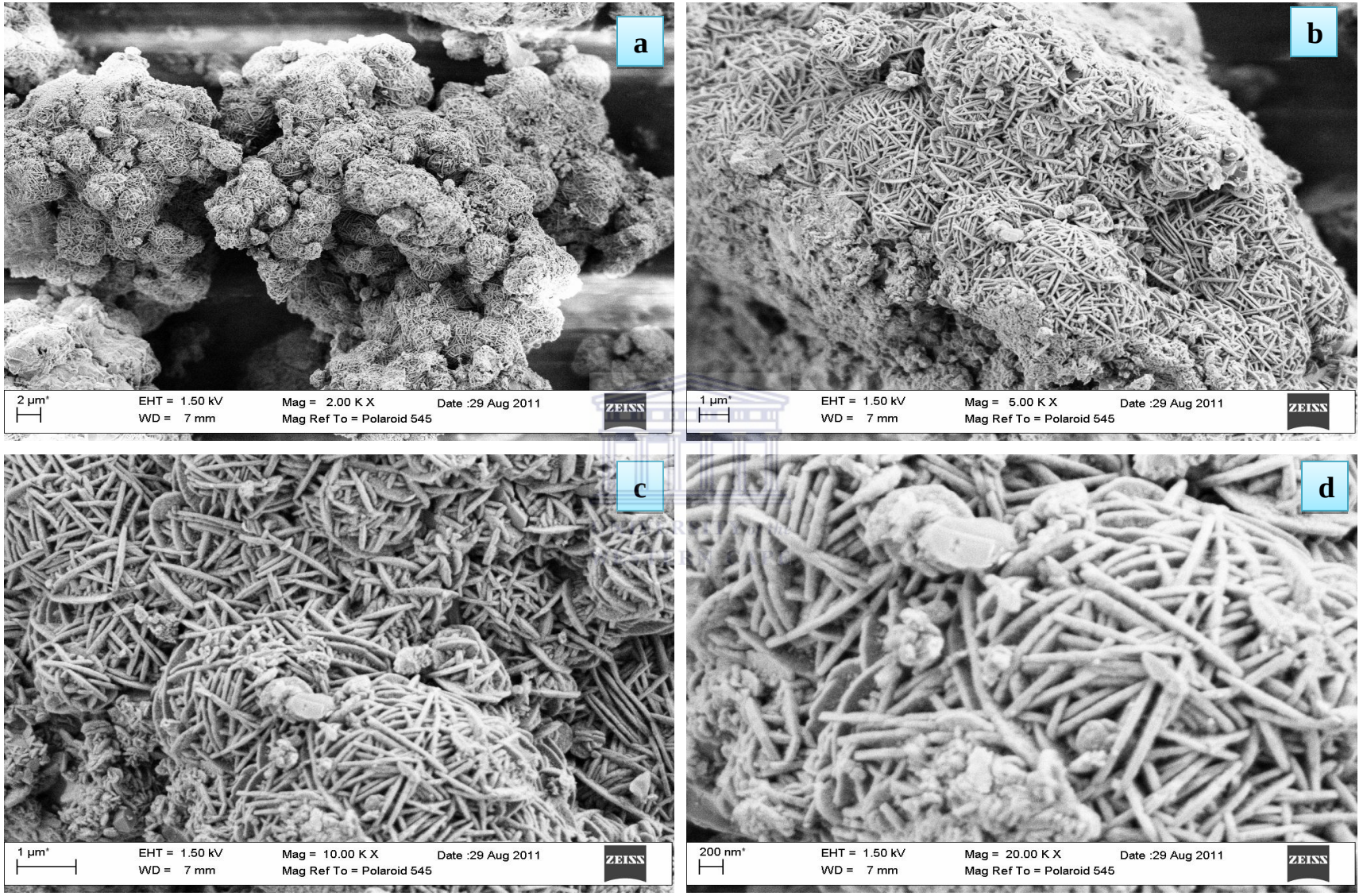

Figure 5-13: SEM micrographs of hierarchical zeolite X synthesized from clear fused fly ash extract at 90˚C for 24 hours (Con X90) - shown at different magnifications a) x 2,000 b) x 5,000 c) x 10,000 and d) x 20,000.

Figure 5-14: SEM micrographs of hierarchical zeolite X synthesized from clear fused fly ash extract at 94 ˚C for 24 hours (Con X94) - shown at different magnifications a) x 2,000 b) x 5,000 c) x 10,000 and d) x 20,000.

Morphological analysis of zeolite P synthesized at 60 ºC (Figure 5.10) shows agglomerated crystals with spiky outer surface. This morphology was different from that reported in a previous study (Musyoka, 2009). Other researchers have reported that zeolite P forms mostly on the outer surface of the unreacted fly ash particles (Murayama *et al*., 2002; Fansuri, 2008). Since the starting synthesis mixture was from a clear extract of fused fly ash (without fly ash particles), the zeolite obtained from this study is expected to be of a higher quality compared to the cases when unseparated fly ash slurry was used because no Quartz or Mullite or fly ash residues were present as is evident in the XRD spectra. In the SEM images presented in Figure 5.11 (for synthesis at 70 °C), two kinds of morphologies could be observed. The agglomerated spiky crystals (as been identified in Figure 5.10) could be associated with zeolite P whereas the larger crystals with distinct disc like morphology could be associated with zeolite X crystals which is also supported by the XRD analysis presented in Figure 5.9.

The SEM micrographs of synthesis product obtained when hydrothermal synthesis was conducted at 80, 90 and 94 ºC (Figures 5.12, 5.13 and 5.14 respectively) show a unique morphology comprising of intergrown disc-like platelets that was identified as mostly zeolite X from the XRD analysis presented in Figure 5.9. The peaks of zeolite P were seen to decrease in intensity upon increase in hydrothermal synthesis temperature and disappeared completely by 94 ºC. It was also interesting to observe that there was broadening of the disc-shaped platelets of zeolite X crystals in one dimension as the synthesis temperature was increased to 94 ºC. This observation is clearly shown by comparing part d of Figures 5.12, 5.13 and 5.14. For instance, the width of disc-shaped platelets for the synthesis product obtained at 80 ºC was about 50 – 100 nm whereas that for the product obtained at 90 ºC was close to 100-130 nm. For synthesis at 94 ºC the width of the platelets was close to 200 nm. The XRD diffraction peaks observed at 13.97 and 24.31 ° 2θ could be due to preferred orientation in the sample or be as a result of intergrowth of the sodium aluminium silicate hydrate phase presented in Figure 5.15A. The intensity of the peak marked by * was also seen to increase with an increase in temperature.

The morphology observed in Figures 5.12, 5.13 and 5.14 was closely similar to the hierarchical zeolite X that had flower-like assembly of nanoplatelets as recently reported by Inayat *et al.* (2012). In Inayat's studies, zeolite X with hierarchical interconnection of pores was synthesized

using sodium silicate and aluminate solution derived from pure analytical grade chemicals together with an organosilane template (TPHAC). After a thorough literature search, there was no published evidence that has reported the synthesis of this unique morphology of zeolite X from fly ash hence this finding is novel. The synthesis of hierarchical zeolites and other porous materials have been of intense scientific and technological interest because the presence of tailored micro, meso and macro pores at different scales has the potential of solving the well-known problems of diffusional constraints and mass transfer limitations that are often associated with the internal micropores in zeolites (Liu *et al.,* 2009; Yang *et al*., 2009; Inayat *et al.,* 2012*).*

The self-formation of this hierarchical zeolite X from South African fly ash, without requiring the use of additional ingredients or post synthesis treatment, is advantageous compared to the complicated procedures that are reported in literature that are based either on chemical or physical techniques that are discussed in detail in a recent review by Yang *et al.* (2009).

5.2.2 Effect of variation of the quantity of water during the extraction of fused fly ash

The effect of varying the mass ratios of fused fly ash to water content (1:5 and 1:1.25) prior to the extraction of the clear solution that was used in the hydrothermal crystallization step were investigated in this sub-section. The procedure for extraction of clear solution from the fused fly ash is presented in Chapter 3, Section 3.2.2.2. It is important to emphasize that no additional chemicals were added in the synthesis solution apart from the NaOH that was used during the fly ash fusion step. The hydrothermal treatment temperature and time were held constant at 80 ˚C and 24 hours respectively. Figure 5.15 presents the XRD patterns together with the corresponding SEM images for the synthesis product obtained after the variation of water quantity during the extraction of the synthesis mixture from fused fly ash.

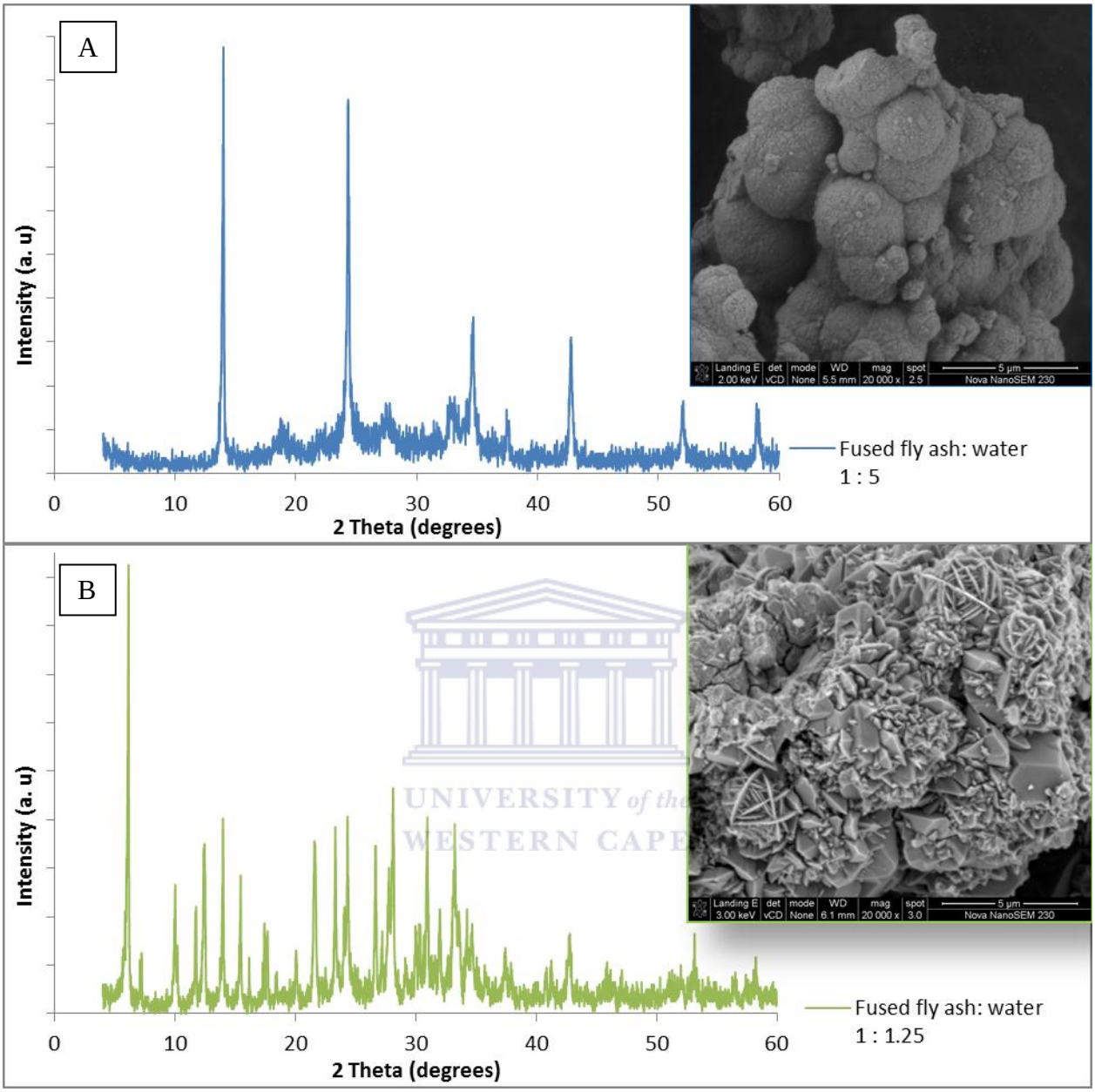

Figure 5-15: XRD patterns and respective SEM micrographs for the synthesis products obtained when fused fly ash-water ratio was varied as a) 1:5 and b) 1: 1.25 during the extraction of the clear solution used during hydrothermal synthesis temperature at 80 ºC for 24 hours.

As shown in Figure 5.15 (insert a), when the fused fly ash to water mass ratio of 1:1.25 was used during the extraction of the clear solution that was then subjected to hydrothermal synthesis at 80 ºC for 24 hours, a zeolitic phase identified as sodium aluminium silicate hydrate phase (PDF No. 00-131-1271) was crystallized. A mixture of crystals that had the triangular crystal face

associated with the typical octahedral crystals associated with zeolite X together with crystals that had the novel (platelets with disc-like) morphology (hierarchical) zeolite X crystals could be seen when the fused fly ash to water mass ratio of 1:5 was used in the extraction process as shown in (Figure 13 (b)). The use of a fused fly ash to water mass ratio of 1:2.5 that was presented in (Figure 5.15 (b)), which had been discussed earlier in Section 2.1, was observed to led to the crystallization of zeolite X with the novel (hierarchical) morphology. Thus water content was crucial in the new route for generating the hierarchical morphology.

It can be concluded that the amount of water used to extract the clear solution from the fused fly ash played a crucial role in ensuring that the synthesis mixture had the right molar regime in the most suitable proportions that could allow the selective crystallization of the new morphology. The molar regime of the synthesis mixture that led to the formation of the novel morphology was found to be 1 Al_2O_3 : 56.80 Na_2O : 16.62 SiO_2 : 954.05 H_2O and the hydrothermal synthesis temperature ranging from 80 to 94 ˚C for 24 hours.

5.2.3 Effect of ageing of the synthesis mixture

Having identified the synthesis molar regime (1 Al_2O_3 : 56.80 Na_2O : 16.62 SiO_2 : 954.05 H_2O) that led to crystallization of the novel (hierarchical) zeolite X crystals at hydrothermal synthesis conditions of 80 ºC and 24 hours (see Section 5.2.2), the effect of ageing the clear extract was investigated by leaving it to age overnight (12 hours) at room temperature under stirred conditions prior to hydrothermal synthesis. Figure 5.16 present the XRD pattern and respective morphological analysis of the synthesis product resulting after ageing the clear extract for 12 hours prior to hydrothermal synthesis at 80 ºC for 24 hours.

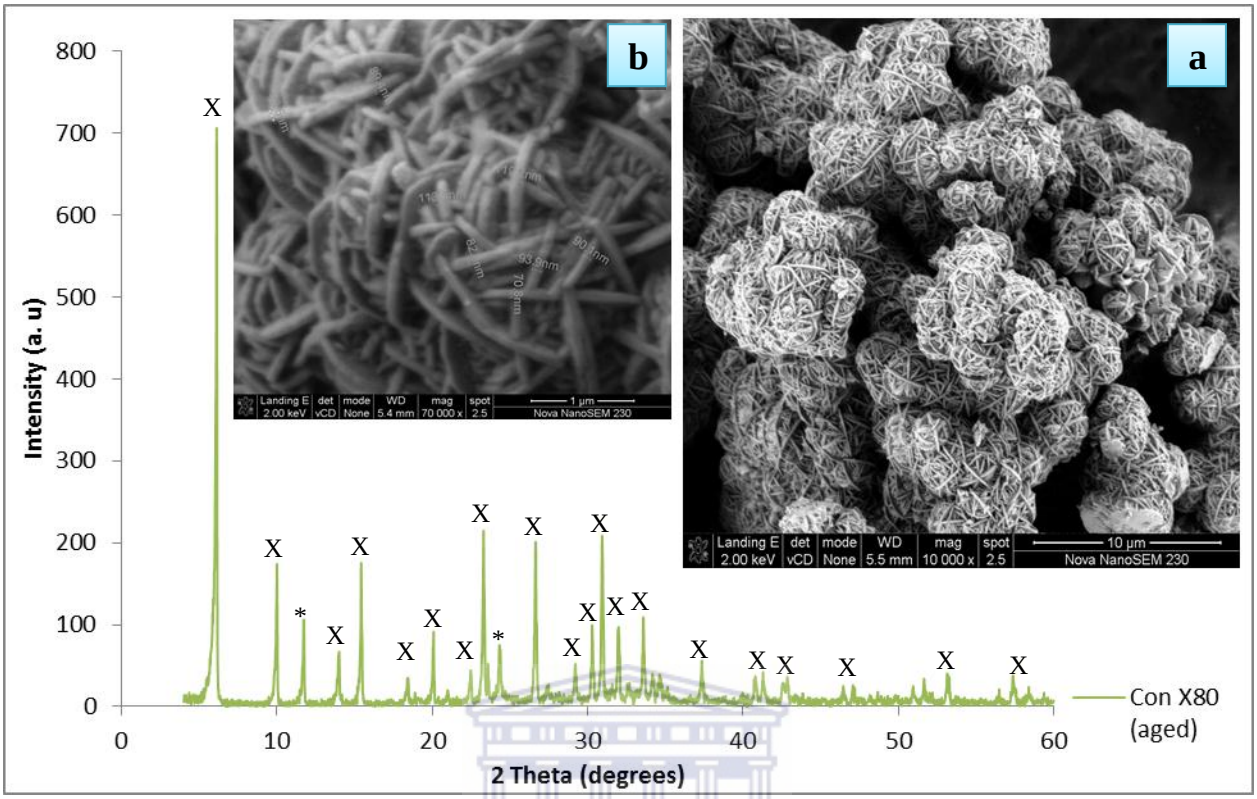

Figure 5-16: XRD pattern and respective SEM micrographs of the novel morphology zeolite X (Con X80, aged) synthesized from the clear extract of fused fly ash (molar regime of 1 Al_2O_3 : 56.80 Na_2O : 16.62 SiO_2 : 954.05 H_2O): effect of ageing for 12 hours prior to hydrothermal synthesis at 80 ºC for 24 hours – SEM shown at a) x 10,000 and b) x 70,000 magnification.

Comparing the morphology of zeolite X generated after ageing the clear extract of fused fly ash (Figure 5.16) with that of the unaged sample (Figure 5.12), it was noted that the crystals generated after ageing were more agglomerated even though the width of 'nano-platelets' was observed to be in the range of 70 – 110 nm. The width of the 'nano-platelets' was close to that of the sample obtained without ageing (see Figure 5.12). It was also interesting to note that the two peaks (marked with *) that had earlier been associated with either preferential growth of zeolite X crystals in one dimension or due to the intergowth with sodium aluminium silicate hydrate phase (Section 5.2.1) were still present even after ageing the clear extract for 12 hours prior to the hydrothermal crystallization. The peaks that correlated to the presence of zeolite P phase where not identified in the XRD pattern for the aged sample.

5.2.4 Further characterization of zeolite X with the novel morphology

In order to gain in-depth understanding of the characteristics of the novel (hierarchical) zeolite X synthesized from the clear extract of fused South African fly ash with a molar regime of 1 Al_2O_3 : 56.80 Na_2O : 16.62 SiO_2 : 954.05 H_2O, different characterization techniques were applied. The results from technique such as HRTEM, FTIR, TGA and BET are presented in the sub-sections that follow.

5.2.4.1 HRTEM analysis

The hierarchical morphology, as was observed earlier in the SEM micrographs, is best understood with the help of high resolution transmission electron microscopy as presented in Figure 5.17.

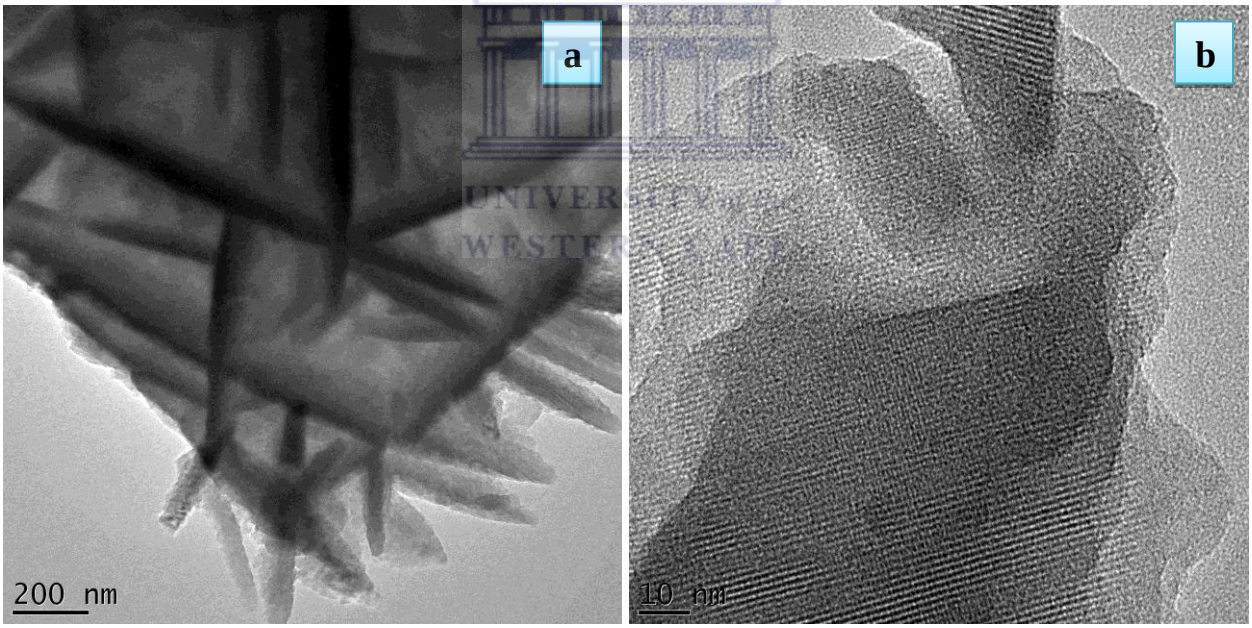

Figure 5-17: HRSEM micrographs of novel morphology zeolite X synthesized from clear extract of fused fly ash at hydrothermal synthesis at 80 ºC for 24 hours (Con X80) - shown at different magnifications.

The agglomerated disc-like platelets for the sample synthesized at 80 ˚C (Con X80) as shown in Figure 5.17 (a) had an individual crystalline width ranging between 100 and 200 nm. Upon

further imaging, at relatively higher magnification, what seemed like overlaid disc-like platelets could be seen from Figure 5.17 (b). The lattice fringes observed in Figure 5.17 (b) exhibit a completely crystallized zeolitic material (lattice fringes shown) that had crystals with noncontinous grain boundaries that could be associated with mesoporosity.

Although it is not currently understood why the zeolite X crystallized in this morphology, competitive adsorption of certain secondary building units promoted during the depolymerization process is speculated to be a driving forces. Further suggestions were presented by Byrappa and Yoshimura (2001) who claimed that the presence of small quantities of metal halides or other non-volatile species (in this case, originating from fused fly ash) could lead to the formation of new products properties.

The Energy dispersive X-ray analysis (EDS) of the novel morphology zeolite X sample (Con X80) synthesized from clear fused fly ash extract at hydrothermal synthesis temperature of 80 ºC for 24 hours is presented in Figure 5.18.

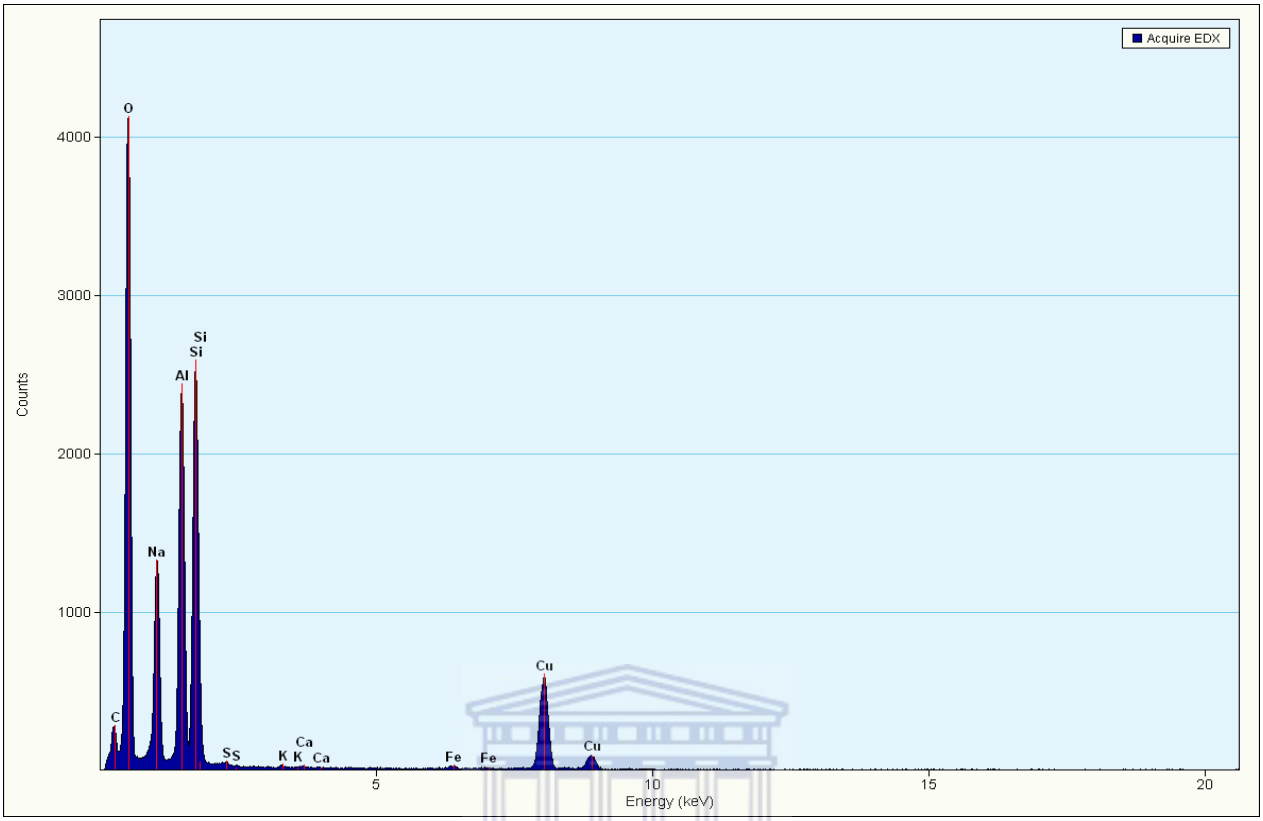

Figure 5-18: EDS of zeolite X obtained during the HRSEM analysis of the sample that was presented in Figure 5.1.

From the EDS analysis presented in Figure 5.18, it is shown that the novel morphology zeolite X had Na as the main exchangeable cation although other elements such as Ca, K, Fe and S could be observed. The presence of Cu and C in the EDS spectrum should be ignored since the holey carbon mounts was made of these elements. The semi-quantitative elemental analysis of the samples revealed that the zeolitic phase obtained had a Si/A1 ratio of 1.2 which falls within the expected range (1-1.5) hence confirming that it was indeed Zeolite X and not Y (Inayat *et al.*, 2012). Chemical analysis of different spots of the same sample (Con X80) done using the EDS attached to the Scanning electron microscope (SEM) further confirmed the ratio, as presented in Figure A1.

5.2.4.2 FTIR analysis

Figure 5.19 presents the infra-red spectra of hierarchical fly ash-based zeolite X, prepared at 80, 90 and 94 ˚C (Con X80, 90 and 94) without ageing according to the procedure highlighted in Chapter 3 (Section 3.2.3.2) and compares them with the spectrum of the commercial counterpart.

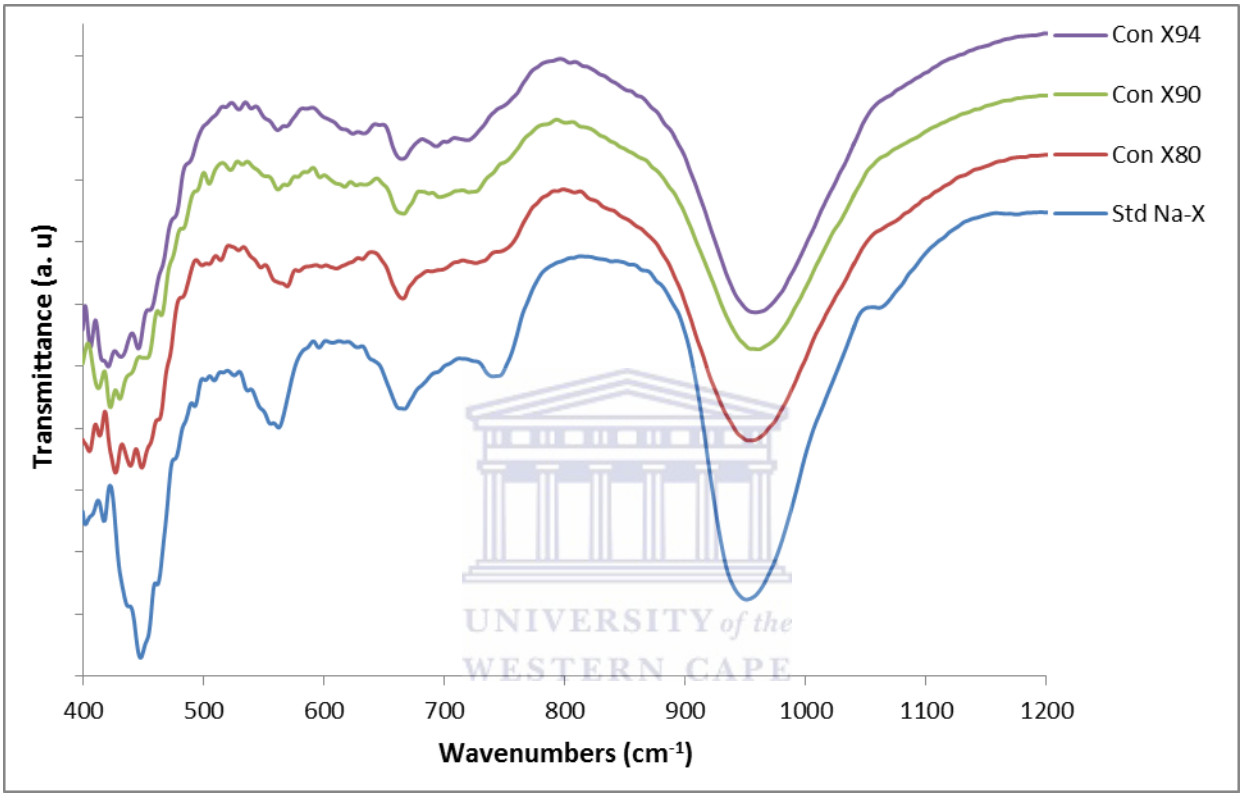

Figure 5-19: FTIR spectra of hierarchical zeolite X synthesized from unaged clear fused fly ash at different temperatures (80, 90 and 94 ˚C, coded as Con X80, 90 and 94) compared to that of commercial zeolite X with conventional pyramidal octahedral morphology.

The Fourier Transform Infra – Red Spectroscopy (FT-IR) vibration bands of the fly ash-based zeolite X together with its commercial counterpart were assigned and compared in accordance to the generally accepted practice for silicates and the zeolite family of compounds as shown in Table 5.4.

Table 5-4: Comparison of mid-Infrared vibrational bands of fly ash based zeolite X, its commercial counterpart as well with vibrational bands reported in literature.

Literature values (Flanigen,1971)		Actual vibration bands of the zeolitic samples (cm^{-1})			
Vibrational band Range (cm^{-1})	Assignment	Std. zeolite X	Con X80	Con X90	Con X94
300 - 420	Pore opening vibrations (internal tetrahedra)	408	422	415	416
420 - 500	T-O bending vibrations (internal tetrahedra)	444	431	433	436
500 - 650	Double ring vibrations (external tetrahedra)	553	557	553	549
650 - 720	Symmetric stretching (internal tetrahedra)	654	654	657	656
750 - 820	Symmetric stretching (external tetrahedra)	736	740	743	743
950 - 1250	Asymmetric stretching (internal tetrahedra)	943	942	944	942
1050 – 1150	Asymmetric stretching (external tetrahedra)	1052	1051	1052	1052

From the comparative infra-red analysis presented in Table 5.13, it can be clearly seen that most of the IR bands identified in the commercial zeolite X closely matched with the bands of fly ash-based zeolite X. The close matching of these IR bands indicated some similarity in their structural units. These observations were also seen to be in good agreement with Flanigen's (1971) assignments for X-type zeolites. IR spectral data can also be used to determine if an impure "contaminant" phase had crystallized with the intended zeolite phase (Balkus and Ly, 1991). Special attention was focussed on the double ring region because it can be used to check the presence or absence of potential contaminant phases that are known to crystalize together with zeolite X. Zeolite A and P are the two common zeolites that have the potential of co-crystalizing with zeolite X (Inayat *et al*., 2012). According to Balkus and Ly, (1991), if zeolite A

was to be an impurity, a significant shift of the double-ring vibration (500 – 650 cm^{-1}) relative to the commercial X-type zeolites would have been noted especially towards the lower wave number because zeolite A has double four-ring units (D4R) instead of the double six-ring (D6R) units associated with zeolite X. The presence of an extra weak band at 741 cm^{-1} for the Con X80 can be associated with the zeolite P what had been identified from the XRD analysis presented in Figure 5.9. This observation is further reinforced by the shift of the peak identified at 431 cm^{-1} 600 cm^{-1} and 660 cm^{-1}.

5.2.4.3 Thermal stability studies

Since the novel fly ash-based zeolite X synthesized in this study may be used in processes that might require elevated temperatures or might need heat treatment during the regeneration process, it was deemed important to understand their thermal stability limits. Comparative TGA-DTA curves of the fly ash based hierarchical zeolite X synthesized at 80 °C for 24 hours (Con X80) (as described in Chapter 3 (Section 3.57)) and commercial zeolite X is presented in Figure 5.20.

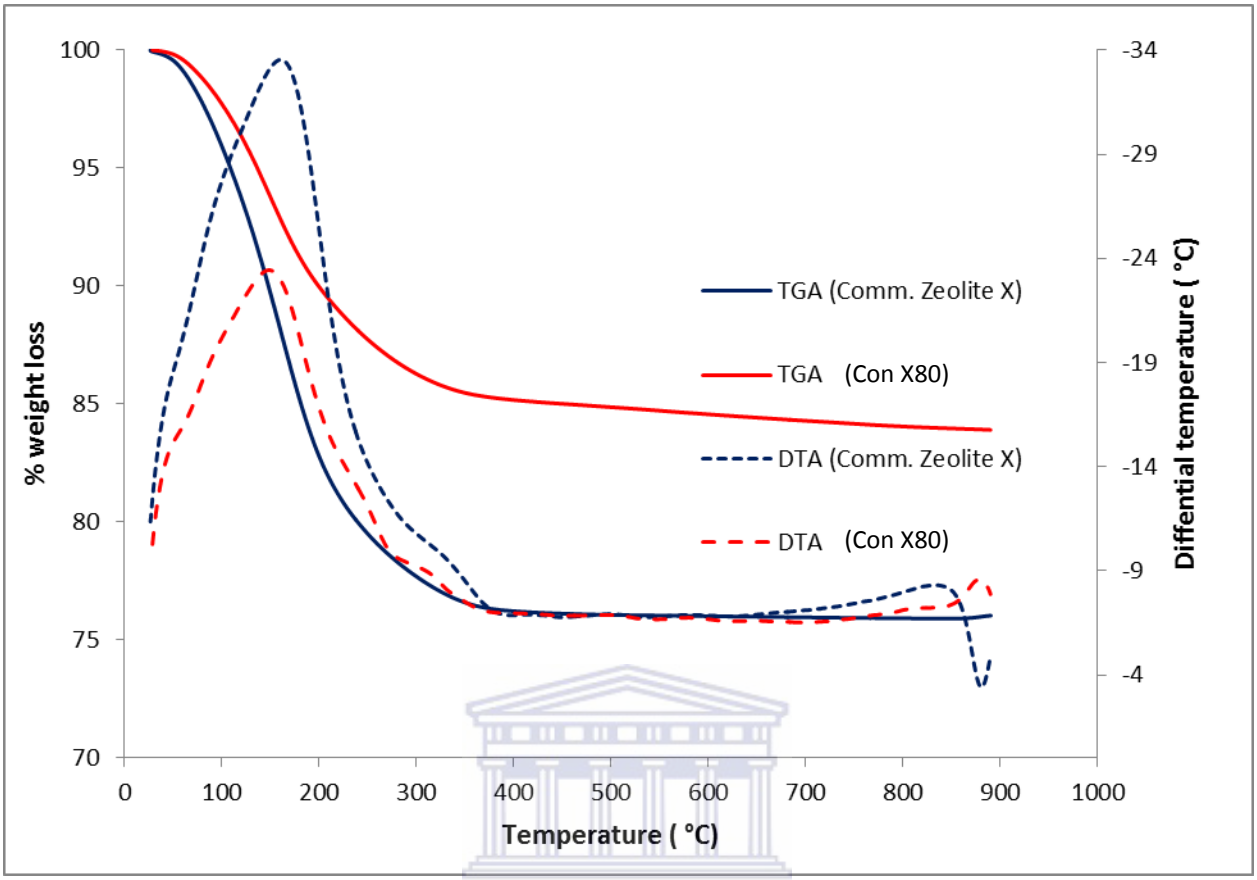

Figure 5-20: Comparative TGA-DTA curves of the fly ash based hierarchical zeolite X (Con X80) and commercial zeolite X.

From the TGA thermographs shown in Figure 5.20, it can be observed that the moisture loss from both fly ash based Con X80 sample and commercial zeolite X started between 40 and 50 ˚C. The initial mass loss of the samples between 40 – 100 °C (around 14 % and 23 % in fly ash Con X80 and commercial zeolite X respectively) is caused by desorption of physically adsorbed water from within the micropores. From DTA inflections of both zeolites, most of this water was lost at 150 °C. Complete dehydration associated with the loss of all the free, sorbed and Na-complexed water is expected to occur between 400 - 450 °C (Akbar *et al.*, 2005) and can be observed as the negligible weight loss occurring in this temperature range. The zeolitic water content has been reported to depend on the porosity as well as nature, size of the exchageable cation and also on the number of Al ions in the zeolitic structure (Akbar *et al.*, 2005). Breck, 1974 reported that hydrothermal stability and hydrophobicity increases as the Si/Al ratio increases. This relationship is due to the variation of the lattice constant which is related to Al-O

(1.728 Å) and Si-O (1.608 Å) bond lengths. Smooth TGA curves of both zeolites were obtained because when zeolites are heated they are known to loose water from their structure in a continuous rather than in separated stages at definite temperatures (Byrappa and Yoshimura, 2001).

In the DTA curves shown in Figure 5.20, the exothermic peaks (seen at 820 °C in commercial zeolite X and 860 °C is fly ash based zeolite X) are thought to be associated with structural collapse of the zeolite X framework. This is because the large amount of surface energy associated with the decreasing surface area as the structure collapses is liberated as heat (Usachev *et al.,* 2003). The temperature induced structural collapse has been reported to depend on temperature, heating time, presence of water vapour among other factors (Akbar *et al.,* 2005). The sharp exothermic peaks observed at around 880 °C in commercial zeolite X could be due to recrystallization. From the TGA-DTA analysis, it can be concluded that the hierachical fly ash-based zeolite X was stable up to temperatures above 800 ˚C similar to a commercial zeolite X sample.

In order to complement the results from thermogravimetic analysis reported above, in-situ temperature programmed XRD analysis (shown in Figure 5.21) was conducted to probe whether there was any temperature induced mineralogical transformations taking place in the hierachical fly ash-based zeolite X. Unfortunately, due to the contraint with the heating stage of the instrument, the temperature could not be studied above 450 ˚C but the information obtained was still valuable.

.

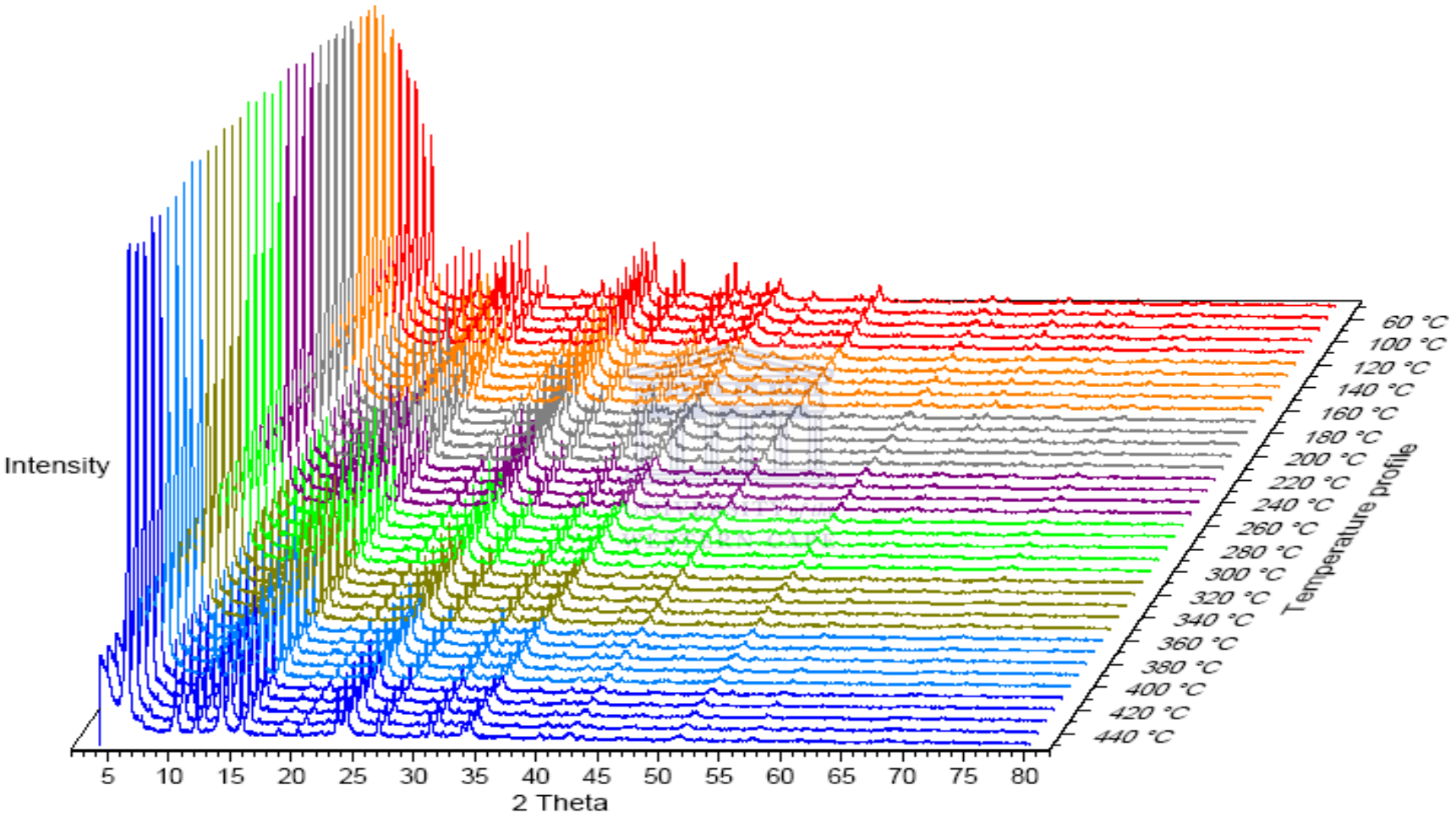

Figure 5-21: XRD patterns for in-situ thermal stability measurements for hierarchical zeolite X synthesized from fly ash (Con X80)

.

As shown in Figure 5.21, the hierachical fly ash based zeolite X (Con X80) was found to retain its structural integrity (crystallinity) and no phase transitions occurred even after being heated up to 440 ˚C meaning that it can be used in applications that require high temperature environments such as in catalysis and adsorption.

5.2.4.4 BET analysis

Figure 5.22 presents a comparison of N_2 adsorption-desorption isotherms for hierarchical fly ash based zeolite X synthesized at different temperatures (80, 90 and 94 °C, coded as Con X80, 90 and 94) following the procedure detailed in Chapter 3, Section 3.5.6.

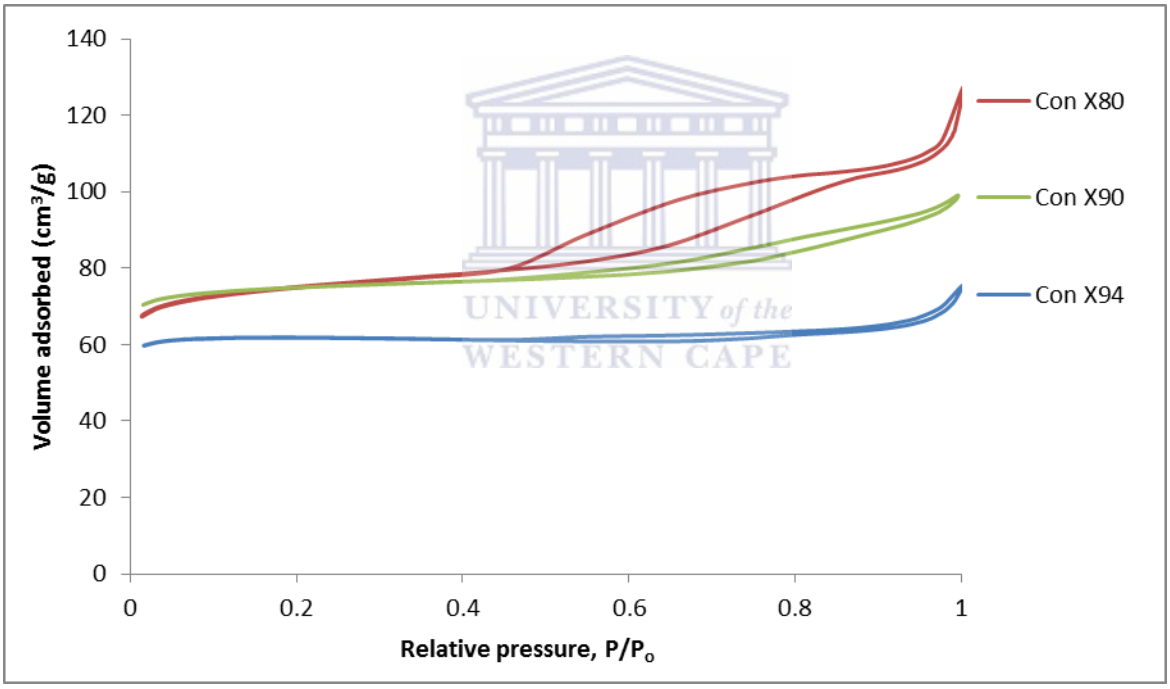

Figure 5-22: Comparison of N_2 adsorption-desorption isotherms for hierarchical zeolite X synthesized at different temperatures (80, 90 and 94 °C, as represented by Con X80, 90 and 94) following the procedure detailed in Chapter 3, Section 3.5.6.

As can be observed in Figure 5.22, all the three N_2 sorption isotherms for hierarchical zeolite X synthesized at different temperatures (80, 90 and 94 ˚C) were observed to have a combination of type I and type IV hysteresis curves which have been associated with materials that have hierarchical porous systems (Bonilla *et al.,* 2009; Liu *et al.,* 2009). The sample synthesized at the lower temperature of 80 ˚C (Con X80) had a wider and steeper hysteresis loop starting at the relative partial pressure (P/P_o) of 0.4 thus indicating an increase in the mesopore volume compared to samples obtained at higher temperatures (Con X90 and 94). The distinct increase in the adsorption quantity in the region $0.4 < P/P0 < 0.9$ can be interpreted as capillary condensation in the mesopores (Liu *et al., 2009).* It can further be noted that the samples that had shown high mesoporosity (Con X80 and 90) also adsorbed a higher volume of nitrogen gas as would be expected. The difference in mesoporosity can be explained by the different sizes of the intraparticle voids (appearing in between the different widths of nano-sized sheets) that had been observed in the SEM micrographs shown in Figures 5.12 to 5.14 which should not be confused with voids caused by interparticle aggregation. This trend was also consistent with erlier observations (Figures 5.12 – 5.14) that had shown that as the temperature increased the voids closed up because the platelets became thicker/wider in one dimension. Also noteworthy of mentioning, this study further proves that the thinner the nano-sized sheets, the higher the overall mesoporosity which has been shown by widening of the hysteresis loop with corresponding increase in the external surface area.

In order to complement the observation shown in Figure 5.2, a comparison of surface areas (BET surface Area, micropore area and external surface area) for fly ash based zeolite X and commercial zeolite X is presented in Table 5.5.

Table 5-5: Comparison of surface areas (BET surface Area, micropore area and external surface area) for fly ash based zeolite X and commercial zeolite X.

	BET Surface Area (m^2/g)	Micropore Area (m^2/g)	External Surface Area (m^2/g)
Con X80	281	233	48
Con X90	282	258	25
Con X94	235	224	12
Comm. Zeo X	746	713	33

The trend in BET surface area presented in Table 5.4 correlates well with the variations of N_2 sorption isotherms presented in Figure 5.22. The corresponding decrease in external surface areas in relation to the increase in temperature of synthesis served to confirm the proposal that creation of mesoporosity leads to an increase in external surface area. According to Bonilla *et al.* (2009), an increase in mesoporosity leads to a decrease in microporosity even in circumstances where desilication conditions are applied to create mesoporores and this observation can be clearly seen in Table 5.4. The relative low BET surface area for the samples synthesizes from fly ahs compared to that of commercial zeolite X sample could either be due to presence of other pore blocking cations or even due to the intergowth of the ealier reported sodium aluminium silicate hydrate phase.

To get a better understanding of the pore size distribution of the fly ash based zeolite X synthesized at different temperatures (80, 90 and 94 °C), curves of incremental pore area versus pore diameter were plotted and are presented in Figure 5.23.

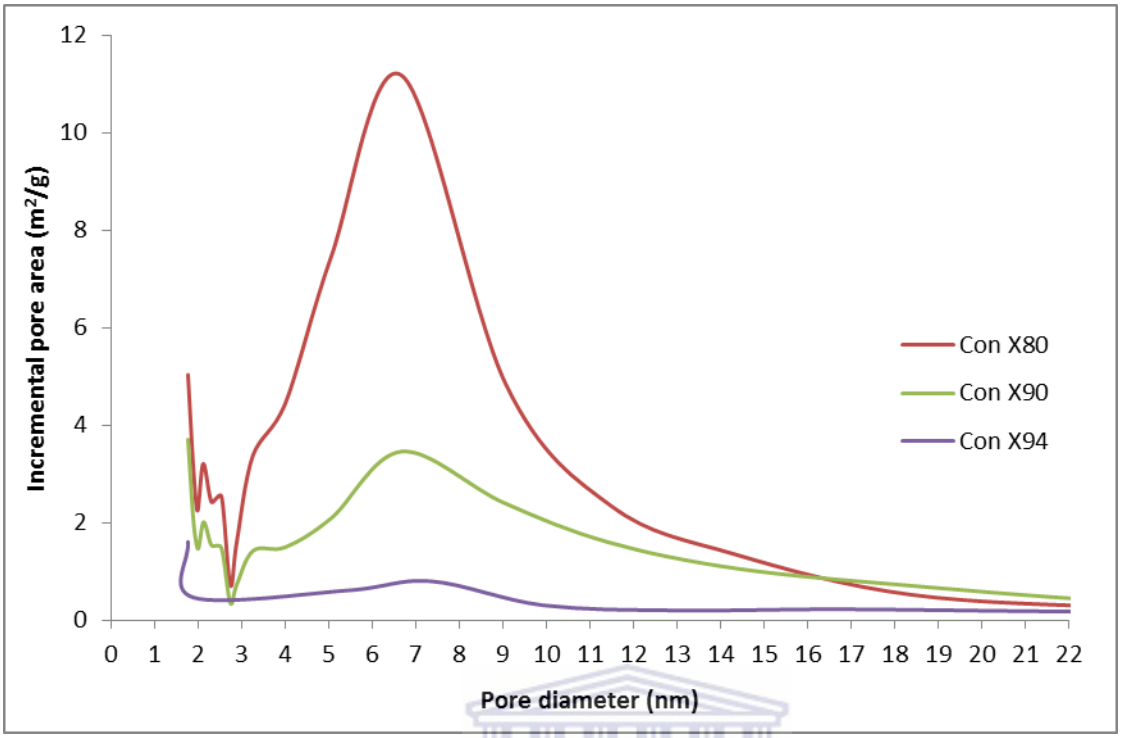

Figure 5-23: Comparative pore size distribution curves of hierarchical fly ash based zeolite X synthesized at different temperatures (80, 90 and 94 °C, coded as Con X80, 90 and 94) following the procedure detailed in Chapter 3, Section 3.5.6.

As was noted during the discussion for the surface areas in the start of Section 5.2.4.4, the variation in pore size distribution (Figure 5.23) for novel morphology fly ash based zeolite X synthesized at different temperatures (80, 90 and 94 °C) show the same trend which correlates well with the trend observed in Table 5.4 and Figure 5.22. Even though the micropore region for the zeolites was not captured in the plots, the increase of the incremental pore area curve as the temperature was changed from 94 °C to 80 °C is clear evidence to complement the results that the thinning of the nano platelets (that were seen in the SEM micrographs that were presented in Figures 5.12, 5.13 and 5.14) led to an increase in mesoporosity.

To confirm that there was a differences in meso pore size distribution of the hierarchical fly ash based zeolite X synthesized at 80 °C (Con X80) and commercial (typical morphology) zeolite X, their pore size distribution plots were overlaid and the results are presented in Figure 5.24.

.

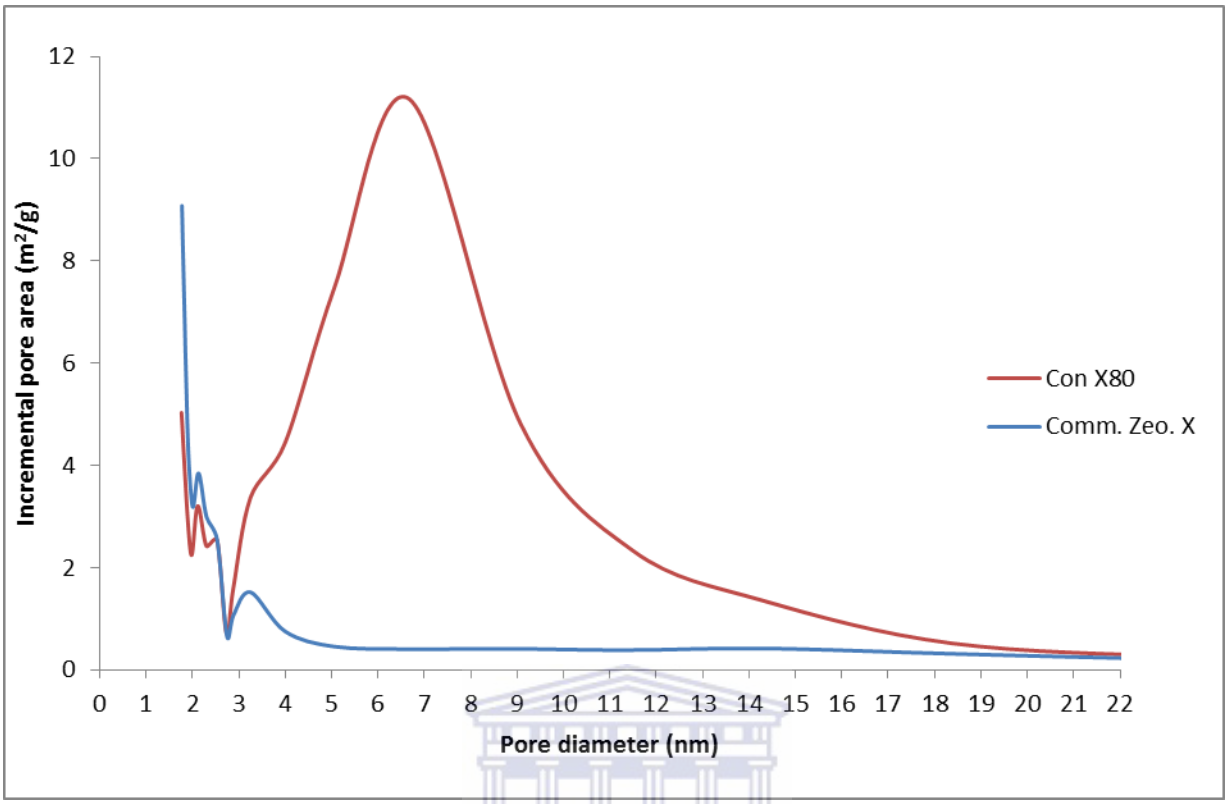

Figure 5-24: Comparative pore size distribution curves of hierarchical fly ash based zeolite X synthesized at 80°C (Con X80) with Commercial (typical morphology) zeolite X.

From Figure 5.24, it was interesting to observe that the mesoporous surface area for fly ash zeolite X between 3 – 12 nm was much greater than that of the commercial zeolite X. This was a further confirmation of the earlier observation that were made using the other characterization techniques.

5.2.5 Chapter summary

In this chapter, two major accomplishments were attained; in the first section, the synthesis conditions to prepare the typical octahedral shaped zeolite X from the South African fly ash were identified. The best synthesis conditions were as follows: molar regime of 1 Al_2O_3 : 4.90 Na_2O : 3.63 SiO_2 : 115.92 H_2O, with hydrothermal synthesis af 80 ºC for 9 hours. Most importantly, it is noteworthy to point out that a single phase zeolite X (with octahedral crystals) was successfully obtained which had been a challenge to the other researchers who had tried to produce the faujasite zeolites from South African fly ash such as Somerset *et al.*, (2005). It was also proved

that zeolite X could crystallize when different qualities of mine waters were used as a synthesis solvent instead of the use of pure water. The novelty of this process of using mine water during the synthesis process is that it has the potential to lead the coal mining and combustion industries to move closer to the attainment of the goal of zero waste production. The benefit of this process can be viewed from both an environmental and economic point of view, since it will lead to the reduction of the environmental burden associated with the disposal and treatment of the mine waters and fly ash wastes. From the economic perspective, the additional income generated from the sale of the synthesized zeolites could be used to reduce the running costs of both coal mining and coal combustion industries hence potential for boosting profits to enable creating of more employment opportunities.

In the second section, a process for producing a novel morphology (hierarchical) zeolite X from a clear extract of the fused South African class F fly ash slurry is presented. The synthesis conditions for this morphology are reported as: molar regime of 1 Al_2O_3 : 56.80 Na_2O : 16.62 SiO_2 : 954.05 H_2O at a hydrothermal synthesis temperature ranging between 80 and 94 ºC for 24 hours. The identified synthesis route leads to self-formation of this hierarchical zeolite X from South African fly ash, without requiring the use of additional ingredients or post synthesis treatment. This is advantageous compared to the complicated procedures that are reported in literature that are based either on chemical or physical techniques that are discussed in detail in a recent review by Yang *et al.* (2009). The aggregates of disc-like nano platelets created a hybrid micro-/mesoporous structures and were shown to have a relatively higher mesoporous surface area that is desirable for most catalytic applications since it has the potential to solve the well-known problem of diffusional and mass transfer constraints that are associated with the presence of only internal zeolitic micropores. The growth mechanism for this unique morphology of zeolite X will be explored in the next chapter that deals with the use of the in-situ ultrasonic monitoring process for zeolite formation.

CHAPTER 6

IN-SITU ULTRASONIC MONITORING OF FORMATION PROCESS OF ZEOLITE A AND X FROM SOUTH AFRICAN FLY ASH

In this chapter the formation process for Zeolite A and X from coal fly ash precursors was monitored in detail using an in-situ ultrasonic system and the results were complemented by use of ex-situ techniques such as XRD, SEM and FTIR. The chapter is divided into two main sections. The first section presents the findings for the in-situ ultrasonic monitoring of the formation process of zeolite A while section two deals with presentation of results for the in-situ investigation of the formation mechanism of the novel morphology (hierarchical) zeolite X.

6 Introduction

A deeper understanding of the formation mechanism of zeolites from fly ash will not only help in controlling and predicting the best conditions for synthesis but will also unmask the cooperative phenomena dictating the physicochemical-structure relationship. Many attempts have been made by other researchers to comprehend the zeolite formation process from fly ash but they are mostly based on the use of ex-situ monitoring techniques (Murayama *et al*., 2002; Fansuri, 2008). These techniques rely on periodic quenching of the reaction mixture i.e. separating the solid and liquid phase prior to independent analysis. The challenge with this approach is that it is not so reliable since there could be artefacts caused by the quenching process. The use of in-situ ultrasound diagnostic of zeolite crystallization had been reported earlier (Schmachtl *et al*., 2000; Herrman *et al*., 2005; Baser *et al*., 2007; Baser and Schwieger, 2008) to successfully enable monitoring of the complex formation process of zeolites from pure analytical grade sources of Si and Al. In this study, zeolite type A and X were chosen as models for investigating the crystallization mechanisms using South African fly ash because these zeolites are well understood and a lot of effort has already been made to understand their formation from pure analytical grade sources aluminate and silica (Cundy and Cox, 2005). In addition, these zeolites are also known to crystallize under reasonable hydrothermal conditions and short synthesis times.

CHAPTER 6

6.1 In-situ ultrasonic monitoring of zeolite A from fly ash

The goal of this subsection was to explore the mechanism of formation of zeolite A from South African fly ash. This study follows on from the identification and optimization studies for zeolite A from South African fly ash (sourced from Arnot power station) reported in Chapter 4. The procedure followed during the investigations of the zeolite A formation process is described in Chapter 3 (Section 3.3.2). The synthesis precursor solution had a molar ratio of 1 Al_2O_3 : 30 Na_2O : 4 SiO_2 : 414 H_2O. A schematic of the in-situ ultrasonic monitoring set-up is shown in Chapter 3 (Figure 3.10 and 3.11). After investigating the formation mechanism of zeolite A at 80 ºC, a synthesis mixture prepared using analytical grade sources of Si and Al was also monitored and used for comparison with the fly ash system. The influence of ageing the fly ash based precursors solution at room temperature prior to hydrothermal synthesis was also studied. To understand the effect of temperature, three hydrothermal crystallization temperatures (i.e 80, 90 and 94 ºC) were investigated. The results obtained from each set of experiments are initially presented before an overall discussion is presented.

6.1.1 Measurements of attenuated ultrasound signal

The in-situ ultrasonic monitoring technique is an indirect, non-invasive, structure insensitive method that is based on the investigation of the degrees of interaction of ultrasonic wave transport properties as ultrasound waves travel through the synthesis mixture (Schmachtl *et al*., 2000; Herrman *et al*., 2005). The use of ultrasonic attenuation as an investigation tool is an improvement on the earlier use of ultrasound velocity and amplitude since there were challenges encountered due to the scattering from the solid products which made it difficult to correlate ultrasound phase and amplitude with the increasing zeolites crystallinity during the crystal growth step (Baser *et al*., 2007).

6.1.1.1 Effect of ultrasound on blank solutions

The study began by conducting in-situ ultrasonic monitoring of blank demineralized water and NaOH (6 M) solution. The heating rate was about 0.5 ºC/min to the final predetermined temperature of 80 ºC. The results for these blank runs are presented in Figures 6.1.

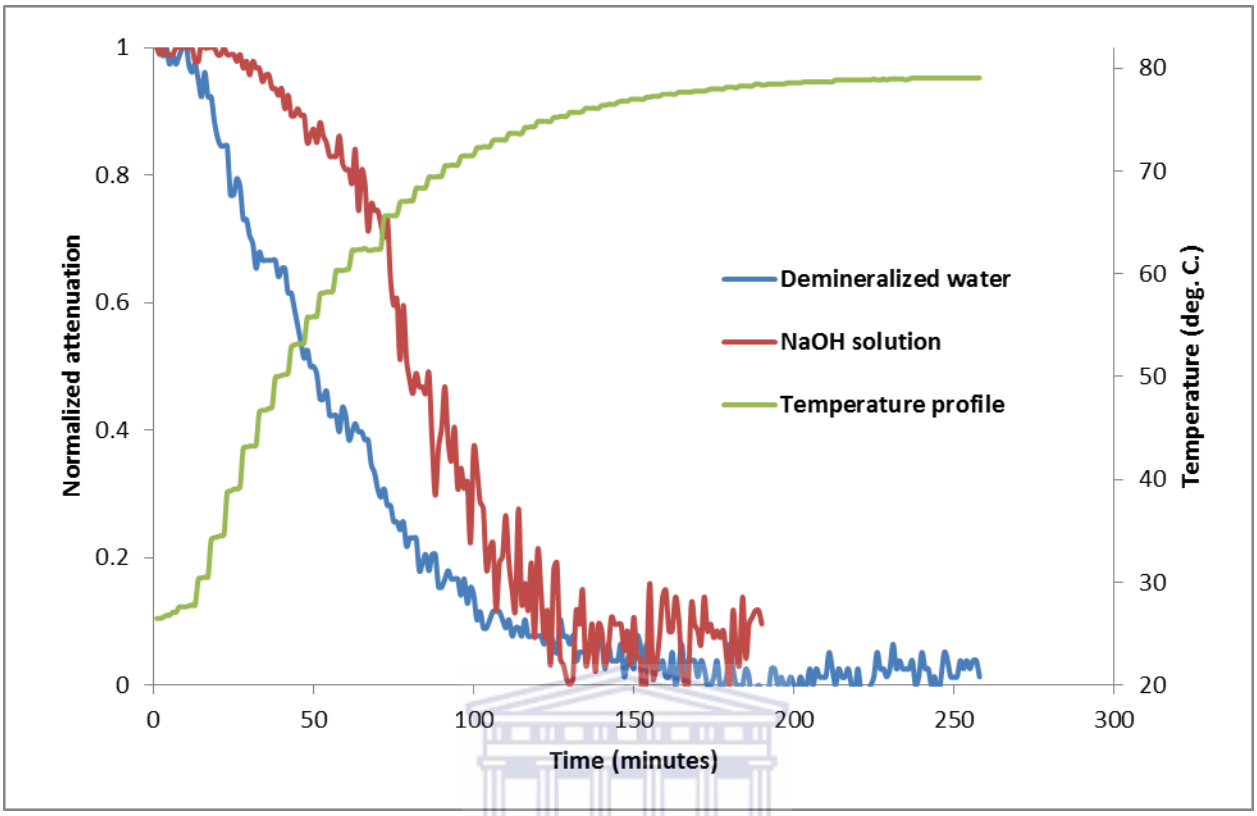

Figure 6-1: Plots of normalized attenuation vs. time of blank runs of demineralized water and NaOH (6 M) conducted at a heating rate of about 0.5 ºC/min.

As shown in Figure 6.1, there was a reduction of ultrasonic attenuation for the first 120 minutes before stabilization once the temperature of 80 °C was attained. These blank experiments enabled decoupling of interferences (background noise) that might complicate the analysis of reactions taking place in the actual synthesis mixture which is presented in the next sub section.

6.1.1.2 Effect of ultrasound on the solutions

The synthesis of zeolite A from a synthesis mixture with a molar ratio of 1 Al_2O_3 : 30 Na_2O : 4 SiO_2 : 414 H_2O that was prepared from the clear extract of fused South African fly ash was monitored under real reaction conditions using the in-situ ultrasonic monitoring set up presented in Chapter 3 (Section 3.3). The plots of normalized attenuation vs. time of crystallization of zeolite A from clear extract of fused South African fly ash together with the heating profile are presented in Figure 6.2. A reproducibilty test was also conducted and the results are presented in the same US-attenuation plot.

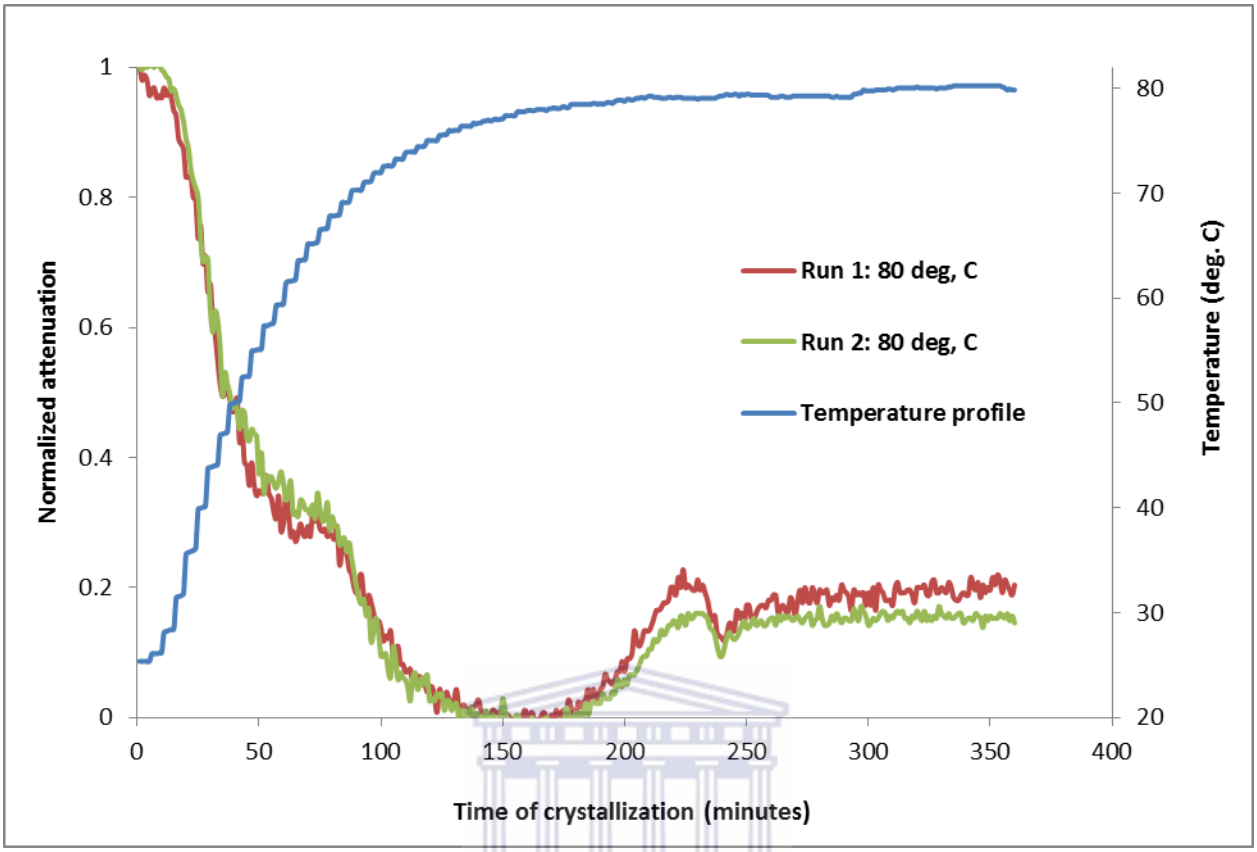

Figure 6-2: Plots of normalized attenuation vs. time of crystallization of zeolite A from clear extract of fused fly ash (Reproducibility tests) conducted at a heating rate of about 0.5 ºC/min.

As shown in Figure 6.2, the signal generated from run 1 and 2 of the in-situ monitoring of crystallization of zeolite A from the clear solution extracted from fused fly ash was reproducible. The temperature profile, generated from the online temperature measurements, show that the heating rate was about 0.5 ºC/min with the final predetermined temperature of 80 ºC achieved after about 140 minutes. In the initial 30 minutes of in-situ ultrasonic monitoring of the synthesis mixture when the heating had reached 50 ºC, the ultrasonic attenuated signal was observed to decrease but as the synthesis time progressed there was a slight increase that occurred between 50 and 80 minutes during the heating profile. Thereafter, a decrease of US-attenuation up to about 140 minutes was observed. Between 140 and 180 minutes at an isothermal temperature of 80 ºC, the attenuated signal was noted to stabilize without any noticeable increase or decrease but then increased steadily between 180 and 220 minutes. Still at the isothermal temperature of 80 ºC, a sharp inflection point in the ultrasound signal was noted at 220 minutes which was

followed by an increase of the ultrasonic attenuation that occurred between 240 and 260 minutes before it stabilized until the end of the monitoring process.

In order to compare the different processes taking place during the hydrothermal synthesis of zeolite A from the clear extract of fused fly ash or from the unseparated fused fly ash slurry (see image a and b in Figure 6.3), the in-situ ultrasonic signals generated when these two different precursor mixtures were investigated when the final temperature was set to 80 ˚C are presented in Figure 6.3.

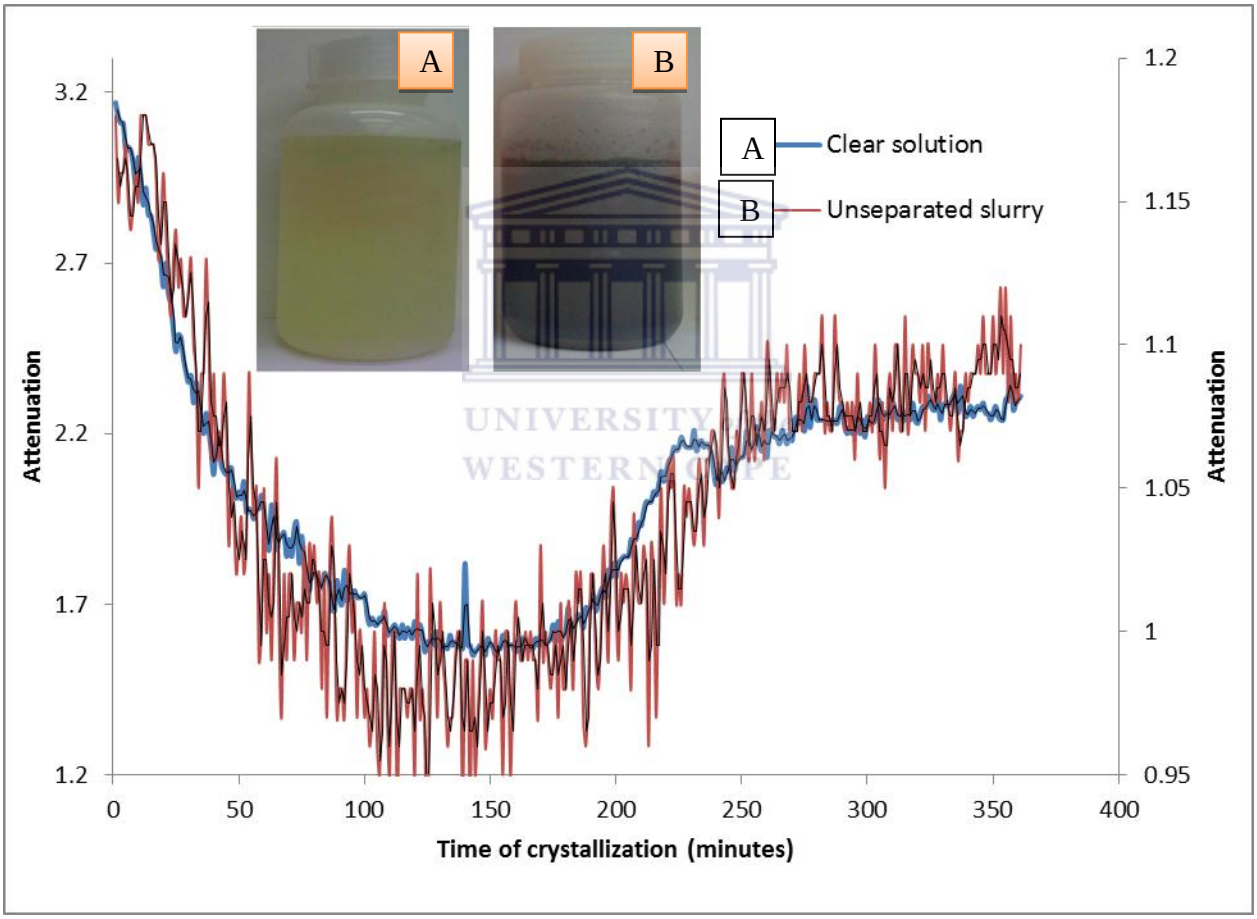

Figure 6-3: Comparison of plot of attenuation vs. time of crystallization of zeolite A synthesized from clear fused fly ash extract or unseparated fly ash slurry conducted at a heating rate of about 0.5 ºC/min to 80 C.

As shown in Figure 6.3, when the in-situ ultrasonic signals generated using clear solution was compared with that obtained using unseparated fused fly ash slurry it can be seen that the signal to noise ratio of the US-attenuation for the unseparated fused fly ash slurry was higher than that of the clear solution. The reason for this difference could be due to the presence of undissolved fused fly ash precursor species which caused scattering of the ultrasound waves, whereas these precursor species did not interfere after filtration and removal of the undissolved matter.

6.1.1.3 Effects of ageing of synthesis mixture

Ageing studies have been widely used to generate indirect experimental data to understand the processes taking place in the early stages of crystallization of zeolites (Zhadanov *et al*., 1971; Li *et al*., 2001). Figure 6.4 shows the effect of the ageing process as monitored by the in-situ ultrasonic technique. The ageing of the reaction mixture with a molar ratio of 1 Al_2O_3 : 30 Na_2O : 4 SiO_2 : 414 H_2O that was prepared starting from the clear extract of fused fly ash was conducted at room temperature for different times (0, 360, 720 and 1050 minutes) before heating was commenced. The start point of the heating is marked with an arrow in Figure 6.4. The temperature profile of heating was as shown in Figure 6.2.

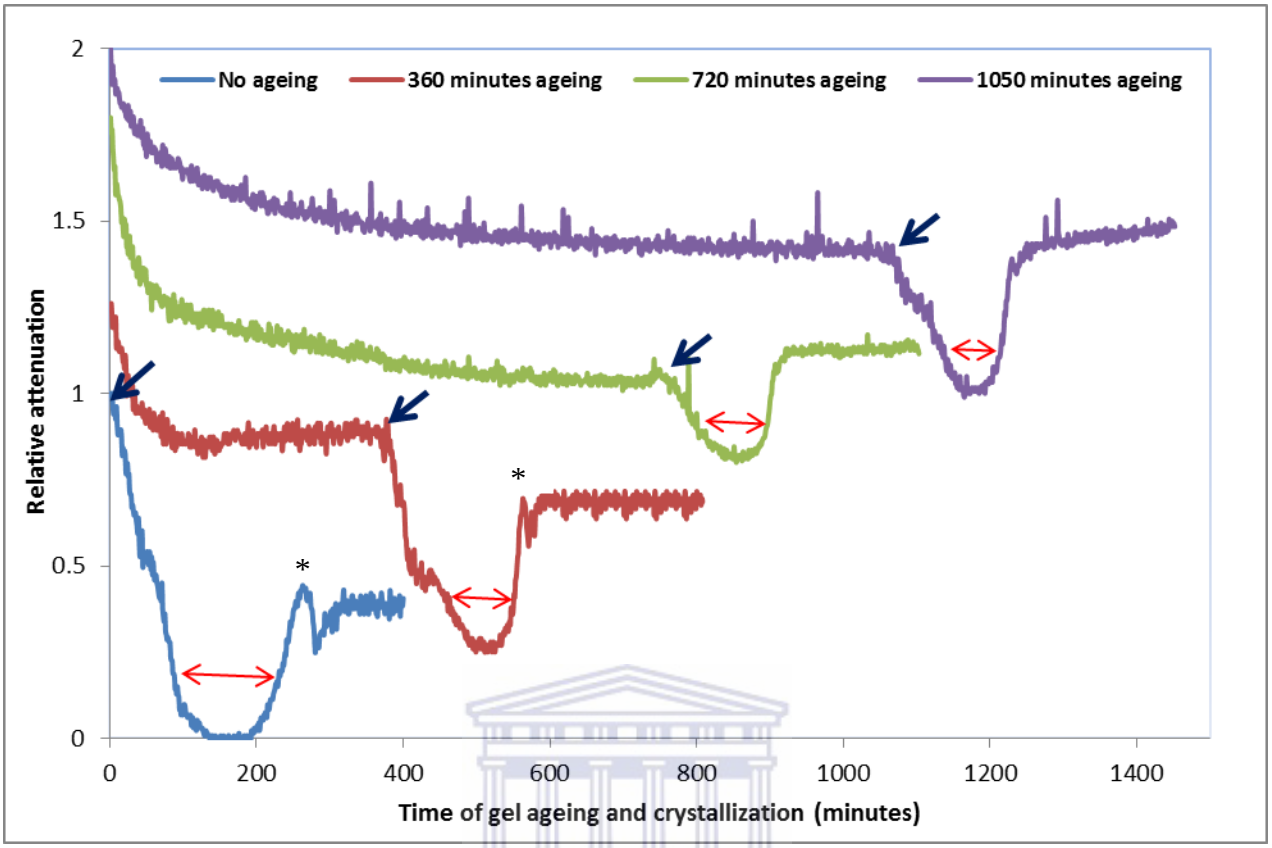

Figure 6-4: Plots of attenuation vs. time of crystallization of zeolite A: effect of gel ageing before crystallization of zeolite A from clear solution at 80 ºC (the start point of the heating up is marked with an arrow).

From Figure 6.4, two effects could be observed when comparing the US-attenuation signals generated from synthesis conducted at 80 ºC after ageing the reaction mixture at room temperature for the four different ageing times. These ageing-time dependent influences were; i) disappearance of the 'hump' in the US-attenuation pattern which could be seen at around 220 minutes (marked by *) for the unaged synthesis mixture; ii) shortening of the syncline region of the US-attenuation plot (shown by a double sided arrow) as ageing time was prolonged. The 'hump' fully disappeared after ageing the reaction mixture for 720 minutes.

6.1.1.4 Effects of simulating fly ash molar regime (use of pure chemicals instead of fly ash)

Figure 6.5 compares the in-situ attenuated ultrasonic signals generated when studying the hydrothermal synthesis of zeolite A with fly ash as feedstock (starting from the clear extract of

fused fly ash) to that of zeolite A prepared using Si, Al and Na derived from pure analytical grade commercial chemicals. This study was performed to enable a better understanding of the differences in processes taking place during the crystallization of zeolite A from different feedstocks (raw materials). The study was conducted without ageing the synthesis mixture. The simulation of the fly ash based molar composition using pure analytical grade sources of silica and sodium hydroxide follows calculations presented in the MS-excel generated data presented in Figure A2.

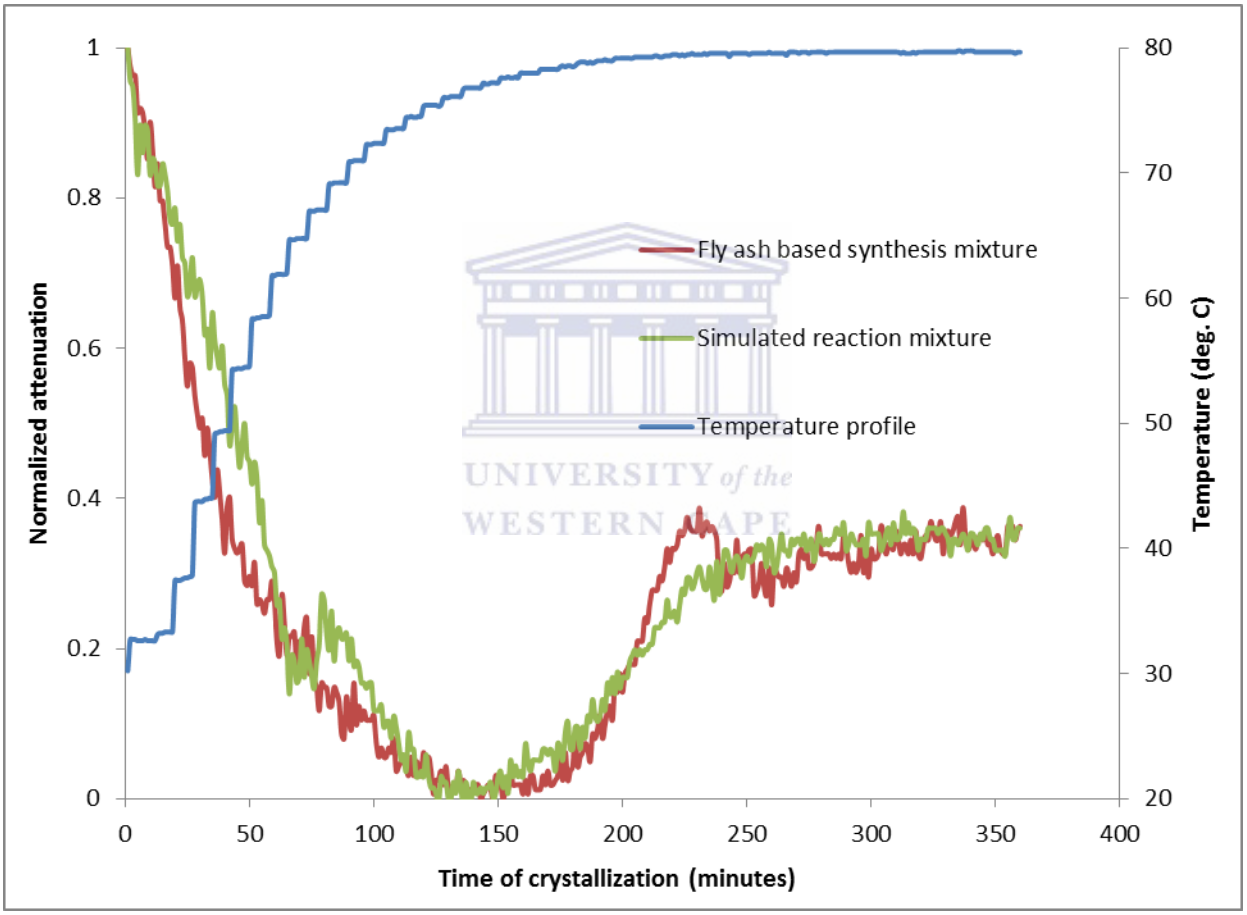

Figure 6-5: Comparison of plots of attenuation vs. time of crystallization generated when studying the hydrothermal synthesis of zeolite A with fly ash as feedstock (starting from the unaged clear extract of fused fly ash) to that of zeolite A prepared using Si, Al and Na derived from pure analytical grade commercial chemicals (simulated reaction mixture).

The immediate cloudiness of the precursor solution that had been observed after preparing the fly ash based precursors was not seen after mixing pure analytical grade aluminate and silicate chemicals but upon further stirring and concurrent heating in the in-situ ultrasonic set up for about 60 minutes the simulated precursor mixture became cloudy. This naked-eye observation was also confirmed by the US-attenuation signal in the case of the simulated reaction mixture, and the cloudiness correlated with the peak between 60 and 80 minutes in the ultrasonic attenuation pattern when the temperature was about 70 ˚C as shown in Figure 6.5. This observation also served to further demonstrate the sensitivity of the ultrasonic attenuation to changes in the viscosity or optical transparency of the synthesis mixture. The hump observed in the US-attenuation signal after 220 minutes in the case of the synthesis using fly ash based precursors was not observed in the attenuated pattern of the simulated composition. The discussion on the presence of the 'hump' is presented in section 6.1.3.

6.1.1.5 Effect of variation of hydrothermal crystallization temperature

In order to investigate the effect of temperature during the in-situ ultrasonic monitoring of zeolite A starting from the clear extract of fused fly ash and also from the unseparated fused fly ash slurry the synthesis was conducted at three temperatures (80, 90 and 94 ºC). The temperature profiles for each of the three temperature variations are presented in Figure 6.6.

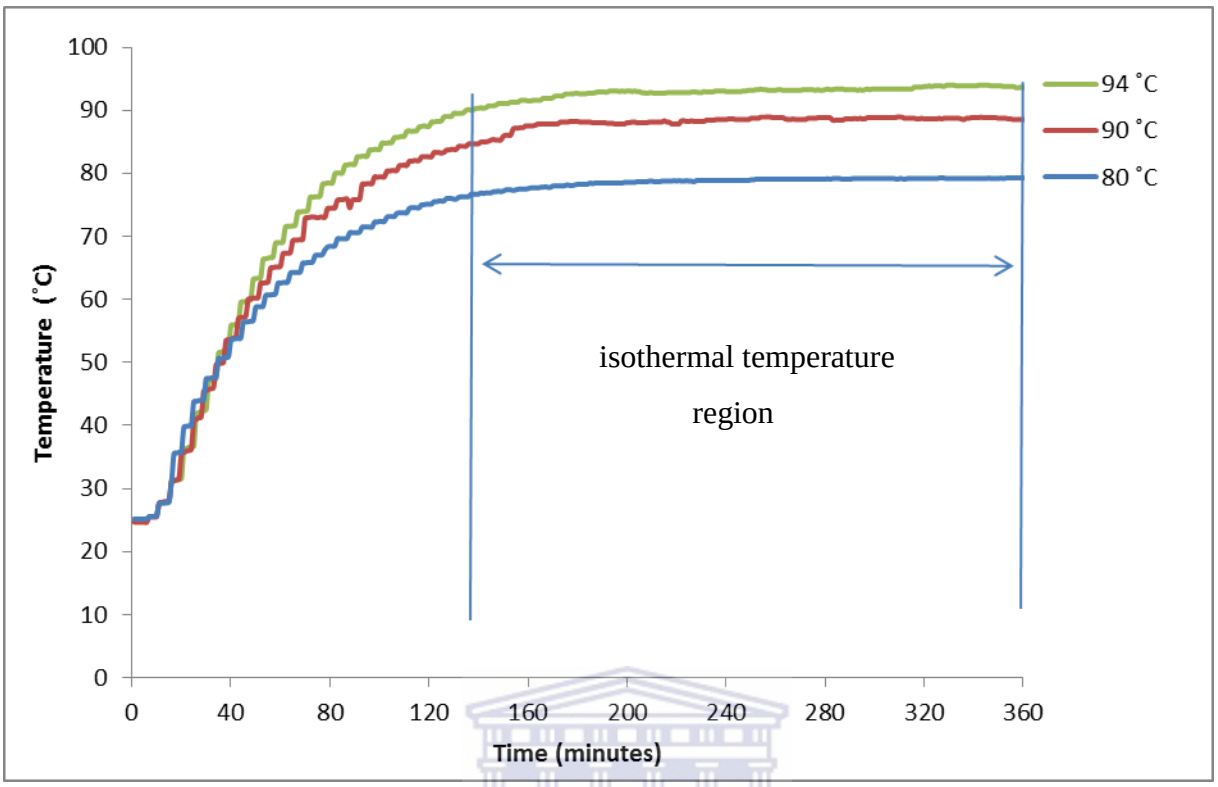

Figure 6-6: Online temperature profiles generated during the in-situ ultrasonic monitoring of crystallization of zeolite A from the clear extract of fused fly ash; the heating rate was about 0.5 ºC/min to 80, 90 and 94 ℃.

From Figure 6.6, the heating rate is shown to be constant at around 0.5 ºC/minute. Isothermal heating for the three temperature variations (80, 90 and 94 ºC) was achieved at around 140 minutes and remained constant up to when the synthesis process was terminated. The real-time temperature monitoring was performed for each experimental run and was a good way to ensure reproducible heating in order to rule out any inconsistencies.

Figure 6.7 presents the comparative plots of normalized attenuation vs. time of crystallization for the in-situ ultrasonic monitoring of zeolite A starting from the clear extract of fused fly ash when the hydrothermal synthesis was conducted at three temperatures (80, 90 and 94 ºC).

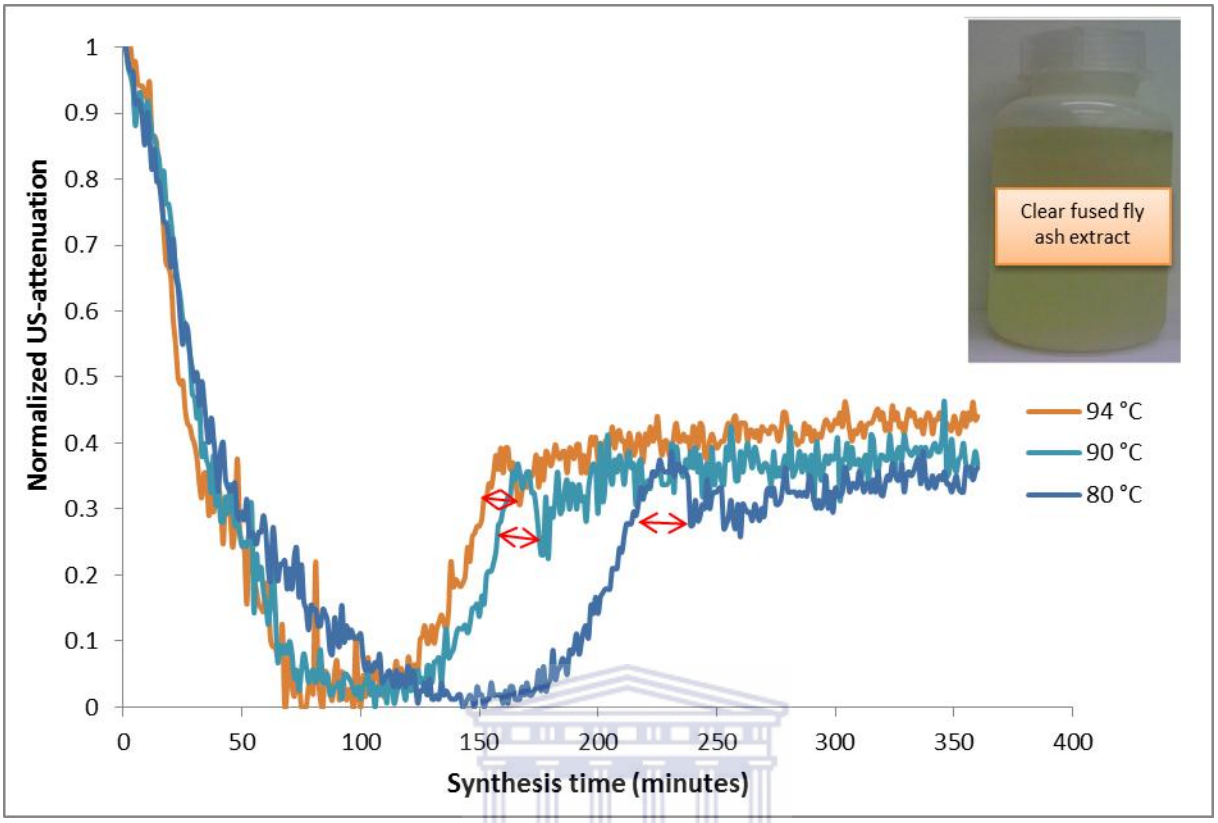

Figure 6-7: Comparative temperature dependent plots of normalized attenuation vs. time of crystallization for the in-situ ultrasonic monitoring of zeolite A starting from the unaged clear extract of fused fly ash when the hydrothermal synthesis was conducted at three temperatures (80, 90 and 94 ºC).

It can be deduced from Figure 6.7 that an increase in the hydrothermal synthesis temperature lead to faster crystallization of zeolite A from fly ash as noted by the shift in the plots of US-attenuation towards shorter synthesis times as the temperature increased. Also noteworthy of mentioning, the base of the hump shown at 220 minutes in the synthesis conducted at 80 ºC grew shorter as the synthesis temperature increased. This observation (shown by double sided arrows in Figure 6.7) will be discussed in detail in Section 6.1.3. Similar effects of variation of temperature were also observed during the in-situ ultrasonic monitoring of zeolite A starting from the unseparated fused fly ash slurry as shown in Figure 6.8.

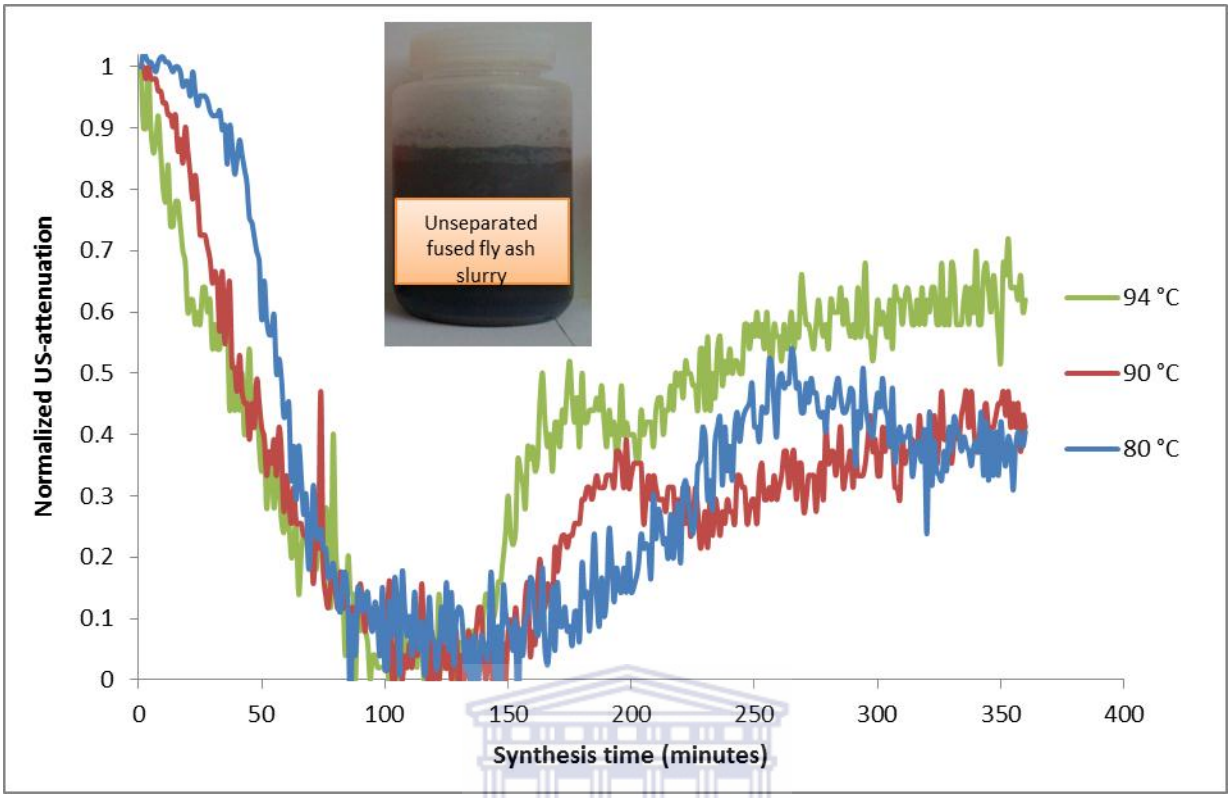

Figure 6-8: Comparative temperature dependent plots of normalized attenuation vs. time of crystallization for the in-situ ultrasonic monitoring of zeolite A starting from the unseparated fused fly ash slurry (unaged) when the hydrothermal synthesis was conducted at three temperatures (80, 90 and 94 ºC).

Figure 6.9 presents a time shift plot of the maxima of the hump vs crystallization temperature calculated from the results that were obtained during the in-situ ultrasonic monitoring of zeolite A starting from the unaged clear extract of fused fly ash (Figure 6.7) when the hydrothermal synthesis was conducted at three temperatures (80, 90 and 94 ºC).

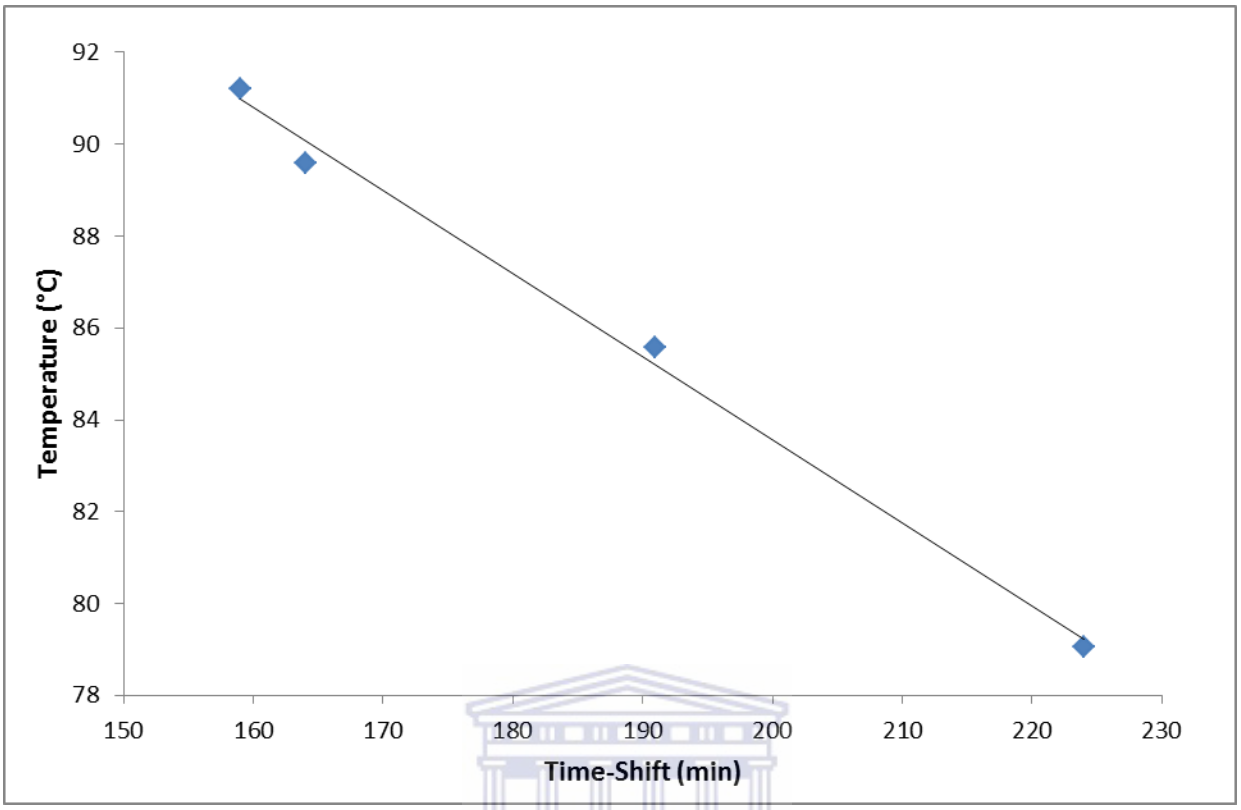

Figure 6-9: Time shift of the maxima of the hump vs crystallization temperature calculated from the results that were obtained during the in-situ ultrasonic monitoring of zeolite A starting from the unaged clear extract of fused fly ash (Figure 6.7) when the hydrothermal synthesis was conducted at three temperatures (80, 90 and 94 ºC).

From Figure 6.9, a linear curve was obtained from the time shift of the maxima of the hump in relationship to the crystallization temperature. The relationship derived from this plot can be used to predict the time of appearance of the hump when the hydrothermal synthesis is conducted at different temperatures.

6.1.2 Complementary ex-situ analyses

Since no single technique is suitable to fully elucidate the key steps of zeolite crystallization, other ex-situ techniques such as X-ray diffraction (XRD), scanning electron microscopy (SEM), fourier transform infrared spectroscopy (FTIR) and Inductively Coupled Plasma Atomic Emission Spectrometry (ICP-AES) were employed to complement the in-situ ultrasonic

monitoring process, to confirm the results and support the findings for the entire crystallization process. Results from these techniques are presented in the sub sections that follow.

6.1.2.1 XRD analysis

Figure 6.10 presents results of XRD analysis of solid products extracted from the synthesis mixtures at different predetermined times (60, 120, 220 and 360 minutes) during the in-situ monitoring process starting from a clear extract of fused fly ash at a hydrothermal synthesis temperature of 80 ºC without ageing. The procedure for preparing the synthesis mixture and sample extraction process is described in detail in Chapter 3, section 3.3.4. The XRD patterns of the extracted solid samples are also compared with the diffraction pattern of standard zeolite A.

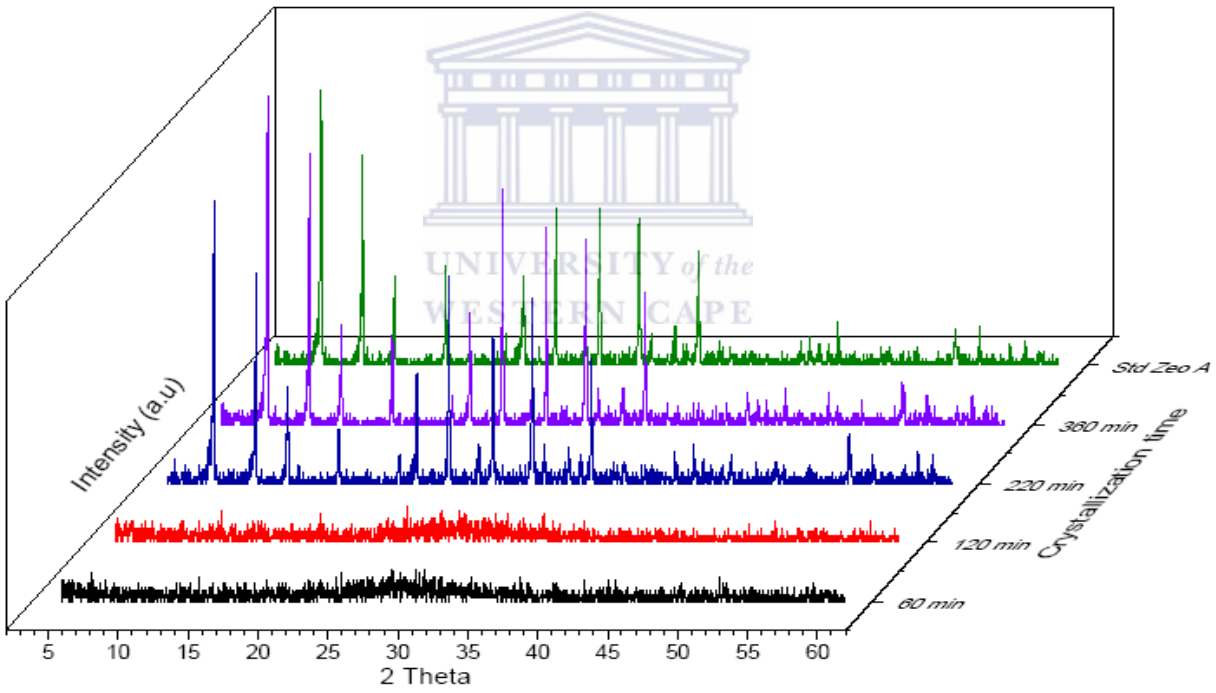

Figure 6-10: XRD patterns analysis of solid products extracted from the synthesis mixture at different predetermined times (60, 120, 220 and 360 minutes) during the in-situ monitoring process starting from a clear extract of fused fly ash at a hydrothermal synthesis temperature of 80 ºC without an ageing step.

The broad hump, observed between 20 and 40˚ 2θ, in the XRD patterns (Figure 6.10) obtained for samples extracted in the initial stages of the zeolite formation process (60 and 120 minutes) is associated with the presence of amorphous precursor material (Inayat *et al.*, 2012). It is important to point out that the original mineral identified in the as-received fly ash (Quartz, Mullite, Hematite and Magnetite) were not observed in the XRD pattern because they had been transformed into soluble sodium aluminosilicate precursors that were further depolymerized to noncrystalline or amorphous species during the extraction of the clear fused fly ash extract. The absence of diffraction peaks in the initial stages (0 – 120 minutes) of the in-situ ultrasonic monitoring process implied that zeolite A had not started to form at that time. After 220 minutes, the characteristic diffraction peaks of zeolite A became more prominent up to 360 minutes and were comparable to the diffraction pattern of standard zeolite A. The data presented in Figure 6.10 highlights the disadvantages of ex-situ XRD investigation due to the fact that fewer data points could be obtained which limits the extent of detailed information compared to results obtained from in-situ ultrasonic analysis.

In order to compare the quality of the synthesis products that were obtained when in-situ ultrasonic monitoring was conducted at different hydrothermal synthesis temperatures (80, 90 and 94 ºC), XRD analysis of the resulting product obtained after 360 minutes were conducted. Comparative XRD results obtained when zeolite A was synthesized at 80, 90 and 94 ºC starting from clear extract of fused fly ash (Figure 6.11) and unseparated fused fly ash slurry (Figure 6.12) are presented below.

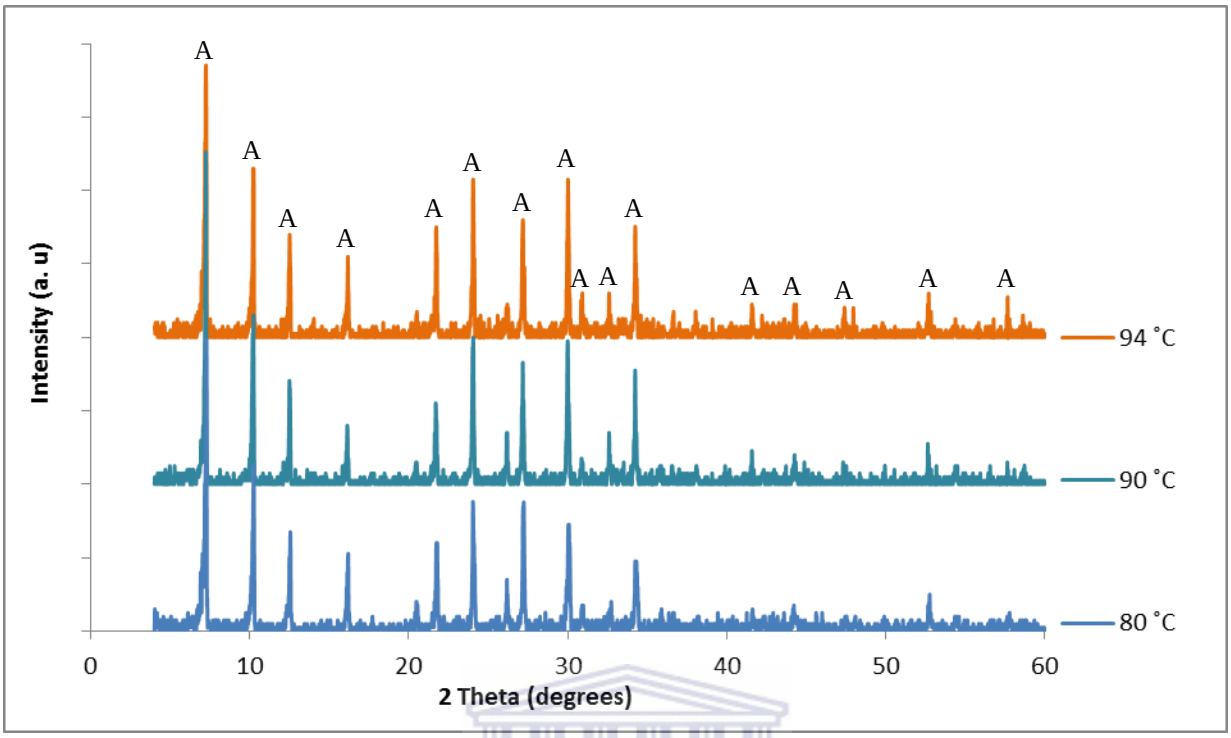

Figure 6-11: Comparative XRD patterns obtained when zeolite A was synthesized for 360 minutes at 80, 90 and 94 ºC using the in-situ ultrasonic monitoring set up starting from the unaged clear extract of fused fly ash.

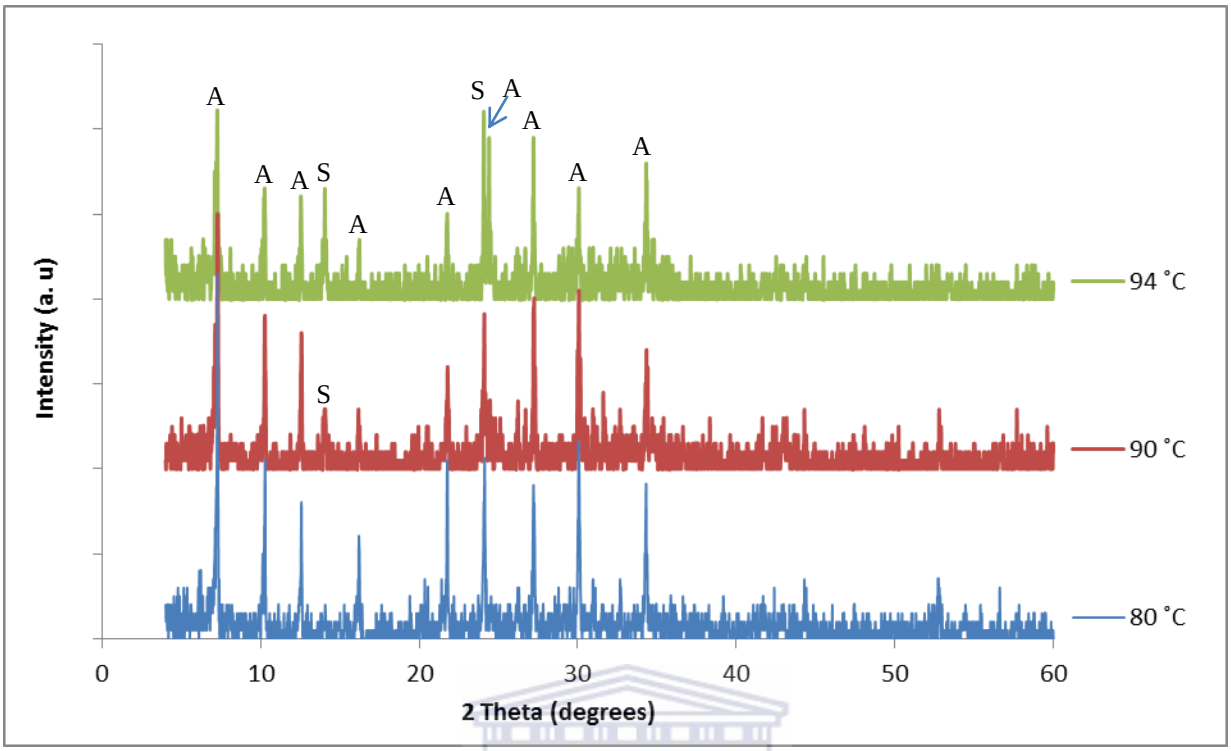

Figure 6-12: Comparative XRD patterns obtained when zeolite A was synthesized for 360 minutes at 80, 90 and 94 ºC using the in-situ ultrasonic monitoring set up starting from the unseparated fused fly ash slurry.

From the XRD patterns presented in Figure 6.11, it is evident that only single phase zeolite A had crystallized when starting from the clear extract of fused fly ash for all the cases when the temperature of the in-situ ultrasonic monitoring was set at 80, 90 and 94 ºC. Results from the synthesis solid products obtained after the in-situ monitoring starting from unseparated fused fly ash slurry (Figure 6.12) show that single phase zeolite A was only obtained when the synthesis temperature was set at 80 ºC. A contaminant phase (hydroxy-sodalite) was seen to co-crystallize with zeolite A when the temperature was set at 90 and 94 ºC using the in-situ ultrasonic monitoring. Changes in the Si/Al ratio, which could be driven by further dissolution of the amorphous precursor species overtime, during the synthesis from unseparated fused fly ash slurry is thought to be the reason for differences in the quality of the synthesis product. The other reason could be due to Oswald phase transformation that occurred at the higher temperatures.

6.1.2.2 SEM analysis

Figure 6.13 presents results of SEM analysis for the solid samples extracted after the predetermined times (0, 150, 200, 210, 220, 240, 280, 360 and 700 minutes) during the in-situ ultrasonic monitoring process at 80 ºC starting from the clear extract of fused fly ash. The procedure followed during the sampling process in described in detail in Chapter 3, Section 3.3.4. In each case the solid and liquid phase was separated by filtration after centrifuging the sample. The morphological analyses (using SEM) of the recovered solid samples, obtained after separating the extracted sample by filtration after centrifuging, were used to track the crystallization process during hydrothermal synthesis. This technique has also been used by other researcher (Cundy and Cox, 2005) and has always proved to be useful. In this case, it would complement the observations noted from the in-situ ultrasonic monitoring process reported in Section 6.1.1.2.

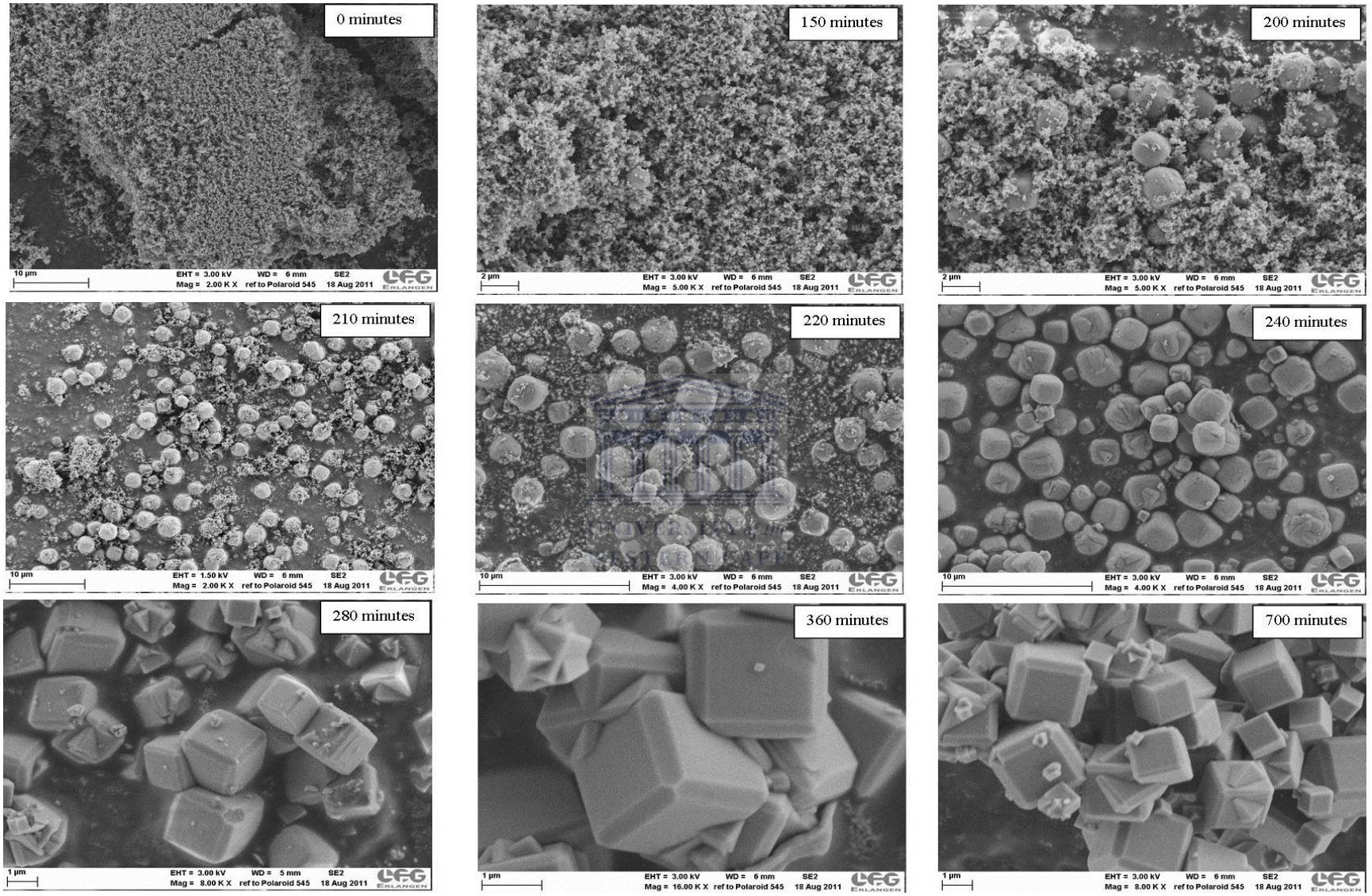

Figure 6-13: SEM micrographs of the solid samples extracted after the predetermined times (0, 150, 200, 210, 220, 240, 280, 360 and 700 minutes) during the in-situ ultrasonic monitoring process at 80 ºC starting from the clear extract of fused fly ash.

The progress of the hydrothermal crystallization of zeolite A is well captured in the SEM micrographs presented in Figure 6.13. The SEM micrographs of the solid sample extracted at time 0 (i.e. before the start of in-situ ultrasonic monitoring) show a 'sponge-like' material which was found to be amorphous from the XRD analysis presented in Figure 6.10. There was no evidence of the typical fly ash cenopheres (shown in Figure 4.3, Chapter 4) giving further evidence that the fly ash fusion step and filtration during the extraction of the clear solution removed all undigested fly ash particles. This amorphous phase was also reported by Cundy and Cox (2005). For the sample obtained after 150 minutes, small round crystals that were about 1 μm could be seen surrounded by the 'sponge-like' amorphous material. For the samples that were extracted between 150 and 220 minutes, the small round crystals that had been confirmed to be of zeolite A (by XRD in Figure 6.10) were seen to increase in size as the synthesis time progressed. For the sample that was obtained after 240 minutes, the SEM image shows that almost all the amorphous material had disappeared and only different crystal sizes of zeolite A could be seen. During these early stages of crystal growth, the crystal morphology is not well defined and the typical morphology (chamfered-edged) of zeolite A is only obtained after 280 minutes. This shape remained distinct until the reaction was terminated after 360 minutes.

Figure 6.14 compares the morphology of zeolite A after 700 minutes of hydrothermal synthesis using a unaged clear extract of fused fly ash precursor solution (Figure 6.14 (a)) with that from unseparated fused fly ash slurry (Figure 6.14 (b)). In both cases, the synthesis was conducted in the in-situ ultrasonic monitoring set up at 80 ºC.

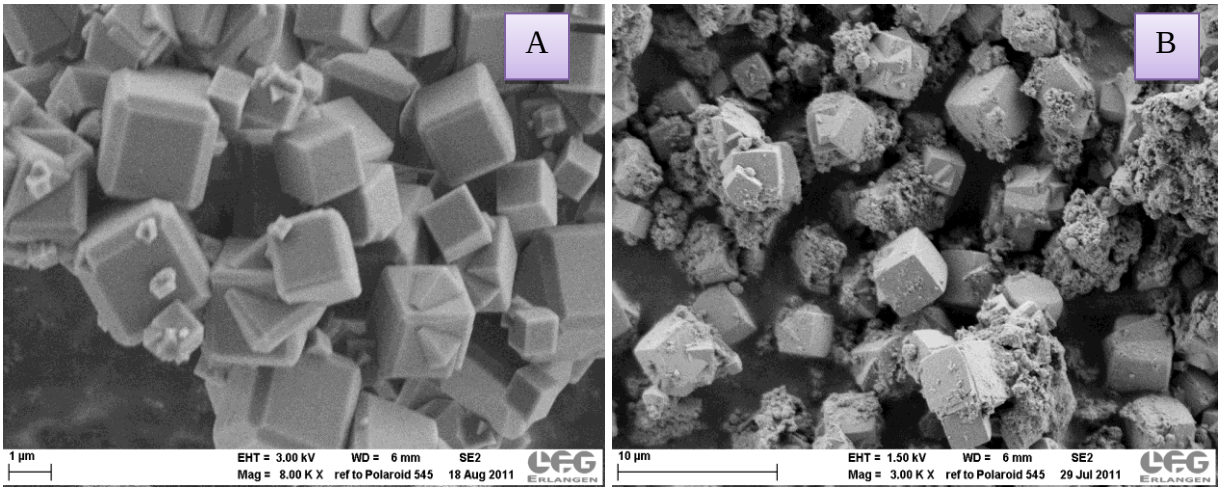

Figure 6-14: Comparative SEM images for zeolite A obtained after 700 minutes of synthesis using a unaged clear extract of fused fly ash precursor solution (A) and unseparated fused fly ash slurry (B) for the synthesis conducted in the in-situ ultrasonic monitoring set up at 80 °C.

From Figure 6.14, it was found that zeolite A crystals prepared from the unseparated precursor slurry had sharp edged cornered morphology (Figure 6.14 (b)) which was different from the chamfered edged crystals obtained from the clear extract of fused fly ash solution (Figure 6.14 (a)). There is also evidence of crystal intergrowth as seen in the SEM image obtained from the clear extract of fused fly ash solution. The small round agglomerates that occur together with the crystals of zeolite A (Figure 6.14 (b)) are thought to be traces of amorphous precursor materials that had not been fully zeolitized.

6.1.2.3 ICP analysis

The product samples which were extracted during the in-situ ultrasonic monitoring process at 80 ºC using the unaged clear extract of fused fly ash precursor solution, following the procedure referred in Chapter 3 (Section 3.3.4), were separated by filtration (after centrifuging) to obtain a supernatant liquid and solid phase. Analysis of the supernatant solution was preferred for monitoring the depletion of the species in the synthesis mixture. It was done to minimize analytical errors that could have otherwise have arisen from the total digestion of the solid product. The ICP results for changes in the concentration of Al and Si in the supernatant liquor, relative to synthesis time, are presented in Figures 6.15 and 6.16 respectively.

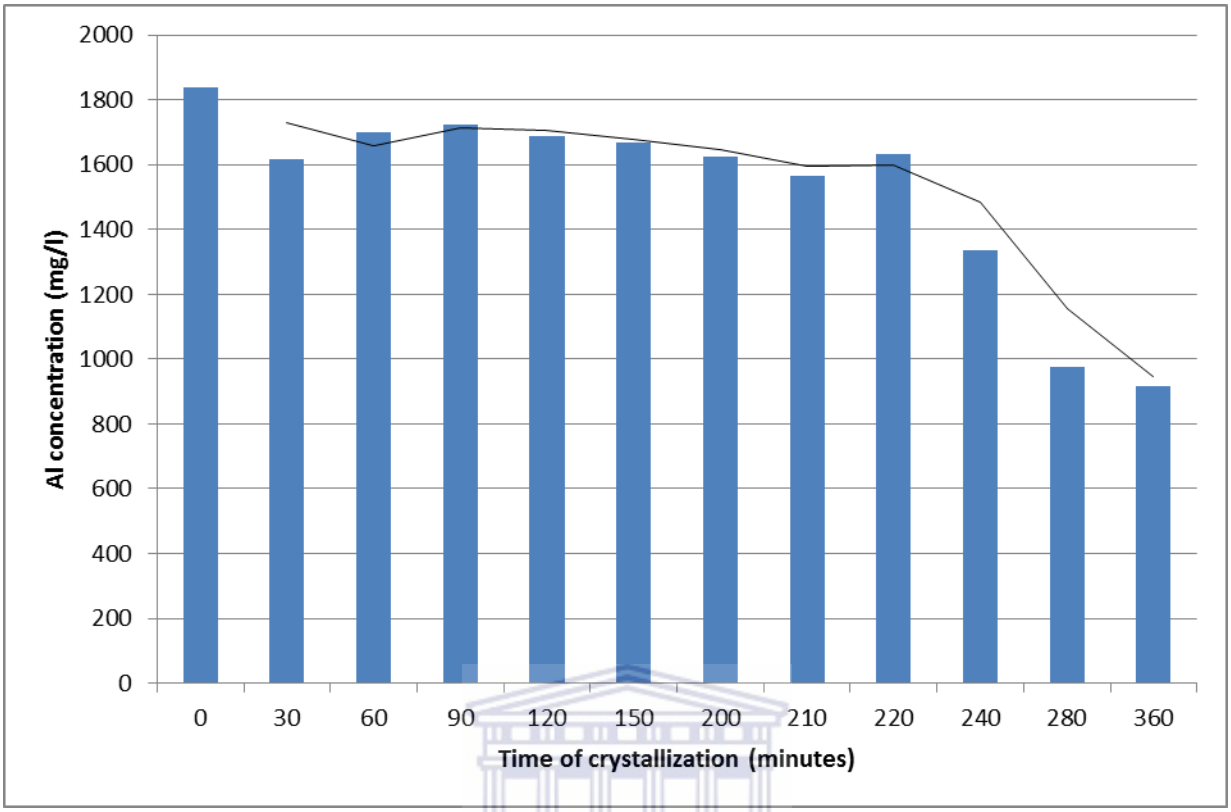

Figure 6-15: ICP analysis: Concentration of Al in the supernatant solution for samples that were extracted at different predetermined times during the in-situ ultrasonic monitoring process at 80 ºC starting from the unaged clear extract of fused fly ash precursor solution.

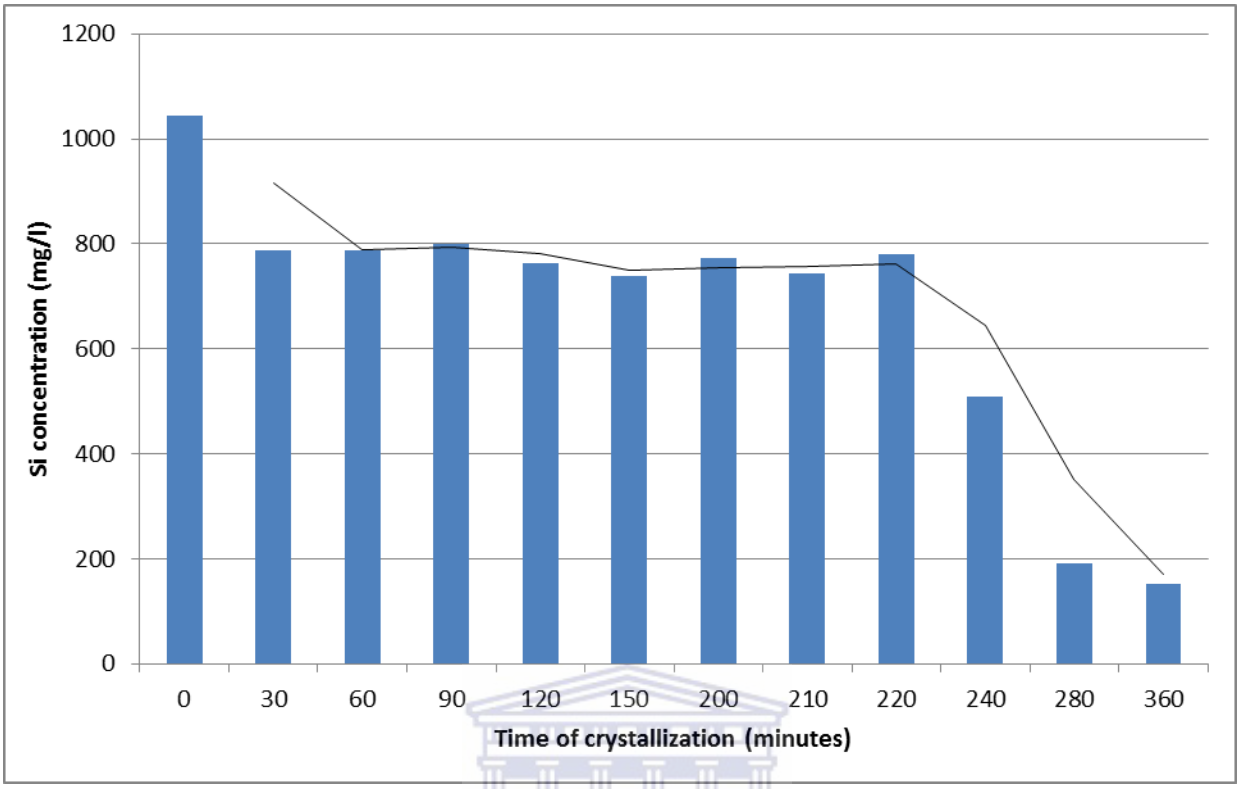

Figure 6-16: ICP analysis: Concentration of Si in the supernatant solution for samples that were extracted at different predetermined times during the in-situ ultrasonic monitoring process at 80 ºC starting from the unaged clear extract of fused fly ash precursor solution.

Both Figure 6.15 and 6.16 indicate the indirect connection between the molar composition of the reaction mixture and the rate of crystal growth. The concentration of Al and Si in the supernatant liquid was observed to decrease after the initial 30 minutes when the temperature was at about 48 ºC but levels increased slightly between 60 and 90 minutes (63 and 70 ºC). As earlier noted (Figure 6.6), after the synthesis time of 140 minutes the isothermal temperature of 80 ºC had already been achieved. As time progressed up to about 150 minutes, the concentration of the Al and Si precursors in the solution was noted to show small fluctuations. A steady decrease in the concentration of Al was noted to occur between 150 and 210 minutes. An inflection point occurring at around 220 minutes for both the concentration of Al and Si was observed and was then followed by a steady depletion of the precursors occurring between 220 and 360 minutes of hydrothermal synthesis. By the time the in-situ ultrasonic monitoring was stopped, after 360 minutes, there was still some Al (about 900 mg/L) and Si (150 mg/L) left behind in the

supernatant solution which in this case can be considered as wastage. Future work, which fall outside of the scope of this work, can be conducted to re-use the excess Si and Al. This investigating of the trend in the consumption or depletion of precursor species out of solution, by integration into the growing zeolite A crystals, acted as an indirect way of monitoring the progress of zeolite A formation process. A more detailed discussion will be presented in Section 6.1.3.

To understand the relationship of depletion of Al to Si precursors, the trend of Si/Al ratio in the supernatant liquor is presented in Figure 6.17.

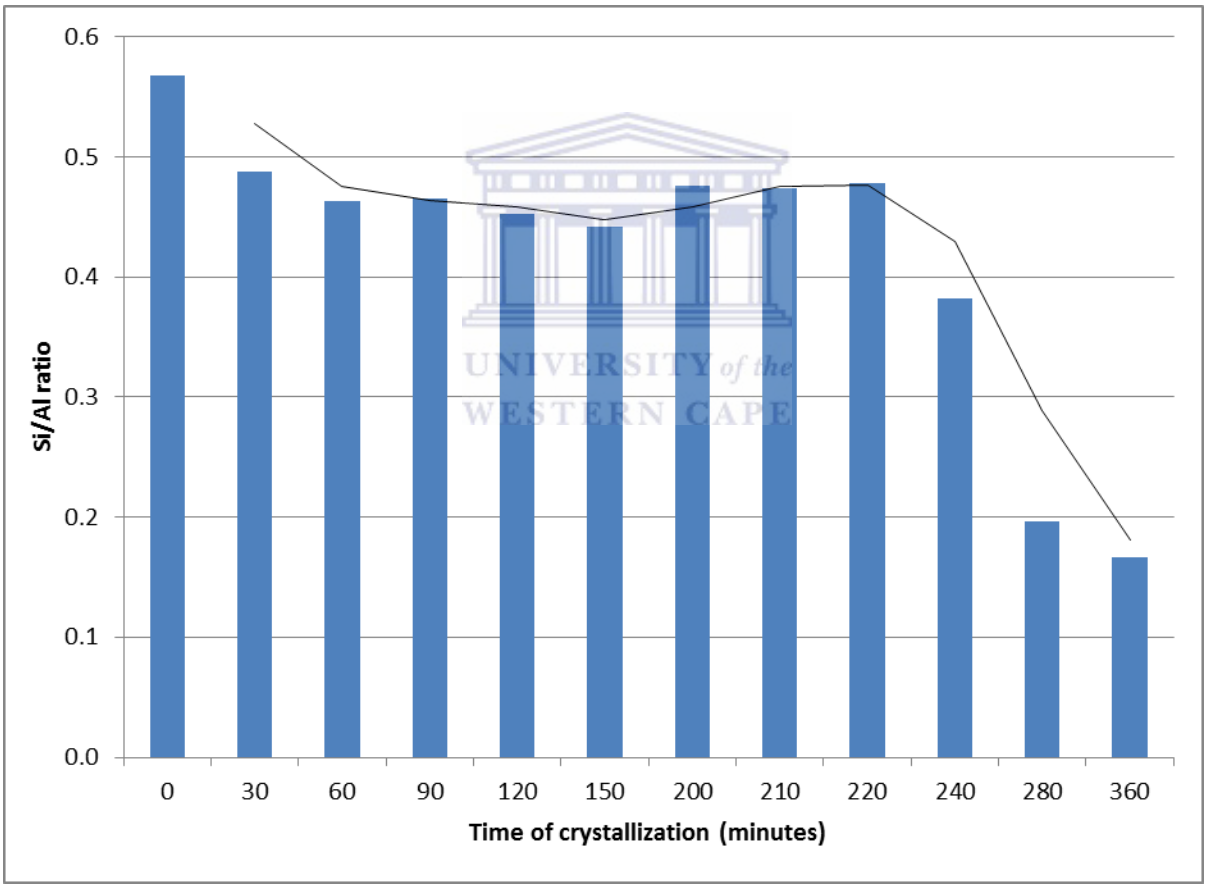

Figure 6-17: ICP analysis: Si/Al ratio of the supernatant solution for samples that were extracted at different predetermined times during the in-situ ultrasonic monitoring process at 80 ºC starting from the unaged clear extract of fused fly ash precursor solution.

Figure 6.17 shows that the trend in the Si/Al ratio was the same as was that found in Figures 6.15 and 6.16. The relative amount of Si and Al is known to play a significant role in determining the outcome of the crystallization process (Bryappa and Yoshimura, 2001). The excess Al towards the end of the synthesis could be explained by Lowenstein's law which rationalized the absence of Al-O-Al linkages in the zeolite framework (Bryappa and Yoshimura, 2001).

6.1.2.4 FTIR analysis

IR spectroscopy has been extensively used to monitor the development of crystallinity during zeolite synthesis (Shigemoto *et al.,* 1995; Fernández-Jiménez and Palomo, 2005). Figure 6.18 and 6.19 compares the infra-red spectra of the synthesized zeolite A with its amorphous precursors and intermediates. These analysis were conducted on the solid phase of the samples which were extracted during the in-situ ultrasonic monitoring process (0, 30, 60, 90, 120, 150, 200, 210, 220, 240 and 360 minutes) for the synthesis conducted at 80 ºC using the unaged clear extract of fused fly ash precursor solution. The procedure for extracting the samples is described in detail in Chapter 3 (Section 3.3.4).

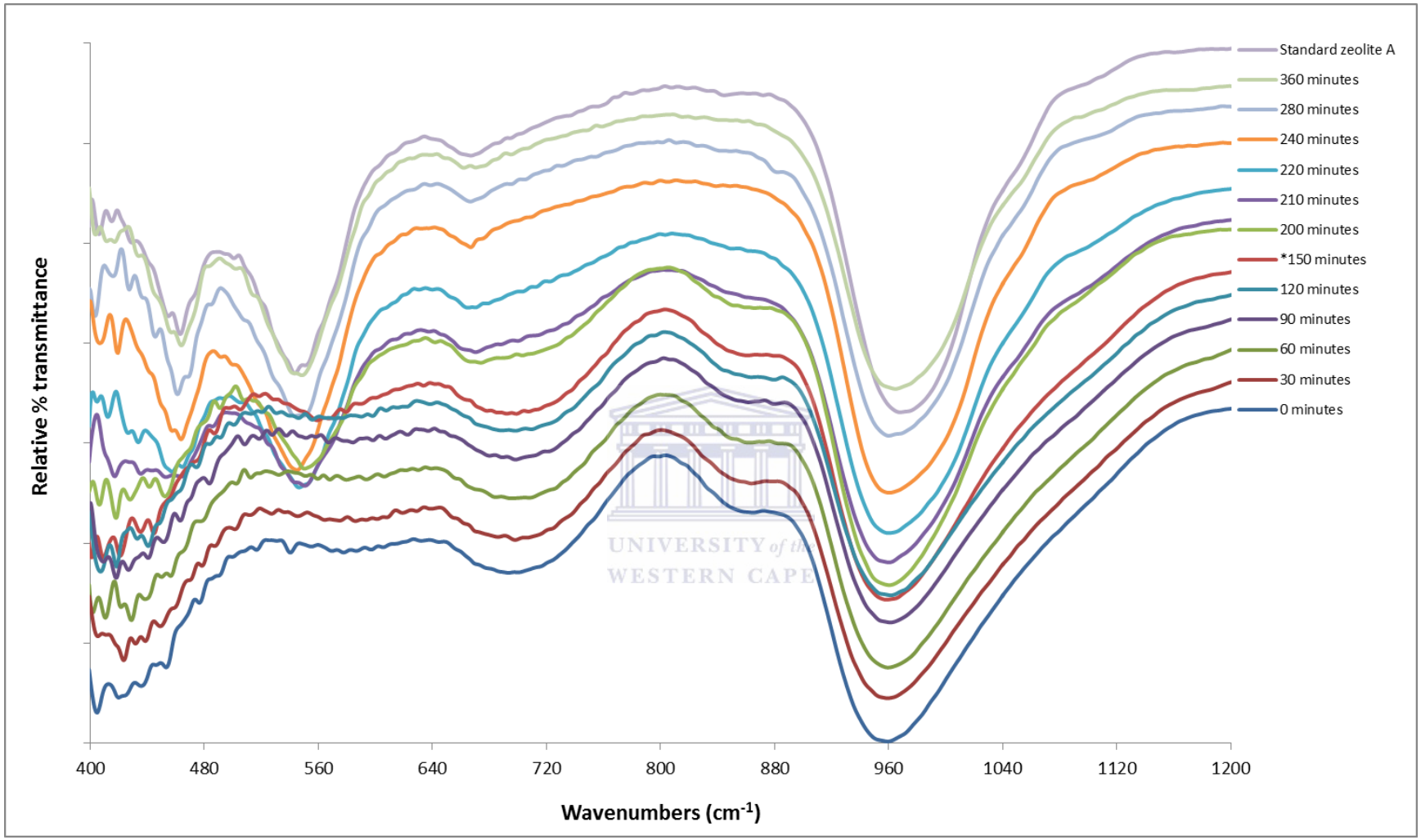

Figure 6-18: FT-IR analysis of solid samples that were extracted at different predetermined times during the in-situ ultrasonic monitoring process of zeolite A for synthesis conducted at 80 ºC starting from the unaged clear extract of fused fly ash precursor solution.

An excerpt of Figure 6.18 that compares bands appearing at 1640 cm^{-1} for the synthesized zeolite A with its amorphous precursors and intermediates is presented in Figure 6.19. This band is associated with the characteristic bending mode of water molecules.

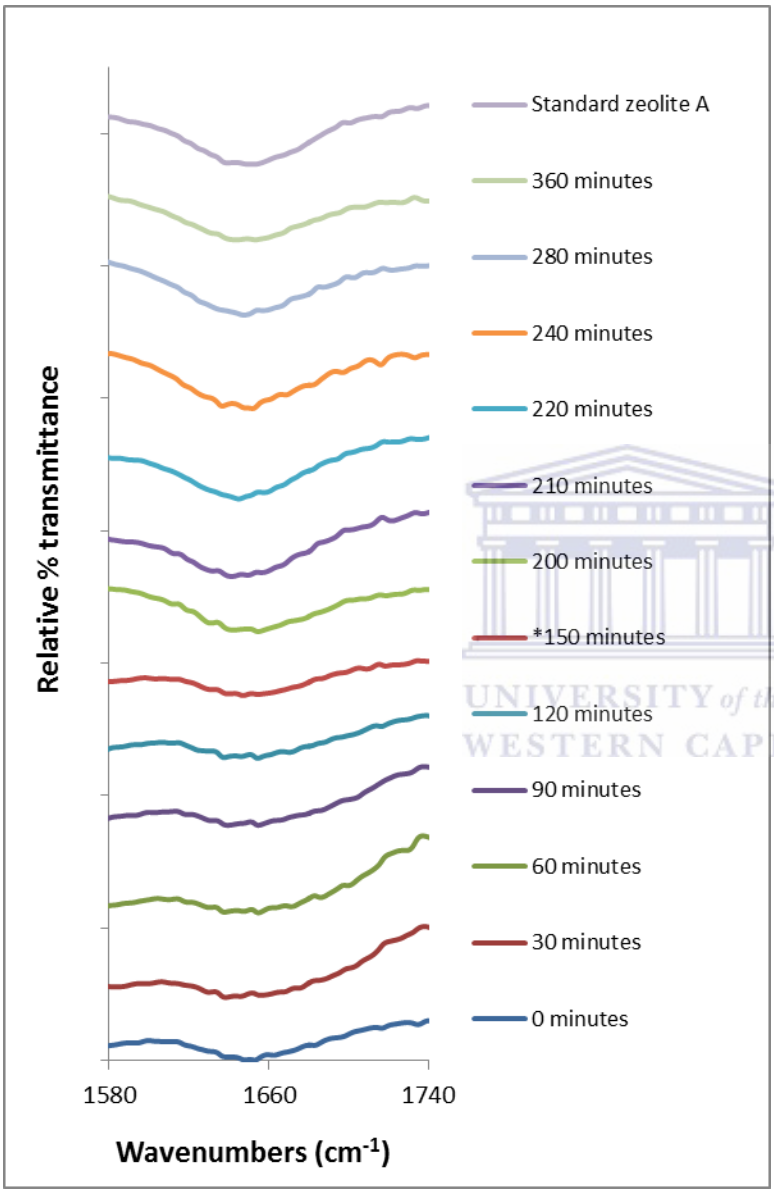

Figure 6-19: FT-IR analysis of solid samples that were extracted at different predetermined times during the in-situ ultrasonic monitoring process of zeolite A for synthesis conducted at 80 ºC starting from the unaged clear extract of fused fly ash precursor solution.

The close matching of IR bands of the fully crystalline zeolite A sample obtained after 360 minutes (at 80 ˚C) to that of standard (commercial) zeolite A indicated the similarity of their structural units and chemical moieties. Although a more detailed discussion will be presented in Section 6.1.3, it is evident from Figure 6.18 and 6.19 that development of crystallinity during the entire zeolite synthesis process can be followed by FTIR analysis. This information derived from this analytical technique also primarily served to complement the observations that were noted from real-time in-situ ultrasonic monitoring of zeolite A formation presented in Figure 6.2 as well as XRD (Figure 6.10) and SEM (Figure 6.13) analysis.

6.1.3 Discussion of the in-situ ultrasonic diagnostic of zeolite A crystallization from fly ash

A thorough discussion correlating the findings from in-situ ultrasonic monitoring process of zeolite A together from fly ash in relation to the results from the complementing ex-situ monitoring is presented in this sub section. The use of complementing ex-situ techniques served to confirm and support the deductions that were made from the in-situ ultrasonic monitoring technique since there is no existing literature that discusses the formation mechanism of zeolites from fly ash using in-situ monitoring techniques.

During the initial mixing of Si and Al source materials prior to hydrothermal conditions, the immediately formed species has been reported to be mostly non-equilibrated amorphous aluminosilicate precursor material (Cundy and Cox, 2005; Angel *et al*., 1977). This primary amorphous phase undergoes changes due to stirring and heating during hydrothermal conditions which in effect causes changes in reaction fluid properties such as viscosity and density (Herrmann *et al*., 2005). The reported observations can be seen from the fluctuations in the initial trend of in-situ ultrasonic attenuation presented in Figure 6.2 and further confirmed by the changes in the concentration of Al and Si shown in Figures 6.15 and 6.16 as well as the FTIR bands at 880 cm^{-1} until 200 minutes shown in Figure 6.18. Furthermore, Zhdanov (1971) and Kerr (1996) reported that equilibration with time of the initial amorphous gel with the liquid phase leads to the release of soluble species which is clearly noted by ICP analysis. Schmachtl *et al*. (2000) had also pointed out that during the initial stages of synthesis of aluminous zeolites structures such as LTA and FAU types, an amorphous aluminosilicate gel results after mixing reactive silica and aluminate source materials with alkali metal hydroxide ions in water. This

observation can be confirmed by the presence of non-crystalline amorphous phase which acted as the precursor material prior to the crystallization of zeolite A as seen in the XRD results presented in Figure 6.10. The slight increase of US-attenuation seen between 50 and 80 minutes in Figure 6.2 deviates from the observation that was noted by Baser and Schwieger (2007) who reported a decrease of US-attenuation at the beginning of the hydrothermal synthesis process which they had ascribed to the dissolution of the amorphous phase. This deviation of the US-attenuation trend can be explained by Cundy and Cox's (2005) concept of the formation of the 'pseudo-steady-state intermediate' which they had referred to as 'secondary amorphous phase' occurring via solution transport mechanism during the process of evolution of order. The existence of primary (visible gel) and secondary amorphous phases had also been proposed by Angell and Flank (1977). During the nucleation period, between 120 and 150 minutes (see Figure 6.2), complex rearrangements have been reported to take place leading to the formation of 'islands of order' which propagate with time and temperature (crystal growth) to form visible zeolite crystals (Cundy and Cox, 2005). The interface between solid and solvent during the nucleation stage has been reported to move faster (Pienack and Bensch, 2011) to an extent that it is not possible to notice significant changes in the concentration of Al and Si species in the solution (Figure 6.15 and 6.16). This observation can further be confirmed by the negligible fluctuations occurring between 120 and 150 minutes in the in-situ ultrasonic attenuation plot (Figure 6.2). During this period, Pienack and Bensch (2011) suggested that the reaction medium becomes supersaturated, leading to the generation of a high free energy, which is reduced by the rapid formation of a solid phase from the dissolved species, which is supported by the decrease of Si and Al from the supernatant solution noted after 210 minutes in Figures 6.16 and 6.17.

The chemical and physical processes leading to formation of the nuclei as well as the duration of nucleation has been reported (Cundy and Cox, 2005; Kerr, 1977) to depend on the structure being formed as well as on the synthesis conditions. The acquisition of experimental data is very difficult during the nucleation process due to the extremely small nature of nuclei and only few researchers have been successful in providing direct experimental evidence of the nucleation phenomenon (Chang and Bell, 1991; Cundy *et al*., 1993; Gora *et al*., 1997). The crystal growth period can be correlated to the steady increase of the US-attenuation occurring between 180 and 220 minutes in Figure 6.2 and further confirmed by the increase in crystallinity of zeolite A as

shown by XRD analysis in Figure 6.10. This period is associated with systematic periodic propagation of zeolite crystal structure and can further be confirmed by the SEM images presented in Figure 6.13 that show a reduction of the amorphous material as the size and number of zeolite A crystals increase. The steady depletion of Al and Si species from the supernatant that occurred after 220 minutes shown in Figure 6.2 also correlated well with the rapid incorporation of the precursors into the crystals (crystal growth). The growth rate of zeolite A crystals was reported to be around 37 nm/min at near optimum compositions at around 80 ˚C (Gora *et al*., 1997) reported during investigations of zeolite A crystallization starting from Si and Al precursors derived from pure chemicals. The chemistry of development of order during the fundamental steps of crystal formation and growth has been discussed in depth by Cundy and Cox (2005) as well as by Chang and Bell (1991). Studies conducted by Miladinovic *et al*. (2009) reported a 'stop effect' that was observed while carrying out in-situ ^{27}Al NMR monitoring of crystallization process of zeolite A. In this study, an almost similar observation was also made by the use of in-situ ultrasonic monitoring as the attenuation hump occurring at around 220 minutes in Figure 6.2 and further confirmed by the slight increase in the concentration of Al and Si in solution at 220 minutes as shown in Figures 6.15 and 6.16 respectively. This observation can be correlated to the breakdown of the amorphous gel structure in this case where the ageing time was zero. Similar observation was demonstrated by Mintova *et al*., (2002) using high resolution electron microscopy (HR-TEM) suggesting that the nucleation also occurred within the amorphous gel particles. The breakdown of the gel structure facilitated the release of nuclei 'germs' that was reported by Zhdanov (1971) to lie dormant in the amorphous phase until activated by release into the solution. This observation is seen by the increase in the rate of crystallization as shown by the sharp increase in the ultrasonic attenuated signal occurring between 240 and 260 minutes in Figure 6.2 (also shown in Figure 6.5) and further demonstrated indirectly by the rapid decrease in the concentration of Al and Si occurring in the same range as seen in Figure 6.15 and 6.16. This unique behaviour can also be related to the autocatalytic model of zeolite crystallization that was discussed by Walton *et al*., (2001). Since there are two distinct inflection points observed during the crystallization monitoring process, it should be possible for independent calculation of kinetic parameters before and after the destruction of the gel structure since two S-shaped crystallization curves can be generated independently to mark

the beginning and end of the attenuation decay. The second S–shaped curve (after gel structure destruction) can be generated by extrapolation.

During the investigation of the ageing process, the initial decrease of the US-attenuation can be associated with the temperature dependent influences on ultrasonic wave properties due to the exothermic nature of reactions taking place upon mixing fly ash extract with the aluminate solution. The observations noted in this study support the effects of ageing which have been reported to result in acceleration of the overall crystallization process (Zhdanov, 1971; Li *et al*., 2001). The information on acceleration of the crystallization process by ageing the reaction mixture at different times can be derived indirectly from the progressive shortening of the nucleation period (shown by double arrows in Figure 6.4). Cundy and Cox (2005) suggested that ageing facilitates 'product-formation' effects such as formation of primary entities 'nuclei' or increasing their number hence generating a different nucleation profile which would have otherwise not been the case if the reaction mixture followed a straight-forward (conventional) heating profile. Other researchers (Cook and Thompson, 1988) have concentrated on trying to generate direct experimental evidence to prove the conclusion that the ageing process enhances the formation of viable nuclei even though it is not easy to get such evidence from chemical and spectroscopic studies. Modelling studies (Bronić *et al*., 1988), kinetic analysis (Katović *et al*., 1989; Toufar et el., 1995) and experiments based on analysis of ultimate product particle sizes as a function of different ageing times (Cook and Thompson, 1988) have allowed interpretation of ageing-nucleation relationship and supported the conclusion. XRD analysis of the solid samples extracted before heating began could not detect formation of any crystalline material. To answer the question why the 'hump' in the US-attenuation pattern disappeared in Figure 6.4 during longer ageing time, two scenarios are proposed; i) the possibility of agglomeration of nuclei formed in the amorphous gel phase may have occurred during the longer ageing periods hence minimizing the unique physico-chemical behaviour that was associated with breakdown of the gel structure ii) after the long ageing all the depolymerisation may have proceeded enough to free all silicate species into the solution as small mono- or dimeric species so no gel formation occurred when heating started.

From infra-red analysis presented in Figure 6.18, the amorphous aluminosilicate samples (0 to 120 minutes) showed a broad band centered at around 946 cm^{-1} that corresponded to T-O-T

(where T is either Si or Al that is tetrahedrally coordinated). This band shifted slightly and became sharper as the amorphous material was transformed into crystalline zeolites A. The IR band at 870 cm^{-1}, which can be assigned to T-OH bond in the amorphous precursor of zeolite A, was also observed by Shigemoto *et al*., (1995). Decottignies *et al*. (1978) noted that this band disappears as the sample became more crystalline. According to Bass and Turner (1997), the peaks appearing at around 856 cm^{-1} in the samples extracted between 0 and 200 minutes mostly belong to vibrations of monomers and small dimeric Si species supporting the second proposition namely that deploymerization had freed monomers and dimers into the solution. A general zeolite vibrational band assignment was summarized and reported by Flanigen (1971). The IR bands that shows the formation of the zeolite lattice (i.e the crystalline samples that were extracted between 150 and 360 minutes) were assigned as follows; IR band at 452 cm^{-1} can be assigned to Si-Al-O bending mode (Shigemoto *et al*., 1995), band at 660 cm^{-1} was assigned to Si-Al-O symmetric stretching while the band appearing 560 cm^{-1} has been related to the presence of the double ring (D4R) structure in the framework structure of zeolite A (Rayalu *et al*., 2005). These bands can clearly be seen after 150 minutes in Figure 6.18. The band at 1640 cm^{-1} that is shown in Figure 6.19 has been associated with the characteristic bending mode of water molecules. Comparing the spectra generated from amorphous sample (from 0 to 120 minutes), the 1640 cm^{-1} band is not so prominent but becomes distinct for samples obtained after 150 to 360 minutes signifying that these samples had a higher percentage of water of hydration. Rayalu *et al*., (2005) reported that by investigating the intensity of the peaks appearing at 537 and 452 cm^{-1}, the most crystalline zeolite A sample can be identified. In this case, the sample extracted after 360 minutes had the most intense peak at 537 and 452 cm^{-1} with almost similar intensity as the standard (commercial) zeolite A sample.

Comparing the formation process of zeolite A from fly ash precursors with that obtained from the molar composition prepared from pure chemicals, the naked-eye milky observation seen in the later case was also confirmed by the US-attenuation signal which could seen as a peak (hump) in the US-attenuation pattern occurring between 60 and 80 minutes in an unaged scenario when the temperature was about 70 ºC (Figure 6.5). This observation can be correlated to the formation of the secondary amorphous gel that was reported by Cundy and Cox (2005). The complex electrolyte solution generated from the coal fly ash as the starting material contains

many different charged species whose concentrations and valence may complicate the understanding of the gel-solution-crystal interactions. This could be the reason why the hump in the US-attenuation that had been observed after 220 minutes during the study of unaged clear extract of fused fly ash based gel was not observed in the attenuated pattern of the pure chemical composition (see Figure 6.5). The presence of the additional ions in the fly ash-based reaction medium/mixture is expected to complicate the zeolitic crystal growth process by generating extra electrostatic contributions. The analysis of Si/Al ratio in Figure 6.17 agreed well with studies by Miladinovic *et al*. (2009) who had reported that an excess amount of Al leads to an increase of both the crystallization rate and crystal growth of zeolite A. The trend observed for Si and Al species in the extracted supernatant liquid compares very well with the ultrasonic signal that was obtained during the in-situ monitoring process (Figure 6.2) and can be used to explain the gel dissolution, equilibration, nucleation and consequent crystal growth processes which are key processes during the zeolitization process. The overall decrease in the amount of amorphous material in relation to the increasing number of crystals of zeolite A shown in Figure 6.13 is indicative and confirms the autocatalytic process which suggest that the 'rate of gel dissolution must increase with the rate of consumption of growth species by increasing cumulative crystal surface area' (Angell *et al*., 1977; Walton *et al*., 2001b; Cundy and Cox, 2005).

The differences in morphology of zeolite A synthesized using clear solution with that from raw unseparated slurry can be attributed to the differences in the Si/Al ratios during the respective synthesis process. Differences in morphology in relation to differences in Si/Al ratios of different reaction compositions have also been reported by other researchers (Basaldella and Kikot, 1997). Othe factors such as the type of metal cation, type of silica, alkalinity of the reaction mixture as well as quantity of water have also been found to affect the crystal morphology (Mostowicz and Berak, 1985).

6.1.4 Conclusion for the in-situ ultrasonic monitoring of formation process of zeolite A from fly ash

The results presented herein have demonstrated that the in-situ ultrasonic diagnostic method can contribute to a better understanding of the conversion process of coal fly ash to zeolites when compared with other studies conducted using other techniques reported in the literature. The findings from both the in-situ ultrasonic monitoring system and the complementing ex-situ

techniques not only provided deeper insights into the reactions taking place during the conversion of coal fly ash into zeolites but also supported the hypothesis that formation of zeolite A from coal fly ash follows both the solution and solid-phase mediated mechanisms for the zeolite formation. The solution mediated model is supported by the observation of small fluctuations of Al and Si concentration during nucleation and crystal growth step as shown by ICP analysis presented in Figure 6.15 and 6.16 and by FTIR (Figure 6.18) at 856 cm^{-1} showing the presence of small monomeric and dimeric species in the solution. Whereas the solid-phase transformation growth model can be supported by the observation of the ultrasonic attenuation hump at around 220 minutes during the in-situ ultrasonic monitoring as shown in Figure 6.2. This observation was complemented by an increase of Si and Al at around 220 minutes (Figure 6.15 and 6.16) which signified the destruction of the amorphous gel structure in unaged solutions which suggests that the amorphous phase is both the nutrient reservoir and also the host of the nucleation sites. In this amorphous gel phase, localized reconstruction took place to yield the dormant nucleation sites that were later released, activated in readiness to grow to visible zeolite A crystals. Once the precursors are aged, the solid phase transformation mechanism no longer operates.

6.2 In-situ ultrasonic monitoring of zeolite X crystallization from coal fly ash

Owing to the complexity of the starting composition, it is recommended that the zeolite crystallization mechanism of each zeolite type synthesized from fly ash be studied independently since it is not expected that the process will always follow the same reaction pathway. This suggestion was also supported by Walton *et al*., 2001a, 2001b and Toufar *et al*. (1995) who had highlighted that each zeolite type follows a complex crystallization scheme even when using pure analytical grade sources of silica and alumina. Therefore this technique was also applied to study the formation of zeolite X from South African fly ash. More specifically, the investigation focused on the formation process of the new morphology (hierarchical) zeolite X that had been reported in Chapter 5 Section 5.2.

The procedure for synthesizing the novel morphology (hierarchical) zeolite X from South African fly ash was based on the use of the clear solution extracted from the fused Arnot fly ash as given in Chapter 3, Section 3.3.5. The solid-to-liquid ratios used during the extraction of the

clear solution was 1:2.5. The same setup that was used for ultrasonic monitoring of formation process for zeolite A was used for zeolite X. In order to evaluate the effect of temperature on the synthesis process, three temperatures (80, 90 and 94 ºC) were investigated. As mentioned in Section 6.2, the main different between the procedure for synthesis of zeolite X compared with that of zeolite A was that the procedure for producing zeolite A required addition of extra Al to the synthesis mixture. It has to be stressed that unlike the procedure used when synthesizing zeolite X from unseparated slurry under static hydrothermal conditions (reported in Chapter 5, Section 5.1), the ultrasonic monitoring of the crystallization process was performed on a magnetically stirred heating system to avoid settling of the product as it was being formed, which if left to sediment, would have interfered with the monitoring process.

6.2.1 Measurements of attenuated ultrasound signal

The synthesis precursor solution for preparing zeolite X had a molar ratio of 1 Al_2O_3 : 56.80 Na_2O : 16.62 SiO_2 : 954.05 H_2O prepared as per the conditions detailed in Chapter 3, Section 3.3.5. The heating rate was about 0.5 ºC/min with the final predetermined temperature set at 80 ºC. The results for the plots of normalized attenuation vs. time of crystallization of the hierachical zeolite X from the clear extract of fused South African fly ash together with the heating profile are presented in Figure 6.20.

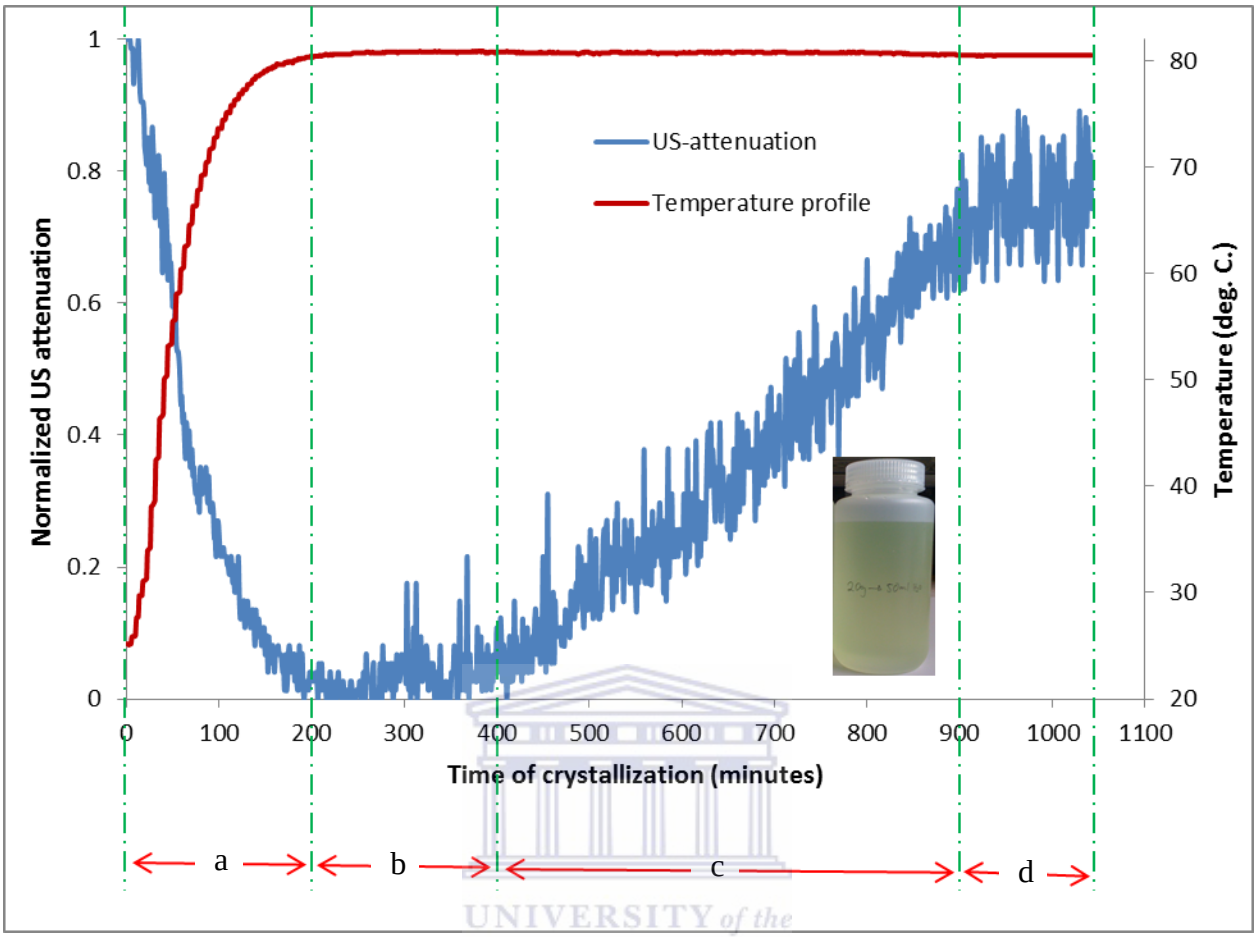

Figure 6-20: Plots of normalized attenuation vs. time of crystallization of zeolite X from unaged clear extract of fused fly ash (see inset image) for the heating rate of about 0.5 ºC/min up to the predetermined temperature of 80 ºC.

As shown in Figure 6.20, in the initial 200 minutes (region a) of in-situ ultrasonic monitoring of the synthesis mixture when the heating had reached the isothermal temperature region (80 ºC), the ultrasonic attenuated signal was observed to decrease as the synthesis time progressed. Thereafter, between 200 and 400 minutes (region b) (still at an isothermal temperature region of 80 ºC), the attenuated signal was noted to stabilize with only negligible fluctuations but then increased steadily between 400 and 900 minutes (region c). Still at the isothermal temperature of 80 ºC, the utrasonic attenuation was observed to stabilize between 900 minutes until the end of the monitoring process at 1040 minutes (region d). In reference to the earlier discussion on the in-situ monitoring of the crystallization of zeolite A presented in Section 6.13, the four regions (a, b c and d) presented in Figure 6.20 can be correlated to induction, nucleation, crystal growth

and zeolite crystal stabilization periods respectively. During the induction period, the zeolite precursor species undergo complex physicochemical changes that lead to supersaturation. According to Herrmann *et al*. (2005), several processes such as gel precipitation, dissolution and/or rearrangement of precursor species take place during this period.

In the nucleation stage (region b, Figure 6.20), the minor fluctuations in the US attenuation can be due to the rapid interfacial changes taking place between solid and solvent which makes it almost impossible to notice significant changes in the in-situ ultrasonic attenuation signal. According to Cundy and Cox (2005), zeolite nucleation is a complex 'discreet chain of event' that involves reversible condensation reactions. These reactions are associated with the formation and destruction of the T-O-T bonds leading to the establishment of sufficient ordered sites in preparation to the commencement of the crystal growth stage (region c, Figure 6.20). The use of in-situ ultrasonic monitoring system provided sufficient data points which enable closer estimation of the time of transition from nucleation to crystal growth step. Hu and Lee, (1990) had earlier indicate that lack of detailed investigation during this period makes it difficult to pinpoint this elusive transition period.

The crystal growth period has been reported by many researchers (Zhadanov, 1971; Ouden and Thomson, 1992; Cundy and Cox, 2005) to result in the S-shaped growth curve that is clearly shown in region c of Figure 6.20. Even though the samples were not extracted during this period as was done during the investigation of the crystal growth stage of zeolite A (Section 6.2.2.2), increase in number and size of the crystals is the main observation that would have been seen in this period. The smaller size of the reaction container together with the low yield of the final product was the main challenge that made the sample extraction exercise difficult.

Comparing the period required to get fully crystalline Zeolite X with novel (hierarchical) morphology to that required for zeolite A (Section 6.1.1.2), it can be shown that zeolite A crystallized within a shorter time than the time required to obtain zeolite X. Similar observations were also reported by Chang and Shih (2000). The difference in the rate of formation can be attributed to the fact that zeolite X has a more complex structure with larger structural units (D6R) and sparser structure than zeolite A, which is composed of D4R structural units.

According to Chang and Shih (2000), apart from the structural differences between these two zeolites, their differences in densities (1.99 g/cm^3 and 1.93 g/cm^3 for zeolite A and X respectively) is also thought to be a contributing factor that influences their formation rates. As for the mechanism of formation of the novel morphology (hierarchical) zeolite X from fly ash, only the solution phase-mediated mechanisms could be supported in this case since the hump that was observed around 220 minutes in the US attenuation signal (Figure 6.2) during the investigation for formation process of zeolite A was not observed. The hump observed in the US attenuation signal (between 50 and 80 minutes in Figure 6.2) during the in-situ ultrasonic monitoring of zeolite A crystallization, that had been associated with the formation of secondary amorphous phase, was not observed in the case of formation of zeolite X even though the clear extract of fused fly ash was unaged. These observations conclusively show that the mechanism of formation of zeolite A is different from that of the novel morphology zeolite X.

6.2.2 Effect of variation of hydrothermal temperature

In order to investigate the effect of temperature during the monitoring of the crystallization process of the novel morphology zeolite X, in-situ ultrasonic monitoring was conducted at different hydrothermal synthesis temperatures (80, 90 and 94 ºC) and the comparative plots of normalized attenuation vs. time of crystallization of the hierachical zeolite X from the unaged clear extract of fused South African fly ash for sythesis at three different hydrothermal synthesis temperatures (80, 90 and 94 ºC) is presented in Figure 6.21.

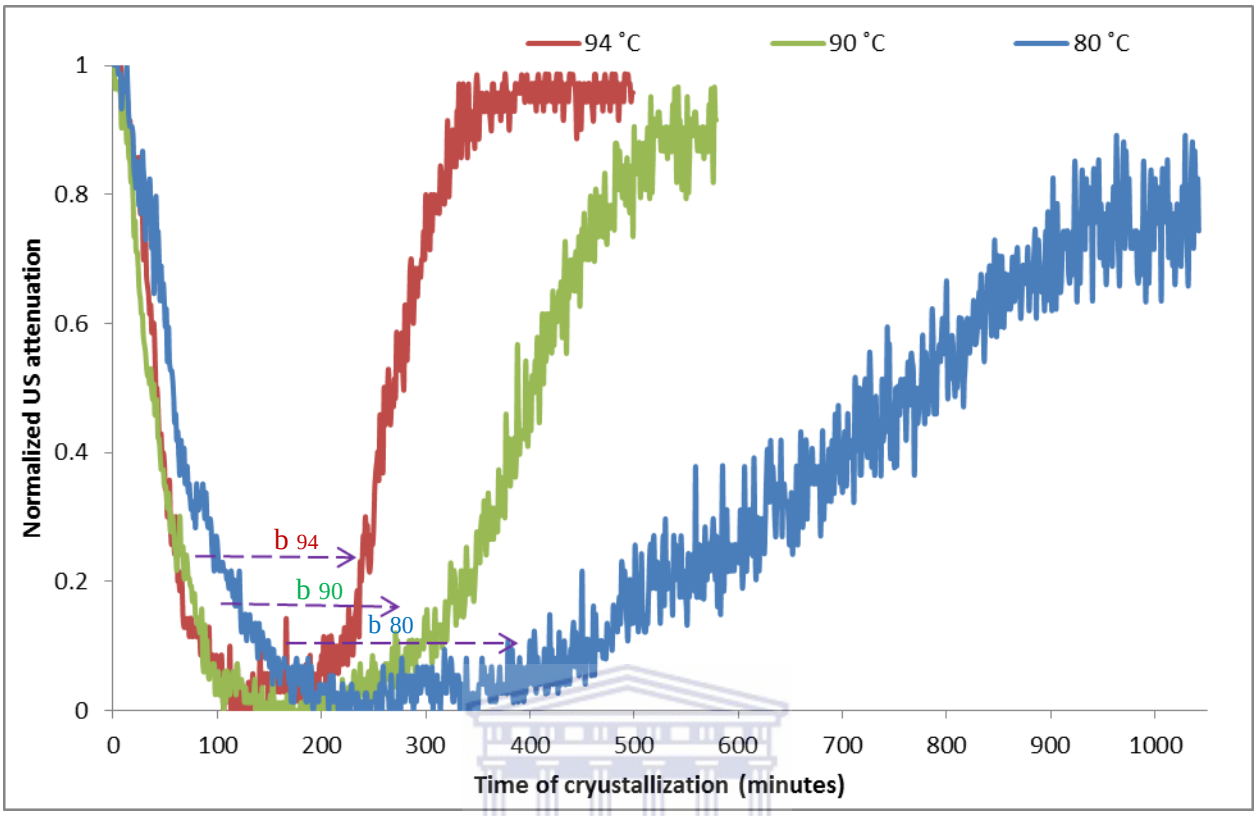

Figure 6-21: Comparative plots of normalized US attenuation vs. time of crystallization for the in-situ ultrasonic monitoring of the novel morphology zeolite X starting from the unaged clear extract of fused fly ash when the hydrothermal synthesis was conducted at three temperatures (80, 90 and 94 ºC).

As shown in Figure 6.21, an increase in the hydrothermal synthesis temperature led to shortening of the nucleation period as noted by the shift in the plots of US-attenuation towards lower crystallization time when the temperature was increased from 90 to 94 ℃ as illustrated in the respective b-80, b-90 and b-94 regions. The XRD patterns and SEM micrographs of the resulting synthesis products are presented in Chapter 5, Section 5.2.1. As earlier discussed in Chapter 5, Section 5.2.1, the resulting zeolite X had a novel morphology that had hierarchical characteristics.

6.2.3 Overall conclusion for in-situ ultrasonic monitoring of zeolite A and X crystallization from fly ash

The results presented in this chapter have demonstrated that the in-situ ultrasonic diagnostic technique can contribute to a better understanding of the conversion process of coal fly ash to either zeolite A and X. The investigation of the zeolite crystallization process starting from this complex feedstock (fly ash) under real reaction conditions has not been conducted before, implying that the contributions from this study will enrich the existing body of literature. In the first Section (6.1) of this chapter, the findings from both the in-situ ultrasonic monitoring system and the complementing ex-situ techniques supported the hypothesis that zeolite A formation from coal fly ash follows both the solution and solid-phase mediated mechanisms for the zeolite formation. The solution-mediated model was supported by the observation of small fluctuations of Al and Si concentration during nucleation and crystal growth step as was shown by ICP analysis presented in Figure 6.15 and 6.16. Whereas the solid-phase transformation growth model was supported in the case of unaged reaction mixture by the observation of the hump at around 220 minutes during the in-situ ultrasonic monitoring as was shown in Figure 6.2. This was further complemented by an increase of Si and Al as shown by the IPC analysis in Figure 6.15 and 6.16. This 'unique' observation signified the destruction of the amorphous gel structure at around 220 minutes hence suggesting that the amorphous phase is both the nutrient reservoir and also the host of the nucleation sites in the unaged reaction mixture hence localized reconstruction of the gel particle to yield the dormant nucleation sites that are later released and activated. The effect of ageing of the reaction mixture for zeolite A was studied and it was found that the hump observed at around 220 minutes (Figure 6.4) in the US attenuation signal disappeared during longer periods of ageing hence suggesting that the solution mediated pathway of crystallization mechanism is followed, once ageing is extended beyond 360 minutes.

In the second Section (6.2) of the chapter, the formation process of the novel morphology (hierarchical) zeolite X from fly ash was investigated using in-situ ultrasonic diagnostic method. Since the hump that occurred at around 220 minutes in the US attenuation signal during the monitoring process of zeolite A formation was not observed in the case of the formation process of zeolites X, only the solution phase mediated mechanisms could be supported. A comparison of the time of crystallization from the generated attenuation signals for formation of zeolite A

with that of zeolite X, it was found that zeolite A crystallized much faster than zeolite X. The investigation of the effect of temperature during the in-situ monitoring of the formation process of zeolites showed that higher temperatures led to faster crystallization as was shown by the shift of the ultrasonic attenuation signals to the lower crystallization time when the temperature had been increased from 90 to 94 °C.

The in-depth investigation of the formation mechanism of zeolite A and X from fly ash conducted in this study could be helpful in controlling and predicting the best conditions for synthesis. The use of in-situ ultrasonic monitoring system provided sufficient data points which enabled closer estimation of the time of transition from nucleation to crystal growth step. In summary, the goal for the research conducted in this chapter which was set as to answer research question number 4 (is it possible to study the formation process of zeolite A and X under real reaction conditions using the in-situ ultrasonic monitoring system?) was fulfilled.

CHAPTER 7

DIRECT AND ULTRASONIC ASSISTED SYNTHESIS OF ZEOLITES FROM SOUTH AFRICAN FLY ASH

This chapter presents results obtained from studies when ultrasound was used during the synthesis of zeolites. The chapter is divided into two sections. The first section presents and discusses results obtained when ultrasound was used to improve the conventional hydrothermal synthesis of zeolites A using the molar compositions that had been identified in Chapter 4. The second section presents results of a novel process for direct ultrasonic synthesis of hydroxy-cancrinite zeolite from the as-received South African class F coal fly ash.

7 Introduction

There has been increasing interest to find alternatives to the classical hydrothermal synthesis of zeolites from fly ash in order to deal with the challenges of high consumption of energy and prolonged synthesis time. Different improvements prior to the conventional hydrothermal synthesis route such as introduction of an alkaline fusion stage (Shigemoto *et al*., 1993), introduction of a two way stage synthesis procedure (Hollman *et al.,* 1999), and introduction of a desilification step (Yaping *et al*., 2008) have been reported together with other synthesis alternatives such as use of a dry or molten-salt method (Park *et al.,* 2000) and application of microwave heating conditions (Querol *et al*., 1997; Kim *et al*., 2004; Inada *et al*., 2005). All the above improvements were conducted to either achieve high synthesis efficiency and/or reduce the energy consumption. Since application of ultrasound during synthesis is known to enable achievement of reactions under normal conditions (Ashokkumar *et al.,* 2007), the ultrasonic assisted route is expected to provide an alternative to the above reported synthesis methods.

Although direct application of ultrasound to crystallize zeolite A from metakaolinite without the conventional hydrothermal treatment step was reported by Kim *et al.,* 2010, there are no papers in the literature reporting on production of zeolites by direct sonication of fly ash. Other authors are acknowledged to have reported the possibility of preparation of zeolites directly from pure sources of Si and Al by the application of ultrasound (Andaç *et al*, 2005; Run *et al* 2004) and only a recent study by Belviso *et al*. (2011) has shown that ultrasonic assisted ageing of fly ash prior to the convetional hydrothermal process can lead to the reduction of hydrothermal synthesis temperature. The use of the ultrasound to control the course of crystallization

(sonocrystallization) is known to lead to synthesis condition within short periods, which would otherwise require harsh conventional reaction conditions such as high temperatures and pressures (Dolores *et al*., 2007, Luque de Castro and Priego-Capote, 2007b). Although the mechanism of zeolite formation by the use of ultrasound is not well understood, Lindley (1992) proposed that during the expansion stage of the cavitation bubble there is localized cooling which in turn leads to localized increase in the degree of supersaturation that triggers the formation of germ nuclei that are distributed through the solution upon the collapse of the bubble which later grow to form the crystalline material. This proposal is also backed by Luque de Castro and Priego-Capote (2007).

The study carried out in this chapter aimed at investigating the extent to which application of ultrasonic energy would improve the earlier optimized hydrothermal synthesis procedure for producing of zeolite A from fused South African class F fly ash that was reported in Chapter 4. More importantly, the second section of the study further aimed to investigate the possible to synthesis of zeolites by direct application of ultrasound to the as-received South African class F fly ash which has not yet been reported in the literature. The experimental strategy in Section 7.1 of this chapter sought to provide answers to research question number 5 (To what extent can application of ultrasound improve the synthesis conditions for producing zeolite A from South African fly ash?) whereas Section 7.2 aimed to answer research question number 6 (Is it possible to synthesize zeolites by direct application of ultrasound?). In both sections, ultrasonic energy was provided by the use of the Omni Sonic Ruptor 400 ultrasonic homogenizer whose power had been adjusted to 100% with the pulse control set to read 100% as detailed in Chapter 3, Section 3.4.1.

7.1 Ultrasonic assisted synthesis of zeolites from coal fly ash

The results presented in this section built on the findings presented in Chapter 4. The reaction mixture was derived from a clear extract of fused South African fly ash that had a molar regime of 1 Al_2O_3 : 30.84 Na_2O : 4 SiO_2 : 414.42 H_2O. Instead of subjecting the clear extract reaction mixture directly to the heated hydrothermal crystallization step, 10 minutes of sonication of the reaction mixture was conducted prior to heating, where after, the mixture was transferred to the heated hydrothermal crystallization step following the procedure described in Chapter 3, Section

3.4.2. Figure 7.1 compares the XRD patterns and respective SEM images obtained when synthesis was conducted with and without the sonication ageing step prior to the hydrothermal synthesis step.

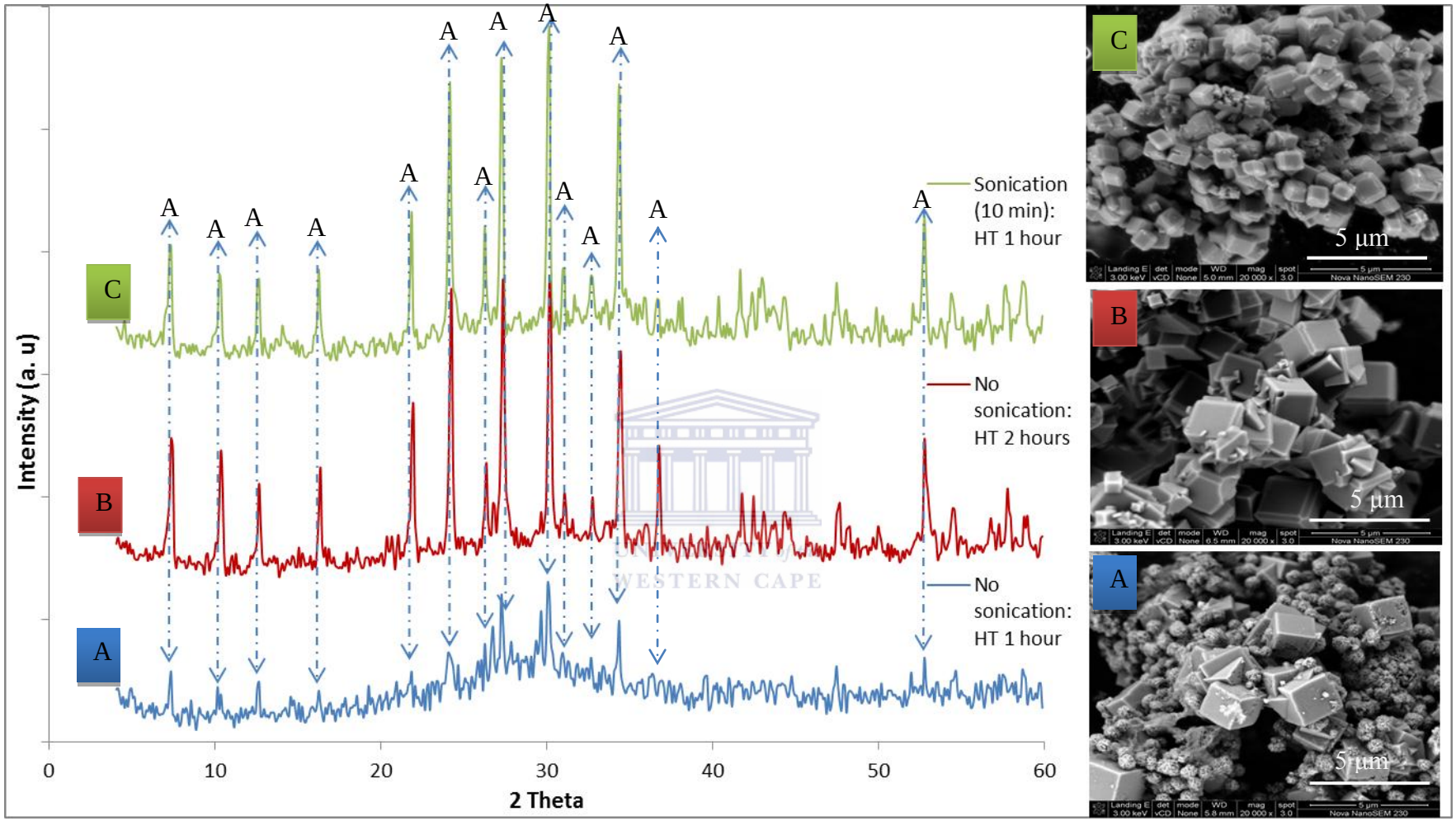

Figure 7-1: XRD patterns and corresponding SEM images obtained when synthesis was conducted A) without sonication prior to the hydrothermal synthesis (HT) at 100 °C for 1 hour B) without sonication prior to the hydrothermal synthesis (HT) at 100 °C for 2 hour C) with sonication (10 minutes) prior to hydrothermal synthesis (HT) at 100 °C for 1 hour during the synthesis of zeolite A starting from clear extract of South African class F fused fly ash that had a molar regime of 1 Al_2O_3 : 30.84 Na_2O : 4 SiO_2 : 414.42 H_2O.

From the XRD patterns presented in Figure 7.1 (b and c), it can be observed that upon sonication (10 minutes) of the unaged clear extract of fused fly ash prior to the heated hydrothermal crystallization step, almost the same quality of zeolite A was crystalized after only one hour instead of two hours with no amorphous material remaining. From the SEM images shown in Figure 7.1 (c), the quality of produced zeolite A upon sonication (10 minutes) of the reaction mixture prior to the heated hydrothermal crystallization step was closely similar to that obtained after two hours of heated hydrothermal crystallization (Figure 7.1 (b)). Figure 7.1 (a) shows that without sonication of the hydrothermally crystallized product after one hour, the obtained zeolite A still had amorphous precursors present which is visible in the respective SEM image as small particulates. The reduction of hydrothermal synthesis time by half could be expected to have a significant impact when the synthesis process is up scaled. The reduction in hydrothermal synthesis time after the 10 minutes ultrasonic pre-treatment can be attributed to acceleration of the nucleation rate. The possible explanation can be obtained indirectly from comparing the crystal sizes of zeolite A when the hydrothermal synthesis was conducted without sonication. From the SEM image obtained when synthesis mixture was sonication for 10 minutes prior to the hydrothermal synthesis step for at 100 °C for 1 hour (Figure 7.1 (c)), the zeolite A crystal are seen to be smaller than those obtained for 2 hours synthesis without sonication (see SEM image in Figure 7.1 (b)), this observation can suggest that more nucleation sites were created during acceleration of the primary and secondary gel dissolution step (see Chapter 6, Section 6.1.3) which in turn led to quicker supersaturated hence providing favourable conditions for the formation of the zeolite A nuclei. Numerous nuclei in the reaction mixture can lead to competition for the zeolite growth species thereby leading to many zeolite crystals with smaller sizes. This observation can also be related to the effects of ageing the synthesis mixture that was reported to result in a decrease in the crystal size of the synthesis product (Cundy and Cox, 2005). Ultrasound effectively replaced extended ageing times and enhanced the earlier reported (Chapter 6, Section 6.2.3) solution mediated mechanism by breaking down the precursor species rapidly and preventing the formation of the gel.

Figure 7.2 presents the XRD pattern and corresponding SEM images obtained when synthesis was conducted with sonication (10 minutes) prior to hydrothermal synthesis (HT) at 100 °C for 1 hour during the synthesis of zeolite A starting with unseparated fused South Africa class

F fly ash that had a molar regime of 1 Al_2O_3 : 5.39 Na_2O : 2.75 SiO_2 : 111.82 H_2O as given in Chapter 3, Section 3.4.2.

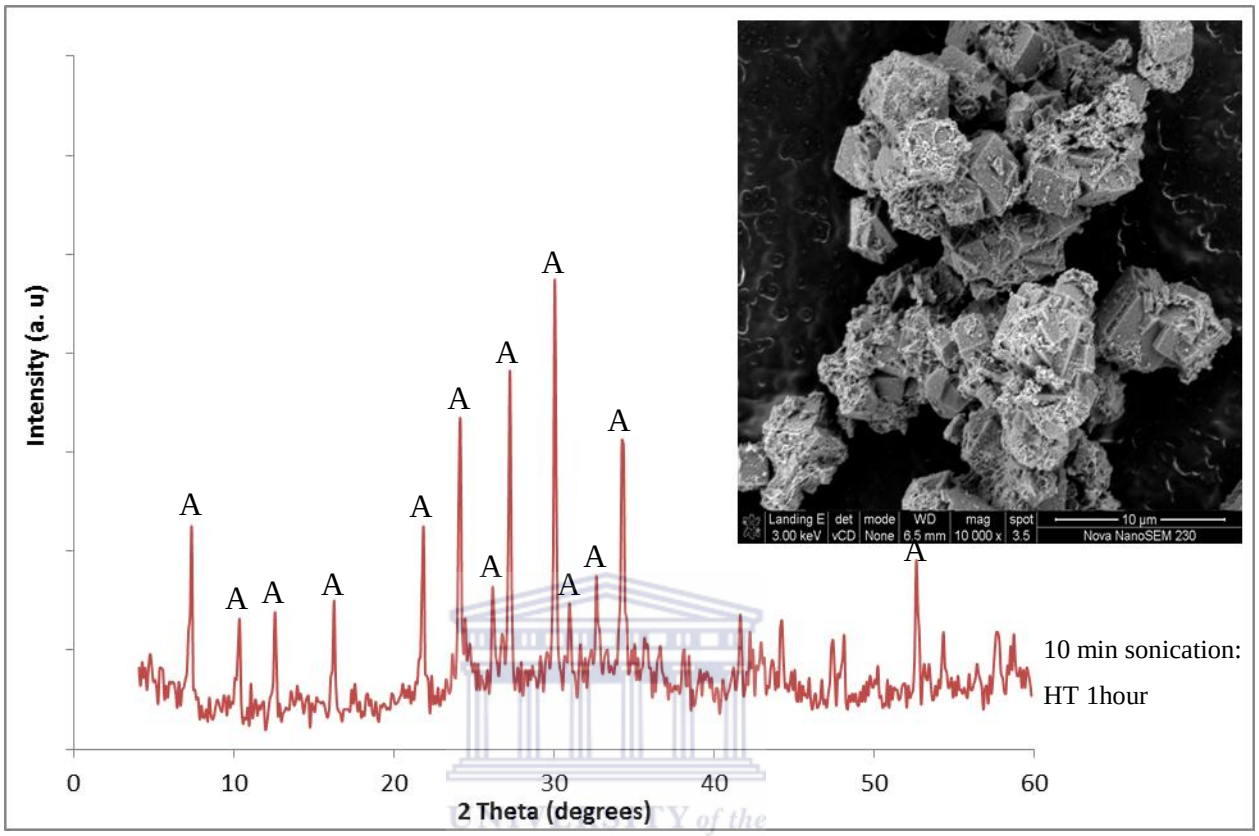

Figure 7-2: XRD patterns and corresponding SEM image obtained when synthesis was conducted with 10 minutes sonication prior to the hydrothermal synthesis (HT) at 100 °C for 1 hour during the synthesis of zeolite A starting from unseparated South African class F fused fly ash slurry that had a molar regime of 1 Al_2O_3 : 5.39 Na_2O : 2.75 SiO_2 : 111.82 H_2O.

Figure 7.2 shows that a single phase zeolite A was also obtained when the unseparated fused fly ash slurry was sonicated for 10 minutes prior to the conventional hydrothermal crystallization step at 100 °C for 1 hour. In this case the crystals habit showed multiple twinning with absence of the amorphous phase which was present without sonication.

Figure 7.3 presents XRD patterns and corresponding SEM images obtained when synthesis was conducted with and without sonication (10 min) prior to hydrothermal synthesis (HT) at 100 °C for 1 hour during the synthesis of zeolite A starting with clear extract of fused fly ash using circumneutral mine water that was obtained from Middleburg coal mine instead of pure

water as set out in Chapter 3, Section 3.4.2. The synthesis mixture had a molar regime of 1 Al_2O_3 : 28.75 Na_2O : 3.06 SiO_2 : 380.16 H_2O.

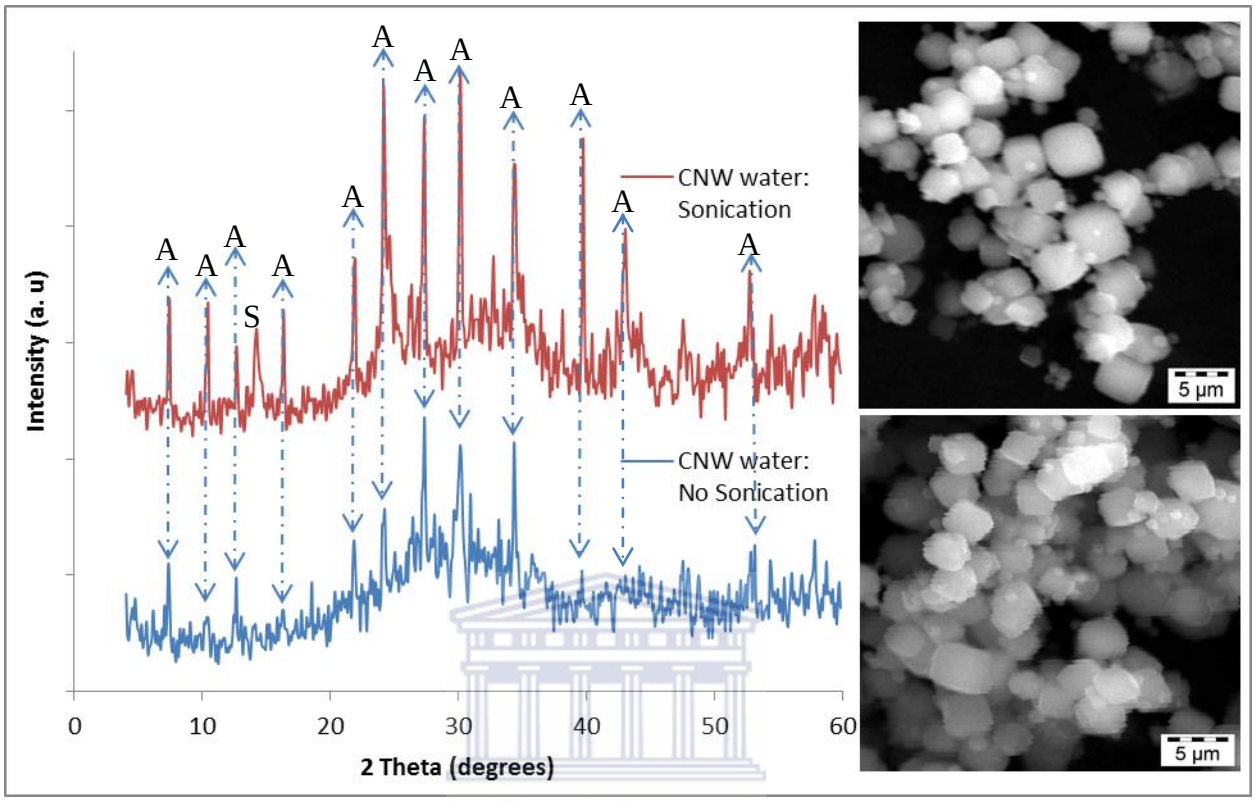

Figure 7-3: XRD patterns and corresponding SEM images obtained when synthesis was conducted with and without sonication (10 min) prior to hydrothermal synthesis (HT) at 100 °C for 1 hour during the synthesis of zeolite A starting from clear extract of South African class F fused fly ash using circumneutral mine water instead of pure water.

Even though smaller crystals of zeolite A were obtained when circumneutral mine water was used as a replacement of pure water (Figure 7.3), it was interesting to note that a contaminant 'hydroxy-sodalite phase' also co-crystallized with zeolite A in the case where 10 minutes sonication was applied. The presence of the amorphous material was also detected from the broad hump appearing between 20 - 40 ° 2θ in both diffraction patterns. Unlike the case when pure water was used in the synthesis with sonication pre-treatment before the heater hydrothermal crystallization for 1 hour (Figure 7.1 (c)), it seemed that the hydrothermal synthesis time of one hour used to crystallize a single phase zeolite A without the amorphous phase was too short when circumneutral mine water was used as the synthesis solvent.

Figure 7.4 presents XRD patterns and corresponding SEM images obtained when synthesis was conducted with and without sonication (10 min) prior to hydrothermal synthesis (HT) at 100 °C for 1 hour during the synthesis of zeolite A starting with clear extract of South African class F fused fly ash using acid mine water that was obtained from Navigation coal mine instead of pure water as set out in Chapter 3, Section 3.4.1. The synthesis mixture had a molar regime of 1 Al_2O_3 : 23.32 Na_2O : 2.82 SiO_2 : 315.60 H_2O.

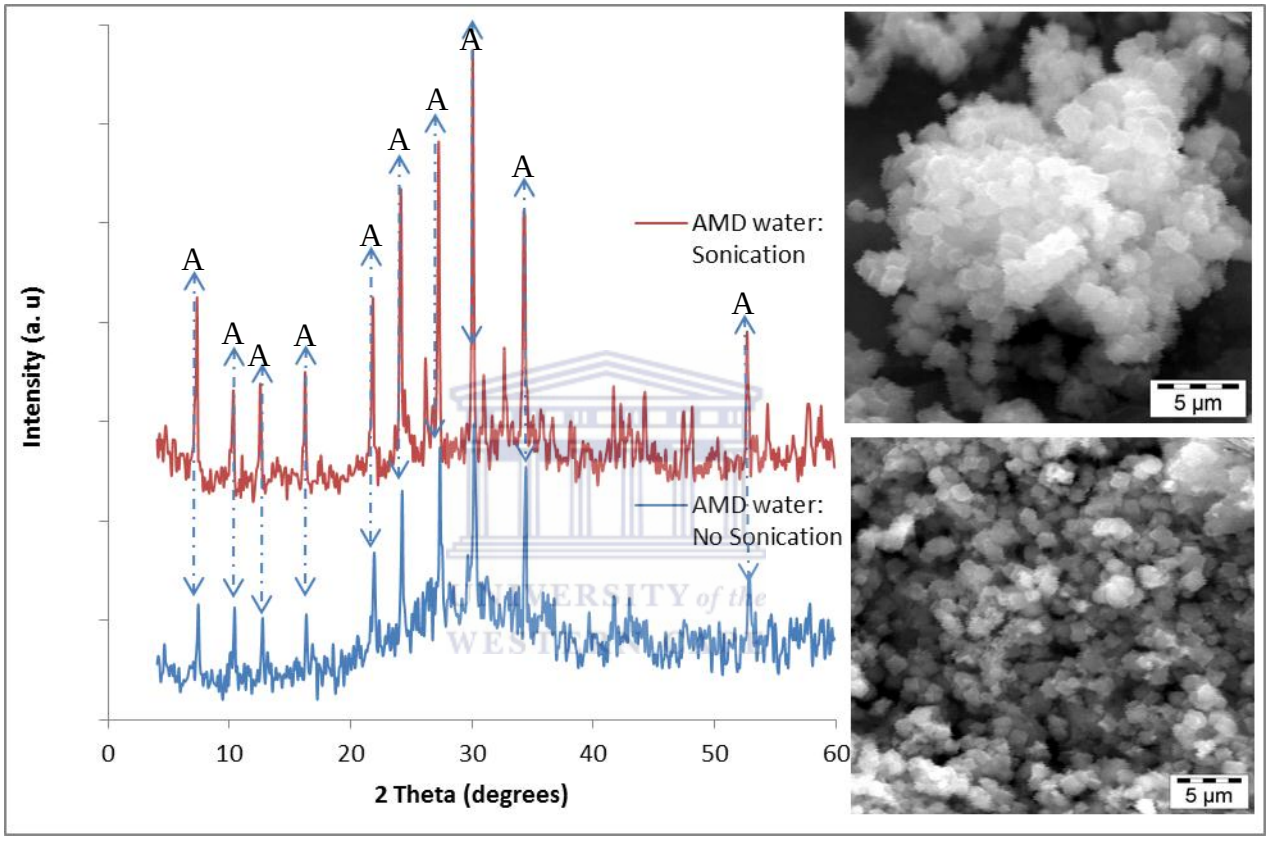

Figure 7-4: XRD patterns and corresponding SEM images obtained when synthesis was conducted with and without sonication (10 min) prior to hydrothermal synthesis (HT) at 100 °C for 1 hour during the synthesis of zeolite A starting from clear extract of South African class F fused fly ash using acid mine drainage water instead of pure water.

As shown in Figure 7.4, a different observation from the case of use of circumneutral mine water was noted when the solvent was substituted with acid mine water. A single phase zeolite A with no amorphous material crystallized after 10 minutes of sonication and one hour hydrothermal synthesis meaning that the high concentration of Fe in the mine water (see Chapter 4, Table 4.8) did not interfere with the formation process of zeolite A. It could not be established why hydroxy-sodalite did not co-crystallize with zeolite A as had been earlier

observed when hydrothermal synthesis was conducted at 100 °C for 2 hours without sonication (see Chapter 4, Figure 4.22). It can only be speculated that the complex dynamics of the ionic balance in the synthesis mixture could have been the contributing factor. Since it had earlier been established that most of the iron in acid mine drainage was trapped in the zeolitic matrix as shown from previous experiments presented in Chapter 4 (Section 4.7.3), the resulting zeolitic material and supernatant solution was not further analyzed.

7.2 Direct ultrasonic synthesis of zeolites from the as-received South African coal fly ash

Although perfoming an ultrasonic enhanced ageing step prior to the heated hydrothermal crystallization step of zeolites from fly ash is not a new process process (Belviso *et al*. 2010), there is no evidence in the literature reporting synthesis of zeolites by direct sonication of the as-received coal fly ash. This section of the study was aimed at investigating the possibility of applying ultrasonic energy using the Omni Sonic Ruptor 400 Ultrasonic Homogenizer to generate zeolites directly from the as-received South African fly ash. The target was to avoid the energy intensive alkali fusion of fly ash that was reported in Chapter 3 (Section 3.2.1). The section started by understanding reactivity of fly ash in terms of dissolution behaviour of Si and Al under the influence of ultrasound to avoid fusion and ageing. The variables investigated during the initial phase of the study include effects of varying the NaOH concentration, sonication time, stirring and fly ash particle size.

7.2.1 Effect of variation of NaOH concentration on the dissolution behaviour of Si and Al, when fly ash was sonicated

During the investigation of the effect of the NaOH concentration on the dissolution behaviour of Si and Al from the as-received South African class F fly ash, four concentrations (1M, 3M, 4M and 7M) were studied. The sonication time of the as-received South African class F fly ash had been fixed to 10 minutes. The experimental details for the sonication studies are detailed in Chapter 3, Section 3.4.3. Figure 7.5 presents the effect of variation of NaOH concentration on the dissolution behaviour of Si and Al when the as-received South African class F fly ash was sonicated for 10 minutes.

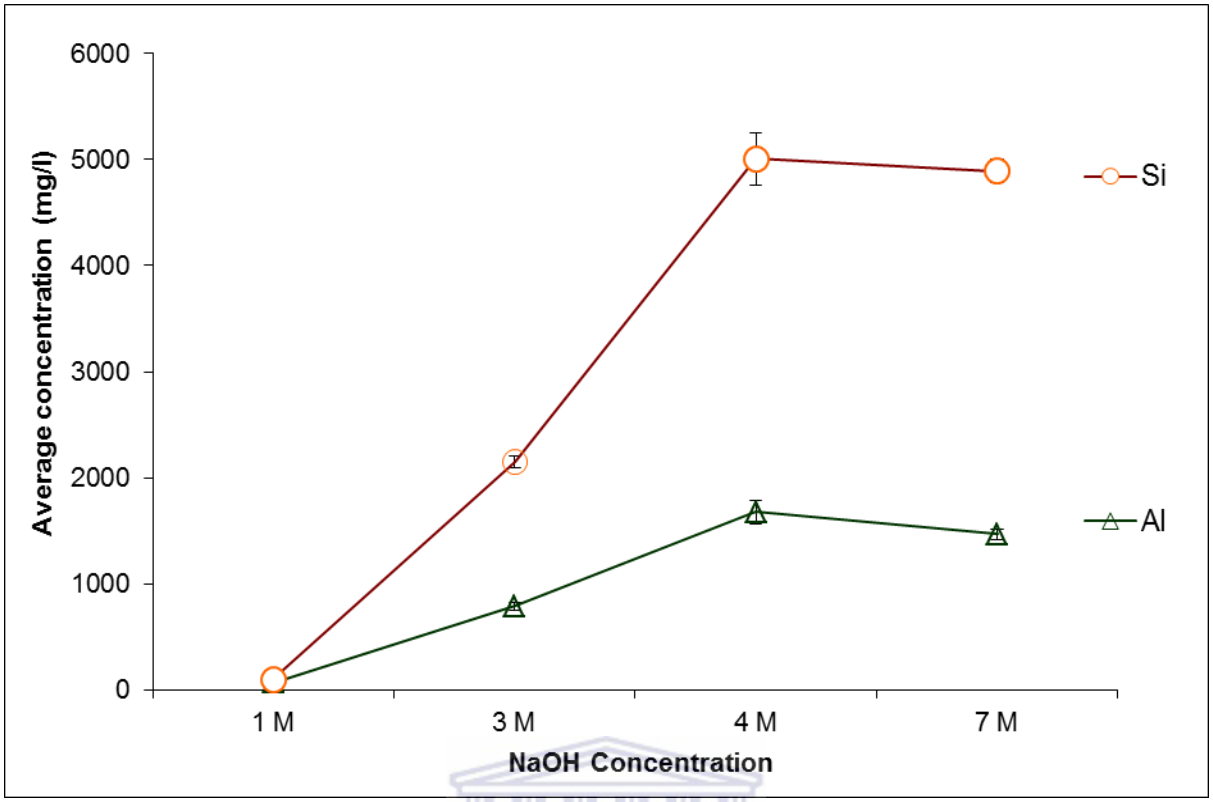

Figure 7-5: Effect of NaOH concentration on dissolution behaviour of Si and Al from the as-received South African class F fly ash after sonication for 10 minutes.

As shown in Figure 7.5, after sonication of the as-received fly ash for 10 minutes the concentration of Si in solution was seen to rapidly increase from 35 mg/L when 1 M NaOH was used up to 3331 mg/L when 4 M NaOH was used. Upon the use of 7 M NaOH, the Si concentration was found to be 3432 mg/L which was only a slight increase compared to the use of 5M NaOH. A similar trend was also observed for the case of dissolution of Al since it was was seen to rapidly increase from 64 mg/L (1 M NaOH) to 1674 mg/L (4 M NaOH) with a decrease to 1466 mg/L when 7 M NaOH was used. The highest temperature reached during the sonication experiments was 76 °C. The increase in temperature is common during sonication. The dissolution of Si and Al from the as-received fly ash was found to be directly dependent on the NaOH concentration between 1 and 4 M when a fixed sonication time was applied.

The Si content was higher than that of Al since the content of SiO_2 in the fly ash had been reported to be higher than that of Al_2O_3 content (see Chapter 4, Table 4.1). This finding is also consistent with results obtained by Wang *et al.* (2008). The use of NaOH as the mineralizing agent is reported to strongly influence the nature of the reacting species (either

monomeric or polymeric) present in the mixture, the concentration of dissolved silico-aluminate fragments, the charge of the species and also the rate of hydrolysis of solid and liquid phases (Nagy *et al*., 1998).

7.2.2 Effect of sonication time on the dissolution behaviour of Si and Al from fly ash

The effect of sonication time on the dissolution behaviour of Si and Al from the as-received South African class F fly ash was investigated by fixing NaOH concentration at 5 M. The experimental details are presented in Chapter 3, Section 3.4.3. The choice of the 5 M NaOH concentration was guided by the experiments that had shown that dissolution of Si and Al from the as-received fly ash had reached its maximum at around 4 M NaOH concentration (Section 7.1.1). The decision was also influenced by previous studies (Musyoka, 2009) that had shown that 5 M had led to high quality zeolite Na-P1 from fly ash. The sonication time was then varied as follows; 5, 10, 15 and 30 minutes. Figure 7.6 presents the results for the effect of sonication time on the dissolution behaviour of Si and Al from the as-received South African class F fly ash.

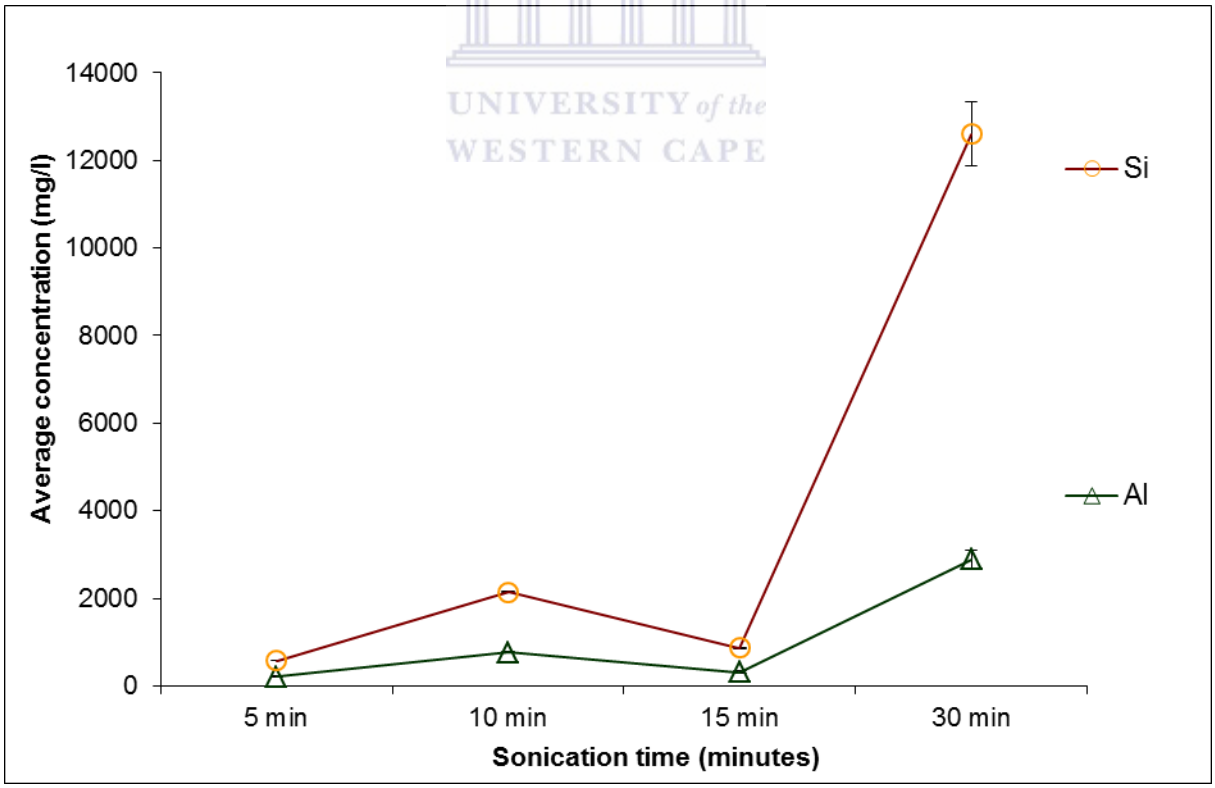

Figure 7-6: : Effect of sonication time (5, 10, 15 and 30 min) on dissolution behaviour of Si and Al from the as-received South African class F fly ash; NaOH concentration was held at 5 M.

Figure 7.6 shows that the concentration of Si was increased from 358 mg/L when the as-received South African class F fly ash was sonicated for 5 minutes to 1385 mg/L after 10 minutes of sonication. A decline in the Si concentration (547 mg/L) was observed occur after 15 minutes of sonication which was followed by a very rapid increase up to 9708 mg/L after 30 of sonication. A similar trend was also observed in the Al concentration which was 218 mg/ L after 5 minutes sonication and increased to 2890 mg/L after sonication for 30 minutes with a similar concentration decrease (320 mg/L) after 15 minutes of sonication. Previous studies by Luque de Castro and Priego-Capote (2007b) pointed out that ultrasound irradiation of solid particles suspended in a liquid phase enhances their dissolution mainly due to the induced mechanical effects. The mechanical disaggregation and breakdown of fly ash particles as well as the glassy amorphous materials phase resulted in enhanced dissolution.

7.2.3 Effect of stirring of the sonicated solution on the dissolution behaviour of Si and Al from fly ash

The effect of stirring the fly ash-NaOH mixture during sonication was investigated by fixing NaOH concentration and sonication time at 5 M and 10 minutes respectively. The stirring was conducted using a magnetic stirrer whilst sonication continued. Further experimental details are described in Chapter 3, Section 3.4.3. Figure 7.7 presents results of the effect of stirring on dissolution behaviour of Si and Al whilst fly ash was sonicated for 10 minutes for a slurry prepared using 5 M NaOH.

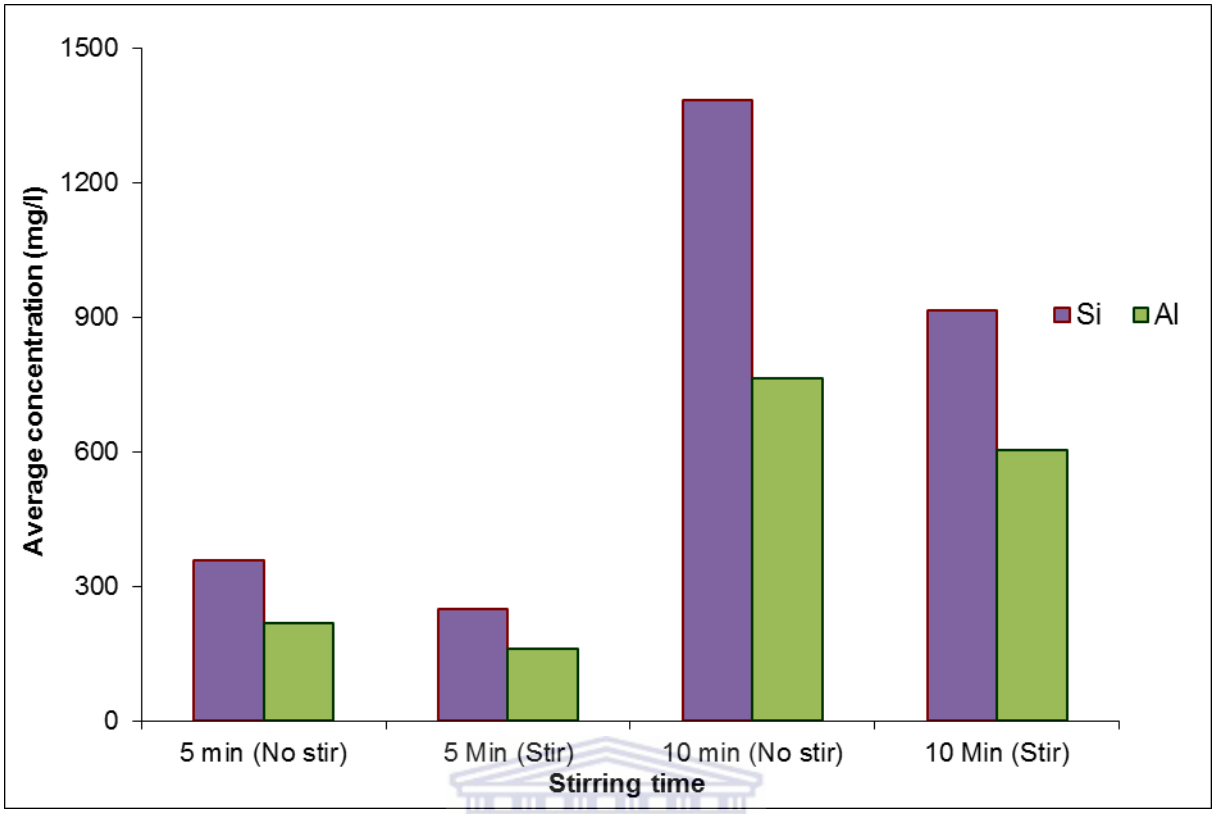

Figure 7-7: Effect of magnetic stirring during sonication fly ash-NaOH slurry on the dissolution behaviour of Si and Al from the as-received South African class F fly ash; mixture was sonicated for 10 minutes and NaOH concentration was held at 5 M.

Ultrasonic irradiation in known to cause a stirring effect in a solution due to the microjetting and microstreaming of the collapsed bubbles (Lindley, 1992). It was expected that the additional magnetic stirring during sonication could enhance dissolution of the fly ash mineral phases but it turned out to be the opposite. As shown in Figure 7.7, sonication of fly ash for 10 minutes without the additional magnetic stirring led to dissolution (358 mg/L of Si and 218 mg/L of Al) but with the additional stirring, the Si concentration was observed to decrease to 250 mg/L whereas that of Al decreased to 162 mg/L. A similar trend was also observed when the fly ash-NaOH slurry was sonicated for 10 minutes. This decrease in the dissolution of Si and Al upon additional magnetic stirring could be due to the interruption of the microstreaming and microjetting effects which are thought to be the main contributors of the mechanical effects affecting dissolution of fly ash.

7.2.4 Effect of fly ash particle size on the dissolution behaviour of Si and Al from fly ash

The study of the effect of fly ash particle size, obtained by sieving the as-received South African class F fly ash through 90 µm, 150 µm and 212 µm mesh sieves, was studied by fixing the NaOH concentration at 5M and sonication time for 10 minutes. Figure 7.8 presents the effect of effect of fly ash particle size on the dissolution behaviour of Si, Al, Ca and Mg when fly ash was sonicated for 10 minutes with NaOH concentration was kept constant at 5 M.

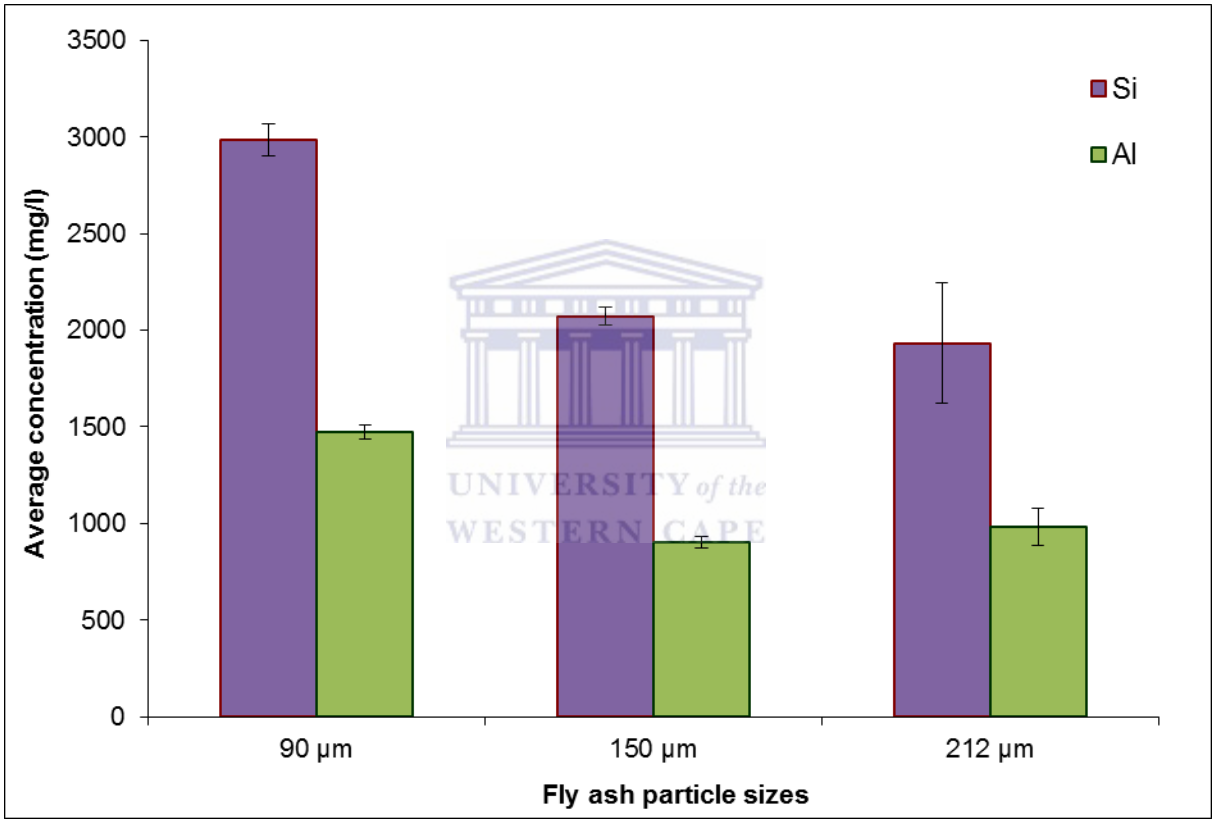

Figure 7-8: Effect of fly ash particle size on dissolution behaviour of Si and Al from the as-received South African class F fly ash after sonication for 10 minutes with NaOH concentration kept constant at 5 M.

From Figure 7.8, the concentration of Si obtained from sonicating fly ash having 90 µm, 150 µm and 212 µm particle sizes was found to be 2985 mg/L, 2073 mg/L and 1933 mg/L respectively while that for Al was 2985 mg/L, 2073 mg/L and 1933 mg/L respectively. The trend shows that the concentration of Si and Al decreased with the increase of fly ash particle size which was understandable since the smaller fly ash particles had earlier been reported to

contain less Quartz (Muriithi *et al*., 2010) and dissolved much easier upon sonication. The high surface area of the smallest particles is also thought to have enhanced the mechanical effects emanating from the cavitation phenomenon of ultrasonication as expected.

7.2.5 XRD Analysis of sonicated fly ash

XRD analysis results for experiments conducted to investigate the effect of sonication time as detailed in Section 7.2.2 are presented in Figure 7.9. The reason for the choice of this set of data was mainly to probe and explain the interesting trend of dissolution of Si and Al that had been observed when the sonication time was varied.

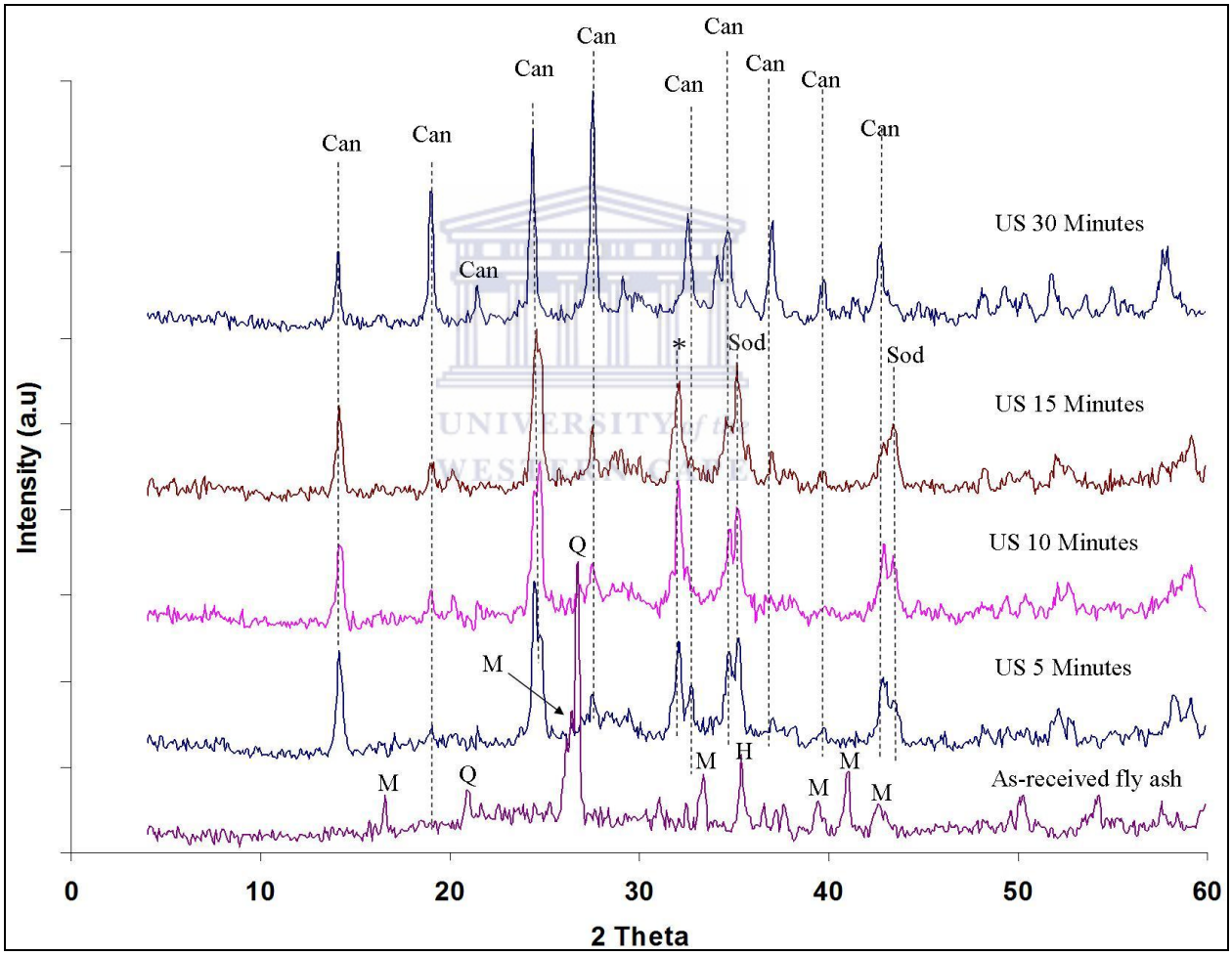

Figure 7-9: X-ray diffraction pattern of the as-received South African class F fly ash compared with diffraction patterns for ultrasonic assisted synthesis products obtained from the same fly ash by variation of sonication time from 5 to 30 minutes (Can = hydroxy-cancrinite, Sod = hydroxy-sodalite, Q = Quartz, M = Mullite, H = Hematite).

As shown in the XRD data patterns presented in Figure 7.9, sonicating the as-received South African class F fly ash for 5, 10 and 15 minutes resulted in direct production of a mixture of hydroxy-cancrinite and hydroxy-sodalite zeolites without a hydrothermal treatment step. All the mineral phases that were identified in the as-received phases had almost immediately been totally dissolved within 5 minutes during the sonication process and transformed into zeolitic materials. Even though only two peaks have been labelled to denote the presence of the hydroxy-sodalite, there was an overlay of some of the low angle diffraction peaks (such as at, 4, 19 and 24° 2θ) which had lower intensities for the case of hydroxy-cancrinite as shown in Figure A3. The cancrinite and sodalite-group of minerals have been known to have strong structural similarly with the only difference being in the stacking of the aluminosilicate layers (Okubo *et al*., 2001). The ABC stacking sequence in cancrinite leads to hexagonal symmetry whereas that of sodalite zeolites leads to cubic symmetry as shown in Figure 7.10.

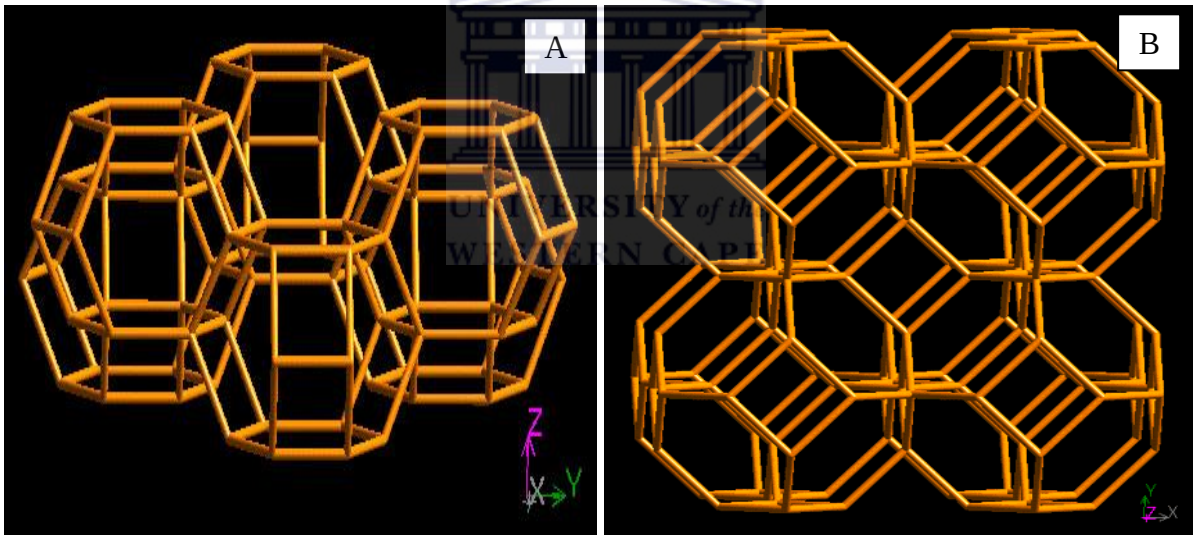

Figure 7-10: Structural projections of a) cancrinite b) sodalite zeolite array of cages viewed along [001] (IZA, 2010).

From Figure 7.9, when sonication of the as-received South African class F fly ash was extended to 30 minutes, a single phase hydroxy-cancrinite zeolite phase was obtained directly without a hydrothermal treatment step. The peak shift marked by * could be due to the crystallite orientation effect because of the needle-like morphology of hydroxy-cancrinite zeolite (Figure 7.12 (d)). Cancrinite is a low-silica zeolite (Si/Al=1) with one-dimensional, 12-membered-ring pores that are about 5.9 Å in diameter (Burton *et al*., 1999). The 6-

membered aluminosilicate rings that act as basic building units of cancrinite are also shared by other zeolites such as sodalite, herschelite and nepheline (Oh *et al*., 2011). Cancrinite zeolites have been reported to have potential uses in the fertilizer industry where they can act as a source of soil nutrients for instance by slowly releasing phosphates and nitrates during the weathering process (Barrer and Cole, 1969; Fansuri *et al*., 2008).

As was shown in Section 7.2.2, the high dissolution of Si and Al which was accelerated by ultrasound in this study is thought to have resulted in high supersaturation of these elements which consequently led to accelerated direct nucleation and crystallization of hydroxy-cancrinite zeolite. Even though ultrasonic enhanced crystallization is not a new process (Lindley, 1992), the mechanism of direct zeolite formation by the use of ultrasound is not well understood. Lindley (1992) proposed that during the expansion stage of the cavitation bubble there is localized cooling which in turn leads to a localized increase in the degree of supersaturation that triggers the formation of germ nuclei that are distributed through the solution upon the collapse of the bubble which later grow to form the crystalline material. The transformation of hydroxy-sodalite to hydroxy-cancrinite zeolite crystals after 15 minutes of sonication is thought to be the main reason why there was a decrease and later an increase in the Si and Al concentration that was reported in Figure 7.6. This observation will be substantiated further during the discussion for SEM analysis.

The findings reported in this section are novel because no evidence was found in the literature reporting synthesis of zeolites by direct sonication of the as-received coal fly ash. In particular, hydroxy-cancrinite zeolite has mostly been synthesized previously from fly ash using solutions of NaOH (.> 5 M) following the conventional heated hydrothermal crystallization process at high temperatures (> 130 ºC) (Querol *et al*., 1997; Chung *et al*., 2003; Oh *et al*., 2011). A study conducted by Querol *et al*. (1997) showed that it was also possible to obtain hydroxy-cancrinite within 30 minutes upon application of microwave conditions using fly ash which was treated with 5 M NaOH at microwave temperature of 235 ºC. Studies on crystallization of zeolites by direct sonication have only been conducted using pure chemicals as was shown by Andaç *et al*. (2005) who reported that a highly crystalline zeolite A had formed by direct application of ultrasound to the reaction mixture. A study conducted by Feng *et al*. (2004) reported that some unidentified semi-crystalline to crystalline phases were formed during the dissolution of fly ash and metakaolin. A good

semi-review paper by (Luque de Castro and Priego-Capote, 20007) discusses the numerous potential applications that ultrasound-assisted crystallization can offer.

Figure 7.11 presents the XRD pattern of synthesis product obtained when the already sonicated (30 minutes) product of the as-received South African class F fly ash that was presented in Figure 7.10 was subjected to hydrothermal treatment at 140 °C for 48 hours. The results of these experimental run acted as a control.

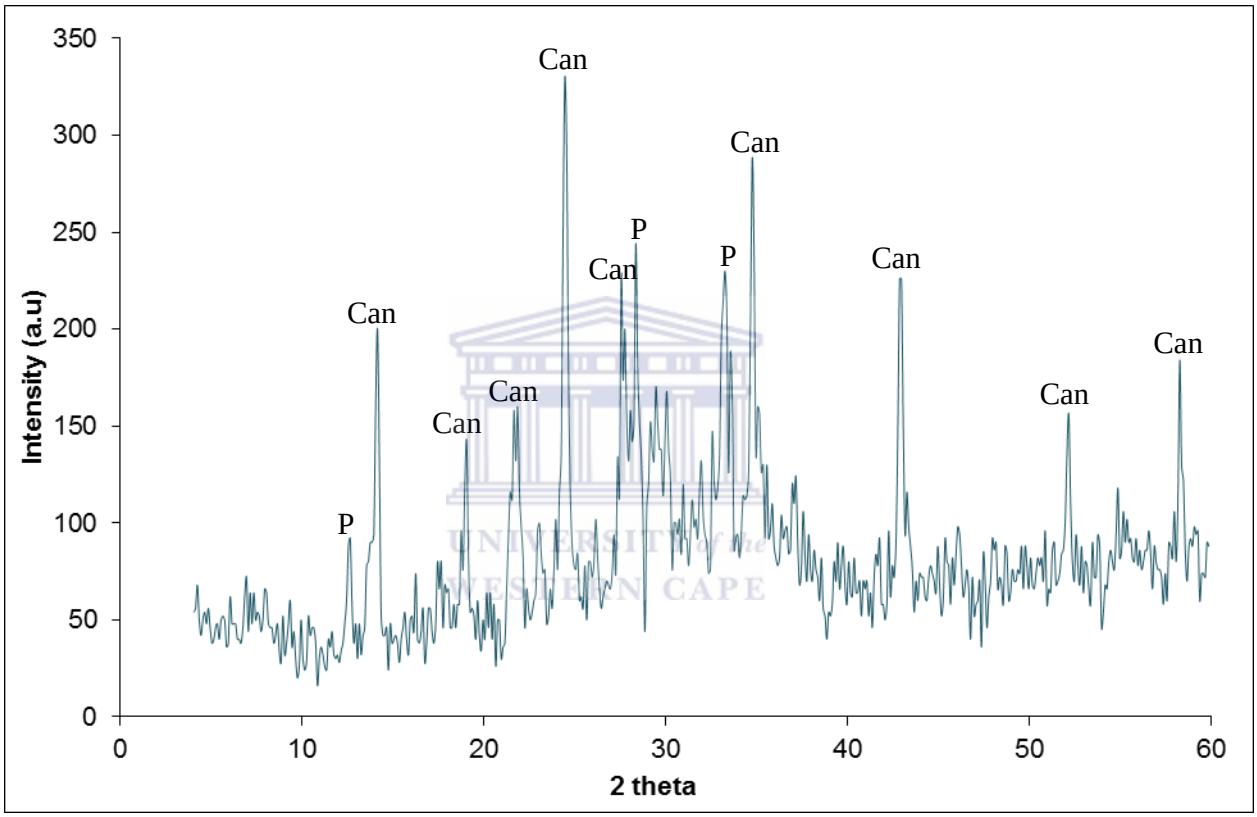

Figure 7-11: XRD pattern of synthesis product obtained when the already sonicated (30 minutes) product of the as-received South African class F fly ash that was presented in Figure 7.10 was further subjected to hydrothermal treatment at 140 °C for 48 hours. (Can = hydroxy-cancrinite, P = zeolite P).

From Figure 7.11, it was interesting to note that further hydrothermal treatment of the already sonicated as-received South African class F fly ash (which had shown presence of hydroxy-cancrinite zeolite) resulted in the development of another zeolitic phase (zeolite Na-P1) together with the hydroxy-cancrinite. Amorphous material was also identified by the 'hump' in the XRD diffraction pattern appearing between 20 – 40° 2θ. This zeolitic transformation is

thought to be due to the Ostwald‘s step rule on the law of successive phase transformations (Byrappa and Yoshimura, 2001).

7.2.6 Morphological studies of sonicated fly ash

Figure 7.12 presents the SEM images of synthesis product obtained when the as-received South African class F fly ash was sonicated for 5, 10, 15 and 30 minutes as was presented in the respective XRD patterns shown in Figure 7.9. The procedure for SEM analysis is detailed in Chapter 3, Section 3.5.4.1.

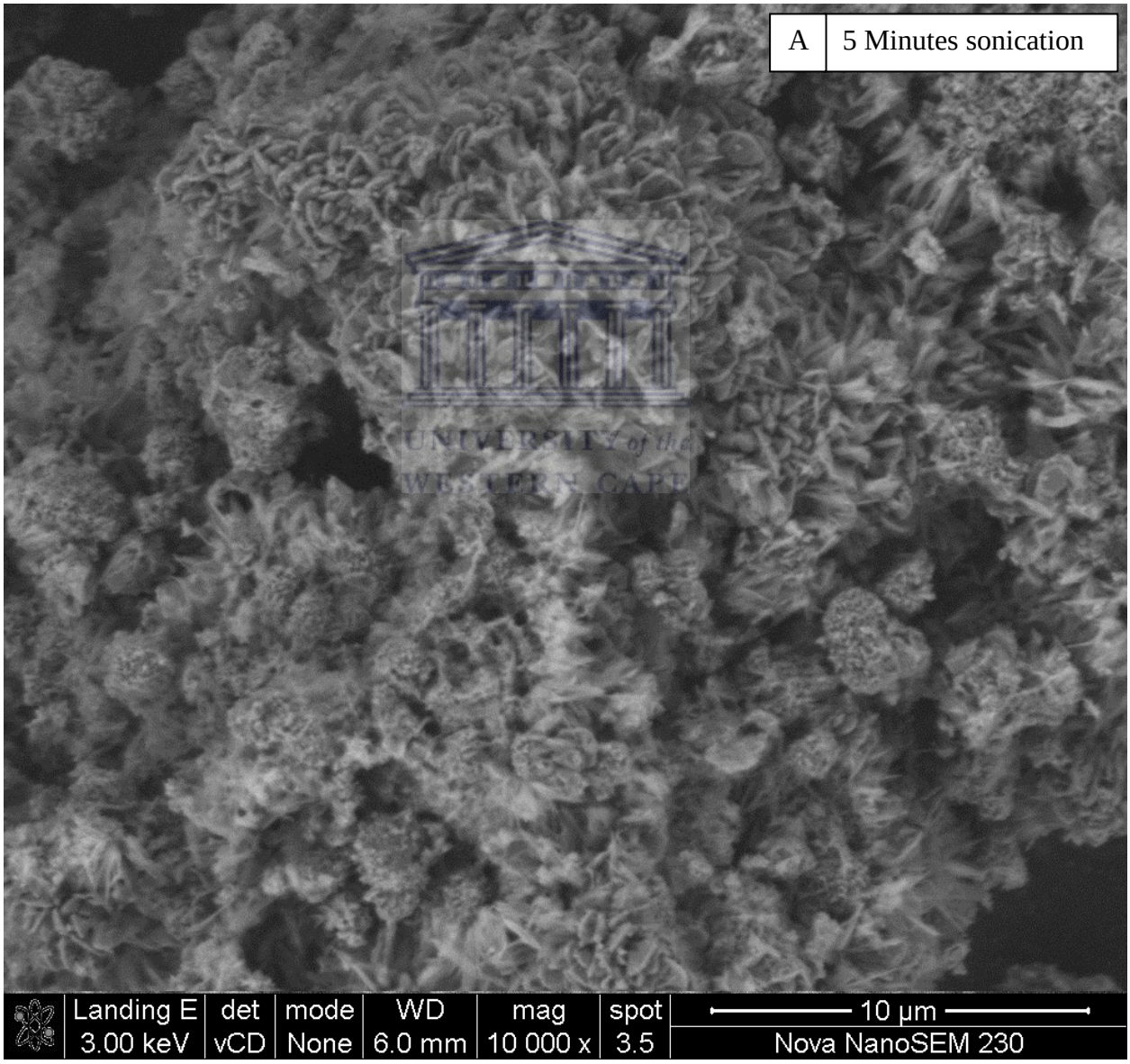

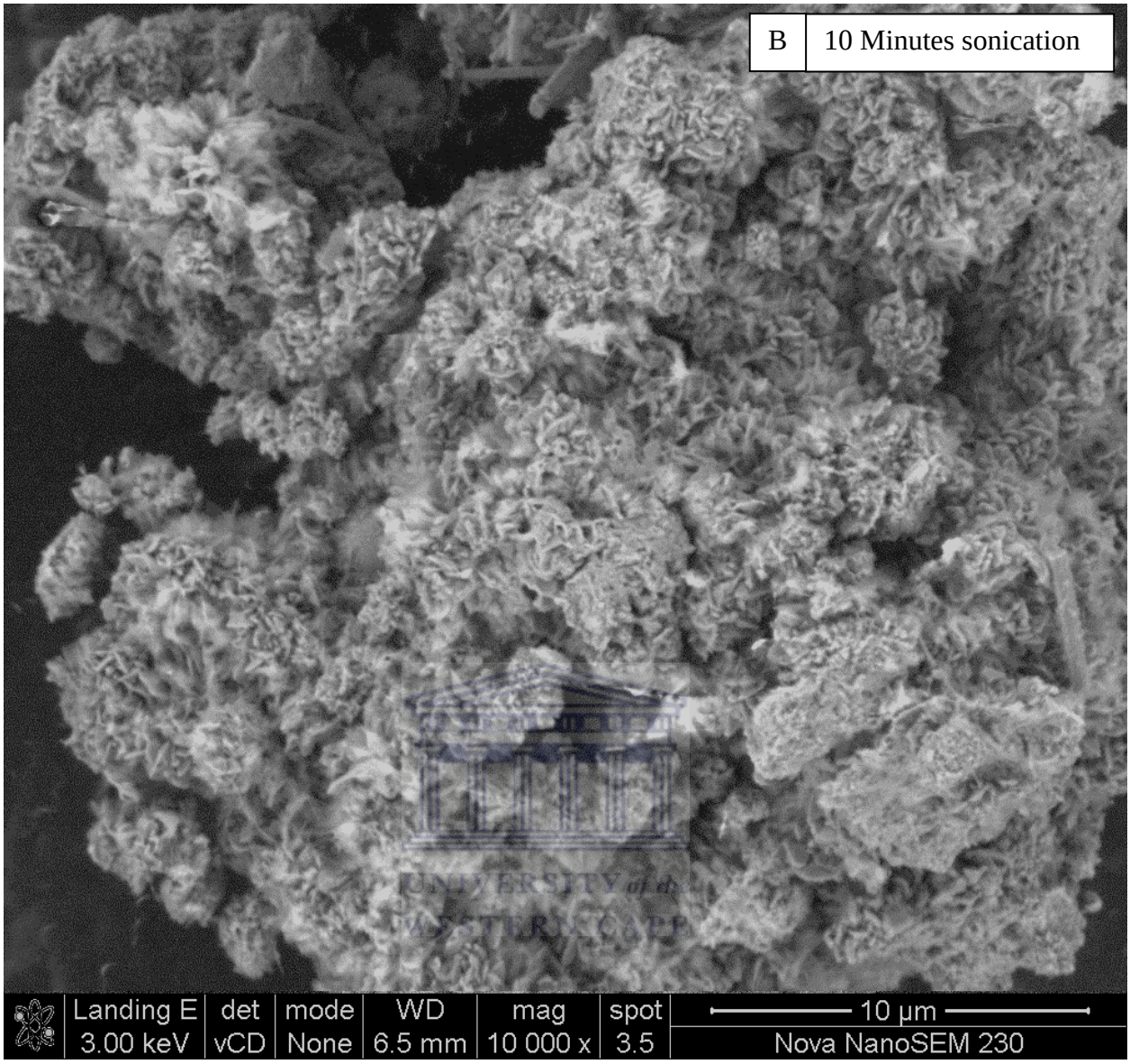
B
10 Minutes sonication
Landing E
3.00 keV
det
vCD
mode
None
WD
6.5 mm
mag
10 000 x
spot
3.5
10 µm
Nova NanoSEM 230

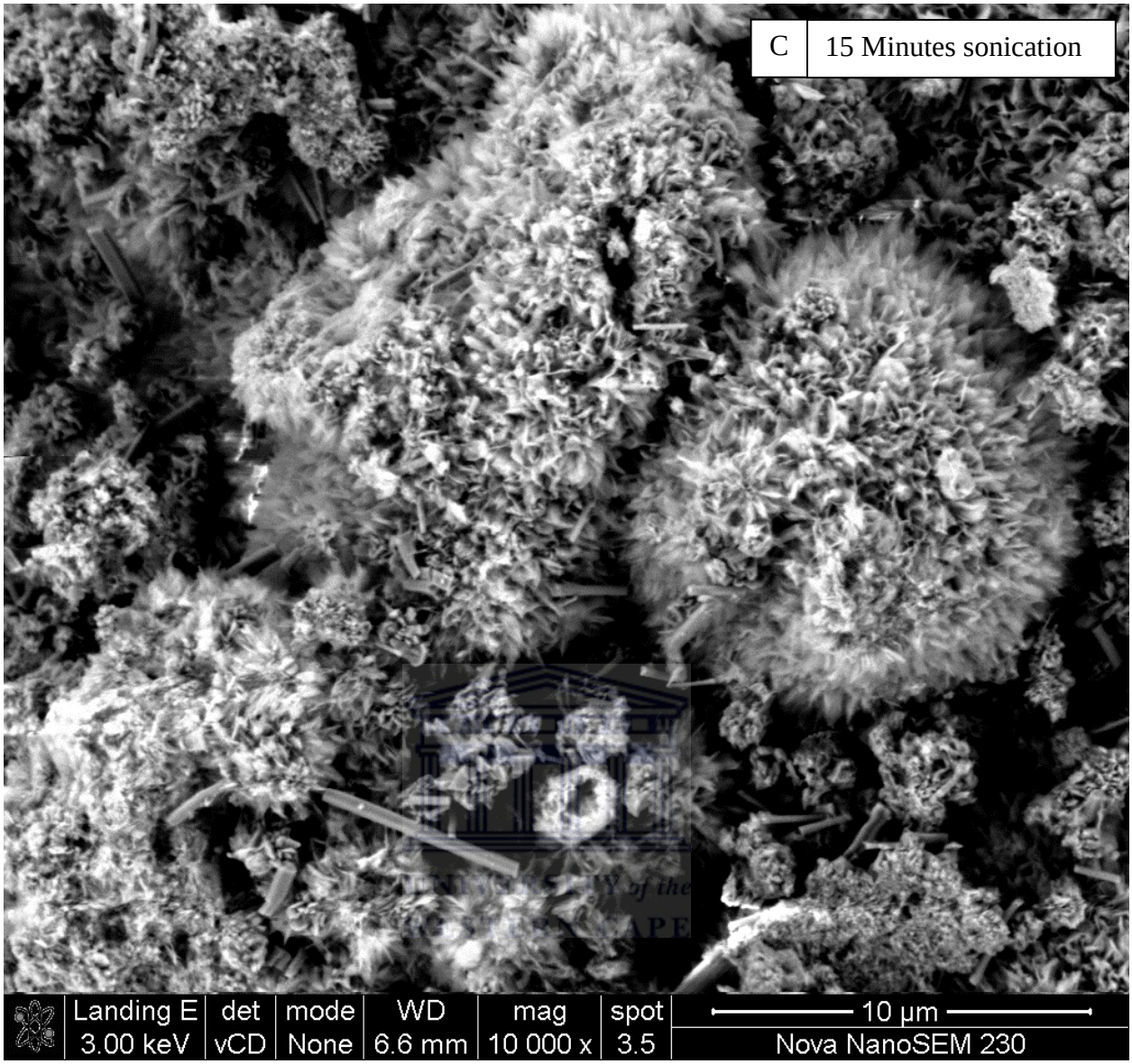
C
15 Minutes sonication
Landing E
3.00 keV
det
vCD
mode
None
WD
6.6 mm
mag
10 000 x
spot
3.5
10 µm
Nova NanoSEM 230

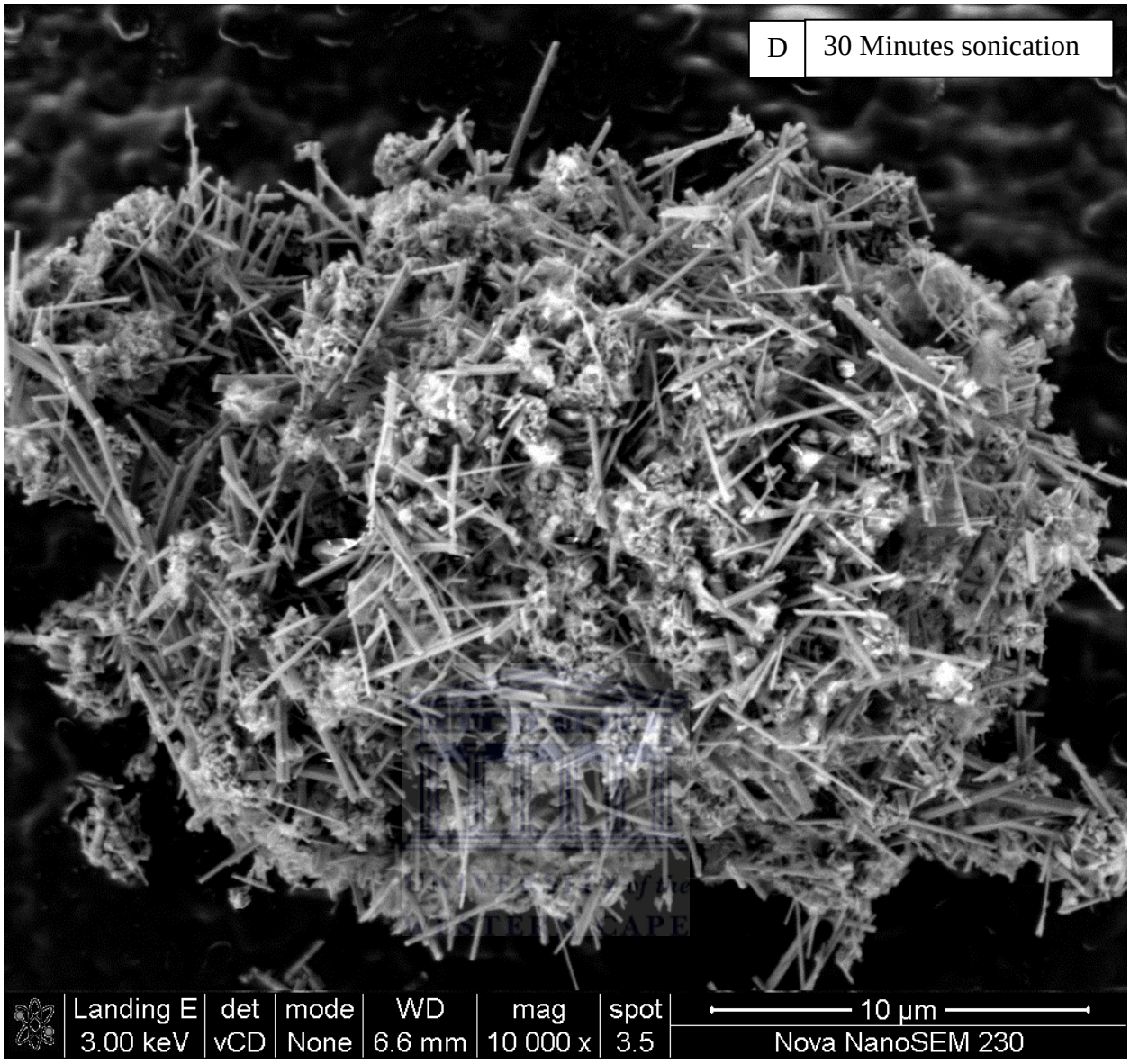

Figure 7-12: SEM images of synthesis product obtained when the as-received South African class F fly ash was sonicated for a) 5, b) 10, c) 15 and d) 30 minutes as was presented in the respective XRD patterns shown in Figure 7.9.

As shown in Figure 7.12, when the as-received South African class F fly ash was sonicated for 5 minutes, the fly ash particles which had been shown to be spherical in shape and smooth surface (see Figure 4.3 (a), Chapter 4) were transformed to small irregular crystallites had been identified from XRD analysis in Figure 7.9 to be a mixture of hydroxy-sodalite and hydroxy-cancrinite. As the time of sonication was increase up to 30 minutes, thin needle-like morphology of hydroxy-cancrinite zeolite was developed. Sonication for 30 minutes led to direct crystallization of a single phase hydroxy-cancrinite zeolite phase without the need for any hydrothermal step. The above SEM images served to complement the XRD analysis

presented in Figure 7.19. The increase of concentration of Si and Al that was observed in Figure 7.6 when the as-received South African class F fly ash was sonicated for 15 minutes can be attributed to the transformation of hydroxy-sodalite to hydroxy-cancrinite.

Figure 7.13 presents the SEM image of the synthesis product obtained when the already sonicated (10 minutes) as-received South African class F fly ash that was shown in Figure 7.10 was further subjected to hydrothermal treatment at 140 °C for 48 hours.

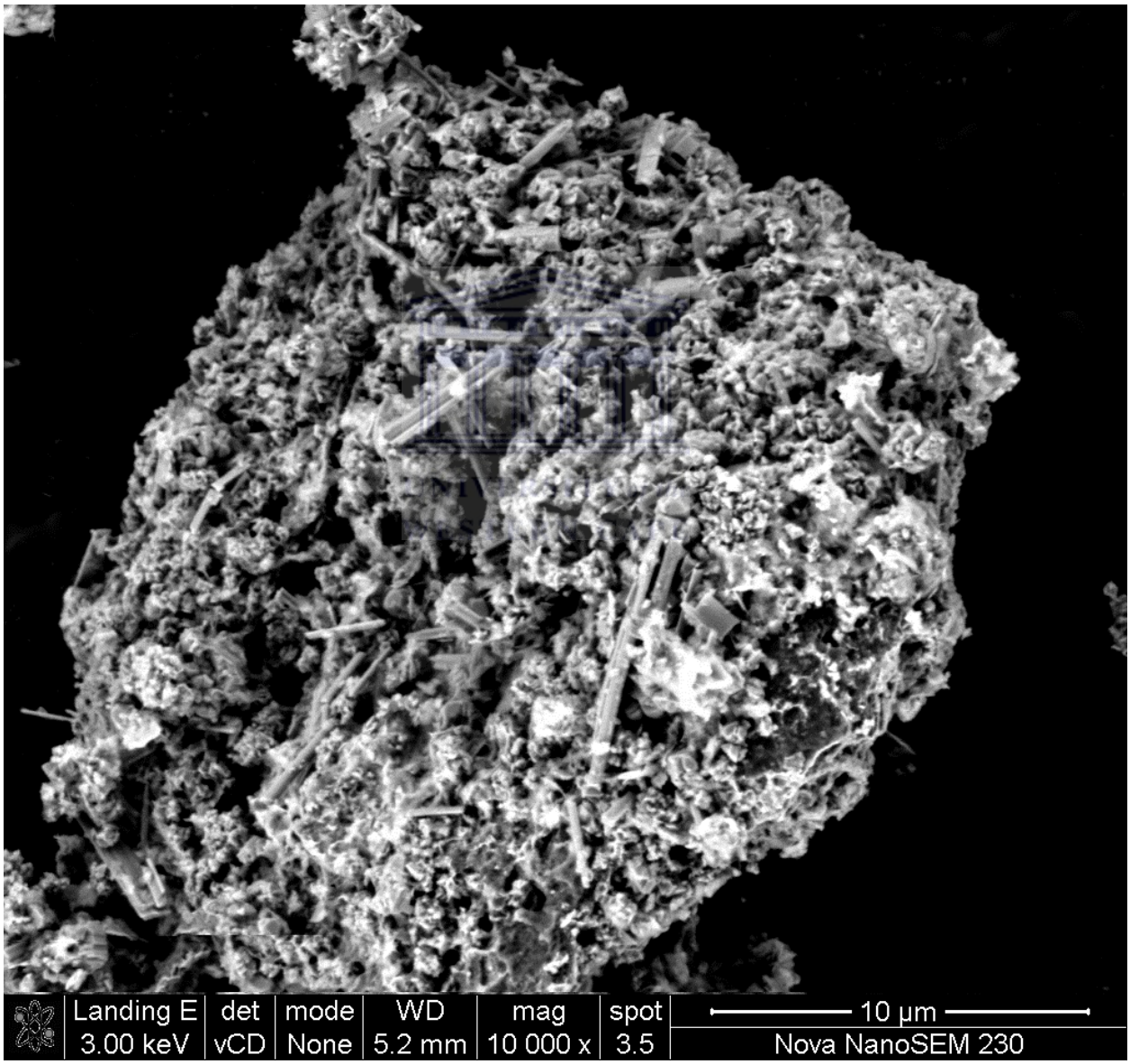

Figure 7-13: SEM image of the synthesis product obtained when the already sonicated (30 minutes) as-received South African class F fly ash that was shown in Figure 7.10 was further subjected to hydrothermal treatment at 140 °C for 48 hours.

The SEM images presented in Figure 7.13 show the presence of longer needle-like crystals that had been identified in Figure 7.12 (d) to be of hydroxy-cancrinite. Even though zeolite P and amorphous material had been identified from the XRD pattern presented in Figure 7.11, a clear distinction of these two phases could not be easily made from the above SEM image.

7.2.7 FTIR analyses of the sonicated fly ash

Figure 7.14 compares the FTIR spectra generated when the as-received South African class F fly ash was sonicated at different times (5, 10, 15 and 30 minutes) together with that generated when the already sonicated (30 minutes) as-received South African class F fly ash was further subjected to hydrothermal treatment at 140 °C for 48 hours. These spectra serve to complement the XRD and SEM analyses that were presented in Figures 7.10, 7.11, 7.12 and 7.13.

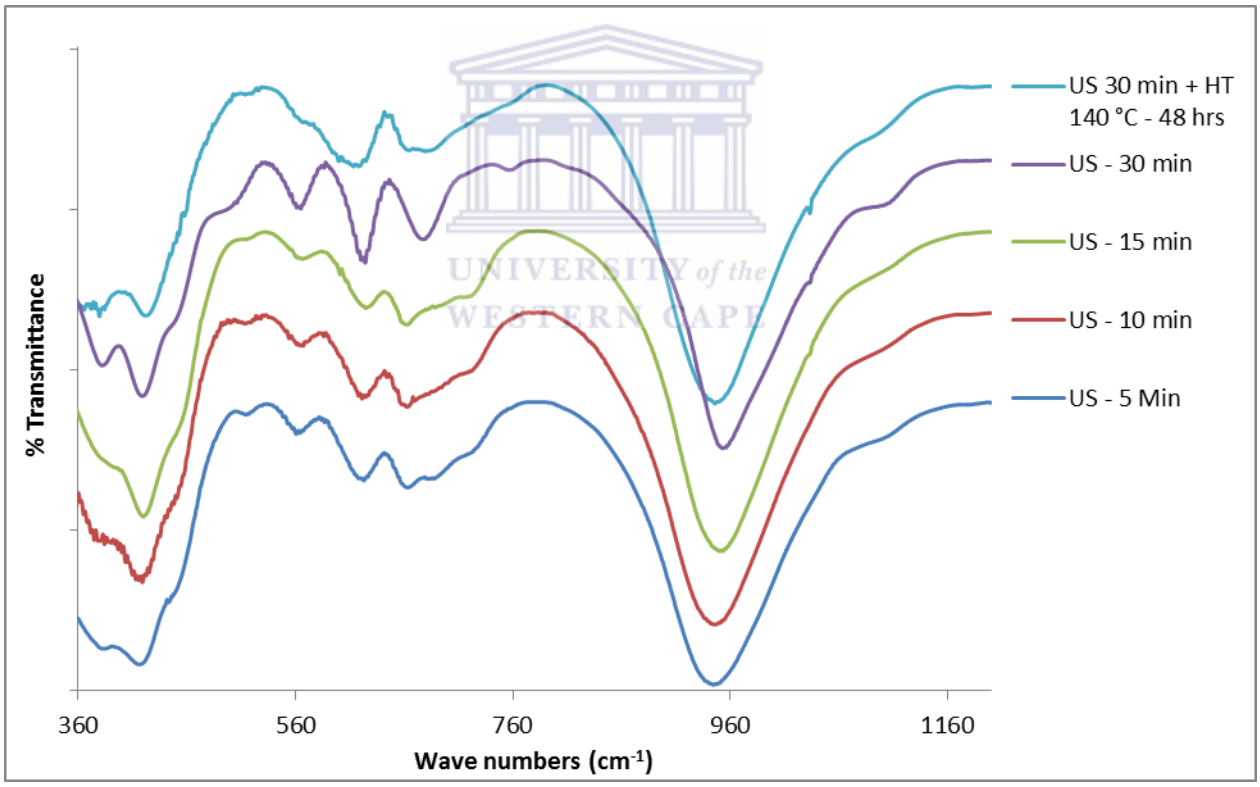

Figure 7-14: Comparative FTIR spectra generated when the as-received South African class F fly ash was sonicated at different times (5, 10, 15 and 30 minutes) together with that generated when the already sonicated (30 minutes) fly ash was further subjected to hydrothermal treatment at 140 °C for 48 hours.

The assignments of the vibrational bands from the FTIR spectra presented in Figure 7.14 are summarized in Table 7.1.

Table 7-1: Comparison of mid-Infrared vibrational bands generated when the as-received South African class F fly ash was sonicated at different times (5, 10, 15 and 30 minutes) together with that generated when the already sonicated (30 minutes) fly ash was further subjected to hydrothermal treatment at 140 °C for 48 hours.

Literature values (Flanigen,1971)		Actual vibration bands of the zeolitic samples (cm^{-1})				
Vibrational band Range (cm^{-1})	Assignment	US 5 Min	US 10 Min	US 15 Min	US 30 Min	US 30 Min + HT 140 °C-48 hrs
300 - 420	Pore opening vibrations (internal tetrahedra)	391	390	392	391	389
420 - 500	T-O bending vibrations (internal tetrahedra)	425	426	425	425	428
650 - 720	Symmetric stretching (internal tetrahedra)	673	671	673	686	695
750 - 820	Symmetric stretching (external tetrahedra)	729	729	730	767	769
950 - 1250	Asymmetric stretching (internal tetrahedra)	955	956	957	961	938
1050 – 1150	Asymmetric stretching (external tetrahedra)	1109	1113	1109	1110	1105

Apart from identifying the common vibrational bands of zeolitic materials, the bands observed around 428 cm^{-1} (in this case, between 425–428 cm^{-1}) are related to the single four-membered ring (S4R) of the sodalite and cancrinite units (Yao *et al*., 2006). The inability to get a clear cut differences of the FTIR spectrum obtained when sodalite and cancrinite had co-crystallized together (such as in the first 15 minutes) is due to their structural similarities, since their aluminosilicate layers of six-membered rings are identical to each other, with the only difference being in the stacking sequences of these layers as shown in Figure 7.10 (Okubo *et al*., 2001). The well-defined and prominence of peak at 686, 627 and 569 cm^{-1} for

the sample that was obtained after 30 minutes sonication of the as-received South African class F fly ash can be used to explain its higher crystallinity when compared to samples obtained at lesser (5, 10 and 15 minutes) sonication times. This argument in good agreement with the observations noted from XRD and SEM analysis presented in Figure 7.9 and 7.12 respectively.

Comparing the mid-Infrared vibrational bands of the ultrasonic assisted synthesis products obtained after 30 minutes sonication of the as-received South African class F fly ash with that obtained after the same sample was further subjected to hydrothermal treatment at 140 °C for 48 hours, the partial transformation of hydroxy-cancrinite to zeolite P is evident from the significant shift of the peak appearing at 938 cm^{-1}. This shift is due to the differences of the Si/Al ratio between zeolite P and cancrinite zeolite. The shift caused by differences in Si/Al ratio has also been affirmed by Flanigen (1971) in the case where dealumination of zeolites was conducted. Though there are some noticeable differences in the intensity of the peaks in the spectra for the single phase hydroxy-cancrinite with that of the mixture of hydroxy-cancrinite with zeolite P and amorphous material, it is important to point out that the joint presence of T-O vibrations (T = Al , Si) in both samples yields overlapping spectral bands that make interpretation difficult. This challenge was also affirmed by Fernandez-Jimenez and Palomo (2005).

7.3 Chapter summary

In Section 7.1 of this chapter, it had been demonstrated that application of 10 minutes of sonication prior to the conventional hydrothermal synthesis step for the clear extract of fused fly ash whose composition (1 Al_2O_3 : 30.84 Na_2O : 4 SiO_2 : 414.42 H_2O) had been optimized in Chapter 4 for zeolite A formation led to reduction of the hydrothermal synthesis time of zeolite A by half. This significant improvement could have been due to ultrasonic accelerated ageing effect of the reaction mixture which is known to lead to enhanced nucleation that often leads to a decrease in the crystal size of the synthesis product as was demonstrated in this study. Similar effects of the application of ultrasound to the reaction mixture were also observed when the pure water was substituted with mine waters (circumneutral and acid drainage mine waters), as the synthesis solvent. The improvement in the hydrothermal synthesis (halving of the synthesis time) caused by sonication can be expected to have a significant impact when the synthesis process is up scaled.

CHAPTER 7

Section 7.2 of the study demonstrated, for the first time, that hydroxy-cancrinite zeolite can be synthesized by direct application of ultrasound to the as-received South African class F fly ash. This novel synthesis route led to production of a single phase hydroxy-cancrinte zeolite from the as-received South African class F fly ash after only 10 minutes of sonication avoiding fusion and ageing.

CHAPTER 8

CONCLUSIONS AND RECOMMENDATIONS

This chapter summarizes the findings of this thesis by presenting an overview of the achievements of the research objectives, a discussion of the importance and contributions of the results from a scientific and industrial point of view and provides recommendations for future work.

8 Introduction

The four main objectives that were set out in the introductory chapter i.e to identify, customize and optimize the synthesis conditions for producing zeolite A and X from South African class F fly ash; ii) to comparatively explore the use of unconventional solvents (mine waters) as a substitute for pure water during the synthesis of zeolite A and X from South African class F fly ash; iii) to study the formation mechanism of zeolites from South African class F fly ash using in-situ ultrasonic monitoring process and iv) to apply ultrasound as a substitute to the conventional ageing step as well as a replacement for the overall hydrothermal synthesis process, were successfully achieved.

8.1 Summary of the key findings of this research

From the research presented in this thesis, several novel findings were reported. These findings were;

1. Use of mine waters, as a solvent instead of ultra-pure water, was applied successfully during the synthesis of either zeolite A or X from South African fly ash.

2. The in-situ ultrasonic method was successfully applied to study the mechanism of formation of zeolite A and X from fly ash under real reaction conditions and ultrasound attenuation correlated with results from ex-situ techniques and provided much deeper insight into the zeolite formation mechanisms.

3. A new synthesis route was discovered leading to the formation of a novel morphology (hierarchical) zeolite X from South African fly ash without the need for use of expensive templates or post synthesis treatments (applied for a patent).

4. A new process was discovered for producing hydroxy-cancrinite zeolite by direct sonication of the as-received South African fly ash (applied for a patent).

A summary of the specific key findings from each of the four chapters is presented below.

8.1.1 Identification and customization of synthesis conditions for conversion of South African fly ash to pure phase zeolites A and X.

8.1.1.1 Zeolite A

A route to prepare single phase, high purity, zeolite A from South African class F fly ash using either unseparated fused fly ash slurry or a clear extract of the fused fly ash slurry was developed. The best synthesis conditions were; hydrothermal synthesis at 100 °C for 2 hours, reaction mixture with a molar regime of 1 Al_2O_3 : 30.84 Na_2O : 4 SiO_2 : 414.42 H_2O for synthesis starting from clear extract of fused fly ash whereas when the unseparated fused fly ash slurry was used, the molar ratio was 1 Al_2O_3 : 5.39 Na_2O : 2.75 SiO_2 : 111.82 H_2O. Comparing the synthesis conditions identified in this study with those reported in the literature, it is evident that the process of producing zeolite A from South African fly ash presented in this study was less complicated and also led to a reduction of hydrothermal synthesis time. Additionally, there was considerable improvement in the quality of zeolite A when the clear extract of fused fly ash was used instead of starting from the unseparated fused fly ash slurry. The less complicated synthesis procedure, relatively better quality zeolite and more rapid crystallization of zeolite A from South African fly ash is expected to trigger interest in scale up studies and further allow high end applications of fly ash based zeolite A.

Furthermore, it was also proven, for the first time, that zeolite A could be prepared when mine waters (circumneutral and acid drainage mine waters) were used as a substitute of pure water during the synthesis process. An almost similar quality single phase zeolite A was obtained when circumneutral mine waters was used whereas a mixture of zeolite A and hydroxysodalite was obtained when acidic mine water was used as solvent. The quality of the obtained zeolite A was dependent on the type of mine water used. It was interesting to note that the presence of the extra cations in the circumneutral and acid drainage mine water did not have a negative effect on the crystallization of zeolite A.

8.1.1.2 Zeolite X

The synthesis conditions for preparing a pure phase with the typical octahedral shaped crystals of zeolite X from the South African fly ash were identified. The best synthesis conditions were: alkali fusion of fly ash followed by mixing with water to generated a molar regime of 1 Al_2O_3 : 4.90 Na_2O : 3.63 SiO_2 : 115.92 H_2O, which formulation was subjected to hydrothermal synthesis conditions of 80 ºC for 9 hours. It is noteworthy to point out that a single phase zeolite X was successfully obtained, which had been a challenge to other researchers who had tried to produce faujasite from South African fly ash. Additionally, it was shown that the use of mine waters as a substitute of pure water during the synthesis of the typical octahedral shaped zeolite X did not lead to a single phase zeolite X under the same conditions which was unlike the case when zeolite A was targeted using mine waters. The zeolite X product obtained when mine waters were used, still had some unconverted amorphous precursor species meaning that the synthesis conditions applied still needed further optimization. This could be attributed to the differences in the formation mechanisms between zeolite A and X or could be due to the presence of higher concentrations of the additional cations such as Fe, Ca, Mg and Al in the mine waters.

Most importantly, a process for producing a novel morphology (hierarchical) zeolite X from the clear extract of the fused South African class F fly ash slurry was discovered. The hydrothermal synthesis conditions for producing this novel zeolite X were: alkali fusion of fly ash and extraction of clear solution with a molar regime of 1 Al_2O_3 : 56.80 Na_2O : 16.62 SiO_2 : 954.05 H_2O followed by hydrothermal synthesis at a temperature ranging between 80 and 94 ºC for 24 hours. Although the driving force behind the crystallization of this unique morphology zeolite X from the clear extract of the fused fly ash feedstock is not currently clearly understood, a combination of effects are postulated to be the factors allowing the crystallization of this unique morphology of zeolite X from fly ash namely; removal of less soluble precursors by filtration and using a clear extract, stirring during the hydrothermal crystallization step and applying the right molar regime under suitably mild hydrothermal conditions .

From the BET analysis, it was shown that the new morphology of zeolite X had a relatively higher external surface area. This enhanced external surface area was due to the presence of intergrowths of disc-like nano platelets which created a bimodal micro-/mesopore structured

zeolite X giving a hierarchical pore size distribution. These properties of the new morphology of zeolite X are desirable for most catalytic applications and have the potential of solving the well-known problem of diffusional and mass transfer constraints that are associated with the presence of only internal zeolitic micropores. A recent jointly published paper (Babajide *et al.,* 2012) that used the new morphology zeolite X in its K-form (zeolite produced from this study) reported a high catalytic activity when used as a solid catalyst for biodiesel production. A patent application for the synthesis process leading to the production of the new morphology zeolite X has also been made.

8.1.2 In-situ ultrasonic monitoring of zeolite A and X crystallization from South African fly ash.

The investigations conducted in this study on the formation mechanism of zeolite A and X under real reaction conditions using the in-situ ultrasonic monitoring set-up enriched the fundamental understanding of zeolite A and X formation from fly ash. To the best of the author's knowledge, no previous effort had been made to understand the formation process of zeolites from fly ash under real reaction conditions. From the in-situ diagnostic of the formation of zeolite A starting from either clear extract or unseparated fused fly ash slurry, it was demonstrated that zeolite A formation from coal fly ash follows both the solution and solid-phase mediated mechanisms. In addition, it was further demonstrated that longer periods of ageing of the precursor species (synthesis mixture) showed a change of the mechanism to only solution-mediated mechanism. The observations of the ultrasonic attenuation signal together with information from complementing ex-situ analysis points out that ageing prior to the hydrothermal synthesis of zeolite A prevented the formation of the secondary gel during the hydrothermal synthesis process. In this case, the avoidance of the secondary amorphous gel allowed supersaturation to occur more rapidly thus further shortening the synthesis time.

The diagnostic of the formation process of the novel morphology (hierarchical) zeolite X from fly ash could only support the solution-mediated model. A comparison of the time of crystallization from the generated ultrasonic attenuation signals for the formation of zeolite A with that of zeolite X, further confirmed that zeolite A crystallizes much faster than zeolite X. The investigation of the effect of temperature during the in-situ monitoring of the formation process of both zeolite A and X showed that higher temperatures led to faster crystallization

as was shown by the shift of the ultrasonic attenuation signals which correlated directly with a more rapid crystallization time when the temperature had been increased from 80 to 90 to 94 °C. The use of in-situ ultrasonic monitoring system also provided sufficient data points which enabled closer estimation of the time of transition from nucleation to crystal growth step during the monitoring of formation mechanism of both zeolite A and X.

8.1.3 Use of ultrasound during the synthesis of zeolites from South African fly ash.

The study has demonstrated that application of 10 minutes of sonication as a substitute for the lengthy ageing prior to the conventional hydrothermal synthesis step for producing zeolite A using the optimized fused reaction mixture, led to a reduction of the hydrothermal synthesis time by half. A similar effect was also observed when the pure water was substituted with mine waters (circumneutral and acid drainage mine waters), as the synthesis solvent. The improvement in the hydrothermal synthesis (halving of the synthesis time) caused by prior sonication of the precursor feedstock solution can be expected to have a significant impact when the synthesis process is up scaled.

A novel process that involved direct sonication of coal fly ash slurry without fusion or ageing to produce hydroxy-cancrinite zeolite was also reported in this thesis. On a fundamental level, the study started by understanding the dissolution behaviour of Si and Al under the influence of ultrasound by investigating variables such as; effect of sonication time, NaOH concentration, stirring and fly ash particle size. Upon characterization of the products of sonicated fly ash slurry, it was found that a single phase hydroxy-cancrinte zeolite had formed directly from the sonicated South African class F fly ash after only 30 minutes of sonication. The new synthesis route can be used to overcome the challenges of high consumption of energy and prolonged synthesis time which is often associated with use of fly ash as feedstock namely, fusion, followed by ageing, followed by the conventional hydrothermal synthesis procedures. A patent application for this novel procedure route to prepare hydroxy-cancrinite has been made. The invention is advantageous and can play a significant role in the transfer of technology to industry since it can contribute to addressing the shortcomings of the popular hydrothermal synthetic approaches.

8.2 Significance of the current study to the scientific and industrial community

The novel findings from this thesis are of importance to both the scientific and industrial community. The significance of the contributions from this research can be summarized as follows;

1. It was shown that fly ash sourced from different South African coal-fired power stations have variation in chemical compositions, thus the research findings should stimulate interest by the coal burning industries to optimize the zeolite synthesis conditions that were identified for Arnot fly ash, for each source of fly ash.

2. The application of the two main industrial waste materials, fly ash and mine waters, to form high value zeolites serves a dual purpose. Firstly, it serves to reduce the environmental pollution associated with waste disposal and at the same time the high quality zeolitic product has the potential to be applied for the treatment of polluted mine waters to remove cations and toxic metals before the treated effluents are further processed or released to the environment. With the increasingly strict environmental regulation and shortage of landfill sites, reuse of fly ash and mine waters that are found together in close proximity provides an attractive option that could help in mitigating the environmental degradation of coal mining and burning hence promoting sustainable development. Secondly, the production of saleable products (zeolites) from a low-cost source of Si and Al as well as use of mine waters as a cheaper source of synthesis solvent has the potential of generating extra income for the mining industry which can be used to offset other costs of mitigating pollution and/or even create jobs.

3. The identified synthesis route leading to the formation of the novel morphology (hierarchical) zeolite X from South African fly ash, without requiring the use of additional ingredients or post synthesis treatment, is advantageous compared to the complicated procedures to make hierarchical catalysts, which are reported in literature that are based either on chemical or physical techniques. This synthesis route is expected to be a low cost alternative to the commercial zeolite X synthesized from conventional raw materials (sodium silicate and aluminate). It is also expected to trigger new applications for fly ash based zeolites which are expected to perform

much better when compared to the standard zeolite X counterpart that has the well-known conventional octahedral crystal morphology.

4. The demonstration of in-situ, in-depth investigation of the formation mechanisms of zeolite A and X from fly ash under real reaction conditions conducted in this study could be helpful in controlling and optimizing the synthesis process of various other zeolite types. The results obtained by use of in-situ ultrasonic monitoring revealed new insights into the mechanism of formation of zeolites from fly ash which cannot be observed when only ex-situ techniques are used to follow the reaction. The study showed that zeolite formation processes proceed through either a solution or a solid-phase mediated mechanism of formation depending on the conditions applied. Therefore, the result obtained from this study enriches the existing body of literature by contributing to a better understanding of the mechanism of zeolite formation from fly ash.

5. The novel direct ultrasonic synthesis route for generating zeolites from as-received fly can contribute to addressing the shortcomings of the popular hydrothermal synthetic approaches by minimising the high consumption of energy for fusion, aging and hydrothermal stages and reducing synthesis times. The economic and environmental benefits associated with direct sonocrystallization of zeolites from fly ash can be expected to trigger research interest at pilot plant scale hence stimulating more beneficial fly ash utilization. The integration of the developed process into waste management is expected to minimize disposal costs, reap financial gains generated from the sale of products obtained and also serve as a replacement of some of the expensive and scarce natural resources. It is further expected that other predetermined high value zeolites can be made by using the well-known molar regimes of the starting synthesis feedstocks through direct application of ultrasound.

8.3 Recommendations for future work

Even though all the initial objectives that were set for this study were achieved, there are still some other aspects, which were not within the scope of this study either due to time or resource constraints, that were not fully explored and could serve as areas of future

investigations. The following is a summary of possible further work that can contribute to a holistic view on the zeolites formation from fly ash and provide more understanding of the entire synthesis process and the synthesized zeolite application potential.

1. Since fly ash sourced from different South African coal-fired power stations was shown to have variation in its chemical compositions, it will be of interest to optimize the conditions identified in the present study to investigate and compare zeolites formation using different ash compositions obtained from different South African coal or municipal incinerators.

2. It will also be important to explore the possibility of adjusting Si/Al ratio by using silica and alumina obtained from other waste sources agricultural wastes such as maize, wheat and rice stalks instead of using pure chemical compounds. Use of these low-cost sources of extra Si and Al will lead to reduction of the cost of zeolite synthesis process.

3. Further fundamental understanding of the reasons that led to the formation of the hierarchical zeolite needs to be explored in order to establish the most essential factors in controlling its formation process. At this stage, it is not clearly known whether the preferred morphology was formed due to the suitable distributions of cations/anion species in the synthesis mixture or whether it could be related to factors such as pH, water content and mild synthesis conditions among others variables.

4. Due to the potential leachability of heavy metals from some of the synthesis products, thorough studies need to be conducted to do mass balance and determine the fate of toxic elements. The findings from these studies could give better perspectives in terms of possible and best match for the zeolite applications. Even though some applications such as biodiesel production are not affected by presence of “these toxic elements”, as it has been reported in this thesis and in published subsidiary studies, such knowledge will also influence the best way to safely dispose the spent zeolites after their specific applications.

5. Since zeolites from fly are low-cost adsorbents, future work needs to be done to evaluate their potential in treatment of the waste mine waters before other

technologies are used. Through these, they could act as sinks for recovery of precious elements as well as other rare earth elements which could even stimulate their re-use.

6. The possible recovery and recycling alternatives for the heavy metal saturated zeolitic materials should be considered after their use for mine water effluent treatment.

7. The application of these fly ash based catalysts for gas separation, flue gas treatment and hydrocarbon processing should be further explored. On the other hand, a study on the conditioning and regeneration methods under different experimental conditions and from an economical and feasibility point of view should be carried out.

REFERENCES

A´lvarez-Ayuso, E., Querol, X., Plana, F., Alastuey, A., Moreno, N., Izquierdo, M., Font, O., Moreno, T., Diez, S., V´azquez, E., Barra M., (2008), "Environmental, physical and structural characterisation of geopolymer matrixes synthesised from coal (co-) combustion fly ashes" *Journal of Hazardous Materials*, Vol. 154, pp. 175–183.

Abrishamkar, M., Azizi, S. N., Kazemian. H., (2010), "Synthesis of borosilicate MFI type zeolite using different aging techniques", *Chemistry of Metals and Alloys*, Vol. 3, pp. 1-6

Adriano, D.C., Page, A.L., Elseewi, A.A., Chang, A.C. & Straughan, I. (1980), "Utilization and disposal of fly ash and other coal residues in terrestrial ecosystems", *A review Journal of Enviromental Quality,* Vol. 9, pp. 333-344.

Ahmaruzzaman, M. (2010), "A review on the utilization of fly ash", *Progress in Energy and Combustion Science*, Vol. 36, pp. 327–363.

Akbar, S., Dad, K., Shah, T. H. & Shahnaz, R., (2005), "Thermal studies of NaX zeolite with different degrees of cadmium exchange" *Journal of the Chemical Society of Pakistan,* Vol. 27, pp. 456-461.

Akinyemi, S. A. (2011), "Geochemical and mineralogical evaluation of toxic contaminants mobility in weathered coal fly ash: as a case study, Tutuka dumpsite, South Africa" Unpublished PhD thesis, University of the Western cape, South Africa.

Alonso, J. L., & Wesche, K. (1991), "Characterisation of Fly Ash, In: Fly Ash in Concrete-Properties and Performance", K. Wesche (Ed), First Edition, E & FN Spon, London, pp. 8.

Al-Shawabkeh, A., Matsuda, H. & Hasatani, M. (1995), "Comparative reactivity of treated FBC- and PCC-fly ash for SO_2 removal", *Canadian Journal* of *Chemical Engineering,* Vol. 73, pp. 678–685.

REFERENCES

Amrhein, C., Gaghnia, G.H., Kim, T.S., Mosher, P.A., Gagajena, R.C., Amanios, T. & Torre, I.D.L. (1996), "Synthesis and properties of zeolites from coal fly ash" *Environmental Science and Technology,* Vol. 30, pp. 735 - 742.

Andaç, Ö. Telli, Ş. M., Tatlier, M., & Erdem-Şenatalar, A., (2006), "Effects of ultrasound on the preparation of zeolite A coatings", *Microporous and Mesoporous Materials,*Vol. 88, pp. 72–76.

Andaç, Ö., Tatlier, M., Sirkecioğlu, A., Ece, I., & Erdem-Şenatalar, A. (2005) "Effects of ultrasound on zeolite A synthesis", *Microporous and Mesoporous Materials,* Vol. 79 pp. 225–233.

Angell, C. L. & Flank, W .H. (1977), "Molecular Sieves-II", American Chemical Society Symposium Series, Katzer, J. R. (Ed.), Vol. 40, pp. 194.

Anuwattana, R. & Khummongkol, P. (2009), "Conventional hydrothermal synthesis of Na-A zeolite from cupola slag and aluminum sludge", *Journal of Hazardous Materials,* Vol. 166, pp. 227–232.

Askari, S., Alipour, S. M., Halladj, R. & Hossein, M. F. D. A. (2012), "Effects of ultrasound on the synthesis of zeolites: a review". *Journal of Porous Materials.* DOI 10.1007/s10934-012-9598-6.

ASTM, (2005), "standard specification for coal fly ash and raw or calcined natural pozzolan for use in concrete (C618-05)", Annual book of ASTM standards, concrete and aggregates, American Society for Testing Materials, Vol. 04.

Auerbach, S. M., Carrado, K.. A. & Dutta, P. (2003), "Handbook of zeolite science and technology", Marcel Dekker, Inc., New York.

Auroux, A. (1994), "Catalyst characterization: Physical techniques for solid Materials", Plenum Press, Imelik B, Vedrine JC (eds), New York, pp. 611.

REFERENCES

Avrami, M, (1939). "Kinetics of Phase Change. I. General Theory", *Journal of Chemical Physics*, Vol. 7, (12), pp. 1103–1112.

Azizi S. N., & Yousefpour, M., (2010), "Static and Ultrasonic-assisted Aging Effects on the Synthesis of Analcime Zeolite", *Zeitschrift für anorganische und allgemeine chemie*, Vol. 636, pp. 886–890.

Babajide, O., Petrik, L., Musyoka, N., Amigun, B. & Ameer. F. (2010), "Use of coal fly ash as a catalyst in the production of biodiesel", *Petroleum and Coal*, Vol. 52, pp. 261-272.

Baerlocher, C. & McCusker, L.B. (2011) "Database of Zeolite Structures" available at http://www.iza-structure.org/databases/ [accessed on 12th June 2011].

Baerlocher, C., Meier, W.M., & Olson, D.H. (2007), "*Atlas of Zeolite Structure Types"*, 7th edn, Elsevier, Amsterdam.

Balkus, K. J., & Ly, K. T., (1991) "The preparation and characterization of an X-type zeolite: An experiment in solid-state chemistry" *Journal of Chemical Education*, Vol. 68, pp. 875-877.

Bandopadhyay, A. K., (2010), "A study on the abundance of Quartz in thermal coals of India and its relation to abrasion index: Development of predictive model for abrasion", *International Journal of Coal Geology*, Vol. 84, pp. 63-69.

Bang J. H., & Suslick, K. S., (2010), "Applications of Ultrasound to the Synthesis of Nanostructured Materials" *Advanced Materials*, Vol. 22, pp. 1039–1059.

Banks, D., Younger, P.L., Arnesen, R.L., Egil R. Iversen, E.R. & Banks, S.B. (1997), "Mine-water chemistry: the good, the bad and the ugly", *Environmental Geology, Vol.* 32, pp. 157-174.

REFERENCES

Barnes, M.C., Addai-Mensah, J., Gerson, A. R. (1999), "The mechanism of the sodalite-to-cancrinite phase transformation in synthetic spent Bayer liquor" *Microporous and Mesoporous Materials,* Vol. 31, pp. 287–302.

Barrer, R. M. & Cole, J. F. "Aluminosilicates containing sodalite and/or cancrinite cages encapsulating salts", United States Patent 3674709, Filled in 1969.

Barrer, R.M. (1982), "Hydrothermal Chemistry of Zeolites", Academic Press, London.

Barzetti, T., Selli E., Moscotti, D. & Forni, L. (1996), "Pyridine and ammonia as probes for FTIR analysis of solid acid catalysts", *Journal of the Chemical Society, Faraday Transactions,* Vol. 92, pp. 1401-1407.

Basaldella, E. I., Kikot, A. & Tara J. C. (1997), "Effect of aluminum concentration on crystal size and morphology in the synthesis of a NaAl zeolite", *Materials Letters,* Vol. 31, pp. 83-86.

Baser, H. & Schwieger, W. (2008), "Zeolites and Related Materials: Trends, Targets and Challenges" Proceedings of 4th International FEZA Conference, Gédéon, A. Massiani, P. and Babonneau, F. (Eds.).

Baser, H., Selvam, T., Ofili, J., Herrmann, R. & Schwieger, W. (2007), "From Zeolites to Porous MOF Materials" Proceedings of the 40th Anniversary of International Zeolite Conference, Xu, R., Gao, Z. Chen, J. and Yan, W. (Eds.).

Bass, J. L. & Turner, G. L. (1997), "Anion Distributions in Sodium Silicate Solutions. Characterization by 29SI NMR and Infrared Spectroscopies, and Vapor Phase Osmometry", *Journal of Physical Chemistry, B.*, Vol. 101, pp. 10638-10644.

Bayati, B., Babaluo, A.A, & Karimi, R., (2008), "Hydrothermal synthesis of nanostructure NaA zeolite: The effect of synthesis parameters on zeolite seed size and crystallinity" *Journal of the European Ceramic Society,* Vol. 28, pp. 2653–2657.

REFERENCES

Bekkum, V.H., Flanigen, E.M. & Jansen, J.C. (1991), "Introduction to zeolite science and practice", Elsevier Science, Amsterdam, Netherlands.

Belviso, C. Cavalcante, F., Lettino, A., & Fiore, S., (2011), "Effects of ultrasonic treatment on zeolite synthesized from coal fly ash", *Ultrasonics Sonochemistry*, Vol. 18, pp. 661-668.

Belviso, C., Cavalcante, F. & Fiore, S. (2010), "Synthesis of zeolite from Italian coal fly ash: Differences in crystallization temperature using seawater instead of distilled water", *Waste Management*, Vol. 30, pp. 839–847.

Berkgaut, V. & Singer, A. (1996), "High capacity cation exchanger by hydrothermal zeolitization of coal fly ash", *Applied Clay Science,* Vol. 10, pp. 369-378.

Betti, C., Fois E., Mazzucato, E., Medici, C., Quartieri, S., Tabacchi, G., Vezzalini, G. & Dmitriev, V. (2007), "Gismondine under HP: Deformation mechanism and re-organization of the extra-framework species", *Microporous and Mesoporous Materials,* Vol. 103, pp. 190–209.

Bhanarkar, A.D., Gavane, A.G., Tajne, D.S., Tamhane, S.M. & Nema, P. (2008), "Composition and size distribution of particules emissions from a coal-fired power plant in India", *Fuel*, Vol. 87, pp. 2095–2101.

Bonilla, A., Baudouin, D., Pérez-Ramírez, J. (2009), "Desilication of ferrierite zeolite for porosity generation and improved effectiveness in polyethylene pyrolysis" *Journal of Catalysis*, Vol. 265, pp. 170–180.

Bosman, D.J., Clayton, J.A., Maree, J.P., & Adlem, C.J.L. (1990), "Removal of sulphates from mine water with sulphide", *Proceedings of the Lisbon 90 International Symposium: Acidic Mine Water in Pyritic Environments*, Lisbon, Portugal, pp. 16

Breck, D.W. (1974), "Zeolite Molecular Sieves", John Wiley & Sons, Ltd, New York.

REFERENCES

Bronic, J., Subotic, B., Šmit, I. & Despotovic, Lj.A. (1988), "Innovation in Zeolite Materials Science, Studies in Surface Science and Catalysis", P.J. Grobet, W.J. Mortier, E.F. Vansant, G. Schulz-Ekloff (Eds.), Elsevier, Amsterdam, Vol. 37 pp. 107.

Brown, M.E. & Gallagher, P.K. (2008). "Handbook of thermal analysis and calorimetry, Volume 5: Recent advances, techniques and applications", Elsevier, Amsterdam, The Netherlands.

Burton, A., Feuerstein, M., Lobo, R. F. & Chan, J. C. C. (1999), "Characterization of cancrinite synthesized in 1,3-butanediol by Rietveld analysis of powder neutron diffraction data and solid-state ^{23}Na NMR spectroscopy", *Microporous and Mesoporous Materials,* Vol. 30, (2–3), pp. 293–305.

Burton, A.W. (2010), "Powder diffraction in zeolite science, an introductory guide" In Chester, A. W. & Derouane, E. G. (Eds). "Zeolite Characterization and Catalysis, a tutorial" Springer-Verlag, Berlin.

Butler, J. N. (1998) "Ionic equilibrium: solubility and pH calculations". Wiley-Interscience, pp. 365 – 448.

Byrappa, K. & Yoshimura, M. (2001), "Handbook of Hydrothermal Technology", Noyes Publications / William Andrew Publishing, LLC, New York,

Catalfamo, P., Corigliano, F., Primerano, P. & Pasquale, S. D. (1993), "Study of the pre-crystallisation stage of hydrothermally treated amorphous aluminosilicates through the composition of the aqueous phase", *Journal of the chemical Society, Faraday Transactions,* Vol. 89, pp. 171 – 175.

Catalfamo, P., Pasquale, S. D., Corigliano, F. & Mavilia, L. (1997), "Influence of the calcium content on the coal fly ash features in some innovative applications", *Resources, Conservation and Recycling*, Vol. 20, pp. 119 – 125.

Chandrasekhar, S. & Pramada, P.N. (2008), "Microware assisted synthesis of zeolite A from metakaolin", *Microporous and Mesoporous Materials*, Vol. 108, pp. 152-161.

Chang, C. D. & Bell, A. T. (1991), "Studies on the mechanism of ZSM-5 formation", *Catalysis Letters, Vol.* 8, No 5/6, pp. 305-316.

Chang, H. L. & Shih, W. H. (2000) "Synthesis of zeolites A and X from fly ashes and their ion-exchange behavior with cobalt ions", *Industrial & Engineering Chemistry Research,* Vol. 39, pp. 4185-4191.

Chang, H.L. & Shih, W.H. (1998), "A general method for the conversion of fly ash in to zeolites as ion exchangers for cesium", *Industrial & Engineering Chemistry Research,* Vol. 37, pp. 7178.

Chareonpanich, M., Namto, T., Kongkachuichay, P. & Limtrakul, J. (2004), "Synthesis of ZSM-5 zeolite from lignite fly ash and rice husk ash", *Fuel Processing Technology,* Vol. 85, pp. 1623–1634.

Chester, A.W. & Derouane, E.G. (2009), "*Zeolite Characterization and Catalysis: A Tutorial"*, Springer-Verlag, Berlin.

Chung, S., Kim, S., Nam, Y., Kim S. & Lee, B. (2003), "Synthesis and application of fly ash-derived zeolites from pyrolysis of polyolefins", *Journal of Industrial and Engineering Chemistry*., Vol. 9, pp. 181-187.

Ciric, J. (1968), "Kinetics of zeolite A crystallization", *Journal of Colloid and Interface Science*., Vol. 28, pp. 3l5-324.

Clarke, L. B. & Sloss, L. L. (1992), "Trace elements - emissions from coal combustion and gasification", IEACR/49, London, UK, IEA Coal Research.

Colella, C. & Gualtieri, A.F. (2007), "Cronstedt's zeolite", *Microporous and Mesoporous Materials,* Vol. 105, pp. 213–221.

REFERENCES

Cronstedt, A. F. (1756), "Natural Zeolite and Minerals", Acad. Handl. Stockholm , Vol. **17**, pp. 120.

Colthup, N. B., Daly, L.H. & Wiberley, S.E. (1964), "Introduction to infrared and Raman spectroscopy", Academic Press, New York.

Cook, J. D. & Thompson, R.W. (1988), "Modelling the effect of gel aging", *Zeolites*, Vol. 8, pp. 322-326.

Coombs, D. S., Alberti, A., Armbruster, T., Artioli, G., Colella, C. Galli, E., Grice, J. D., Liebau, F., Mandarino, J. A., Minato, H., Nickel, E. H., Passaglia, E., Peacor, D. R., Quartieri, S., Rinaldi, R., Ross, M., Sheppard, R. A., Tillmanns, E., Vezzalini, G. (1997) "Recommended nomenclature for zeolite minerals: report of the subcommittee on zeolites of the international mineralogical association, commission on new minerals and mineral names". *The Canadian Mineralogist*, Vol. 35, pp. 1571-1606.

Coutanceau C., J.M. da Silva, M.F. Alvarez, F.R. Ribiero, M. Guisnet, *Journal de Chimie Physique*, 1997, Vol. 94, pp. 765.

Crelling, J. C., Hagemann, H. W., Sauter, D. H., Ramani, R. V., Vogt, W., Leininger, D., Krzack, S., Meyer, B., Orywal, F., Reimert, R., Bonn, B., Bertmann, U., Klose, W. & Dach, G. (2010), "Coal", Ullmann's Encyclopedia of Industrial Chemistry.

Criado, M. (2007), "Alkali activation of fly ash: Effect of the SiO2/Na2O ratio Part I: FTIR study", *Microporous and Mesoporous Materials*, Vol. 106, pp. 180–191.

Cubillas, P. & Anderson, M. W. (2010) "Synthesis Mechanism: Crystal Growth and Nucleation, in Zeolites and Catalysis: Synthesis, Reactions and Applications" (eds) J. Čejka, A. Corma and S. Zones), Wiley-VCH Verlag GmbH & Co. KGaA, Weinheim, Germany.

Cundy, C. S. & Cox, P.A. (2005), "The hydrothermal synthesis of zeolites: Precursors, intermediates and reaction mechanism", *Microporous and Mesoporous Materials*, Vol. 82, pp. 1-78.

REFERENCES

Cundy, C.S., Lowe, B.M. & Sinclair, D.M. (1993), "Crystallisation of zeolitic molecular sieves: direct measurements of the growth behaviour of single crystals as a function of synthesis conditions", *Journal of the Chemical Society, Faraday Discuss,* Vol. 95, pp. 235-252.

Czurdo, K. A. & Haus, R. (2002), "Reactive barriers with fly ash zeolites for in-situ ground water remediation", *Applied Clay Science*, Vol. 21, pp. 13 – 20.

Davini, P. (1996), "Investigation of the SO_2 adsorption properties of $Ca(OH)^{2-}$ fly ash systems", *Fuel,* Vol. 75, pp. 713–716.

Decottignies, M., Phalippou, *J.* & Zarzycki, *J.* (*1978*), "Synthesis of glasses by hot-pressing of gels", *Journal of Materials Science, Vol. 13, No. 12, pp. 2605-2618.*

Derkowski, A., Franus, W., Beran, E., Czímerová, A., (2006), "Properties and potential applications of zeolitic materials produced from fly ash using simple method of synthesis". *Powder Technology,* Vol. 166, pp. 47–54.

Derkowski, A., Franus W.,Waniak-Nowicka, H., Czímerová, A., (2007), "Textural properties vs. CEC and EGME retention of Na–X zeolite prepared from fly ash at room temperature". *International Journal of Mineral Processing,* Vol. 82, pp. 57–68.

Ouden, D. C. J. J. & Thompson, R. W. (1992), "Analysis of Zeolite Crystallizations Using the Crystallization Curve", *Industrial and Engineering Chemistry Research*, Vol. 31, pp.369-373.

Di Renzo, F. (1998), "Zeolites as tailor-made catalysts: Control of the crystal size", *Catalysis Today,* Vol. 41, pp. 37-40.

Luque de Castro, M. & Priego-Capote, F. (2007), "Lesser known ultrasound-assisted heterogeneous sample-preparation procedures", *TrAC Trends in Analytical Chemistry*, Vol. 26, pp. 154-162,

Dyer, A. (1988), "*An introduction to Zeolite Molecular Sieves*", John Wiley, London.

Eary, L. E., Rai, D., Mattigold, S.V & Ainsworth, (1990), "Geochemical factors controlling the mobilization of inorganic constituents from fossil fuel combustion residues: II. Review of the minor elements", *Journal of Environmental Quality*, Vol. 19, pp. 202 – 214.

Eldik, R., & Hubbard C. D., (1997), "Chemistry under Extreme or Non-Classical Conditions", John Wiley and Sons, New York.

Elliot, A.D. (2006), "An investigation in to the hydrothermal processing of coal fly ash to produce zeolite for controlled release fertilizer applications", PhD Thesis, School of engineering, Curtin University of Technology, Perth.

Eskom, (2011), Electricity Supply Commission, South Africa, annual report, www.eskom.co.za, [accessed on January 31, 2012].

Fansuri, H., Pritchard, D., & Zhang Dong-ke, (2008), "Manufacture of low-grade zeolites from fly ash for fertilizer applications", Research report 91 for Cooperative research Centre for coal in sustainable development, Australia.

Fatoba, O. O. (2011), "Chemical interactions and mobility of species in fly ash-brine co-disposal systems" Unpublished PhD thesis, University of the Western Cape, South Africa.

Feijen, E.J.P., Martens, J.A. & Jacobs, P.A. (1994), "Zeolites and Related Microporous Materials", Weitkamp J., Karge H.G., Pfeifer H., Hölderich W. (Eds.), vol. 84A, Elsevier, Amsterdam, pp. 3.

Feng, D., Aldrich, C. & Tan, H. (2000), "Treatment of acid mine drainage by use of heavy metal precipitation and ion exchange", *Minerals Engineering*, Vol. 13, pp. 623-642.

Feng, D., Tan, H., Van Deventer, J. S. J. (2004), "Ultrasound enhanced geopolymerisation" *Journal of materials science*, Vol. 39, pp. 571– 580.

Fernández-Jiménez, A. & Palomo, A. (2005), "Mid-infrared spectroscopic studies of alkali-activated fly ash structure", *Microporous and Mesoporous Materials,* Vol. 86, pp. 207-214.

Flanigen, E.M., Khatami, H. & Szymanski, H. A. (1971), "Molecular sieve zeolited", *Advances in Chemistry Series*, Vol. 101, pp. 201.

Foner, H. A., Robl, T. L., Hower, J. C. & Graham, U. M. (1999), "Characterization of fly ash from. Israel with reference to its possible utilization". *Fuel*, Vol. 78, pp. 215–223.

Franus, W. (2012), "Characterization of X-type zeolite prepared from coal fly ash", *Polish Journal of Environmental Studies*, Vol. 21, pp. 337-343.

Gaind, S. & Gaur, A.C. (2002), "Impact of fly ash and phosphate solubilising bacteria on soybean productivity", *Bioresource Technology,* Vol. 85, pp. 313–315.

Gazea, B., Adam, K., Gazea, B., Adam, K. & Kontopoulos, A. (1996), "A review of passive systems for the treatment of acid mine drainage", *Journal of Minerals Engineering*, Vol. 9, pp. 23-42.

Gitari, W.M. (2006). "Evaluation of the Leachate Chemistry and Contaminants Attenuation in Acid Mine Drainage by Fly Ash and its derivatives", Unpublished PhD Thesis, University of the Western Cape, South Africa.

Gitari, W.M., Petrik, L.F., Etchebers, O., Key, D.L., Iwuoha, E. & Okujeni, C. (2008), "Utilization of Fly Ash for Treatment of coal mines waste water: Solubility controls on major inorganic contaminants." *Fuel,* 87, pp. 2450-2462.

Goodarzi, F. (2002), "Minerology, elemental composition and modes of occurrence of elements in canadian feed coals", *Fuel*, Vol. 81, pp. 199–213.

Goodarzi, F. (2006), "Morphology and chemistry of fine particles emitted froma Canadian coal-fired power plant", *Fuel*, Vol. 85, pp. 273–280.

REFERENCES

Goodhew, J., Humphreys, J. & Beanland, R. (2001), "Electron Microscopy and Analysis", Electron Microscopy and Analysis, ed. Taylor and Francis, Taylor and Francis, London, pp. 47-48.

Gora, L., Streletzky, K., Thompson, R.W. & Phillies, G.D.J. (1997), "Study of the crystallization of zeolite NaA by quasi-elastic light scattering spectroscopy and electron microscopy", *Zeolites*, Vol. 18.

Gottardi, G. & Galli, E. (1985), "Natural Zeolites", Springer-Verlag, Heidelberg.

Guang X., Yi Y, Zhao-chi F., Qin X., Feng-Shou X. & Can L, (2001), "UV Raman spectroscopic study on the synthesis mechanism of zeolite X", *Microporous and Mesoporous Materials*, Vol. 42, pp. 317-323.

Gutierrez, B., Pazos, C. & Coca, J. (1993), "Characterization and leaching of fly ash", *Waste Manage and Research,* Vol. 11, pp. 279–86.

Grutzeck, M. W. & Siemer, D. D. (1997), "Zeolites Synthesized from Class F Fly Ash and Sodium Aluminate Slurry", *Journal of the American Ceramic Society*, VoL. 80, Issue 9, pp. 2449–2453.

Haber, J., Block, H. & Delmon, B. (1995), "Manual of methods and procedures for catalyst characterization (Technical report)", *Pure and Applied Chemistry*, Vol. 67, pp. 1257-1306.

Hagenson, L. C, & Doraiswamy, L. K., (1998), "Comparison of the effects of ultrasound and mechanical agitation on a reacting solid-liquid system", *Chemical Engineering Science,* Vol. 53, pp. 131 – 148.

Hammack, R. W., de Vegt, A. L. & Schoeneman, A. L. (1998), "The Removal of Sulfate and Metals from Mine Waters using Bacterial Sulfate Reduction: Pilot Plant Results." Mine Water and the Environment, Vol. 17, pp. 8-27.

Helble, J.J. (1994), "Trace element behavior during coal combustion: results of a laboratory study", *Fuel Process Technology,* Vol. 39, pp. 159– 172.

Hendricks, N.R (2005), "The applications of high capacity ion exchange adsorbent material synthesized from fly ash and acid mine drainage, for the removal of heavy and trace metals from secondary co-disposed process waters", Unpublished master's thesis, University of the Western Cape.

Herrmann, R., Schwieger, W., Scharf, O., Stenzel, C., Toufar, H., Schmachtl, M., Ziberi, B. & Grill, W. (2005), "In-situ diagnostics of zeolite crystallization by ultrasonic monitoring", *Microporous and Mesoporous Materials*, Vol. 80, pp. 1-9.

Holler, H. & Wirsching, U. (1985), "Zeolite formation from fly ash", *Fortschritte der Mineralogie,* Vol. 63, pp. 21 – 43.

Hollman, G.G., Steenbruggen, G. & Janssen-Jurkovicová, M. (1999), "A two-step process for the synthesis of zeolites from fly ash", *Fuel*. Vol. 78, pp. 1225-1230.

Hower, J. C., Robertson, J. D., Gerald, A. T., Wang, A. S., William, S. H., Graham, U. M., Rathbone, R. F. & Robl, T. L. (1996), "Characterization of fly ash from Kentucky power plants", *Fuel*, Vol. 75, pp. 403-411.

Hu, H. C & Lee, T. Y. (1990), "Synthesis Kinetics of Zeolite A", Industrial & *Engineering Chemistry Research,* Vol. 29, pp. 749-754.

Hui K. S., Chao, C. Y .H. & Kot, S. C. (2005), "Removal of mixed heavy metal ions in wastewater by zeolite 4A and residual products from recycled coal fly ash", *Journal of Hazardous Materials B*, Vol. 127, pp. 89–101.

Hui, K. S. & Chao, C. Y. H. (2008), "Methane Emissions Abatement by Multi-Ion-Exchanged Zeolite A Prepared from Both Commercial-Grade Zeolite and Coal Fly Ash", *Environmental Science and Technology,* Vol. *42,* pp. 7392–7397.

Hui, K. S. & Chao, C.Y. H. (2006), "Effects of step-change of synthesis temperature on synthesis of zeolite 4A from coal fly ash" Microporous. Mesoporous Materials, Vol. 88, pp 145–151.

Hui, K. S. & Chao, C. Y. H. (2006), "Pure, single phase, high crystalline, chamfered-edge zeolite 4A synthesized from coal fly ash for use as a builder in detergents", *Journal of Hazardous Materials B,* Vol. 137, pp. 401–409.

Hunger, M. (2009), Solid-State NMR Spectroscopy", In: Arthur W. Chester and E. G. Derouane (Eds.), "*Zeolite Characterization and Catalysis: A Tutorial",* Springer-Verlag, Berlin.

Hurley, J. P. & Schobert, H. H. (1991), "Ash Formation during Pulverized Subbituminous Coal Combustion. 1. Characterization of Coals, and Inorganic Transformations during Early Stages of Burnout", *Energy & Fuels,* Vol. 6, pp. 47-58.

Inada, M., Tsujimoto, H., Eguchi, Y., Enomoto, N. & Hojo, J. (2005), "Microwave assisted zeolite synthesis from fly ash in hydrothermal process", *Fuel,* Vol. 84, pp. 1482 – 1486.

Inayat, A., Knoke, I., Spiecker, E. & Schwieger, W. (2012), "Assemblies of mesoporous FAU-type zeolite nanosheets", *Angewandte Chemie international edition,* Vol. 51, pp. 1962-1965.

Iwasaki, A., Sano, T. & Kiyozumi, Y. (1998), "Effect of additives on the growth behavior of silicalite crystal", *Microporous and Mesoporous Materials,* Vol. 51, pp. 1962-1965.

Iyer, R. S. & Scott, J. A. (2001), "Power station fly ash – a review of value-added utilization outside of the construction industry", *Resource, Conservation and Recycle,* Vol. 31, pp. 217–228.

Jain, A. K. Jasra, R. V. & Bhat, S. G. T. (1990), "Liquid-phase adsorption of olefin/paraffin mixtures on ion-exchanged X zeolite", Separation Science and Technology, vol. 25, pp. 489–505.

REFERENCES

Jansen, K., Arafat, A., Barakat, A.K. & Van Bekkum, H. (1992), "Microwave techniques in zeolite syntheses". Synthesis of Microporous Materials (Eds. M.L. Occelli, H.E. Robson), van Nostrand Reinhold, New York, pp. 507.

Jeffrey, L. S. (2005), "Characterization of the coal resources of South Africa", *The Journal of The South African Institute of Mining and Metallurgy*, Vol. 106, pp. 95 – 102.

Johnson, B. D. & Hallberg, K. B., (2005), "Acid mine drainage remediation options: a review", *Science of the Total Environment*, Vol. 338, pp. 3-14.

Juan, R., Hernandez, S., Andres, J. M. & Ruiz, C. (2007), "Synthesis of granular zeolitic materials with high cation exchange capacity from agglomerated coal fly ash", Fuel, Vol. 86, pp. 1811-1821.

Kalnicky, D. J. & Singhvi, R. (2001), "Field portable XRF analysis for environmental samples", Journal of Hazardous Materials, Vol. 83, pp. 93-122.

Kalyoncu, R. S., (2001), "*Coal Combustion Products (*U.S. GEOLOGICAL SURVEY MINERALS YEARBOOK—2001)" http://minerals.usgs.gov/minerals, [accessed on March 5, 2012].

Katovic, A. , Subotic, B., Šmit, I., Despotovic, Lj. A. & uric, M. C. (1989), " Zeolite Synthesis", American Chemical Society Symposium Series, Occelli, M. L., & Robson H.E. (Eds.).

Karge H. G and Weitkamp (1989), "Zeolites as catalysts, sorbents and detergent builders", Elsevier science publishers. B. V., Amsterdam.

Kerr, G. T. (1968) "Chemistry of crystalline aluminosilicates I.V Factors affecting the format ion of zeolites X and B", *The Journal of Physical Chemistry*, Vol. 72, pp. 1385-1386.

Kerr, G.T. (1996), "Chemistry of Crystalline Aluminosilicates. I. Factors Affecting theFormation of Zeolit A", *Journal of Physical Chemical Chemistry*, Vol. 70, pp. 1047-1050.

Kim, D.S., Chang, J., Hwang, J., Park, S. & Kim, J.M. (2004), "Synthesis of zeolite beta in fluoride media under microwave irradiation", *Microporous and Mesoporous Materials*, Vol. 68, pp. 77-82.

Kim, H., Jung, J., Kim, D., Phuong, N. T., & Kim, K. (2007), "Monitoring of polymorph transformation using in-situ measurement of ultrasonic velocity", BIWIC, 14th International workshop on industrial crystallization. A.E. Lewis & C. Oslen, (Eds.), pp.. 89-94.

Kim, W., Choi, D. & Kim, S. (2010), "Sonochemical Synthesis of Zeolite A from Metakaolinite in NaOH Solution" *Materials Transactions,* Vol. 51, pp. 1694-1698.

Kiricsi I., Flego, C., Pazzuconi, G., Parker, W. O., Millini, R., Perego, C. & Bellussi, G. (1994) "Progress toward understanding zeolite-Beta acidity - An Ir and Al-27 NMR Spectroscopic Study" *Journal of Physical Chemistry,* Vol. 98, pp. 4627-4634.

Kitsopoulos, K. P. (1999), "Cation-exchange capacity (CEC) of zeolitic volcanilastic materials: applicability of the ammonium acetate saturation (AMAS) method", *Clays and clay minerals,* Vol. 47, pp. 688-696.

Kliewer, C. E. (2009), 'Electron Microscopy and Imaging", in Arthur W. Chester and E. G. Derouane (Eds.), "*Zeolite Characterization and Catalysis: A Tutorial",* Springer, Dordrecht.

Klink, M. J. (2003), "The potential use of South African coal as a neutralisation treatment option for acid mine drainage", Unpublished MSc Thesis, University of the Western Cape, South Africa.

Kosanović, C., Bosnar, S., Subotić, B., Svetličić, V., Mišić, T., Dražić, G. & Havancsák, K. (2008), "Study of the microstructure of amorphous aluminosilicate gel before and after its hydrothermal treatment". *Microporous and Mesoporous Materials*, Vol. 110, pp.177-185.

Koukouzas, N., Hämäläinen, J., Papanikolaou, D., Tourunen, A. & Jäntti, T. (2007), "Mineralogical and elemental composition of fly ash from pilot scale fluidised bed

combustion of lignite, bituminous coal, wood chips and their blends", *Fuel*, Vol. 86, pp. 2186–2193.

Koukouzas, N., Vasilatos, C., Itskos, G., Mitsis, I., Moutsatsou, A. (2010), "Removal of heavy metals from wastewater using CFB-coal fly ash zeolitic materials", *Journal of Hazardous Materials*, Vol. 173, pp. 581-588.

Krevelen, D. W. (1993), "Coal: Topology, chemistry, physics, constitution", 3rd edition. Elsevier, Amsterdam.

Kruger R. A & Kruger J. E. (2005), "Historical development of coal ash utilization in South Africa" World coal ash (WOCA) symposium, April 11-15, 2005. Available at http://www.flyash.info/2005/204kru.pdf [accessed on May 2010].

Krüger, J. E. (2003), "South African fly ash: a cement extender South African Coal Ash Association" Monograph publication on behalf of South African Coal Ash Association (SACAA).

Kruger, R. A. (1997), "Fly ash beneficiation in South Africa: creating new opportunities in the market-place" *Fuel*, Vol, 76, pp. 777-779.

Kutchko, B. G. & Kim, A. G. (2006), "Fly ash characterization by SEM–EDS", *Fuel*, Vol. 85, pp. 2537–2544.

Lantz, R. C. & Hinton, D. E. (1984), "Pulmonary toxicity associated with fly ash from fluidized bed coal combustion. II. Cellular morphometry of distal lung following a single intratracheal instillation", *Toxicology* and Applied *Pharmacology*, Vol. pp. 75:44-51.

Lawrence, A. R. (1998), "Energy from municipal solid waste: A comparison with coal combustion technology", *Progress in Energy and Combustion Science*, Vol. 24, pp. 545-564.

Lee, D. B., Matsue, N. & Henmi, T. (2001), "Influence of NaOH concentrations dissolved in seawater and hydrothermal temperatures on the synthesis of artificial zeolite from coal fly ash', *Clay Science*, Vol. 11, pp. 451–463.

Li, M., Hu, S., Xiang, J., Sun, L.S., Li, P. S., Su, S. & Sun, X. (2003), "Characterization of fly ashes from two Chinese Municipal solid waste incinerators", *Energy and Fuels*, Vol. 17, pp. 1487-1491.

Li, Q., Mihailova, B., Creaser, D. & Sterte, J. (2001), "Aging effects on the nucleation and crystallization kinetics of colloidal TPA-silicalite-I", *Microporous and Mesoporous Materials*, Vol. 43, (1), pp. 51-59.

Li, X., Wang, D., Zhou, Q., Liu, G. & Peng, Z. (2011), "Concentration variation of aluminate ions during the seeded precipitation process of gibbsite from sodium aluminate solution" *Hydrometallurgy*, Vol. 106, pp. 93-98.

Lindley, J. (1992) "Sonochemical effects on syntheses involving solid and supported catalysts" *Ultrasonics*, Vol. 30, pp. 163-167.

Liu, Y., Xu, J., Jin, L., Fang, Y. & Hu, H. (2009), "Synthesis and modification of zeolite NaA adsorbents for separation of hydrogen and methane", *Asia-Pacific Journal of Chemical Engineering, Vol.* 4, pp. 666–671

Liu, G., Zhang, H., Gao, L., Zheng, L. & Peng, Z. (2004), "Petrological and mineralogical characterizations and chemical composition of coal ashes from power plants in Yanzhou mining district, China", *Fuel Process Technology*, Vol. 85, pp. 1635–46.

Lottermoser, B.G. (2007), "Mine Wastes: Characterization, Treatment and Environmental Impacts". 2nd edn, Springer Verlag, Berlin Heidelberg.

Lowell, S., Joan, E. S., Martin, A. T. & Matthias, T. (2006), "Characterization of porous solids and powder: surface area, pore size and density", Spinger, Netherlands, pp. 123.

Lu, G. Q. & Do, D. D. (1991), "Adsorption properties of fly ash particles for NO*x* removal from flue gases", Fuel Processing Technology, Vol. 27, pp. 95–107.

Luque-de-Castro, M. D. & Priego-Capote, F., (2007), "Ultrasound-assisted crystallization (sonocrystallization)" *Ultrasonics Sonochemistry*, Vol. 14, pp. 717-724.

Madzivire, G., Petrik, L.F., Gitari, W.M., Ojumu, T.V. & Balfour, G. (2010), "Application of coal fly ash to circumneutral mine waters for the removal of sulphates as gypsum and ettringite", *Minerals Engineering,* Vol. 23, pp. 252–257.

Manz, O.E. (1999), "Coal fly ash: a retrospective and future look", *Fuel,* Vol. 78, pp. 133–136.

Martinez, C. & Perez-Pariente, J. (2011), "Zeolites and ordered porous solids. In: 3rd FEZA School on Zeolites : fundamentals and applications", Valencia, Editorial Universitat Politecnica de Valencia, ISBN 978-84-8363-719-7.

Mason, T. J. (1997), "Sonochemistry" Oxford University press, New York.

Mattigod, S.V., Dhanpat, R., Eary, L.E. & Ainsworth, C.C. (1990), "Geochemical factors controlling the mobilization of inorganic constituents from fossil fuel combustion residues: I. Review of the major elements", *Journal of Environmental Quality,* Vol. 19, pp. 188–201.

McLennan, A. R., Bryant, G. W., Stanmore, B. R. & Wall, T. F. (2000). "Ash Formation Mechanisms during pf Combustion in Reducing Conditions", *Energy & Fuels*, Vol. 14, pp. 150-159.

Meier, W.M., Olson D.H., & Baerlocher, C. (1996), "Atlas of Zeolite Structure Types", 4th revised edition, Structure Commission of the International Zeolite Association.

Miladinović, Z., Zakrzewska, J., Kovačević, B. & Bačić, G. (2007), "Monitoring of crystallization processes during synthesis of zeolite A by in-situ ^{27}Al NMR spectroscopy", *Materials Chemistry and Physics*, Vol. 104, pp. 384-389.

Mintova, S., Olson, N.H. & Bein, T. (1999), "Electron microscopy reveals the nucleation mechanism of zeolite Y from precursor colloids", *Angewandte Chemie International Edition,* Vol. 38, pp. 3201-3204.

Mintova, S., Olson, N.H., Senker, J. & Bein, T. (2002), "Mechanism of the transformation of silica precursor solutions into Si-MFI zeolite", *Angewandte Chemie International Edition,* Vol. 41, pp. 2558-2561.

Molina, A. & Poole, C. (2004), "A comparative study using two methods to produce zeolites from fly ash", *Minerals Engineering*, Vol. 17, pp. 167-173.

Mostowicz, R. & Berak J. M. (1985), "Factors Influencing the Crystal Morphology of ZSM-5 Type Zeolites" , in Studies in Surface Science and Catalysis, Proceedings of an International Symposium, Vol. 24, pp. 65–72.

Mollah, M. Y. A., Promreuk, S., Schennach, R., Cocke, D.L. & Güler, R. (1999), "Cristobalite formation from thermal treatment of Texas lignite fly ash", *Fuel*, Vol. 78, pp. 1277-1282.

Mondragón, F., Rincón, F., Sierra, L., Escobar, J., Ramírez, J. & Fernández, J., (1990), "New perspectives for coal ash utilization: Synthesis of zeolitic materials", *Fuel*, Vol. 69, pp. 263-266,

Montanari, T. & Busca, G. (2008), "On the mechanism of adsorption and separation of CO_2 on LTA zeolites: An IR investigation", *Vibrational Spectroscopy*, Vol. 46, pp. 45–51.

Moreno N., Querol, X. Ayora, C., Alastuey, A., Fernández-Pereira, C. & Janssen-Jurkovicová, M. (2001), "Potential Environmental Applications of Pure Zeolitic Material Synthesized from Fly Ash", *Journal of Environmental Engineering,* Vol. 127, pp. 994 – 1002.

Moreno, N., Querol, X. & Ayora, C. (2001), "Utilization of Zeolites Synthesized from Coal Fly Ash for the Purification of Acid Mine Waters", *Environmental Science* & *Technology,* Vol. 35, pp. 3526-3534.

Mosca, A. (2006), "Structured zeolite adsorbents", Msc Thesis, Lulea University of Technology.

Moutsatsou, A., Stamatakis, E., Hatzitzotzia, K. & Protonotarios, V. (2006), "The utilization of Ca-rich and Ca–Si-rich fly ashes in zeolites production", *Fuel*, Vol. 86, pp. 657-663.

Murayama, N., Yamamoto, H. & Shibata, J. (2002), "Mechanism of zeolite synthesis from fly ash by alkali hydrothermal reaction", *International Journal Mineral Processing*, Vol. 64, pp. 1–17.

Muriithi, G. N., Gitari, W. M., Petrik, L. F. & Ndungu, P. G. (2011), "Carbonation of brine impacted fractionated coal fly ash: Implications for CO_2 sequestration", *Journal of Environmental Management*, Vol. 92, pp. 655-664.

Murphy, T.E., Phyllis, C.A., Behrns, R.J. & Jaquier, D.R. (1984), "Fly ash analysis by complementary atomic absorption spectrometry and energy dispersive X-ray spectrometry" *Analytical Chemistry,* Vol. 56, pp. 2534-2537.

Musyoka, N. M. (2009), "Hydrothermal synthesis and optimisation of zeolite Na-P1 from South African coal fly ash", MSc thesis, University of the Western Cape, South Africa,.

Musyoka, N. M., Petrik, L. F., Balfour, G., Gitari W. M. & Hums, E. (2011) "Synthesis of hydroxy sodalite from coal fly ash using waste industrial brine solution", *Journal of Environmental Science and Health, Part A*, Vol. 46, pp. 1–9.

Musyoka, N. M., Petrik, L. F., Gitari, W. M., Balfour, G., Hums, E. (2012), "Optimization of hydrothermal synthesis of pure phase zeolite Na-P1 from South African coal fly ashes", *Journal of Environmental Science and Health, Part A*, Vol. 47, 337–350.

Nagy, J. B., Bodart, P., Hannus, I. & Kiricsi, I. (1998), "Synthesis, Characterization and Use of ZeoliticMicroporous Materials", Deca Gen Ltd, Szeged, Hungary.

REFERENCES

Navarro, C. R., Agudo, E. R., Luque, A., Navarro, A. B. R., & Huertas, M. O. (2009), "Thermal decomposition of calcite: Mechanisms of formation and textural evolution of CaO nanocrystals", *American Mineralogist*, Vol. 94, pp. 578-593.

Ndayambaje, G. (2011), "Sorption properties of natural zeolites for the removal of ammonium and chromium ions in aqueous solution" Unpublished MSc thesis, University of the Western cape, South Africa.

Nisnevich, M., Sirotin, G., Schlesinger, T. & Eshel, Y. (2008), " Radiological safety aspects of utilizing coal ashes for production of lightweight concrete", *Fuel*, Vol. 87, pp. 1610–1616.

Occelli, M.L. & Robson, H.E. (1989), "ACS Symposium Series; Zeolite Synthesis", American Chemical Society (eds.) Washington, DC.

Oh, J. E., Clark, S. M. & Monteiro, P. J. M. (2011), "Determination of the bulk modulus of hydroxycancrinite, a possible zeolitic precursor in geopolymers, by high-pressure synchrotron X-ray diffraction", *Cement and Concrete Composites*, Vol. 33, pp. 1014–1019.

Ojha, K., Pradhan, N.C. & Samanta, A.N. (2004), "Zeolite from fly ash: synthesis and characterization", *Bulletin of Material Science*, Vol. 27, pp. 555–564.

Okubo, T., Wakihara, T., Plíevert, J., Nair, S., Tsapatsis, M., Ogawa, Y., Komiyama, H., Yoshimura, M. & Davis, M. E. (2001) "Heteroepitaxial Growth of a Zeolite", *Angewandte Chemie International Edition*, Vol. 40.

Oslon, D. H. (1970), *Journal of Physical Chemistry*. pp.742- 758.

Ouden, C. J. J. & Thompson, R. W. (1992), "Analysis of zeolite crystallizations using the crystallization curve" *Industrial & Engineering Chemistry Research.*, Vol. 31.

Park, M., Choi, C.L., Lim, W.T., Kim, M.C., Choi, J. & Heo, N.H. (2000), "Molten-salt method for the synthesis of zeolitic materials: I. Zeolite formation in alkaline molten-salt system", *Microporous and Mesoporous Materials.* Vol. 37, pp. 81-89.

Pathan, S.M., Aylmore, L.A.G. & Colmer, T.D. (2003), "Properties of Several Fly Ash Materials in Relation to Use as Soil Amendments", *Journal of Environmental Quality*, Vol. 32, pp. 687–693.

Passaglia, E. & Sheppard, R. A. (2001), "The Crystal Chemistry of Zeolites", *Reviews in Mineralogy and Geochemistry*, Vol. 45, pp. 69-116.

Pecharsky, V. K. & Zavali, P. Y. (2005), "Fundamentals of powder diffraction and structural characterization of materials", Springer, USA.

Peloso, A., Rovatti, M., & Ferraiolo, G. (1983), "Fly ash as adsorbent material for toluene vapours", *Resources, Conservation and Recycling*, Vol. 10, pp. 211–220.

Pengthamkeerati, P., Satapanajaru, T. & Chularuengoaksorn, P. (2008), "Chemical modification of coal fly ash for the removal of phosphate from aqueous solution", *Fuel*, Vol. 87, pp. 2469–2476.

Petkowicz, D. I., Rigo, R. T., Radtke, C., Pergher, S.B. & Dos Santos, J. H. Z. (2008), "Zeolite NaA from Brazilian chrysolite and rice husk", *Microporous and Mesoporous Materials*, Vol. 116, pp. 548-554.

Petrik, L. F., O'Connor, C. T. & Schwartz, S. (1995), "The influence of various synthesis parameters on the morphology and crystal size of ZSM-5 and the relationship between morphology and crystal size and propene oligomerization activity', Proceedings of ZEOCAT'95, Szombathely, HK Beyer, HG Karge, I Kiricsi, JB Nagy (eds.), Elsevier Science B.V., Amsterdam, pp. 517–524.

Petrik, L., White, R., Klink, M., Somerset, V., Key, D.L., Iwuoha, E., Burgers, C. & Fey, M.V. (2005), "Utilization of Fly Ash for Acid Mine Drainage remediation", *Water Research Commission* Report No. 1242/1/05.

Petrik, L.F., White, R.A., Klink, M.J., Somerset, V.S., Burgers, C.L. & Fey, M.V. (2003), "Utilisation of South African fly ash to treat acid coal mine drainage and production of high

quality zeolites from the residual solids. International Ash Utilisation symposium", Lexington, Kentucky, USA.

Pfenninger, A. (1999), "Molecular Sieve, Science and Technology", H.G. Karge and J. Weitkamp (Eds.), Springer-Verlag, Berlin, Vol. 2, pp. 162

Pienack, N., & Bensch, W. (2011), "In-situ monitoring of the formation of crystalline solids", *Angewandte Chemie International Edition*, Vol. 50, pp. 2014-2034.

Pretorius, P.J. & Woolard, C.D. (2003), "The Surface Chemical Properties of Novel High Surface Area Solids Synthesized from Coal Fly Ash", *South African Journal of Chemistry*, Vol. 56, pp. 34–39.

Querol, X., Alastuey, A., López-Soler, A. & Plana, F. (1997), "A Fast Method for Recycling Fly Ash: Microwave-Assisted Zeolite Synthesis". *Environmental Science & Technology,* Vol. 31, pp 2527–2533.

Querol, X., Moreno, N., Umaña, J.C., Alastuey, A., Hernández, E., López-Soler, A. & Plana, F. (2002), "Synthesis of zeolites from fly ash: an overview", *International Journal of Coal Geology,* Vol. 50, pp. 413-423.

Querol, X., Plana, F., Alastuey, A. & López-Soler, A. (1997), "Synthesis of Na-zeolites from fly ash", *Fuel*, Vol. 76, pp. 793-799.

Querol, X., Umana, F., Plana, F., Alastuey, A., López-soler, A., Medinaceli, A., Valero, A., Domingo, M.J. & Garcia-rojo, E. (2001), "Synthesis of zeolites from fly ash at pilot scale. Example of potential applications", *Fuel*, Vol. 80, pp. 857-865.

Querol, X., Umana, J.C., Alastuey, A., Ayora C., Lopez-Soler, A. & Plana, F. (2001), " Extraction of soluble major and trace elements from fly ash in open and closed leaching systems", *Fuel*, Vol. 80, pp. 801-813.

Ratoarinoro, N., Contamine, F., Wilhelm, A. M., Berlan, J. and Delmas, H., (1995), "Activation of a solid-liquid chemical reaction by ultrasound", *Chemical Engineering Science*, Vol. 50, pp. 554-558.

Rayalu, S.S., Udhoji, J.S., Meshram, S.U., Naidu, R.R. & Devotta, S. (2005), "Estimation of crytallinity in fly ash-bsed zeolite-A using XRDand IRspectroscopy*", Current Science*, Vol. 89, pp. 2147-2150.

Rayalu, S.S., Udhoji, J.S., Munshi b, K.N. & Hasan, M.Z. (2001), "Highly crystalline zeolite -A from fly ash of bituminous and lignite coal combustion", *Journal of Hazardous Materials B*, Vol. 88, pp. 107–121.

Reynold, K., Kruger, R. & Rethman, N. (1999), "The manufacture and evaluation of an artificial soil (SLASH) prepared from fly ash and sewage sludge", International Ash Utilization Symposium, Center for Applied Energy Research, University of Kentucky , paper #1.

Ríos, C.A. & Williams, C.D. (2008), "Synthesis of zeolitic materials from natural clinker: A new alternative for recycling coal combustion by-products", *Fuel*, Vol. 87, (12), pp. 2482-2492.

Roland, E. & Kleinschmit, P. (2005), "Zeolites", Ullmann's Encyclopedia of Industrial Chemistry. John Wiley & Sons.

Rotenberg, S. J., Mettzler, G., Poliner, J., Bechtold, W. E., Eidson, A. F. & Newton, G. J. (1991), "Adsorption kinetics of vapor-phase *m*-xylene on coal fly ash", *Environmental Science & Technology*, Vol. 25, pp. 830-935.

Run, M., Wu, S., & Wu, G. (2004), "Ultrasonic synthesis of mesoporous molecular sieve", *Microporous and Mesoporous Materials*, Vol. 74, pp. 37 – 47

Sallam, M. (2006), "Zeolite synthesis from municipal solid waste ash using fusion and hydrothermal treatment", PhD Thesis, University of South Florida.

Sankar, G. & Bras, W. (2009), "Insights into the formation of microporous materials by in-situ X-ray scattering techniques", *Catalysis Today*, Vol. 145, pp. 195–203.

Scheetz, B.E. & Earle, R. (1998), "Utilisation of fly ash", *Current opinion in solid state and material science*, Vol. 3, pp. 510-520.

Schmachtl, M., Kim, T.J., Grill, W., Herrmann, R., Scharf , O., Schwieger, W., Schertlen, R. & Stenzel, C. (2000), "Ultrasonic monitoring of zeolite synthesis in real time", *Ultrasonics*, Vol. 38, pp. 809–812.

Schüth F., Bussian, P., Ågren, P., Schunk, S. & Lindén, M. (2001), "Techniques for analysing the early stages of crystallization reactions", *Solid State Sciences*, Vol. 3, (7), pp. 801-808.

Scott, J., Guang, D., Naeramitmarnsuk, K., Thabout, M. & Amal, R. (2001), "Zeolite synthesis from coal fly ash for the removal of lead ions from aqueous solution", *Journal of chemical Technology and Biotechnology*, Vol. 77, pp. 63 – 69.

Sheng, C. & Li, Y. (2008), "Experimental study of ash formation during pulverized coal combustion in O2/CO2 mixtures", *Fuel*, Vol. 87, pp. 1297–1305.

Shi J., Anderson, M.W. & Carr, S.W. (1996), "Direct observation of zeolite A synthesis by in-situ solid-state NMR", *Chemistry of Materials*, Vol. 8, pp. 369-375.

Shigemoto, N., Sugiyama, S. Hayashi, H. & Miyaura, K. (1995), "Characterization of Na-X, Na-A, and coal fly ash zeolites and their amorphous precursors by IR, MAS, NMR and XPS, *Journal of Materials Science*, Vol. 30, pp. 5777-5783.

Shigemoto, N., Hayashi, H. & Miyaura, K. (1993), "Selective Formation of Na-X Zeolite from Coal Fly Ash by Fusion with Sodium Hydroxide Prior to Hydrothermal Reaction", *Journal of Materials Science*. Vol. 28, pp. 4781-4786.

Shih, W. H. & Chang, H. L. (1996), "Conversion of Fly Ash into Zeolites for Ion- Exchange Applications", Materials Letters, Vol. 28, pp. 263-268.

Singer, A. & Berkgaut, V., (1995), "Cation exchange properties of hydrothermally treated coal fly ash", *Environmental Science and Technology*, Vol. 29, pp. 1748 – 1753.

Somerset, V., Petrik, L. & Iwuoha, E. (2008), "Alkaline hydrothermal conversion of fly ash precipitates into zeolites:3: the removal of mercury and lead ions from wastewater", *Journal of Environmental Management,* Vol. 87, pp. 125-131.

Somerset, V. S., Petrik, L. F.,.White, R. A, Klink, M. J., Key, D. & Iwuoha, E. (2004), "The use of X-ray fluorescence (XRF) analysis in predicting the alkaline hydrothermal conversion of ash precipitates into zeolites", *Talanta*, Vol. 64, pp. 109-114.

Somerset, V. S., Petrick, L., White, R., Michael, J., David, K. & Iwuoha, E. I. (2005), "Alkaline hydrothermal zeolites synthesized from high SiO_2 and AlO_3 co-disposal fly ash filtrates", Fuel, Vol. 84, pp. 2324-2329.

Somerset, V., Petrik, L., & Iwuoha, E.Alkaline, (2005), "Hydrothermal Conversion of Fly Ash Filtrates Into Zeolites 2: Utilization in Wastewater Treatment", *Journal of Environmental Science and Health*, Vol. 40, pp. 1627–1636.

Sonqishe, T. M. (2008), "Treatment of brines using commercial zeolites and zeolites from ash derivative" Unpublished MSc thesis, University of the Western Cape.

Spears, D. A. (2000), "Role of clay minerals in UK coal combustion", *Applied Clay Science*, Vol. 16, pp. 87–95.

Speight, J.G. (2005), "Handbook of coal analysis", John Wiley & Sons, NJ, USA.

Srinivasan, A. & Grutzeck, M. W. (1999), "The Adsorption of SO_2 by Zeolites Synthesized from Fly Ash", *Environmental Science & Technology*, Vol. *33*, pp. 1464–1469.

Stumm, W. & Morgan, J.J., (1981), "Aquatic chemistry", 2nd edn, John Wiley & Sons, New York.

Subotić, B. & Bronić, J. (2003), "Theoretical and Practical Aspects of Zeolite Crystal Growth", Handbook of zeolite science and technology. Scott M. Auerbach, Kathleen A. Carrado, Prabir K. Dutta (eds.). Marcel Dekker, New York.

Suslick, K. S., & Doktycz, S. J. "The Effects of Ultrasound on Solids " in Mason, TJ. (ed), (1990) "Advances in Sonochemistry", Vol. 1, JAI Press, New York, pp. 197.

Sutarno & Arryanto, Y. (2007), "Synthesis of Faujasite from Fly Ash and Its Applications for Hydrocracking of Petroleum Distillates", *Bulletin of Chemical Reaction Engineering and Catalysis,* Vol. 2, pp. 45-51.

Szostak, R. (1989), "Molecular Sieves, Principles of synthesis and Identification", Van Nostrand Reinhold, New York.

Tanaka, H., Eguchi, H., Fujimoto, S. & Hino R. (2006), "Two-step process for synthesis of a single phase Na-A zeolite from coal ash by dialysis", *Fuel,* Vol. 85, pp. 1329-1334.

Tanaka, H., Furusawa, S. & Hino, R. (2002) "Synthesis, Characterization, and Formation Process of Na-X Zeolites from Coal Fly Ash", *Journal of Materials Synthesis and Processing,* Vol. 10, pp. 143-148.

Toufar H., ESTEC study report, contract no. 12599/97/NL/NB, Noordwijk (1998), pp. 3-23.

Toufar H., Wendlandt, K. & Karge, H.G. (1995), " A simple model for the kinetic evaluation of zeolite crystallization processes", *Journal of the Chemical Society, Faraday Transactions,* Vol. 91, pp. 549-554.

Truter, W.F., Rethman, N.F.G., Reynolds, K.A. & Kruger, R.A. (2001). "The use of a soil ameriolant based on fly ash and sewage sludge", International Ash Utilization Symposium, Center for Applied Energy Research, university of Kentucky, paper #80.

REFERENCES

Ural, S. (2005), "Comparison of fly ash properties from Afsin–Elbistan coal basin, Turkey", *Journal of Hazardous Materials B*, Vol. 119, pp. 85–92.

Usachev, N. Y., Belaruva, E. P., Krukousky, L. M, Kanaev, S. A. and Kazakov, O. K. A. (2003), *Russian Chemical Bulletin*. Vo., 52, pp. 1940.

Vadapalli, V.R.K., Gitari, W.M., Ellendt, A., Petrik, L.F. & Balfour, G. (2010), "Synthesis of zeolite-P from coal fly ash derivative and its utilization in mine-water remediation", *South African Journal of Science*. Vol. 106, pp. 62-68.

Vassilev, S.V. & Vassileva, C.G. (2005), "Methods for characterization of composition of fly ashes from coal-fired power stations: A critical overview", *Energy Fuels*, Vol. 19, pp. 1084–98.

Vassilev, S.V. & Vassileva, C.G. (2007), "A new approach for the classification of coal fly ashes based on their origin, composition, properties, and behavior", *Fuel*, Vol. 86, pp. 1490-1512.

Vories, K.C. & Throgmorton, D. (2002), "Proceedings of coal combustion by-products and western coal mines", Technical interactive forum, Denver Marriot west hotel, Golden, Colorado.

Vuthaluru, H.B. & French, D. (2008), "Ash chemistry and mineralogy of an Indonesian coal during combustion: Part II — Pilot scale observations", *Fuel processing technology*, Vol. 89, pp. 608 – 621.

Walek, T., Saito, F., & Zhang, Q. (2008), "The effects of low solid /liquid ratio on hydrothermal synthesis of zeolites from fly ash", *Fuel*, Vol. 87, pp. 3194 – 3199.

Walton R.I., Millange, F., O'Hare, D., Davies, A.T., Sankar, G. & Catlow, R.A. (2001), "An in-situ energy X-ray diffraction study of the hydrothermal crystallisation of zeolite A, Part 1: Influence of reaction conditions and transformation into sodalite", *Journal of Physical Chemistry B*, Vol. 105, pp. 83-90.

Wang, C., Li, J., Wang, L. & Sun, X. (2008), "Influence of NaOH concentrations on synthesis of pure-form zeolite A from fly ash using two-stage method", *Journal of Hazardous Materials,* Vol. 155, pp. 58-64.

Wang, S. & Wu, H. (2006). "Environmental-benign utilisation of fly ash as low-cost adsorbents", *Journal of Hazardous Materials,* Vol. 136, pp. 482-501.

Ward, C.R. & French, D. (2005), "Relation between Coal and Fly Ash Mineralogy, Based on Quantitative X-Ray Diffraction Methods*",* World of Coal Ash (WOCA), April 11-15, Lexington, Kentucky, USA. (http://www.flyash.info).

Weitkamp, J. (2000), "Zeolites and catalysis", *Solid state ionics,* Vol. 131, pp. 175 -188.

Weitkamp, J. & Puppe, L. (1999), "Catalysis and zeolites: fundamentals and applications", (eds.). Springer, German.

White, S. C. & Case, E. D. (1990), Characterization of fly ash from coal-fired power plants. *Journal of Materials Science,* Vol. 25, pp. 5215–5219.

Woolard, C.D., Petrus, K. & Van der Horst, M. (2000), "The use of modified fly ash as a sorbent for lead", *Water SA*, Vol. 26, No. 4.

WCA (World Coal association) publication, The Coal Resource, (2005), "A Comprehensive Overview of Coal", [www.worldcoal.org/resources/wca-publications, accessed on January 31, 2012].

Wu, J., Wang, B., Li, N., & Xiang, S., (2006) "Effect of aging with ultrasound on the synthesis of MCM-49 zeolite" *Chinese Journal of Catalysis,* Vol. 27, pp. 375–377.

Yang, X., Li, Y., Lemaire, A., Yu, J. & Su, B, (2009), "Hierarchically structured functional materials: Synthesis strategies for multimodal porous networks", *Pure and Applied Chemistry,* Vol. 81, pp. 2265–2307.

Yao, J., Wang, H., Ratinac, K. R. & Ringer, S. P. (2006), "Formation of Colloidal Hydroxy-Sodalite Nanocrystals by the Direct Transformation of Silicalite Nanocrystals" *Chemistry of Materials,* Vol. 18, pp. 1394-1396

Yaping Ye, Xiaogiang Zeng, Weilan Qian & Mingwen. (2008), "Synthesis of pure zeolites from supersaturated silicon and aluminium alkali extracts from fused fly ash", *Fuel*, Vol. 87, pp. 1800 – 1886.

Zhadanov S.P. (1971), "Molecular sieve zeolites -1", E.M. Flanigen., L. B. San (Eds.), American Chemical Society-Advances in Chemistry, Series 101, pp. 20-45.

Zhao, X. S., Lu, G. Q., & Zhu, H. Y. *(1997) "*Effects of ageing and seeding on the formation of zeolite Y from coal fly ash", *Journal of Porous Materials,* Vol. 4, pp. *245-251.*

Zheng, K., Gerson, A. R., Addai-Mensah, J. & Smart, R. S. (1997) "The influence of sodium carbonate on sodium ahminosilicate crystallisation and solubility in sodium aluminate solutions" *Journal of Crystal Growth,* Vol. 171, pp. 197-208.

Zholobenko, V.L., Dwyer J., Zhang, R., Chapple, A.P., Rhodes, N.P. & Stuart, J.A. (1998), "Structural transitions in zeolite P An in-situ FTIR study", *Journal of Chemical Society,* Vol. 94, pp. 1779-1781.

APPENDIX

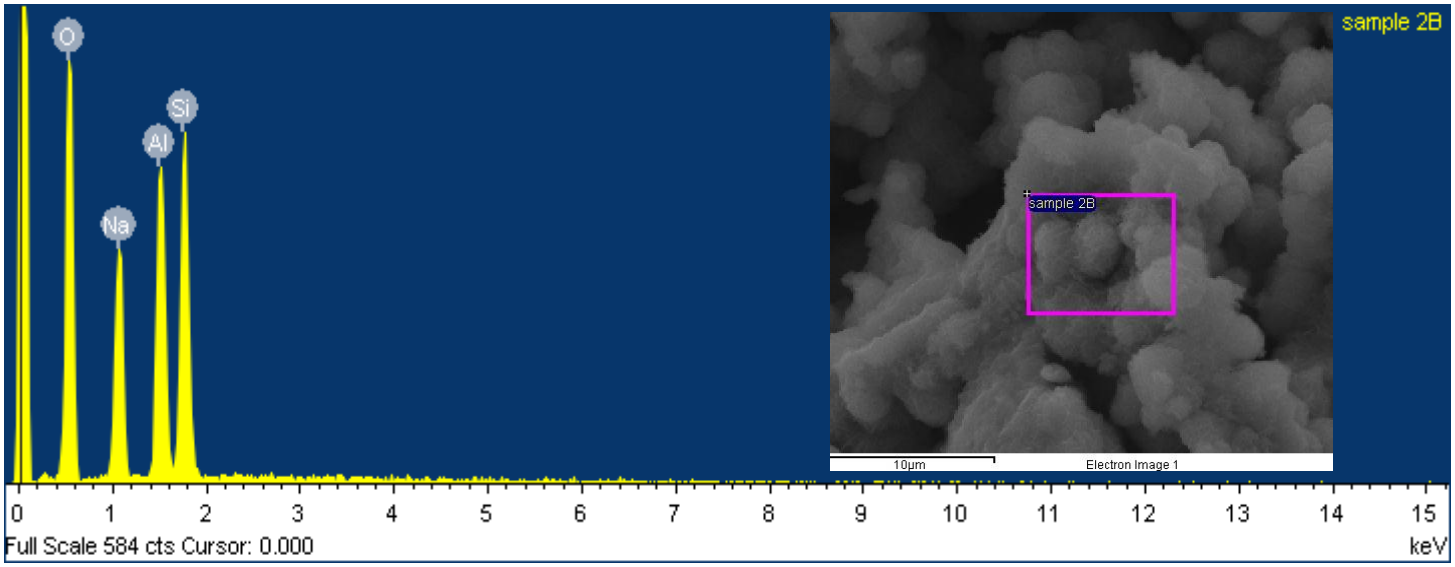

Label : sample 2B
Collected : 20-Dec-2011 02:56 PM
Livetime (s) : 30.00
Real time (s) : 30.44
Detector : X-Max
Window : SATW
Tilt (deg) : 0.1
Elevation (deg) : 35.0
Azimuth (deg) : 0.0

Magnification : 9062 X
Accelerating voltage (kV) : 20.00

Spectrum processing :
No peaks omitted
Processing option : All elements analyzed
(Normalised)
Number of iterations = 5

Element	Weight%	Atomic%
O K	52.44	64.18
Na K	14.54	12.38
Al K	14.29	10.37
Si K	18.73	13.06
Totals	100.00	

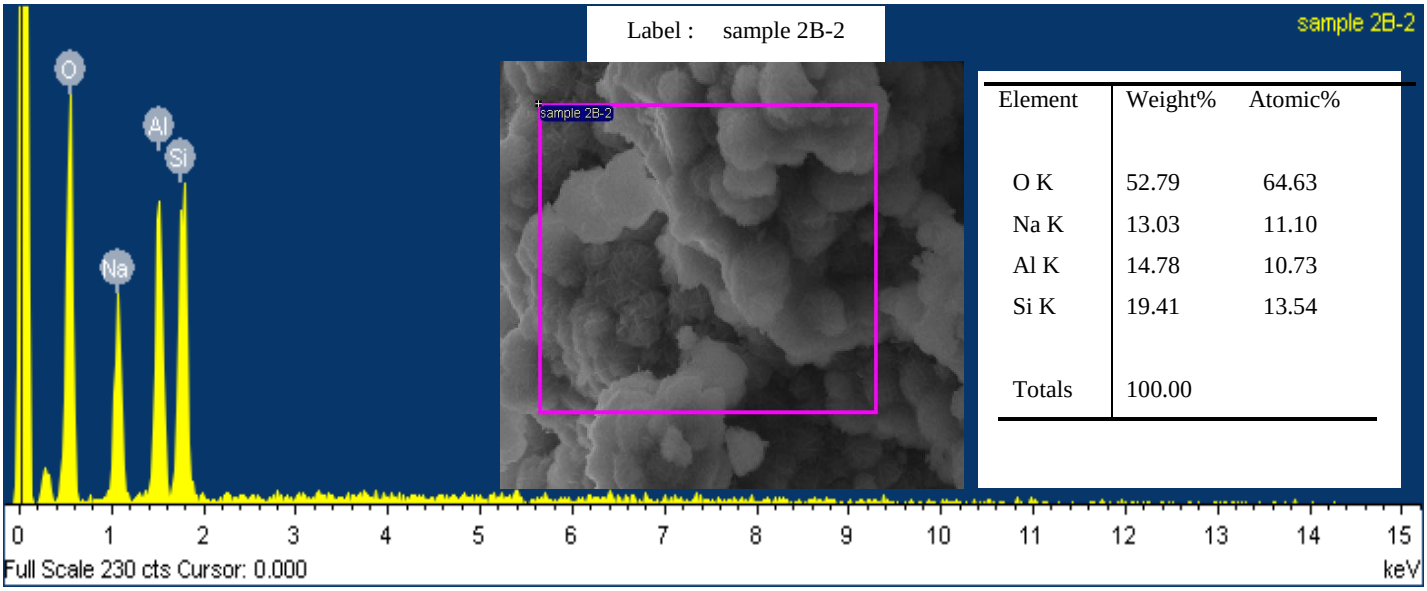

Element	Weight%	Atomic%
O K	52.79	64.63
Na K	13.03	11.10
Al K	14.78	10.73
Si K	19.41	13.54
Totals	100.00	

Figure A 1: EDS analysis of Con X80 sample done using Nova NanoSEM 230

Sample X — Dried sample at time 0 for synthesis of zeolite A from clear extarct of fused fly ash

Proben-Nr.	Einwaage (g)	Si mg/l	Al mg/l	Na mg/l	% Si	% Al	% Na
Sample X	0.1028	11.317	5.437	142.887	2.75	1.32	34.75

% in Amorphous		% water	Total	
23.19		76.81	100.00	From TGA

Total of solid oxide in Amorphous 142.25

Total oxide in solid specursor mixture

	Al_2O_3	Na_2O	SiO_2	H_2O	Total	
	1.05	19.67	2.47	76.81	100.00	Related to 100g
Molar mass	101.96128	61.97894	60.0843	18.0152		
No. of moles	0.01	0.32	0.04	4.26		
Rel. No of mole	1.00	30.84	4.00	414.41	Normalized to Al_2O_3	

Formulation	1.00	Al_2O_3 +	30.84	Na_2O +	4.00	SiO_2 +	414.41	H_2O

Relative % oxide quantities in industrial chemicals

		Al_2O_3	SiO_2	Na_2O	H_2O	Density
Na-Aluminat		28.04%	0.00%	27.40%	44.56%	1.477
Na-Wasserglas		0.00%	27.34%	8.37%	64.29%	1.356
Natriumhydroxid		0.00%	0.00%	77.48%	22.52%	
dest. Wasser		0.00%	0.00%	0.00%	100.00%	1.000

Quantities used during synthesis (simulation)

			Weight	Units	Volume	Units	
Na-Aluminate			5.10	g	3.45	ml	
Na-Waterglass			12.33	g	9.09	ml	
Sodium hydroxide			31.48	g		ml	
Distilled water			87.45	g	87.45	ml	
		Total	136.37	g	Total	100.00	ml

Figure A 2: Calculations for simulation of fly ash based molar regime for synthesis of zoeliet A from extract of fused fly ash using commecially available pure grade analytical chemicals.

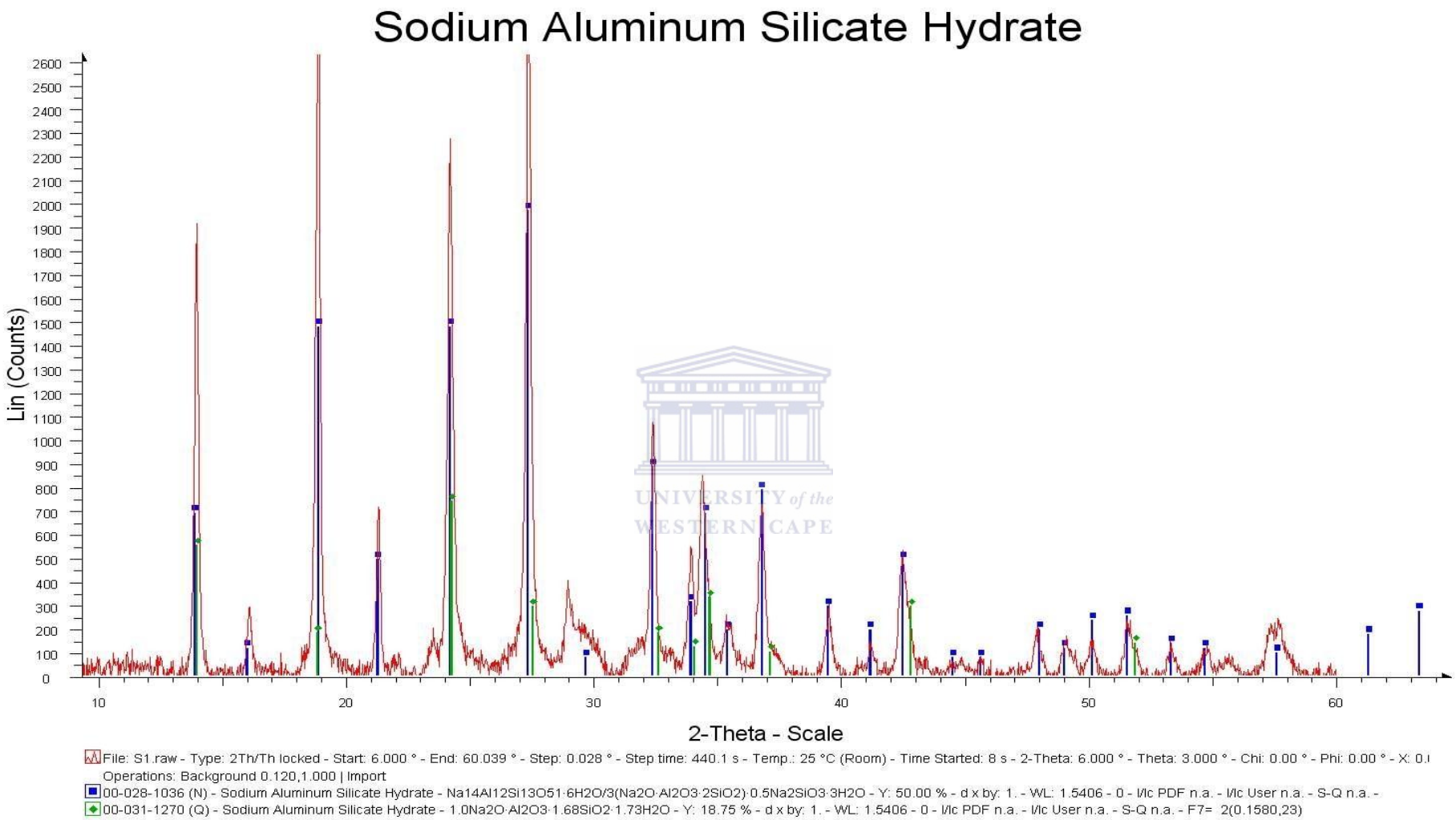

Figure A 3: XRD patterns showing the ovarlapping of peaks of cancrinite and sodalite zeolites.